Computer simulation of 2D and 3D moving conductor problems

Karaguler, Turhan

Award date:
1992

Awarding institution:
University of Bath

COMPUTER SIMULATION OF 2D AND 3D MOVING CONDUCTOR PROBLEMS

Submitted by

Turhan Karaguler

for the degree of Doctor of Philosophy

of the University of Bath

1992

ProQuest LLC
789 East Eisenhower Parkway
P.O. Box 1346
Ann Arbor, MI 48106-1346

" A modern poet has characterised the personality of art and the impersonality of science as follows: art is I; science is we."

Claude Bernard

(Introduction a l'etude de la medecine experimentale 1865, 1,2.4, line 1742)

ACKNOWLEDGEMENTS

I am very grateful to Professor D.Rodger for his invaluable guidance and continuous encouragement throughout this project.

I would also like to thank the ' MEGA Group ', academic, research and technical staff who helped in any way.

TABLE OF CONTENTS

LIST OF SYMBOLS

CHAPTER 1

$D( )$	General differential equation
$f'( )$	Trial solution
W_i	Shape function
a_i	Degrees of freedom
R	Residual function
t_j	Weighting function
dv	Volume integral
f_i	Nodal values
x,y,z	Cartesian coordinates
s,q	Local coordinates
L	Length of element
ξ,η,ζ	Natural coordinates
[K]	"Stiffness matrix"

CHAPTER 2

E	Electric field intensity
D	Electric flux density
B	Magnetic flux density
H	Magnetic field intensity
J	Current Density
ρ	Volume charge density
ε	Permittivity

μ	Permeability
σ	Conductivity
u	Velocity vector
V	Electric scalar potential
K_s	Surface current density
A	Magnetic vector potential
n	Normal vector
J_s	Source current density
ds	Surface integral
dc	Line integral
Φ_T	Total magnetic scalar potential
Φ_R	Reduced magnetic scalar potential
H_R	Reduced magnetic field intensity
H_S	Source magnetic field intensity
r,r'	Position vectors
α_p	Penalty number

CHAPTER 3

C,C_1,C_2	Constants
k,l,m	Constants
h	Grid size
α	Peclet number
W_{bj}	Biasing shape function
u_ξ,u_η	Velocity components (in natural coordinates)
τ	New position of a Gauss point

J_c	Jacobian

CHAPTER 4

f_t	Tensile stress
f_n	Compressive stress
N	Number of turns

CHAPTER 5

J_R	Reference phase current density
J_C	Control phase current density
J_{S1}	Maximum reference phase current density
J_{S2}	Maximum control phase current density
J_S	Total current density of the phases
ω	Angular frequency
s	Pole pitch
t	Time
g	Air-gap length
u_r	Speed of the rotor
u_s	Speed of the stator field
j	Imaginary unit
G	Goodness factor
B_F	Forward component of magnetic flux density
B_B	Backward component of magnetic flux density
ρ_r	Rotor resistivity
t_r	Thickness of rotor plate

Ω_s	Slip
p	Number of pole pairs
T	Torque
n	Harmonic number
[T]	Transfer Matrix
L	Stator length
M	Periodicity number

ABSTRACT

Many devices, such as electromagnetic launchers, magnetic levitation transport systems (MAGLEV) and linear induction machines, involve conducting parts which move. The main thrust of this thesis is to develope and validate effective numerical methods for modelling such problems using the finite element method in 2 and 3 dimensions.

Initially, a basic description of the finite element method which is widely used throughout the work is given. In chapter 2, the field equations which consider only the motional effect (DC case) are obtained for 2D and 3D moving conductor problems. The 2D and 3D finite element equations are derived from the Galerkin's point of view. The 3D formulation uses the magnetic vector potential $\overline{A}$, together with the electric scalar potential V in conductors, coupled to magnetic scalar potentials elswhere. In chapter 3, a difficulty, the occurrence of oscillations in the solution when using the standard Galerkin formula for the moving conductor problem is discussed. A method, upwinding, is suggested and applied to alleviate this particular problem. A new technique not requiring the electric scalar potential V in the 3D formulation is introduced in chapter 4. An experimental set up is also presented in order to verify the results obtained from the application of the new technique. Finally, in chapter 5, AC problems are included in the formulation. A two-phase linear induction servomotor is used as an example. In the same chapter, calculations obtained using a very simple analytic technique, 'layer theory' Fourier harmonic analysis, and 2 and 3 finite elements are compared with experimental measurements.

CHAPTER 1

INTRODUCTION

1.1 Introduction

There is no doubt that one of the most significant events of the 19 th century is Maxwell's discovery of the laws of electrodynamics. However, although Maxwell described the fundamental behaviour of electromagnetism 120 years ago, the solution of his equations for practical applications had to await recent advances in computer hardware and numerical algorithms. Before this, engineers, particularly in the design area, faced severe problems in trying to investigate the electromagnetic nature of their products. Instead of electromagnetic field theory, they used mainly lumped parameter circuit models. However the circuit theory is derived from the field theory under certain assumptions and simplifications which may sometimes lead to an extensive departure from modelling the real problem. More recently solving the problems by means of using the field theory is becoming increasingly popular. This change has been prompted by mainly three developments. Firstly, the arrival of reasonably priced high speed digital computers on the market. In parallel with this, rapid developments in computer graphics systems enabled the visualisation of device geometries and field distribution. Lastly, advances in numerical techniques which represent geometries and Maxwell's equations in a digital or discretized form.

In general terms, the work described in this thesis may fall into the last category above, that of advancing numerical techniques to solve a particular

electromagnetics problem represented directly by the Maxwell equations. There are three common approaches for discretizing the Maxwell equations, namely integral techniques, the finite difference method and the finite element method. The integral techniques use the integral form of the Maxwell equations, solving them for the entire domain or for only the source of the field on the boundaries of the model (boundary element method). Despite the fact that the integral methods possess comparatively less variables than the other two methods, it can be suitable for only simple geometries. This is because the variables in the set of equations are mostly related to each other. Therefore, the resulting matrices are small but highly dense and the entries of the matrices involve complex and time consuming integral operations. The finite difference method solves the Maxwell equations in a differential form at each node of the regularly spaced grid of points. The difference method often requires regular meshes therefore, it can be restrictive in applications. The finite element method is widely regarded as the most powerful method of the three, not only for the solution of Maxwell equations but also for the solution of many different problems experienced in physics and engineering in general. The finite element method divides the geometry into standard elements and solves the problem for each of these elements. It can model complex geometries by using many kinds of regular or irregular elements. The application of it will be closely examined in this work.

The area of electromagnetism concerned in this work is the moving conductor problem. Only the type of moving conductor problem in which the moving member is invarient in the cross section which is normal to the direction of motion is considered. This restriction leads to a steady state solution for the problem at constant speed. Otherwise a full time transient analysis would be required.

According to the well known laws of electromagnetism, there are two ways of inducing currents in a conductor, by either moving the conductor through a steady magnetic field or/and changing the magnitude of the exciting field with time. The first effect produces motional EMF and the second effect produces transformer EMF. Initially only the motional EMF is concerned in this work. The formulae in chapters 2,3 and 4 are exclusively obtained for the field excited by DC currents. The transformer effect is also included in chapter 5, when a 2-phase linear induction servomotor is used as the test problem.

1.2 Brief History and Development of the Finite Element Method

The beginning of the finite element method (FE) goes back to around 1940. Courant's 1943 paper dealing with elasticity problems can be considered as the earliest FE work [1.1]. The paper that signalled the beginning of FE analysis was written by Turner in 1956 [1.2]. The method was first used around 1960 to solve simple static stress problems with linear materials and small displacement.

Although there were some small scale applications of FE analysis in heat transfer, fluid flow and magnetic problems, the main use of the method in the 1960s was limited to structural analysis. The introduction of the Frontal Solution Algorithm by Irons in 1970 made the equation solving phase of the technique more adaptable to a wider variety of hardware [1.3]. Zienkiewicz wrote one of the earliest fundamental text books published in 1971, with emphasis on civil and mechanical engineering applications [1.4]. However, regarding the application of the technique to

electromagnetism, Winslow's work [1.5] is significant. His seminal work at the Lawrence Livermore Laboratory California in 1963, which includes the introduction of a variational method may be seen as the earliest application in electromagnetism. Later, in 1969, Peter Silvester of Mc Gill university used FE to solve a standard electromagnetic problem involving homogeneous waveguides.

As electric circuits which are mathematical abstractions of electromagnetic fields were thought to be easier to understand for engineers than fields, Carpenter's publication of the circuit interpretation of FE in 1975 is considered significant as early work [1.6].

On the other hand, in the late 1960s, and beginning of 1970s the application of the FE method required the use of a large Mainframe computer. Most applications were run on Mainframe IBM and Control Data Machines that had memory sufficient to handle the large sets of matrix equations, therefore the majority of the analyses were performed by specialists. However, in the late 1970s, the introduction of super mini computers such as the digital Vax, the Prime etc. made it possible for the engineers to use 2D FE analysis as part of their work, without necessarily relying on the support of FE specialists or large mainframe computers. During this period, some publications which introduced the use of vector and/or scalar potentials describing field quantities made some impact on spreading the technique to more complex 3D electromagnetic field problems. Particularly the publications of Simkin & Trowbridge [1.7] and Rodger [1.8], along with some other papers [1.9- 1.13] are important as far as the use of the magnetic scalar and vector potentials in this work is concerned. And also, the first FE text book dealing with only electrical engineering problems was

published in 1983 by Silvester & Ferrari [1.14].

The development of work-station computers in the early and mid 1980s such as the Apollo, the Sun and the Micro-Vax helped to promote further the use of FE applications with the cost per second of computing use decreasing at such a rapid rate that engineers were not restricted by computer costs. As a result of these improvements, today, some software companies and research groups have developed FE packages that leave engineers free to focus on design work instead of numerical algorithms.

The introduction of the FE method to moving conductor problems is quite new. There are not many publications available in this field. The analysis of characteristics of a linear induction tachometer published by Rodger and Eastham in 1985 may be the earliest appearance of the method in the 3D moving conductor eddy current problem [1.15]. The papers by Rodger, Karaguler, and Leonard in 1988 and 1989 are believed to be useful as reference publications in the field. As these papers [1.16] and [1.17] are outcome of this work, they are included in the thesis in appendix 1.1.

1.3 General Procedure of the Finite Element Method

The Finite element method, (FE), uses a selected approximation for the unknown variable of the field. Therefore it can be regarded as an example of trial function approximation methods. In the FE method, the domain is divided into subdomains which are basic elements, and the solution is approximated by a

polynomial over each element. The boundary conditions on the boundary between elements need to be defined suitably in order to match with the approximation. Each polynomial is specified by a number of coefficients or equivalently by values of the function and its derivatives at certain points. There is a certain pattern to apply the finite element to any kind of a physical problem. This can be listed as follows;

1) Creation of a FE mesh and subdivision of the mesh into elements which are connected at nodes.

2) Definition of the approximation equation.

3) Formation of the system of equations and description of boundary conditions.

4) Solution of the resulting set of simultaneous equations.

5) Calculation of the desired physical quantities.

1.3.1 Approximation by Trial Functions

As mentioned earlier, the essence of the FE method is to partition the domain of the problem into non-overlapping elements, and to provide an approximate solution that has a simple form within each element. The local representations are then patched together to form a global solution. Therefore the approximation of the problem is the initial step towards the solution. If the governing equation for any physical phenomenon is given as:

$$D(f(r)) = 0 \tag{1.1}$$

where **D()** symbolizes any differential equation, **f(r)** is the unknown quantity, and a function of the independent variables usually space **(x,y,z)** or/and time. The

approximate solution suggests that there is a **f(r)** function which is close to **f(r)** but not the same. The FE method obtains this **f(r)** approximate solution by using a procedure very similiar to the classical trial solution method.

The trial solution procedure is characterized by 3 operations; the first one is that construction of **f(r)**. This is done by constructing suitable trial functions which are generally simple and only functions of geometry so maybe conveniently calculated by computers. The trial solution **f(r)** is usually a finite sum of functions (in fact **f(r)** may consist of an infinite set of numbers but to solve a reasonable number of unknowns, some limitation is needed). This finite sum can be expressed as

$$f(r) = W_0(r) + a_1 W_1(r) + a_2 W_2(r) + \ldots\ldots + a_n W_n(r) \qquad (1.2)$$

or

$$f(r) = W_0(r) + \sum_{i=1}^{n} a_i W_i(r) \qquad (1.3)$$

The functions W_i are called trial functions or sometimes basis functions or more commonly shape functions as they are functions of geometry. The a_i are unknown parameters often called the degrees of freedom. In many cases these parameters represent the value of the function at certain nodes (nodal values) therefore they may be replaced with f_i in the equation. The term $W_o(r)$ is included only to represent the boundary equations. If these trial functions are constructed then all that remains to be done is to find the values of a_i which are only numbers. This will be the second phase of the trial solution method.

An optimising technique has to be applied in order to obtain the necessary set of equations that leads to finding the values of a_i parameters, thus the $\underline{f(r)}$ solution. This optimizing technique in fact originates from some of the general physical or mathematical principles. For instance the well known principle of minimum energy is the basis of the variational method (the minimum energy principle is mathematically equivalent to Laplace's equation) which is one of the most common methods used in the FE applications. The variational method seeks to minimize or find an extremum in some physical quantity, such as energy. It involves the integral of a function that produces a number. When the function produces the lowest number it approximately satisfies a specific differential equation that the function represents. Although the variational method is the basis for many finite element formulations, it has a major disadvantage of failing to solve any differential equation containing a first derivative term. An alternative technique, the weighted residual method, does not possess this drawback of the variational method. It can be applicable to almost any kind of differential equations. In this work, the weighted residual method from the Galerkin point of view is used. This will be examined in the following section.

The third operation is that of the estimation of the accuracy of the $\underline{f(r)}$ solution. In general, this is not an easy task as the exact correct answer is unknown. However it is possible to obtain a certain degree of accuracy. This can be achieved by just simply employing more trial functions or as it will be seen in the element technique, using finer subdivisions in the model. For this purpose, some self adaptive mesh generation techniques have been developed [1.18]. But eventually 'round off' error will effect the results and absolute accuracy can not be obtained on computers for the general case.

The summary of the trial solution procedure is illustrated as a block diagram in fig 1.1.

1.3.2 The Weighted Residual Method and the Galerkin Approach

The weighted residual method uses the residual function. The residual function in fact is an error term obtained from the substitution of the approximate trial solution **f(r)** in the differential equation. As, no matter how accurate the solution **f(r)** is, it is an approximation and will not be in general exact over the whole domain. Therefore, the replacement of **f(r)** with **f(r)** in equation (1.1) will always yield an error term that is named the residual function and is defined as:

$$D(f(r)) = R(r) \tag{1.4}$$

By using equation (1.3), the residue term can be rewritten as;

$$R(r) = D\left(\sum_{i=1}^{n} W_i(r)\, a_i + W_0\right) \tag{1.5}$$

The logic of the weighted residual method is quite simple. Any function that satisfies the differential equation over the entire domain, and the boundary conditions on the boundaries must also make the residual term **R(r)** zero and vice versa. If there is a **f(r)** which makes the residual term zero, this **f(r)** will be the required answer.

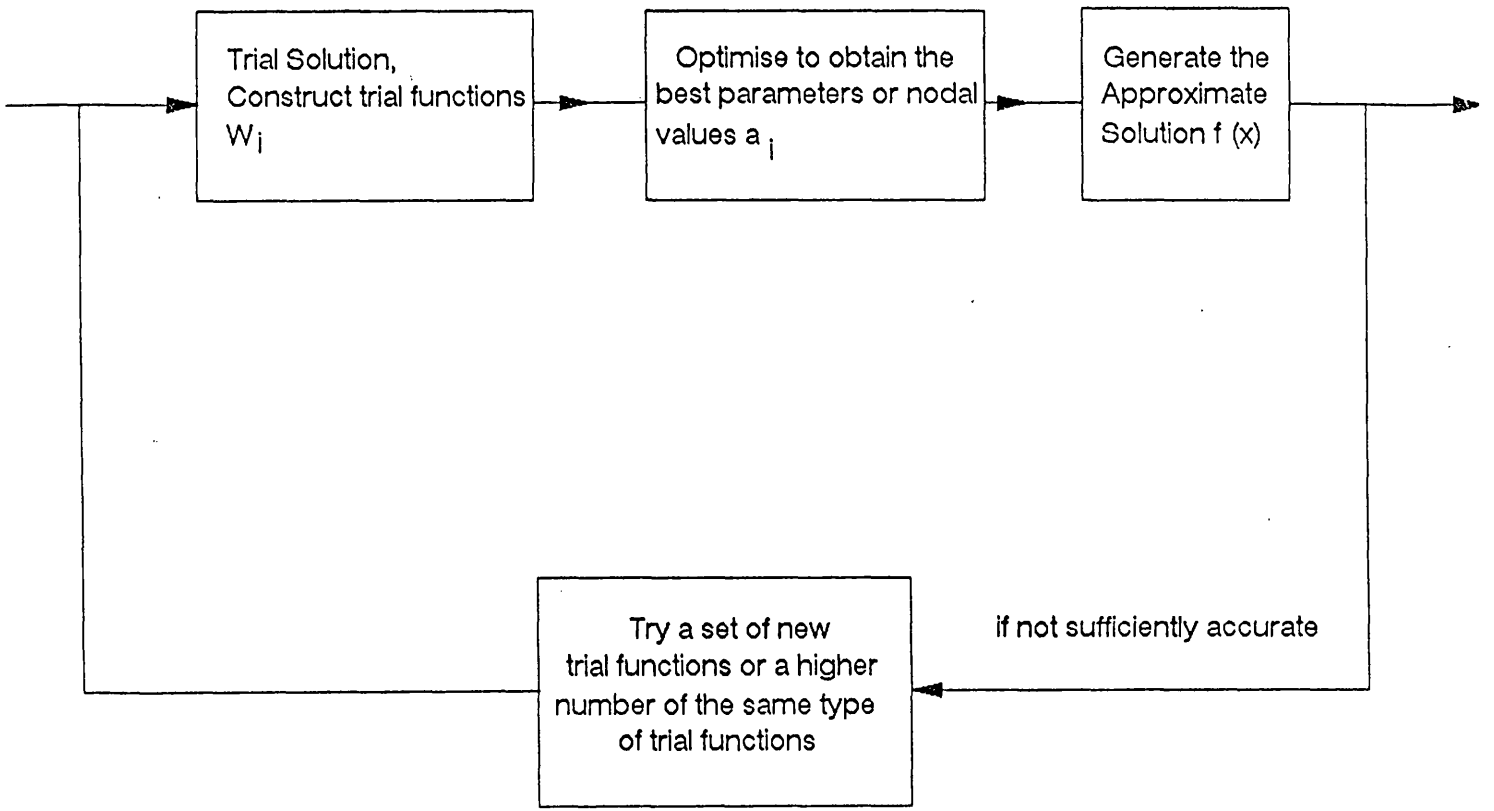

Fig 1.1 Block diagram of Trial function process

Considering the weighted integral (the residual **R(x)** is multiplied by a weighting function) of the residual over the entire domain, the general formula for the weighted residual method can be expressed as:

$$\int_v t_j(r)\, R(r)\, dv = 0 \tag{1.6}$$

and

$$\int_v t_j(r)\, D\,(\sum_{i=1}^{n} W_i(r)\, a_i + W_0)\, dv = 0 \tag{1.7}$$

The number of $\mathbf{t_j}$ (named weighting functions), equals the number of the parameters $\mathbf{a_i}$. Thus **n** equations are obtained to find the **n** unknown $\mathbf{a_i}$ values. At this point, there are several methods distinct from each other in selecting different weighting functions, which can be applied to eqn. (1.6) or (1.7) to find the parameters. For instance; the collocation method uses impulse functions as the weighting functions. The residual is required to vanish at specific points. The subdomain method uses **n** specific intervals, rather than points, where the residual is required to vanish. However, in the most FE applications, as well as in this work, the Galerkin method in which the weighting functions are the same as the trial or shape functions associated with each $\mathbf{a_i}$, is selected for the solution. The technique requires that the weighted average of the residual over the entire domain is zero. Therefore in equation (1.7), the replacement of $\mathbf{t_j}$ weighting functions with $\mathbf{W_j}$ shape functions yields the Galerkin form of FE equations. If this is carried out, equation (1.7) becomes as:

$$\int_v W_j(r)\, D\,(W_i(r) a_i + W_0)\, dv = 0 \tag{1.8}$$

The summary of these residual methods which using different weighting functions is given in table 1.1.

1.4 The Element Technique

So far, the trial solution has been defined over the whole domain regardless of the division into elements. This would be considered only for problems for which the solutions are very smooth and simple. However in many physical phenomena, the solutions are expected to be nonuniform. This is very common in electromagnetism For instance sudden jumps or 'bumps' can often be encountered in the flux distributions caused mainly by having regions with different permeabilities such as air and iron. In these circumstances very high order polynomials are required for the problem. But the desired accuracy may still be difficult to obtain. The problem can be tackled by using the element concept. Here, the shape functions are defined to be non zero only over small, finite regions in the domain, as opposed to being applied over the whole of the domain. These are called finite elements which must join together at certain points (nodes) but not overlap in the domain (Fig 1.2). Relatively larger elements are probably sufficient in areas where the field (or any kind of wanted quantity) does not vary rapidly and, usually where the jumps are expected in the solution, smaller elements are used. In fact, if required, the various combination of different types of elements and functional representations can be employed for the same solution domain.

The simplest element used in the F.E. applications is a line segment with a

METHODS	FORMULAS	DESCRIPTION
1) The Collocation Method	$R(x_1;a)=0$ $R(x_2;a)=0$ . . . $R(x_n;a)=0$	$x_1, x_2, \ldots, x_n$ are the points where the residuals are required to be zero.
2) The Subdomain Method	$\frac{1}{\Delta_{\Delta l_1}}\int_{\Delta l_1} R(r,a)dl=0$ $\frac{1}{\Delta_{\Delta l_2}}\int_{\Delta l_2} R(r,a)dl=0$ . . . $\frac{1}{\Delta_{\Delta l_n}}\int_{\Delta l_n} R(r,a)dl=0$	$\Delta l_1, \Delta l_2, \ldots, \Delta l_n$,are the intervals in which the average of the residuals are required to be zero.
3) The Least Square Method	$\frac{\partial}{\partial a_1}\int_V R^2(r,a)dV=0$ $\frac{\partial}{\partial a_1}\int_V R^2(r,a)dV=0$ . . . $\frac{\partial}{\partial a_1}\int_V R^2(r,a)dV=0$	The least mean square minimisation of the square of the residual over the entire domain with respect to each a_i
4) The Galerkin Method	$\int_V W_1 R(r,a)dV=0$ $\int_V W_2 R(r,a)dV=0$ . . . $\int_V W_n R(r,a)dV=0$	$W_1, W_2, \ldots, W_n$ are the shape functions.

Table 1.1 Some optimisation methods for FE

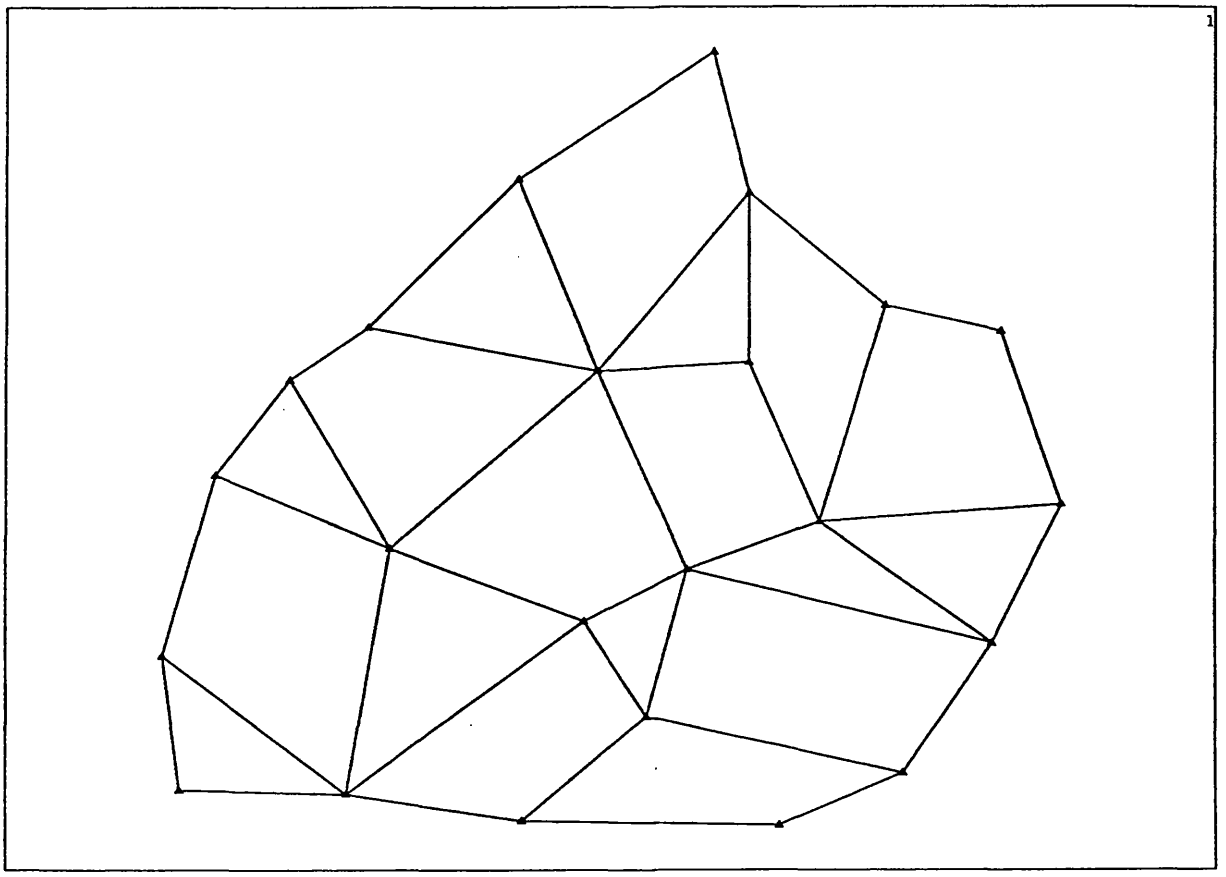

Fig. 1.2 A simple example of division of a domain by the element technique

length **L** and two nodes at each end shown as in figure (1.3a). A 1D linear function can be expressed as:

$$f(x) = a_1 + a_2 x \tag{1.9}$$

By using the nodal values of **f(x)**, the parameters, $\mathbf{a_1}$ and $\mathbf{a_2}$ can be found. If $\mathbf{f_i}$ and $\mathbf{f_j}$ are the values of function at the nodes i and j;

$$f_i = a_1 + a_2 X_i \tag{1.10}$$

$$f_j = a_1 + a_2 X_j \tag{1.11}$$

Then **f(x)** can be obtained by substituting $\mathbf{a_1}$ and $\mathbf{a_2}$ into equation (1.10).

$$f(x) = \frac{X_j - x}{X_j - X_i} f_i + \frac{x - X_i}{X_j - X_i} f_j \tag{1.12}$$

This is a standard form of FE equation in which the unknown field is represented as shape functions multiplied by the function values at the nodes of the element. Remembering the standard form in general as:

$$f(x) = W_i f_i + W_j f_j \tag{1.13}$$

(the $\mathbf{W_0}$ of eqn. (1.5) term is associated with the boundary conditions and is not included in FE as the bondary conditions are generally treated specially) the shape functions $\mathbf{W_i}$ and $\mathbf{W_j}$ can be written from (1.12) and (1.13)

$$W_i = \frac{X_j - x}{X_j - X_i} \quad and \quad W_j = \frac{x - X_i}{X_j - X_i} \tag{1.14}$$

The shape functions in equation (1.12) are evaluated by using the Cartesian

Coordinate System. However the Cartesian System has a disadvantage of involving complex calculations when determining an integral such as

$$\int_{x_i}^{x_j} W_i(x)\, W_j(x)\, dx$$

Nevertheless there are some alternative Coordinate systems which may give arise to some simplifications. For instance, the local Coordinate System whose origin is located on the element, will lead to obtaining the shape functions, refering to fig 1.3b as:

$$W_i(q) = \frac{1}{2} - \frac{q}{L} \quad and \quad W_j(q) = \frac{1}{2} + \frac{q}{L} \tag{1.15}$$

Further simplification in the integrations can be possible when the natural Coordinate System which is the most common one in the applications, is used. The natural system, is in fact, a local system represented by a dimensionless number whose absolute magnitude never exceeds unity. The shape functions for the system, refering to fig 1.3c are:

$$W_i(\xi) = \frac{1}{2}(1 - \xi) \quad and \quad W_j(\xi) = \frac{1}{2}(1 + \xi) \tag{1.16}$$

The advantage of the system is that any integration involving shape functions can be limited between -1 and +1. The integrals are therefore ideally suited to the Gaussian quadrature method which requires these limits.

A similar procedure can be applied to the other 1D, 2D and 3D elements to

obtain the shape functions. Some of these elements and their shape functions (mainly used in this work) in the natural Coordinate System are given in table 1.2.

When using the element technique, the polynomial trial solution is still in force but equation (1.7) will be rearranged into a special form which is a matrix form. The general matrix form is obtained by rearranging equation(1.7) such a way that $\mathbf{a}_i$ parameters (or $\mathbf{f}_i$ nodal variables) will constitute the unknown matrix. For instance, if the simplest element, 1D linear element (shown in fig. 1.4), is considered, the matrix form of equation (1.7) will be

$$\begin{bmatrix} K_{11} & K_{12} \\ K_{21} & K_{22} \end{bmatrix} \begin{bmatrix} a_1 \\ a_2 \end{bmatrix} = \begin{bmatrix} b_1 \\ b_2 \end{bmatrix} \tag{1.17}$$

where the $\mathbf{K}_{ij}$'s include only properties of the differential equation and geometric data. The $\mathbf{b}_i$'s form the RHS of the equation and carry information about the boundary conditions. If the same procedure is followed for two elements then the matrix form becomes

$$\begin{bmatrix} K_{11} & K_{12} & 0 & 0 \\ K_{21} & K_{22} & 0 & 0 \\ 0 & 0 & K_{33} & K_{34} \\ 0 & 0 & K_{43} & K_{44} \end{bmatrix} \begin{bmatrix} a_1 \\ a_2 \\ a_3 \\ a_4 \end{bmatrix} = \begin{bmatrix} b_1 \\ b_2 \\ b_3 \\ b_4 \end{bmatrix} \tag{1.18}$$

When the domain is divided into two (or more) elements, the problem of continuity of the solution at the interelement boundary points arise and introduces the concept of the interelement boundary conditions. These conditions can be satisfied,

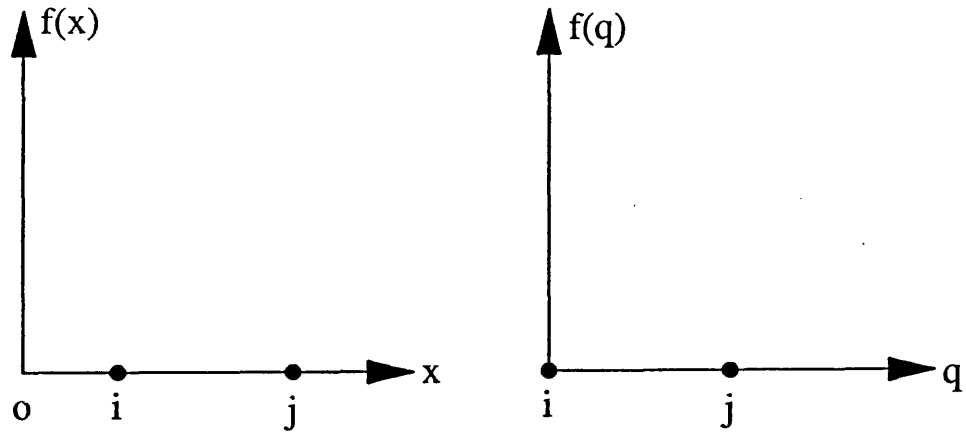

a) Cartesian coordinates b) Local coordinates

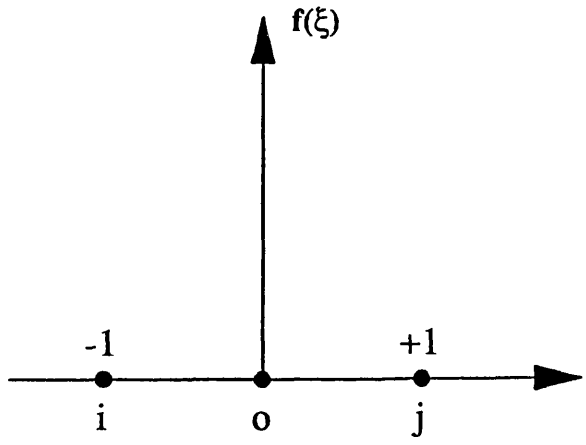

c) Natural coordinates

Fig. 1.3 Common types of coordinate systems used in FE applications

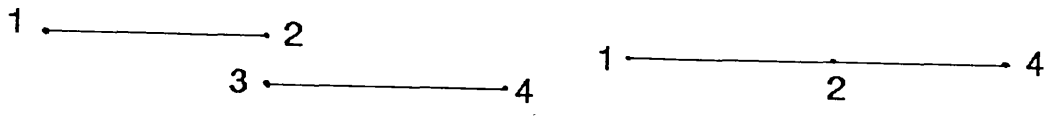

Fig. 1.4 Typical 2 1D elements and their assembly

ELEMENTS		SHAPE FUNCTIONS
1D Linear Element	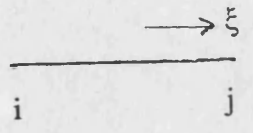	$W_i = \frac{1}{2}(1+\xi)$ $W_j = \frac{1}{2}(1-\xi)$
2D Linear Quadrilateral Element	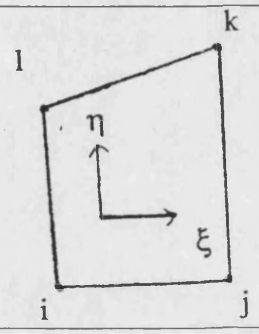	$W_i = \frac{1}{4}(1-\xi)(1-\eta)$ $W_j = \frac{1}{4}(1+\xi)(1-\eta)$ $W_k = \frac{1}{4}(1+\xi)(1+\eta)$ $W_l = \frac{1}{4}(1-\xi)(1+\eta)$
The Lagrangian Element	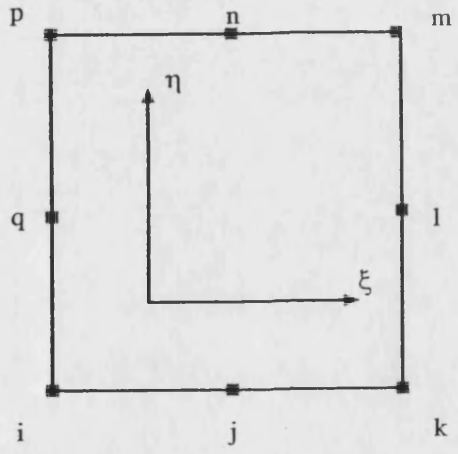	$W_i = \frac{\xi\eta}{4}(\xi-1)(\eta-1)$ $W_j = \frac{-\xi}{2}(\eta-1)(\xi^2-1)$ $W_k = \frac{\xi\eta}{4}(\xi+1)(\eta-1)$ $W_l = \frac{-\xi}{2}(\xi+1)(\eta^2-1)$ $W_m = \frac{\xi\eta}{4}(\xi+1)(\eta+1)$ $W_n = \frac{-\xi}{2}(\eta+1)(\xi^2-1)$ $W_p = \frac{\xi\eta}{4}(\xi-1)(\eta+1)$ $W_q = \frac{-\xi}{2}(\xi-1)(\eta^2-1)$ $W_r = (\xi^2-1)(\eta^2-1)$
Eight Node 3D Solid	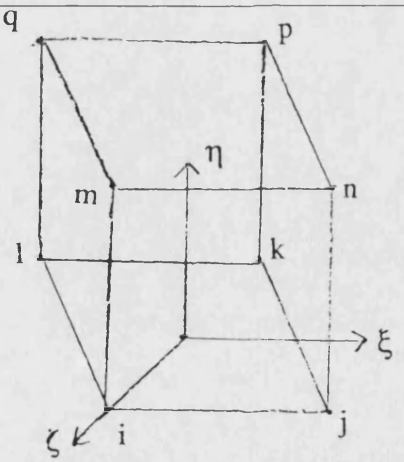	$W_i = \frac{1}{8}(1-\xi)(1-\eta)(1-\zeta)$ $W_j = \frac{1}{8}(1+\xi)(1-\eta)(1-\zeta)$ $W_k = \frac{1}{8}(1+\xi)(1+\eta)(1-\zeta)$ ⋮ ⋮ $W_p = \frac{1}{8}(1-\xi)(1+\eta)(1+\zeta)$

Table 1.2 Shape functions of some common types of Finite Elements

either naturally or essentially (weak form), depending on the differential equation and the property of the unknowns. A good example of this is illustrated in section 2.2.1. The division into elements will also introduce the concept of the assembly of element equations. Instead of considering all the elements of domain separately, the FE method in general combines the elements and eliminates some unknowns or nodal variables which are commonly shared by two or more elements. This also leads to the rearrangement of the 'stiffness matrix' [K]. For the example of two 1D linear elements referring to fig. 1.4, the matrix equation (1.9) will be transformed to

$$\begin{bmatrix} K_{11} & K_{12} & 0 \\ K_{21} & K_{22}+K_{33} & K_{34} \\ 0 & K_{43} & K_{44} \end{bmatrix} \begin{bmatrix} a_1 \\ a_2 \\ a_4 \end{bmatrix} = \begin{bmatrix} b_1 \\ b_2+b_3 \\ b_4 \end{bmatrix} \qquad (1.19)$$

As it can be seen from the rearranged matrix in equation (1.18) that the assembly procedure, in practice actually means adding some of the terms from one pair of element equations to some of the terms in the other pair of element equations. If the procedure is followed for all the elements in entire domain, then the final form of the matrices will be obtained.

The properties of the stiffness matrix are important in solving the equations. (The matrix [K] is usually referred to as the stiffness matrix, since the early applications of FE technique were mainly to structural engineering problems where the terminology is used). As predicted from (1.19), the final form of the [K] matrix obtained for all the elements is sparse (usually very sparse) and banded. A banded matrix has the characteristics that all of the nonzero coefficients are located relatively

close to the diagonal and all of the coefficients beyond the bandwidth are zero. This property should be considered when applying the numerical method for the solution.

In the following chapters, the element technique from the Galerkin point of view will be introduced to the electromagnetic field equations and the concept will be further examined.

CHAPTER 2

MOVING CONDUCTOR PROBLEMS AND THE FE APPROACH

2.1 Electromagnetic Field Equations

The electromagnetic field equations to which the FE method will be applied, can be derived from Maxwell's equations which are valid for all aspects of electromagnetic phenomena. The general form of these equations is as follows:

$$curl\bar{E} + \frac{\partial \bar{B}}{\partial t} = 0 \tag{2.1}$$

$$curl\bar{H} - \frac{\partial \bar{D}}{\partial t} = \bar{J} \tag{2.2}$$

$$div\bar{B}=0 \tag{2.3}$$

$$div\bar{D}=\rho \tag{2.4}$$

where $\bar{E}$ is the electric field intensity [Volt/m]

$\bar{D}$ is the electric flux density [Coulomb/m^2]

$\bar{B}$ is the magnetic flux density [Tesla]

$\bar{H}$ is the magnetic flux intensity [Amper/m]

$\bar{J}$ is the current density [Amper/m^2]

ρ is the volume charge density [Coulomb/m^3]

Since only DC or power frequency cases are being considered, the $\partial\bar{D}/\partial t$ term, which corresponds to displacement currents, can be ignored, and equation (2.2) will be used without this term throughout the rest of this work.

The constitutive equations are also needed together with Maxwell's equations. These are:

$$\bar{D}=\epsilon\bar{E} \tag{2.5}$$

$$\bar{B}=\mu\bar{H} \tag{2.6}$$

$$\bar{J}=\sigma\bar{E} \tag{2.7}$$

where ϵ is the permittivity [Farad/m], μ is the permeability [Henry/m] and σ is the conductivity [Siemen/m].

As far as the moving conductor problem is concerned, in the DC case, the moving region electric field has two components which are expressed in the equation below as:

$$\bar{E} = \bar{u}\times\bar{B} - gradV \tag{2.8}$$

With reference to fig (2.1), the first component on the RHS of equation (2.8) is due to the movement of a conductor with a speed $\bar{u}$ through a constant magnetic field $\bar{\mathbf{B}}$. When the conductor starts moving, a force which is described by the Lorentz law as $q\ (\bar{u}\times\bar{B})$ will act on each charge within the conductor and drive it towards the edges of the conductor. The total displaced charge generates an electrostatic field which opposes the

field produced by the motion. This electrostatic field is represented as $-gradV$ in (2.8) where V is the electric scalar potential.

2.1.1 Boundary Conditions

In order to solve any electromagnetic field problem; in addition to the field equations, the boundary conditions also need to be defined. These conditions describe the transitional properties of the field at a boundary between two different regions. Considering the field quantities $\bar{B}$, $\bar{H}$, $\bar{E}$, $\bar{D}$, the general boundary conditions, between two regions 1 and 2 as shown in fig 2.2, are

$$D_{n2}-D_{n1}=\rho_s \tag{2.9}$$

$$H_{t2}-H_{t1}=K_s \tag{2.10}$$

$$B_{n2}-B_{n1}=0 \tag{2.11}$$

$$E_{t2}-E_{t1}=0 \tag{2.12}$$

where **t** and **n** denote tangential and normal components of the field quantities, respectively. The equations above show that a discontinuity in the field quantities occurs when there are free surface charges or a line current density K_s at the boundary between the two regions.

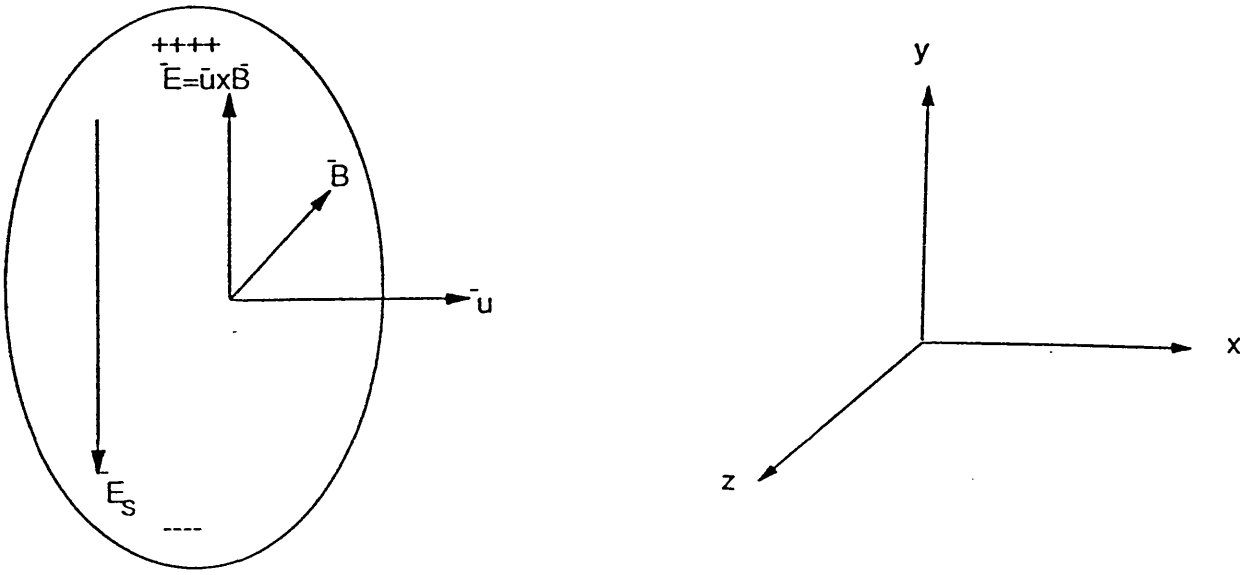

Fig. 2.1 Fields in a moving conductor

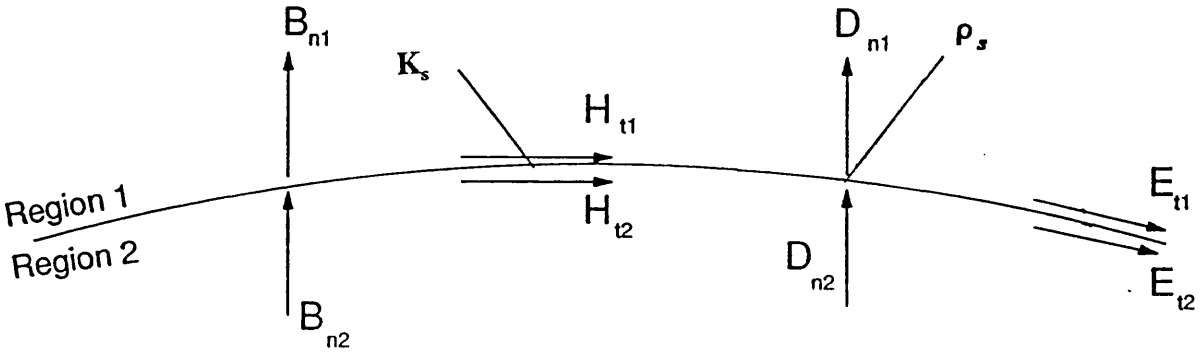

Fig. 2.2 The field components on the boundary between two regions

2.2 2D FE Analysis of Moving Conductor Problem

It is very common in electromagnetism to calculate the desired field quantities such as the $\bar{E}$ and $\bar{B}$ fields via vector and/or scalar potentials. This leads to a considerable simplification of the problem both conceptually and in computation. An example of this is the magnetic vector potential $\bar{A}$, which replaces the magnetic flux density $\bar{B}$ in the equations by a curl operator. This is the most prevailing choice for modelling 2D electromagnetic field problems. The magnetic vector potential vector is defined by

$$curl\bar{A}=\bar{B} \tag{2.13}$$

The first advantage of introducing $\bar{A}$ is that the transformation (2.13) automatically satisfies Maxwell's third equation: $div\bar{B}=0$, since the divergence of any curl function is zero. Secondly, in order to solve a 2D magnetostatic problem, in this cartesian coordinate system depicted in fig (2.1) in which H_z and B_z are zero (as there is no field variation in the z direction), the remaining two components of $\bar{B}$ or $\bar{H}$ must be determined at each node. However when using $\bar{A}$ in this 2D problem only A_z needs to be found. Additionally in the FE method, the interelement boundary conditions would be difficult to obtain if we solve $\bar{B}$ and $\bar{H}$ directly. Since $\bar{B}\cdot\bar{n}$ and $\bar{H}\times\bar{n}$ are required to be continuous on these boundaries, if the permeability of the material on either side of the boundaries is not the same, then $\bar{H}$ and $\bar{B}$ will be discontinuous. However $\bar{A}$ is always continuous and therefore formulating the problems in terms of the latter yields a straightforward procedure for the FE technique as far as the interelement boundary conditions are concerned. This point will be elaborated in detail in the following section when 2D FE equations for the moving

conductor problem are obtained.

In order to get the governing equation expressed by the magnetic vector potential $\bar{A}$ for the moving conductor problem (DC cases only), $\bar{H}$ and $\bar{J}$ in equation (2.2) are replaced with their equivalents in equations (2.6) and (2.7). This together with the substitution $\gamma=1/\mu$ gives

$$Curl\gamma\bar{B}=\sigma\bar{E} \tag{2.14}$$

Substituting the expression (2.13) for $\bar{B}$ and the expression (2.8) for $\bar{E}$ into (2.14) then gives

$$curl\gamma curl\bar{A}=\sigma\ (\bar{u}\times curl\bar{A}-gradV) \tag{2.15}$$

Using the following identity for the curl operator:

$$curl\gamma curl\bar{A}=grad\gamma\ div\bar{A}-div\ \gamma\ grad\bar{A} \tag{2.16}$$

The equation below is obtained.

$$grad\gamma\ div\bar{A}-div\ \gamma\ grad\bar{A}\ =\ \sigma(\bar{u}\times curl\bar{A}\ -\ gradV) \tag{2.17}$$

According to the Helmholtz theorem, any single-valued vector point function that together with its derivatives is finite and continuous can be expressed in terms of a scalar potential and a vector potential taken together. In general terms, a conservative field such as the electric field $\bar{E}$ (in electrostatics) can be expressed as the gradient of a scalar potential as ($\bar{F}=-grad\,\phi$). As the conservative fields are irrotational, the curl product of the conservative field will be zero ($curl\bar{F}=0$). However, the divergence of such field will

be the source term. If the field is nonconservative, such as the magnetic flux density, it will be specified by its curl sources, and the divergence of such field will be zero. Therefore divergence and curl sources are independent of each other, and a general vector field can only be specified, when both types of source are specified. In terms of using the magnetic vector potential, $\bar{A}$, this implies that $curl\bar{A}=\bar{B}$ will not be sufficient to define $\bar{A}$ uniquely (the proof of the uniqueness theorem is given in reference [2.1]). Therefore $div\bar{A}$ must also be specified for an unique solution. The specification of $div\bar{A}$ can be arbitrary. The most common formulation encountered is the Coulomb Gauge which sets $div\bar{A}$ to zero. As it will be explained in the 3D application, this constraint on $div\bar{A}$ is normally imposed by means of a number of well known methods. This brings about some computational convenience in the solution procedure. However in the 2D application $\bar{J}$ and $\bar{A}$ have only longitudinal component, that is $J_x=J_y=0$ and $A_x=A_y=0$ with respect to the coordinate system depicted in fig 2.1, $\bar{A}$, $\bar{J}$ and thus $\bar{E}$, are all z-directed and there is no variation of the fields and currents in the z-direction (they can be represented by only their z components in the formulas). This can lead to simplification of equation (2.17) by specifying $div\bar{A}$ and $gradV$ implicitly to be zero. Substituting $div\bar{A}$ and $gradV$ with zero, and dropping the z subscript from $\bar{A}$, yields

$$-div\ \gamma\ grad\bar{A}=\sigma(\bar{u}\times curl\bar{A}) \tag{2.18}$$

On the other hand, for a general representation of the current in the formula if the source term $\bar{J}_s$ is added in equation (2.18), then the governing equation for general 2D problems at zero frequencies can be obtained as

$$-div\ \gamma\ gradAbax\sigma(\bar{u}\times cur\bar{l}x)\ +\ \bar{J}_s$$

If the problem involves motion in the x-direction only, equation (2.19) becomes

$$-div\,\gamma\,gradA = -\sigma(u_x\frac{\partial A}{\partial x}) + J_s \tag{2.20}$$

2.2.1 Formation of the 2D FE Galerkin Equations

The weighted residual technique in the Galerkin Method is applied to equation (2.20) in order to yield the FE equations. The weighted form of the governing equation (2.20) is explained in the first chapter and can be stated as

$$\int_s t_j[-div\gamma\,gradA + \sigma(u_x\frac{\partial A}{\partial x}) - J_s]\,ds = 0 \tag{2.21}$$

According to the FE procedure A is approximated over a 2D element by

$$A=\sum_{i=1}^{k} W_i\,A_i \tag{2.22}$$

where A_i denotes the potential values at the nodes of the element, W denotes the basis or shape functions of the chosen element and k represents the number of the total nodes of the element. By using the approximation equation (2.22) in the weighted equation and applying integration by parts (see appendix 2.1) to the second order terms of the governing equation, we obtain

$$\sum_{i=1}^{k}\left\{\int_s\left[\frac{\partial t_j}{\partial x}\,\gamma\,\frac{\partial W_i}{\partial x} + \frac{\partial t_j}{\partial y}\,\gamma\,\frac{\partial W_i}{\partial y}\right]A_i\,ds + \sigma u_x\int_s t_j\frac{\partial W_i}{\partial x}A_i\,ds\right.$$
$$\left.-\int_s t_j J_s\,ds - \oint_c t_j(\frac{\partial A}{\partial n})\,dc\right\}=0 \tag{2.23}$$

By the Galerkin Method, the shape function W is selected as the weighting function therefore equation (2.23) can be rewritten as:

$$\sum_{i=1}^{k} \left\{ \int_{s} \left[\frac{\partial W_j}{\partial x} \gamma \frac{\partial W_i}{\partial x} + \frac{\partial W_j}{\partial y} \gamma \frac{\partial W_i}{\partial y} + \sigma u_x W_j \frac{\partial W_i}{\partial x} \right] A_i \, ds \right.$$

$$\left. - \int_{s} W_j J_s \, ds - \oint_{c} W_j \left(\frac{\partial A}{\partial n}\right) dc \right\} = 0 \qquad (2.24)$$

The procedure is carried out for all the nodes until **j** is the maximum number of nodes.

The line integral term in both equations (2.23) and (2.24) is important in the application of the FE technique. When using $\bar{A}$, the boundary condition (equation 2.12) can be automatically but weakly satisfied at a boundary between two elements by simply missing out the line integral term from the formula. This operation is correct as long as the elements are not on the outer boundaries. Because, inside the domain, two elements will have a commonly shared edge, and on this edge, they will have oppositely directed outward normal unit vectors shown in fig 2.3. Therefore, when considering the integration over the entire domain, the line integral terms will cancel out each other. This process is very significant and reduces the great amount of work involved in solving the field problems.

2.2.2 The Boundary Conditions With Magnetic Vector Potential

In the application, the interelement boundary conditions can be satisfied by dropping the line integral term from the FE equation. The only remaining part to

complete the 2D FE transformation from the partial differential equation is that of specifying $\bar{A}$ at the outer or peripheral boundaries of the geometry. There are two common cases that may be experienced in the magnetic field analysis. Either, the flux lines are assumed to cross the boundary at right angles, or the boundary itself is a flux line. In terms of $\bar{A}$, the first case is obtained using the homogeneous Neumann condition which sets the normal derivative of $\bar{A}$ to zero. This corresponds to an assumption that the model includes infinitely high permeable iron surroundings. The Neumann condition can be easily implemented by missing out the line integral term from equation (2.24) for the peripheral boundary. The second case is named Dirichlet Condition and may be obtained by imposing fixed values on the matrix.

2.3 3D FE Analysis of Moving Conductor Problem

1D or 2D techniques may produce good results for many engineering problems by means of taking some calculated or experimentally found coefficients into account. However, there is always a need for realistic 3D modelling techniques for exact representation of geometrically complex problems.

Compared with 2D, the number of unknowns that have to be solved in a 3D FE problem increases sharply. The well known 3D elements such as rectangular bricks or triangular prism, involve a higher number of vertices than 2D ones. And also the addition of 2 components of $\bar{A}$ in the 3D solution will escalate the increase even further. Not only because of the increase in number of unknowns, but as a whole, the application of the

3D FE procedure in general is a very expensive computational process. In order to reduce the cost, an alternative technique which does not need $\bar{A}$ everywhere in the model would be preferable. The alternative technique would replace $\bar{A}$ with scalar potential or potentials which have only a single value to be found at each point in space. Despite the fact that the introduction of new potentials in the modelling will cause discontinuity of potentials when determining the field at the boundaries between the regions, this replacement of scalar potentials is still worth doing as far as computing time and computer storage capacity are concerned.

The $\bar{A}$-ϕ technique detailed in ref. [1.7] and [1.8] is believed appropriate to the problems of this work. The technique uses $\bar{A}$ in only conducting regions, whereas non-conducting regions can be modelled by means of magnetic scalar potentials. The total scalar potential is useful only for regions not involving any source currents where $\mathbf{J}_s$ and therefore $\mathbf{curlH}_s$ is zero. It is well known that any curl operator of the gradient of a scalar function is zero, thus **H** can be expressed as the gradient of a scalar function

$$\bar{H} = -grad\phi_T \tag{2.25}$$

If the region has some source currents whose field is represented as $curl\bar{H}_s = \bar{J}_s$, hence $Curl(\bar{H}-\bar{H}_s)$ will be zero, $\bar{H}-\bar{H}_s$ can be equated to the gradient of a scalar function, that is called the reduced scalar potential as the field is reduced by the source field. It is described in the formula below as:

$$\bar{H}_R = \bar{H}-\bar{H}_s = -grad\phi_R \tag{2.26}$$

2.3.1 General 3D and the Field Equations

Only one governing equation for the entire model was used in the 2D problem. In the 3D application, the geometry is partitioned into 3 separate regions which are modelled by means of different kinds of potential hence the governing equations need to be developed independently for each region of the partitioned model shown in fig. 2.4.

The field equations for region 1 where, the source currents exist but eddy currents do not, are obtained in terms of the Reduced Scalar Potential ϕ_R. By using equations (2.3),(2.6), and (2.26), the field or governing equation for the region 1 is derived as:

$$div\mu_1\bar{H}_s - div\mu_1\, grad\phi_R=0 \tag{2.27}$$

In the equation above, $\bar{H}_s$ is specified by the Biot Savart law as

$$\bar{H}_s=\frac{1}{4\pi}\int_{v_1}\frac{\bar{J}_s\times(\bar{r}-\bar{r}')}{|\bar{r}-\bar{r}'|^3} \tag{2.28}$$

where $\bar{r}$ and $\bar{r}'$ are the position vectors of the field point and source point respectively.

Region 2 contains neither source currents nor eddy currents. There might be a ferro magnetic material in the region whose relative permeability is much greater than one. If the region was modelled by means of the reduced scalar potential, the source and the magnetization field intensities would be nearly equal and opposite valued and will almost cancel each other. Therefore, as pointed out in reference [1.7], possible numerical difficulties might arise in the solution. The exclusion of iron or any kind of high permeable material from region 1 may be the simplest arrangement to prevent the possible inaccuracy. So the governing equation for the region can be obtained from

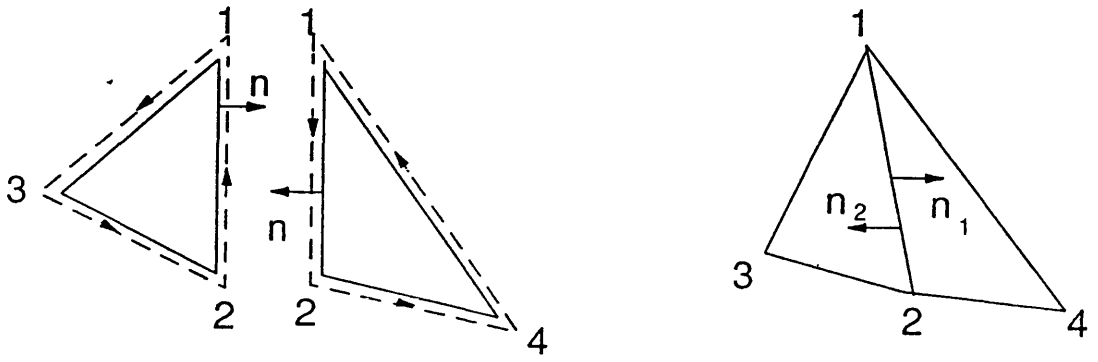

Fig. 2.3 Interelement boundary between two elements

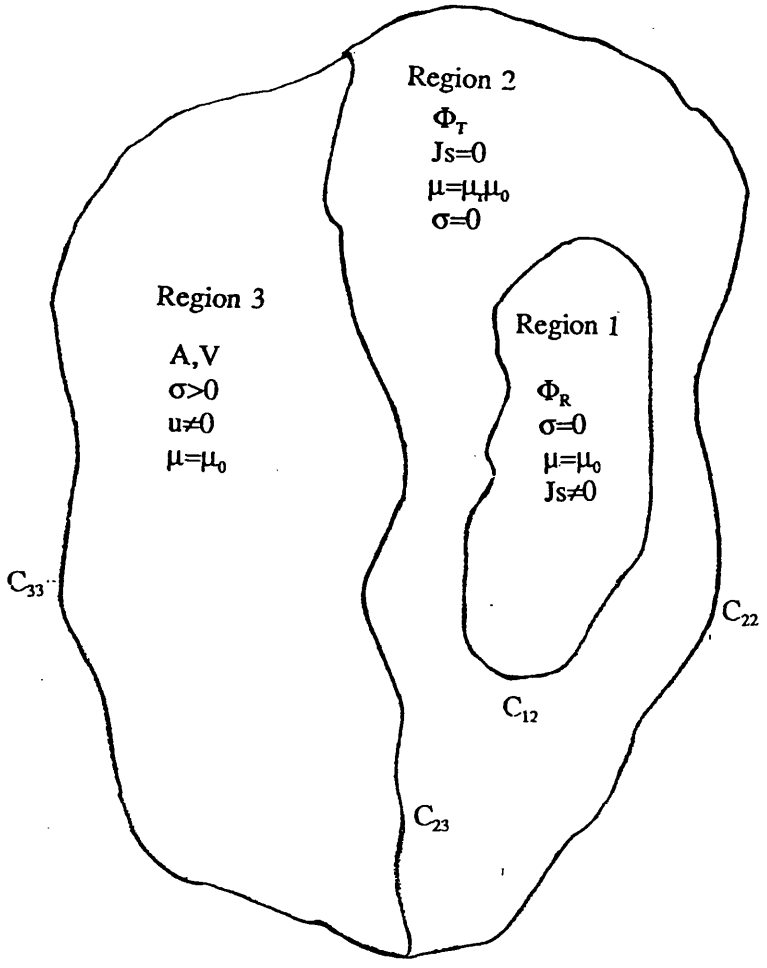

Fig. 2.4 General 3D FE partition of the model for moving conductor problem

(2.3), (2.7) and (2.25) as

$$div\mu_2\ grad\phi_T = 0 \tag{2.29}$$

Region 3 includes only eddy currents hence it is often named as the eddy or conducting region. An eddy current is produced by an electric field acting in conjunction with conductivity. As it was described earlier, the electric field results from the motion of a conductor through a magnetic field. On the other hand, the time variation of the magnetic flux density also produces an electric field which has been excluded from the formulas, as presently only DC problems are concerned. However, the effect of the time variation of the field will be included later when an AC problem is studied in chapter 5.

Hence the problem is 3D, removal of $gradV$ from the formula is not appropriate (a method which does not need V to be used as an unknown is introduced in chapter 4). If $gradV$ is removed without rearrangement of the formula the $\bar{u}\times Curl\bar{A}$ term would define all the components of the eddy currents induced on the conductor. This implies that the current component on the conductor that is parallel to the direction of the motion is zero which may not be the case. So that, with the inclusion of $gradV$, the governing equation to be solved for the region, should be as;

$$curl\,\gamma\, curl\bar{A} = \sigma\,[\bar{u}\times curl\bar{A} - gradV] \tag{2.30}$$

And $div\bar{J}=0$ is also used together with the equation above for the solution. By using the definition of $\bar{J}$ in equation (2.7) and equation (2.8), $div\bar{J}=0$ will yield:

$$div\,\sigma\,(\bar{u}\times curl\bar{A} - gradV) = 0 \tag{2.31}$$

Equation (2.30) comprises 4 unknowns and 3 equations. So that clearly another equation

is necessary for an unique solution. But equation (2.31) does not actually introduce any new information to equation (2.30) as it is obtained from $div\bar{J}=0$ which can be automatically satisfied when applying the div operator to both sides of equation (2.30). Nevertheless the necessary fourth equation can be supplied from the specification of $div\bar{A}$. Incidentally, this will also ensure the uniqueness of the solution with the condition of $\bar{A}\cdot\bar{n}=0$ on the boundary surface (more detail about uniqueness theorem is given in ref.[2.1]) The Lorentz gauge is also widely encountered particularly, in the applications where high frequencies are involved. The Lorentz gauge sets $div\bar{A}$ to $\frac{1}{\mu\epsilon}\frac{\partial V}{\partial t}$.

The Coulomb gauge is most commonly imposed rather than being taken as a separate set of equations along with the governing equations. This is mainly due to having a better shaped element matrix therefore convenience in the solution. The advantage of imposing $div\bar{A}$ will be conspicuous when 3D FE equations are derived in the next section. The enforcement of the Coulomb gauge can be carried out by means of several methods such as the Lagrangian multipliers, the penalty technique etc. In the Lagrangian method, the constraints $div\bar{A}=0$ is multiplied by the Lagrangian multiplier and added to the governing equation. The multiplier is treated as actual degrees of freedom for the new equation which includes the multiplied constraints term. The disadvantage of the method is that it introduces new additional unknowns to be found, and removes a number of degrees of freedom from the original set of equations, which depends on the number of multipliers. An example with the Lagrangian method is explained in reference [1.8]. However, the penalty technique used here, does not possess the drawback of the Lagrangian multiplier method which increases the total number of unknowns. This is an

important reason why the penalty technique is picked in this application. The penalty method adds the term $\alpha_p \, div\bar{N} \, div\bar{A}$ to the usual Galerkin form which will be obtained in the next section, and satisfies the constraints approximately, α_p is the penalty number. Because the solution satisfies the constraints approximately, the larger the value of α_p the better will be the constraint. This is well documented in reference [1.4]. On the other hand the addition of a new penalty term which is $grad1/\mu_0 \, div\bar{A}$ to the governing equation (2.33) will produce exactly similar results if $1/\mu_0$ is equal to α_p [2.2].

2.3.2 Application of Boundary Conditions

The general model for a 3D problem denoted in fig 2.4 introduces 2 interface and 2 outer boundaries. At the interface C_{12}, between two scalar regions, two well known boundary conditions, B_n and H_t continuous, (equations (2.11) and (2.12)), should be expressed in the scalar potentials. Then the conditions are rewritten as:

$$-\mu_1 \frac{\partial \phi_R}{\partial n} + \mu_1 H_{sn} = -\mu_2 \frac{\partial \phi_T}{\partial n} \tag{2.32}$$

$$-\frac{\partial \phi_R}{\partial t} + H_{st} = -\frac{\partial \phi_T}{\partial t} \tag{2.33}$$

H_{sn} and H_{st} are the normal and tangential components of the source current field given in equation(2.28).

The second interface boundary is between region 2 and region 3. The boundary conditions should include $\bar{J}\cdot\bar{n}=0$ and $\bar{A}\cdot\bar{n}=0$ on the conductor surface, as well as conditions

(2.11) and (2.12). $\bar{J}\cdot\bar{n}=0$ automatically satisfies the condition of $\bar{E}\cdot\bar{n}=0$ and, $\bar{A}\cdot\bar{n}=0$ is needed for the condition $div\bar{A}=0$. All these conditions can be expressed in terms of the vector and scalar potentials as follows

$$-\bar{n}\cdot\mu_2 grad\phi_T=\bar{n}\cdot curl\bar{A} \tag{2.34}$$

$$-\bar{n}\times grad\phi_T=\bar{u}\times\gamma_3 curl\bar{A} \tag{2.35}$$

$$\bar{A}.\bar{n}=0 \tag{2.36}$$

$$\bar{n}\cdot\sigma(\bar{u}\times curl\bar{A}-gradV) = 0 \tag{2.37}$$

On the outer boundaries C_{22} and C_{33} a suitable choice of the Dirichlet or Neumann type or mixed conditions are applied depending on the potential which models the region.

2.3.3 Formation of the 3D FE Galerkin Equations

As the model consists of 3 regions the derivation of 3D FE equations from the governing equations should be carried out independently for each region. The procedure is similar to the 2D application. Naturally the elements for the approximation will be selected from the family of 3D standard elements.

Region 1: The reduced scalar region is represented by equation (2.27). However as ferro magnetic materials are excluded from the region (in a region of constant permeability or free space, $div\bar{B}$ and $div\bar{H}$ are both zero.) the first term of the equation can be

omitted, and if the weighted residual technique is applied, the residue term will be ;

$$R_1=\int_{v_1} t_j \ (div\mu_1 \ grad\phi_R \ ) \ dv \ = \ 0 \tag{2.38}$$

in order not to have the second order derivatives, by the Green's theorem, equation (2.38) becomes;

$$\int_{v_1} gradt_j \ \mu_1 grad\phi_R \ dv - \oint_s t_j \mu_1 \frac{\partial \phi_R}{\partial n} \ ds \ = \ 0 \tag{2.39}$$

ϕ_R can be approximated at each node of finite elements by means of:

$$\phi_R=\sum_{i=1}^{k} W_i \ \phi_{Ri} \tag{2.40}$$

where W_i are the shape functions of a standard 3D element, and k is the number of nodes representing the element. On the other hand as shown in ref. [1.7], the surface terms are only needed on the boundary as the element technique gives a way to the elimination of them by means of opposite directed normal unit vectors of two adjacent elements when the integration is implemented. The replacement of t_j with W_j shapes function as usual in the Galerkin method yields;

$$\int_{v_1} \sum_{i=1}^{k} \left(\frac{\partial W_j}{\partial x} \ \mu_1 \ \frac{\partial W_i}{\partial x} + \frac{\partial W_j}{\partial y} \ \mu_1 \ \frac{\partial W_i}{\partial y} + \frac{\partial W_j}{\partial z} \ \mu_1 \ \frac{\partial W_i}{\partial z} \right) \phi_{Ri} \ dv = 0 \tag{2.41}$$

This formula without the surface integral term is valid everywhere in the region except the common boundary with the region 2.

Region 2 : The same procedure is adopted for region 2. The approximation of ϕ_T by

$$\phi_T = \sum_{i=1}^{k} W_i \, \phi_{Ti} \tag{2.42}$$

is applied, and using Galerkin and Green's theorem, the set of FE equations can be obtained as ;

$$\int_{v_2} \sum_{i=1}^{k} \left(\frac{\partial W_j}{\partial x} \mu_2 \frac{\partial W_i}{\partial x} + \frac{\partial W_j}{\partial y} \mu_2 \frac{\partial W_i}{\partial y} + \frac{\partial W_j}{\partial z} \mu_2 \frac{\partial W_i}{\partial z} \right) \phi_{Ti} \, dv = 0 \tag{2.43}$$

On the boundary between two scalar regions, there is more numerical exercise needed. As the regions are modelled by different potentials, the surface integral terms can not be simply missed out on the common boundary. However these integrals can be used to apply the boundary conditions. For the elements sharing a common boundary side in fig 2.5 by using equation (2.32) together with the surface terms in equations (2.41) and (2.43), the continuity of B_n yields

$$\int_{S_{12}} \mu_1 \left(\frac{\partial H_{sn}}{\partial n} - W_j \frac{\partial \phi_R}{\partial n} \right) ds - \int_{S_{12}} \mu_2 \, W_j \frac{\partial \phi_T}{\partial n} \, ds = 0 \tag{2.44}$$

The equation above, and side by side summation of (2.41) and (2.43) will result with an equation expressed in the implicit form as

$$\int_{v_1} \mu_1 \, gradW_j \, gradW_i \, \phi_R \, dv + \int_{v_2} \mu_2 \, gradW_j \, gradW_i \, \phi_T \, dv = \int_{S_{12}} \mu_1 H_{sn} \, ds \tag{2.45}$$

Another set of equations required, as equation (2.45) involves two unknowns. One unknown can be eliminated by using the second boundary condition expressed with equation (2.33). By describing a reference point q ,at which the potentials are zero, the

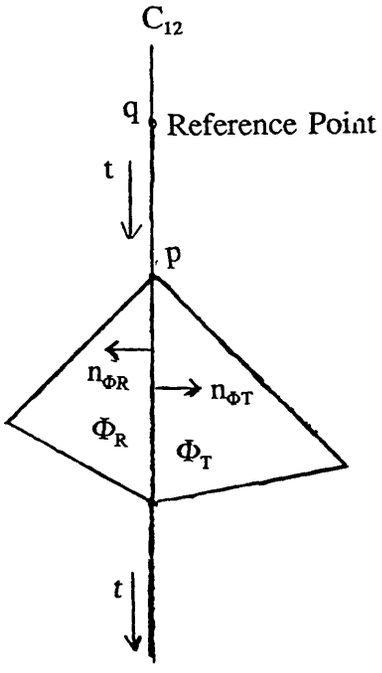

Fig. 2.5 The Interface boundary between two scalar potential regions

boundary equation (2.33) can be rewritten as

$$\phi_{R_p}=\phi_{T_p}+\int_q^p H_s\, dt \tag{2.46}$$

The substitution of (2.46) in (2.45) will eliminate one of the unknown scalar potentials, and ultimately define the final form of the boundary equation.

Region 3 : As the region is modelled by the vector potential $\bar{A}$, the shape function needs to be a vector as well.

$$\bar{W}_i = W_{xi}\,\bar{e}_x + W_{yi}\,\bar{e}_y + W_{zi}\,\bar{e}_z \tag{2.47}$$

The application of the FE procedure and the Galerkin technique to equation (2.30) results in ;

$$\begin{aligned}\int_{v_3} [curl\bar{W}_j\ \gamma curl\bar{A} + \bar{W}_j\sigma(\bar{u}\times curl\bar{A} - gradV)]\, dv \\ -\oint_{s_3} \bar{W}_j\ (\gamma\, curl\bar{A}\times\bar{n})\ ds=0\end{aligned} \tag{2.48}$$

In order to impose $div\bar{A}=0$ by a penalty method the penalty term $\int_{v_3}\alpha_p\, div\bar{W}\, div\bar{A}\, dv$ is added to equation (2.45) where α_p is a large number, and is often of the same order as $1/\mu_0$. The additional term gives ;

$$\begin{aligned}\int_{v_3} \left[\ curl\bar{W}_j\ \gamma curl\bar{A} + \alpha_p div\bar{W}_j\ div\bar{A} + \bar{W}_j\ \sigma\ (\bar{u}\times curl\bar{A} - gradV)\right] dv \\ -\oint_{s_3} \bar{W}_j\ (\gamma Curl\bar{A}\times\bar{n})\ ds\ =\ 0\end{aligned} \tag{2.49}$$

The second set of equations resulting from $div\bar{J}=0$, are derived by using the shape function and Green's theorem

$$\int_{v_3} W_j \, div\bar{J} \, dv = \int_{v_3} grad W_j \, \bar{J} \, dv - \oint_{s_3} W_j \, \bar{J}\cdot\bar{n} \, ds = 0 \tag{2.50}$$

$$\begin{aligned} &\int_{v_3} grad W_j \; \sigma(\bar{u}\times Curl\bar{A} - gradV) \, dv \\ &- \oint_{s_3} W_j \; \sigma(\bar{u}\times Curl\bar{A} - gradV) \cdot \bar{n} \, ds = 0 \end{aligned} \tag{2.51}$$

The surface integral term is important as it yields $\bar{J}\cdot\bar{n}=0$ as the natural boundary condition on the inside of the conducting region.

The field quantities $\bar{A}$ and V are approximated and replaced in equations (2.48) and (2.49) by:

$$\bar{A}=\sum_{i=1}^{k} \bar{W}_i A_i \tag{2.52}$$

$$V=\sum_{i=1}^{k} W_i \, V_i \tag{2.53}$$

where $\bar{A}$ is either A_x or A_y or A_z, and $\bar{W}_i$ is either W_{xi} or W_{yi} or W_{zi}. For simplicity in many cases $W_x=W_y=W_z=W$.

When considering only x-directed motion, the approximations of $\bar{A}$ and V by (2.52) and (2.53), then all the 3D FE equations can be obtained. Ignoring the surface integral terms, these equations are listed as below;

$$\int_{v_3} \sum_{i=1}^{k} \left\{ \frac{\partial W_j}{\partial z} \gamma \left[\frac{\partial W}{\partial z} A_{xi} - \frac{\partial W}{\partial x} A_{zi} \right] - \frac{\partial W_j}{\partial y} \gamma \left[\frac{\partial W}{\partial x} A_{yi} - \frac{\partial W}{\partial y} A_{xi} \right] + \alpha_p \frac{\partial W_j}{\partial x} \frac{\partial W}{\partial x} A_{xi} \right\} dv = 0 \tag{2.54}$$

$$\int_{v_3} \sum_{i=1}^{k} \left\{ \frac{\partial W_j}{\partial x} \gamma \left[\frac{\partial W}{\partial x} A_{yi} - \frac{\partial W}{\partial y} A_{xi} \right] - \frac{\partial W_j}{\partial z} \gamma \left[\frac{\partial W}{\partial y} A_{zi} - \frac{\partial W}{\partial z} A_{yi} \right] + \alpha_p \frac{\partial W_j}{\partial y} \frac{\partial W}{\partial y} A_{yi} + W_j \sigma \left[-u_x \left(\frac{\partial W}{\partial x} A_{yi} - \frac{\partial W}{\partial y} A_{xi} \right) - \frac{\partial W}{\partial y} V_i \right] \right\} dv = 0 \tag{2.55}$$

$$\int_{v_3} \sum_{i=1}^{k} \left\{ \frac{\partial W_j}{\partial y} \gamma \left[\frac{\partial W}{\partial y} A_{zi} - \frac{\partial W}{\partial z} A_{yi} \right] - \frac{\partial W_j}{\partial x} \gamma \left[\frac{\partial W}{\partial z} A_{xi} - \frac{\partial W}{\partial x} A_{zi} \right] + \alpha_p \frac{\partial W_j}{\partial z} \frac{\partial W}{\partial z} A_{zi} + W_j \sigma \left[u_x \left(\frac{\partial W}{\partial z} A_{xi} - \frac{\partial W}{\partial x} A_{zi} \right) - \frac{\partial W}{\partial z} V_i \right] \right\} dv = 0 \tag{2.56}$$

$$\int_{v_3} \sum_{i=1}^{k} \frac{\partial W_j}{\partial y} \left\{ \left[-u_x \left(\frac{\partial W}{\partial x} A_{yi} - \frac{\partial W}{\partial y} A_{xi} \right) - \frac{\partial W}{\partial y} V_i \right] + \frac{\partial W_j}{\partial z} \left[u_x \left(\frac{\partial W}{\partial z} A_{xi} - \frac{\partial W}{\partial x} A_{zi} \right) - \frac{\partial W}{\partial z} V_i \right] \right\} dv = 0 \tag{2.57}$$

Finally the evaluation of 3D boundary equations (2.34) - (2.37) on the boundary, with the scalar region by means of the approximate functions will deliver all the necessary 3D FE equations. The implementation is rather simple. For the boundary S_{23} the surface term in (2.49) can be replaced, according to the boundary equation 2.36, by

$$\int_{s_{23}} \bar{W}_j \gamma \, (\bar{u} \times curl\bar{A} - gradV) \times \bar{n} \, ds = \int_{S_{23}} W_j \, (grad\phi_T \times \bar{n}) \, ds \tag{2.58}$$

Similarly, replacing the surface integral term in equation (2.43) by using (2.34), which expresses the continuity of B_n, will ensure all the boundary conditions.

$$\int_{S_{23}} W_j \mu_2 \frac{\partial \phi_T}{\partial n} \, dS = \int_{S_{23}} W_j \, curl\bar{A} \cdot \bar{n} \, dS \qquad (2.59)$$

2.4 The Solution of the FE Equations

The final step of the technique is that to find a way of solving a number of equations which are normally expressed in a matrix form as **[K]*[a]=[b]**. In general, the number of unknowns involved in a FE problem can be high, from 1000 unknowns for a moderate problem up to 100000 for a complex geometry. This is why the effectiveness of the chosen method is significant.

Commonly the FE method yields K matrices which have a great deal of zero entries, 'sparse matrices'. This is apparent as the FE equations contain only nodal variables belonging to the same element. Therefore the method which will be selected for the solution should take advantage of the sparseness of the A matrix. From this point of view the direct methods such as Gauss elimination, Gauss Jordan, LU decomposition, etc. will not be efficient as they tend to use and store all the elements of **[K]**. Inside the bandwidth, as shown in [2.4] so the possible requirement of a very large memory for an even medium size problem is a big drawback of the direct methods. However, the iterative methods can exploit the spareness. In general these methods can be classified as the stationary and gradient methods. Principally, they employ trial solutions and improve them until the convergence within a desired tolerance is obtained. However when using a stationary method for instance Gauss Seidal or Successive Over Relaxation (SOR)

which is an improved version of Gauss Seidal, the convergence even if assured for a moderate size problem (for not more than 2000 unknowns) can be very slow and the problem of inaccuracy may rise. Nevertheless the Gradient methods are the most likely superior ones for the FE applications. They aim to determine the position of the minimum of an error function defined over n-dimensional space. And trial variables are improved to a lower value of the error function.

A gradient method, the pre-conditioned conjugate gradient , has been used to find the unknown variables of the FE equations. The method is briefly introduced along with the common characteristics of the gradient methods in appendix 2.2.

2.5 'MEGA' FE package

In this work, some facilities of a package, called MEGA, is used in mesh generation and postprocessing. MEGA is a general 2D and 3D package for solving electrostatic, magnetostatic and eddy current problems and has been developed in the School of Electrical Engineering at the University of Bath.

CHAPTER 3

UPWINDING TECHNIQUE IN THE FE METHOD

3.1 Introduction

When solving certain physical problems represented by a second order ordinary or partial differential equation having also a first order derivative term, by numerical methods such as finite difference or finite element, there may arise a severe obstacle to obtaining accurate results, namely the occurrence of oscillations in the solution. Fluid flow and heat transfer are good examples of such problems. The difficulty arises especially at high values of the first derivative term. As the moving conductor problem also contains a similar first order derivative term in its differential representation, the same problem is likely to be encountered. Therefore, when the solution of the moving conductor problem is attempted by the FE method as detailed in the previous chapter from the classical Galerkin point of view, possible spurious oscillations in the solution can occur. The remedy to this problem in the FE technique has long been known as 'upwinding'. The particular upwinding scheme used here is that developed by Hughes for fluid flow problems [3.1].

In this chapter, firstly the occurrence of the oscillations is shown analytically in a general one dimensional problem. Then the problem is also displayed for a typical moving conductor problem, as a 2D model of an electrical machine. The solution method, the upwinding scheme, is investigated and introduced to the problem. Finally the 3D FE technique provided with upwinding is used to determine the drag

and normal forces produced by a coil suspended over an aluminium conducting plate. This problem is of interest in the field of magnetic levitation of vehicles for transport (MAGLEV).

3.1.1 1-Dimensional Approach

Although only 2D and 3D problems are concerned in this work, a 1D approach is very useful for illustrating the occurrence of oscillations in the solution. A typical 1D second order differential equation having a first order derivative term, for any kind of physical problem, expressed as below, is considered as a test problem.

$$\frac{d}{dx}\left(k\frac{df}{dx}\right) + l\frac{df}{dx} = 0 \tag{3.1}$$

where $k,l > 0$ are constants. By using the boundary values $f(0)=1$ and $f(H)=0$, and describing $m=l/k$, the exact solution of the equation is

$$f(x) = \frac{e^{mx} - e^{mH}}{1 - e^{mH}} \tag{3.2}$$

When the classical Galerkin FE method is applied to equation (3.1) by using a simple first order linear element which is a line segment with a length **h** and two nodes, one each end (figure 3.1), a set of linear equations is obtained as:

$$-(1-p)\, f_{i+1} - 2f_i - (1+p)\, f_{i-1} = 0 \tag{3.3}$$

In the equation above p which is equal to $lh/2k$, corresponds to Peclet number (or Reynold number in fluid flow). The solution of the set (3.3) is

$$f_i = C_1 + C_2 \left(\frac{1+p}{1-p}\right) \tag{3.4}$$

where C_1 and C_2 constants are determined by the boundary conditions. From equation (3.4) it can be clearly seen that a stable solution is possible only at certain Peclet numbers lying in the interval between -1 and 1. For values outside this interval, the solution includes oscillations.

It is also clear that in the 1D case, the standard Galerkin FE results give exactly the same set of equations as obtained from the finite difference method using the central difference form. The standard method selects the shape function such that the origin of the element is the sampling point. The solution for the occurrence of oscillations in the finite difference method is the replacement of the central difference form with the backward difference form. This yields the solution as:

$$f_i = \frac{C_1 p^2 + C_2 (1+p)}{2+p} \tag{3.5}$$

This solution above is oscillation free, however this is accomplished at the expense of accuracy, as the error term is proportional with the grid size **h**, in the backward form rather than $\mathbf{h}^2$ in the central difference form. A similar argument can also be used to eliminate the oscillations in the FE method. This is shown in the following section.

3.2 The 2D Moving Conductor Problem and Upwinding

In the previous chapter the 2D governing equation for the moving conductor problem in which motion is only in the x direction, was obtained as:

$$-div\gamma\, grad A + \sigma u_x \frac{\partial A}{\partial x} = J_s \tag{3.6}$$

The Peclet number for the equation above is specified as

$$\alpha = \frac{\sigma u_x \mu h}{2} \tag{3.7}$$

As explained in the case of the 1D problem at high Peclet numbers, the solution of equation (3.6) by the Galerkin method which uses an equivalent of the central difference approach will have non physical oscillations. In fact, the problem can be overcome by reducing the element size, h, to a degree that the Peclet number lies in the desired oscillation free interval. This, however, may well require a very fine mesh particularly at high speeds. Therefore a more practical and applicable method should be recommended. The introduction of a biased weighting function in the process by Hendrics can be one way of solving the problem [3.2]. The technique, as an alternative to the Galerkin method, replaces the shape function with a more general unsymmetrical new function by (for the 1D example)

$$t_j(x) = W_j(x) \pm C_k W_{bj}(x) \tag{3.8}$$

so that the function $C_k W_{bj}(x)$, as shown in fig. 3.2, biases the normal shape function

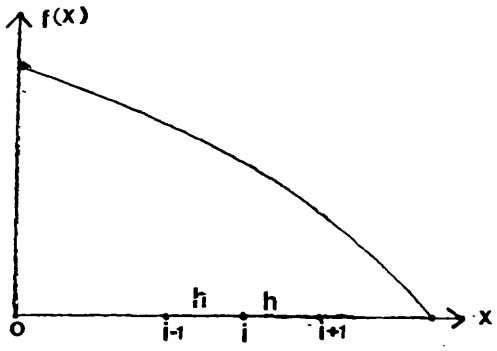

Fig. 3.1 A line segment and 1D approach

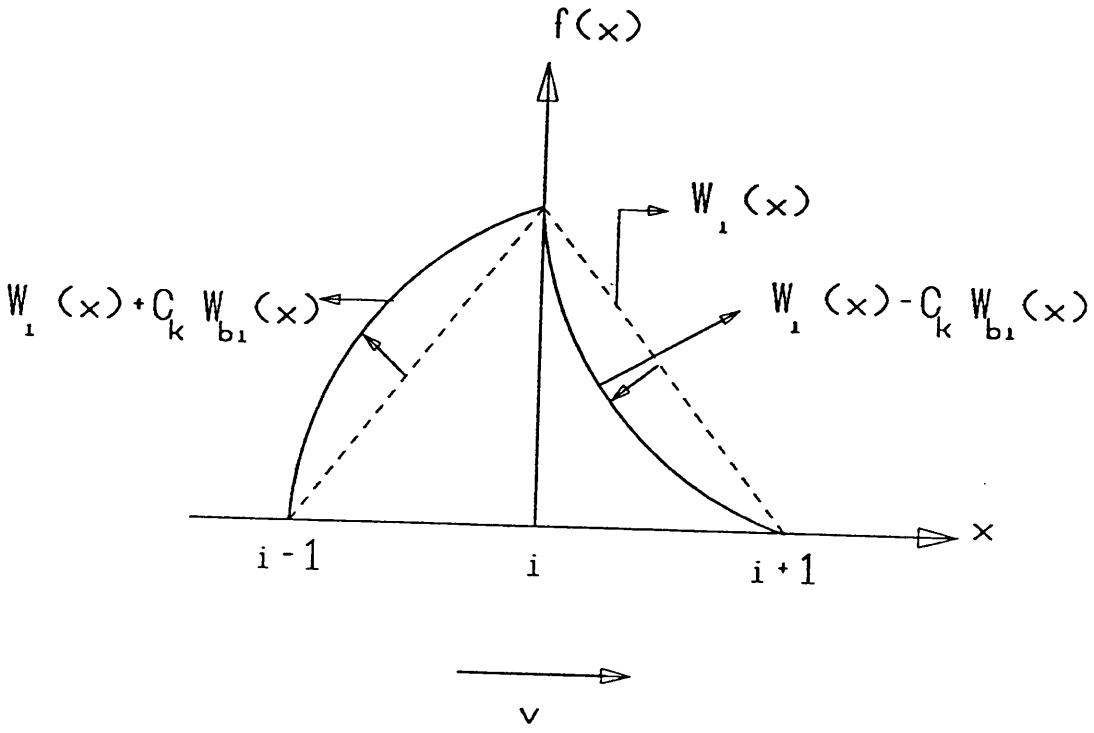

Fig. 3.2 Example of a biased shape function by Heinrich

$W_j(x)$. In reference [3.3] W_{bj} and the optimal choice of C_k are given as

$$W_{bj}(x) = -\frac{3}{h^2}x(x-h) \tag{3.9}$$

$$C_k = \coth\frac{\alpha}{2} - \frac{2}{\alpha} \tag{3.10}$$

Although the technique has been used in some applications [3.4], it increases the order of the polynomials used in the shape function and causes more difficult integral calculations. The upwinding solution by Hughes is simpler and inexpensive as it only modifies the first order term (velocity term) and leaves the rest unchanged. When using a 2D quadrature element with the natural coordinate system (in fig. 3.3) the unit velocity vectors in both directions (for a general 2D problem) are:

$$\bar{u}_\xi = u\bar{e}_\xi \quad \textit{and} \quad \bar{u}_\eta = u\bar{e}_\eta \tag{3.11}$$

and the Peclet numbers are defined as:

$$\alpha_\xi = \frac{\sigma u_\xi h_\xi \mu}{2} \quad \textit{and} \quad \alpha_\eta = \frac{\sigma u_\eta \mu h_\eta}{2} \tag{3.12}$$

According to the Hughes Scheme, a Gauss point at the origin of the element (an element with a centrally located Gauss point corresponds to the central difference approach of the finite difference method and produces the highest accuracy for the integration but causes oscillation) is moved to another position $\tau(\xi,\eta)$ which is decided in accordance with the direction of the motion, by the formulas given below

$$\xi = \coth\alpha_\xi - \frac{1}{\alpha_\xi} \quad \textit{and} \quad \eta = \coth\alpha_\eta - \frac{1}{\alpha_\eta} \tag{3.13}$$

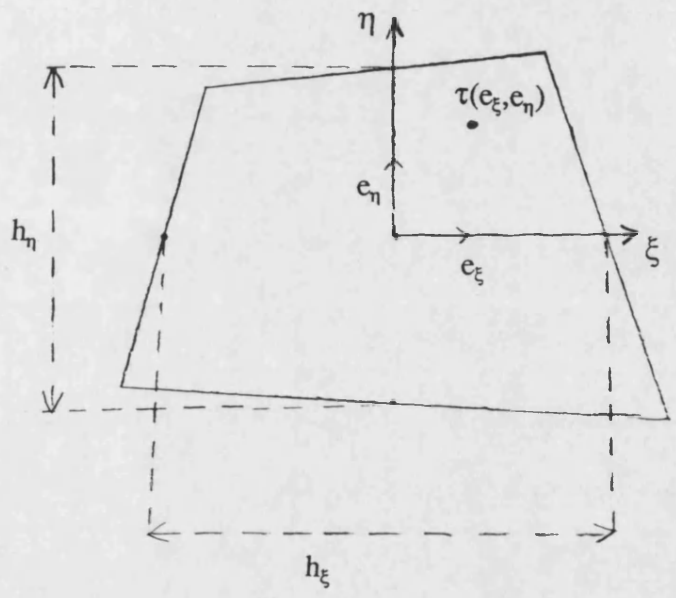

Fig. 3.3 Hughes's upwinding scheme and new position of a sample point

The displacement of the sampling points also leads to a new specification of the Galerkin form of the first order term described in equation (2.24). Then it becomes

$$\sum W_j(\tau)\left(\sigma u_x(o)\frac{\partial W_i(\tau)}{\partial x}A_i\right)J_C(0)\,C \qquad (3.14)$$

where $u_x(0)$ is the velocity evaluated at the origin of the isoparametric element, J_C is the jacobian of the isoparametric transformation, C is a constant and equals 4 for 2D elements (2 and 8 for 1D and 3D elements respectively).

3.2.1 A 2-D Test Problem

The linear electrical machine shown in fig 3.4 is considered as the test problem to show the effect of the FE method with and without upwinding in the solution of the moving conductor problem. The machine involves a highly permeable moving conducting rotor (the value of relative permeability and conductivity of rotor used in the problem are 2000 and 10^7 S/m respectively). The stator contains current sheets on the boundary with the air-gap. The sheets (with a current density of 2.5 10^8 A/m^2) are modelled with 0.25 mm thickness so that almost an exact comparison with the Fourier analysis technique using current sheets with zero thickness would be possible. The Fourier technique is distinctly detailed in chapter 5 and applied to this particular problem in the same manner. Furthermore the Fourier technique can only be applied under the assumption of an infinitely long machine in the x-direction of fig 3.4. Therefore the 2D FE model should also be able to represent this feature. This is carried out by applying the periodicity conditions to the nodes lying on the outer

boundaries marked AB and A'B' on fig 3.5. The periodicity condition implies that the fields are exactly the same at the periodicity boundaries. The condition is implemented by setting the potentials which lie on the two periodicity boundaries, and equally distanced from the x-axis, equal.

3.2.2 Results

The validity of upwinding and its importance in solving the moving conductor problem can be appreciated by comparing results obtained from the FE technique with and without upwinding, with the results of the analytical Fourier method. The air-gap normal flux density and force calculations are considered for the comparison. The drag and normal forces are calculated by using the method of the Maxwell's stresses in the air-gap (section 4.3). Two meshes are utilized for the FE calculations. The average element size, h, is 4mm in the coarse mesh, and 1 mm in the fine mesh shown in figs. 3.6 and 3.7.

The drag force density and normal force density results are shown in tables 3.1 and 3.2, for both fine and coarse meshes at different velocities, thereby at different Peclet numbers. From these results and the force-speed characteristics shown in figs 3.8 and 3.9, it can be noted that, particularly in drag force calculations, the errors in the no upwind case increase rapidly with high Peclet numbers, and that the upwinding technique cures the problem and produces accurate results. The normal and tangential air-gap flux densities at **u=50 m/s** are shown in figs. 3.10 and 3.11. They also indicate a slight inaccuracy for the no upwind case, which leads to vastly different drag force results.

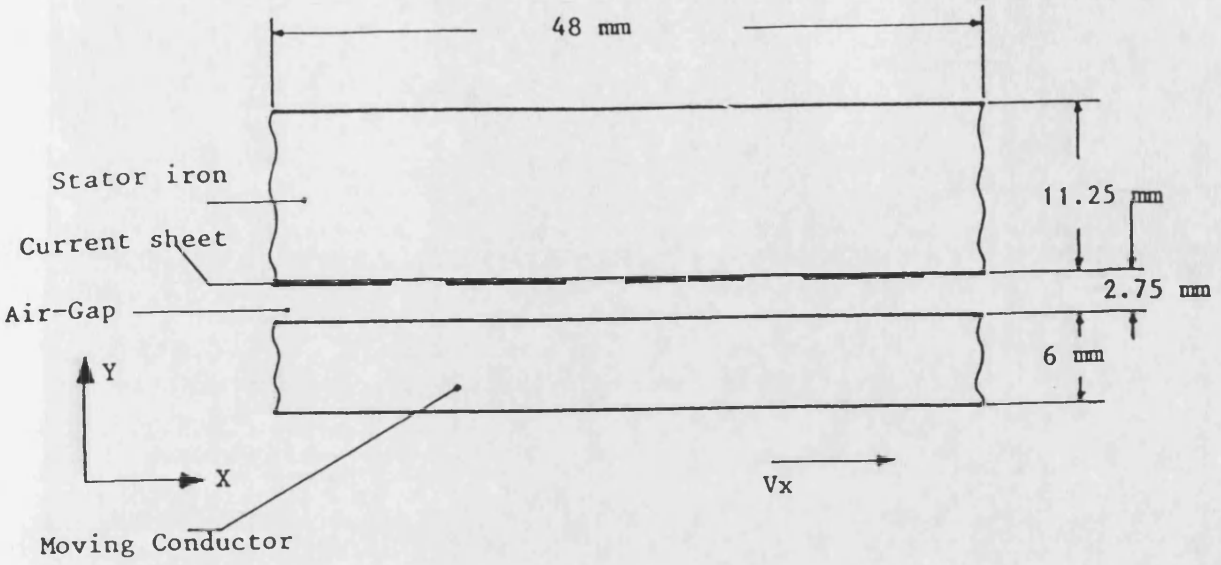

Fig. 3.4 2D test problem with steel rotor

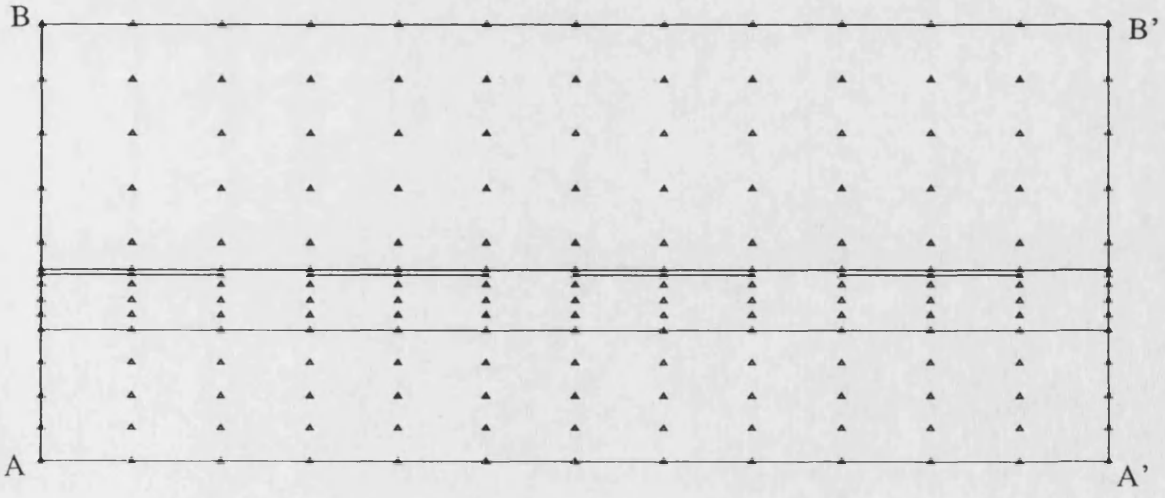

Fig. 3.5 Specification of the periodicity boundaries for the test motor

Fig. 3.6 2D Coarse mesh (h=4 mm)

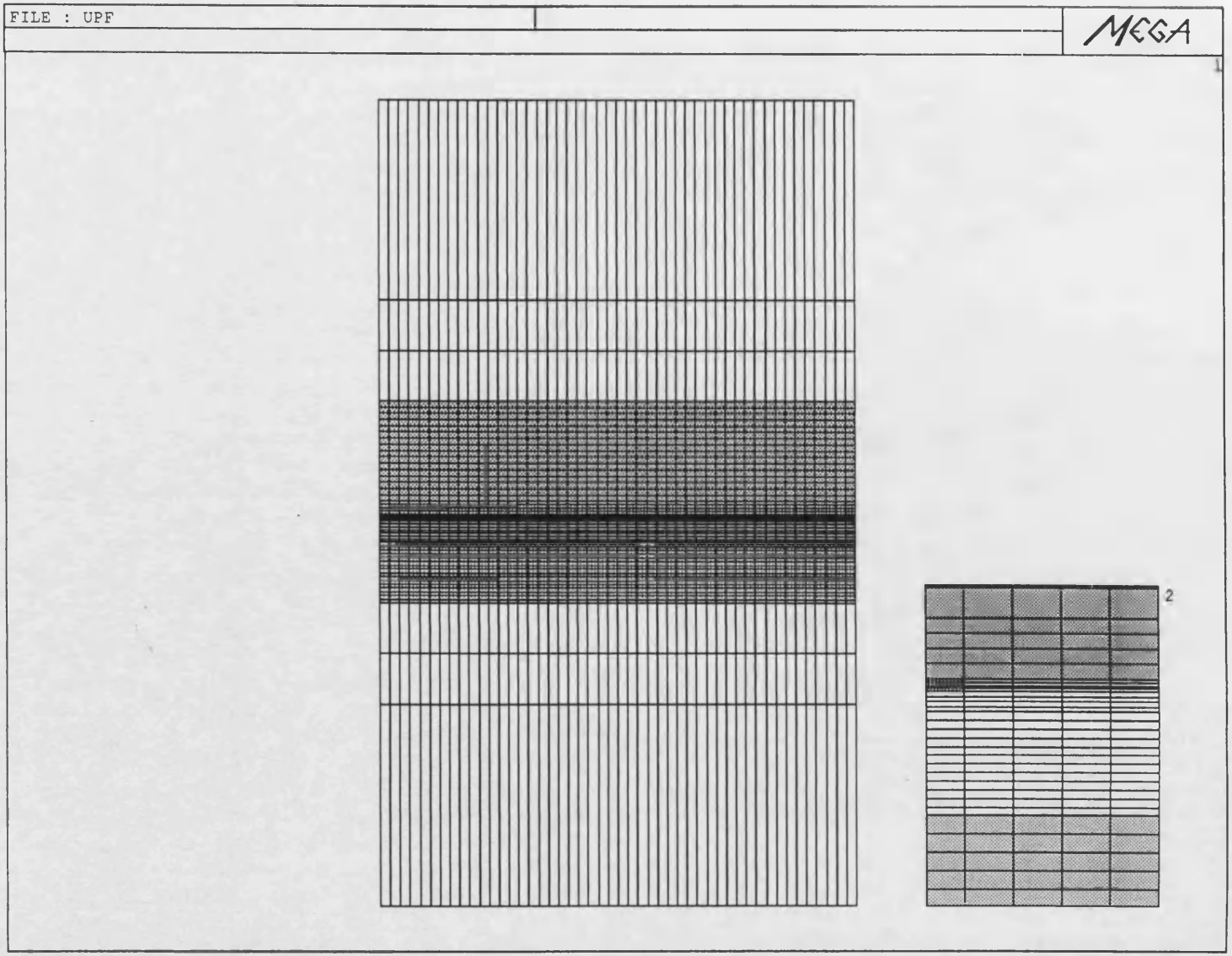

Fig. 3.7 2D Fine mesh (h=1 mm)

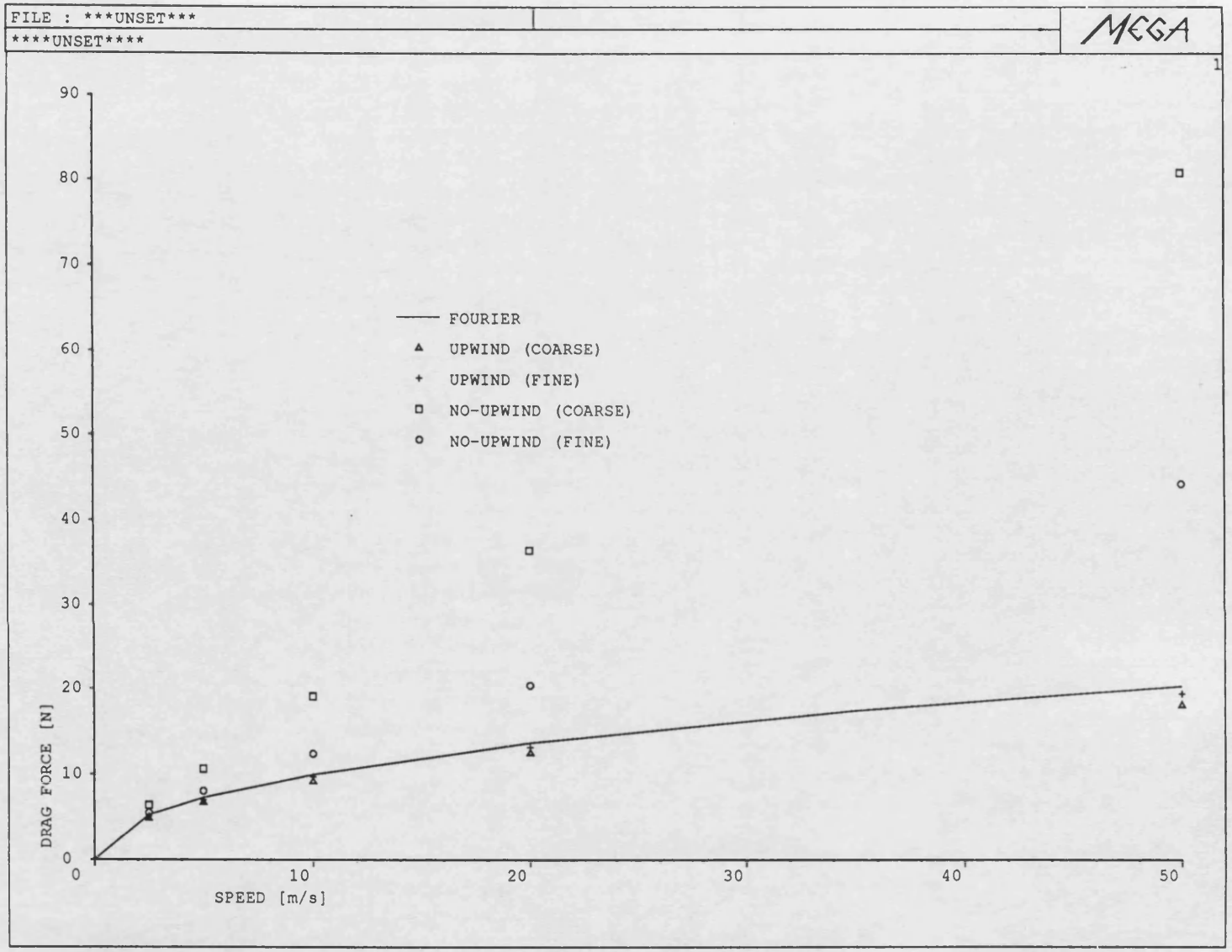

Fig. 3.8 Drag force - speed characteristics with and without upwinding

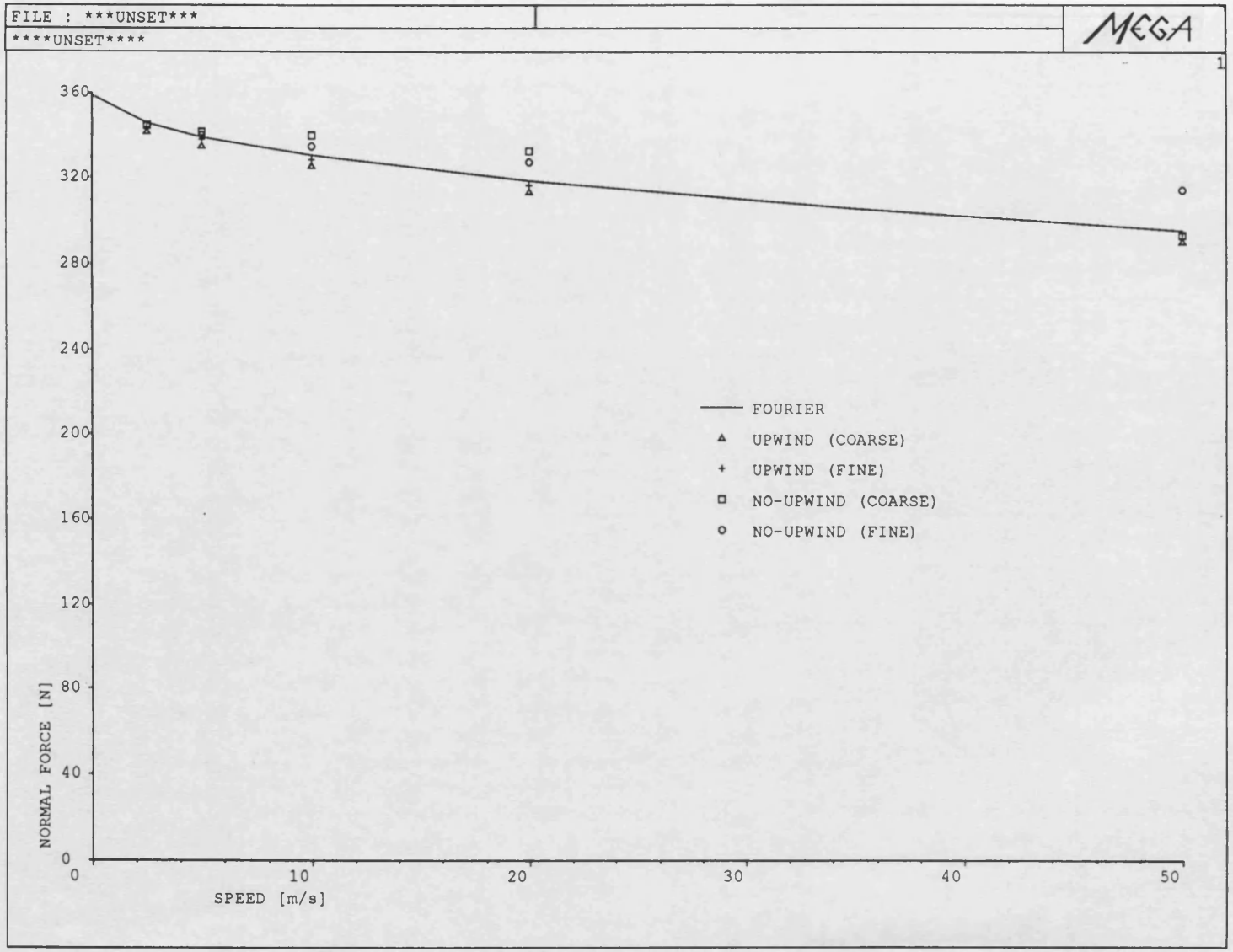

Fig. 3.9 Normal force - speed characteristics with and without upwinding

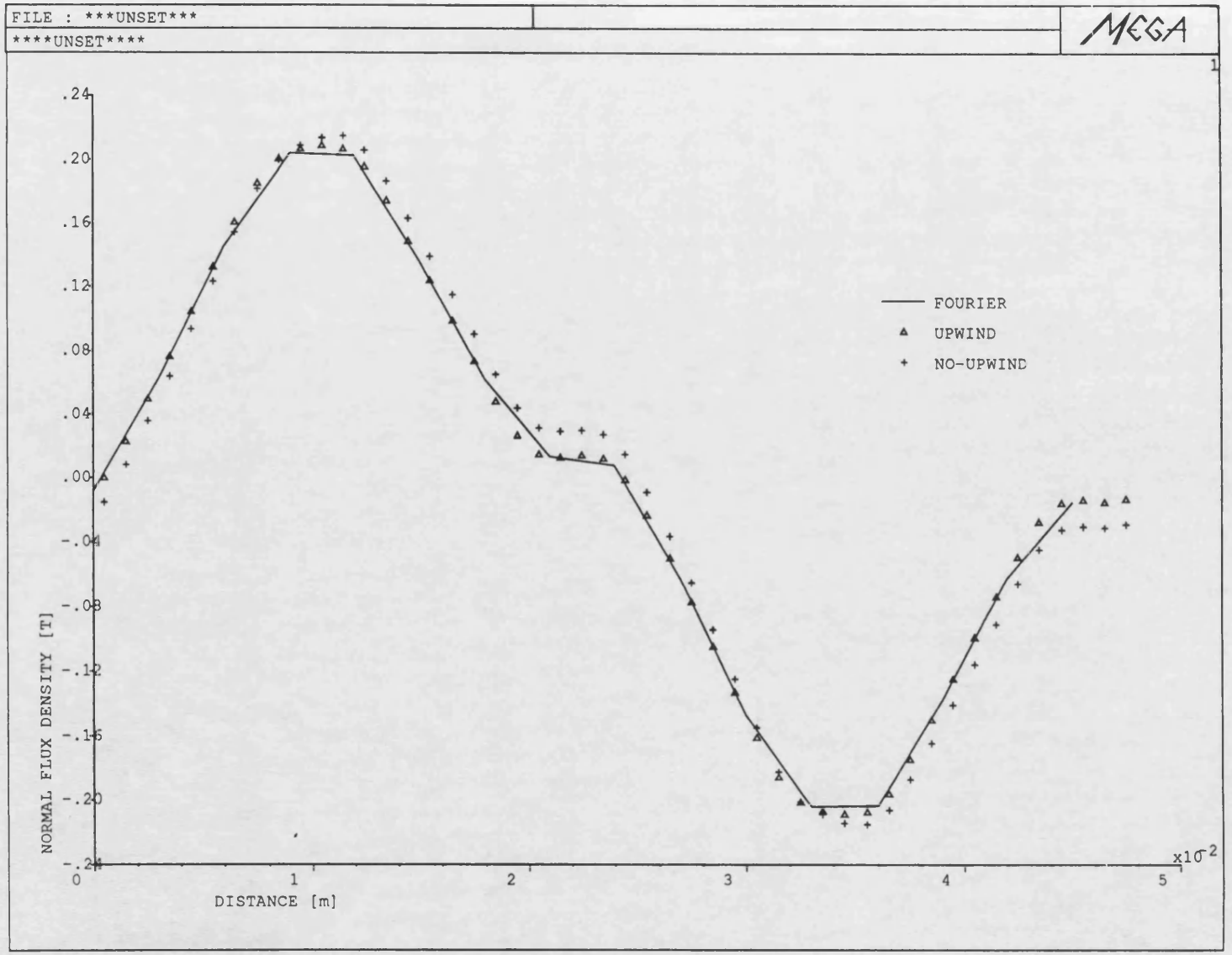

Fig. 3.10 Normal air-gap flux density with and without upwinding at u=50 m/s

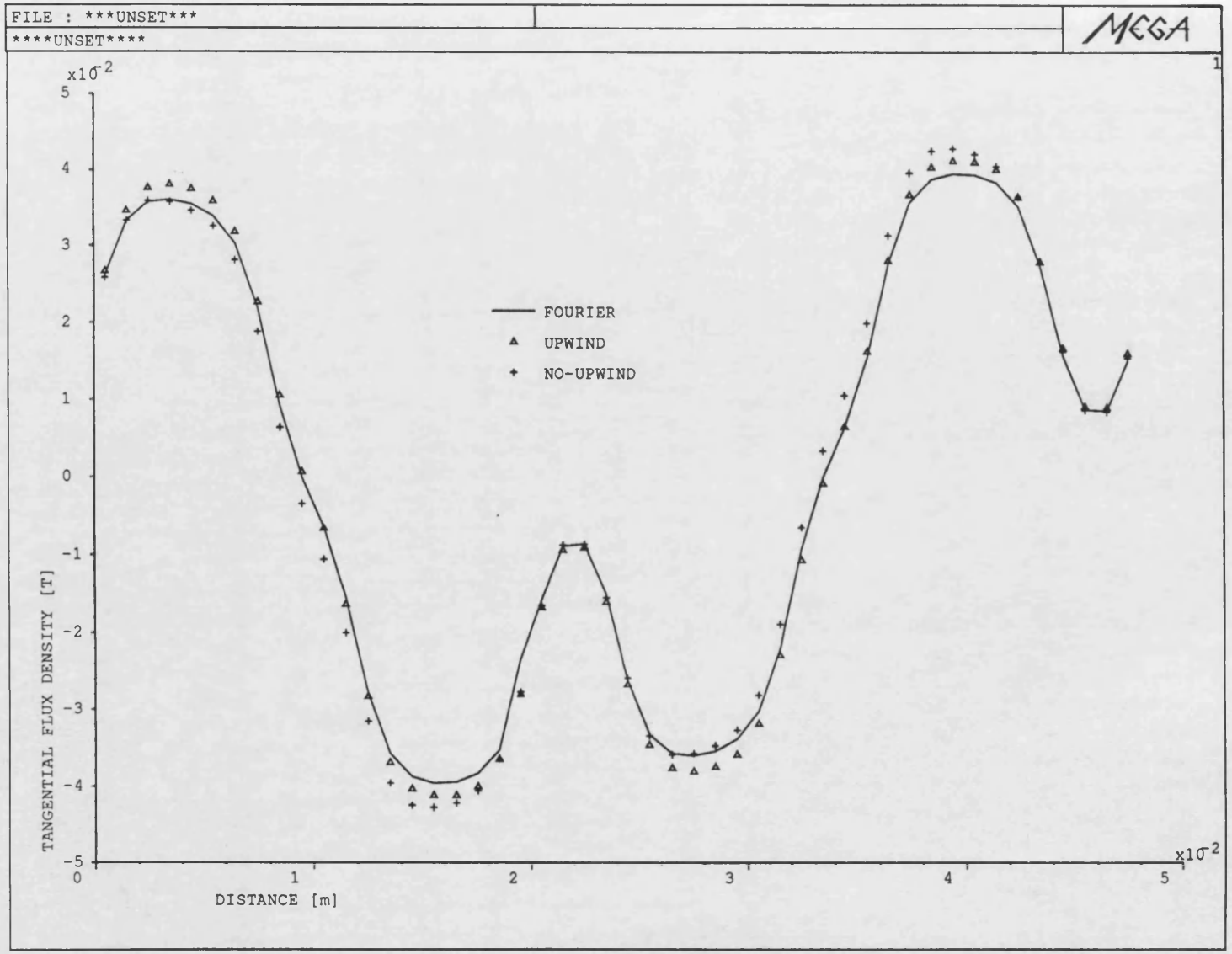

Fig. 3.11 Tangential air-gap flux density with and without upwinding at u=50 m/s

		Drag Force [N]			Normal Force [N]		
Speed [m/s]	Peclet No.	Fourier	Upwind	No-upwind	Fourier	Upwind	No-upwind
2.5	125	5.26	4.84	6.36	346	342	345
5	250	7.3	6.72	10.59	339	335	342
10	500	10.01	9.25	19.19	331	326	340
20	1000	13.72	12.62	36.5	319	314	333
50	2500	20.25	18.17	80.9	296	291	294

Table 3.1 Coarse mesh results

		Drag Force [N]			Normal Force [N]		
Speed [m/s]	Peclet No.	Fourier	Upwind	No-upwind	Fourier	Upwind	No-upwind
2.5	31.2	5.26	5.07	5.53	346	344	345
5	62.5	7.3	7.04	8.11	339	338	340
10	125	10.01	9.70	12.4	331	329	335
20	250	13.72	13.22	20.44	319	317	328
50	625	20.25	19.43	44.35	296	295	315

Table 3.2 Fine Mesh results

3.3 The 3D Moving Conductor Problem And Upwinding

The upwinding technique is also exercised in a 3D application. The test problem is chosen from the area of high speed magnetically levitated ground transport systems, MAGLEV, which stands for magnetic levitation.

The basic concepts of MAGLEV have long been known, but some systems have become economically more interesting after recent successes in obtaining low temperature super conducting materials. There are few possible techniques for magnetic levitation. These are, briefly:

i) Repulsion between permanent magnets

ii) Repulsion between A.C. iron-cored magnets and eddy currrents induced in a conducting guideway.

iii) Attraction between ferromagnetic rails and controlled electromagnets (electromagnetic suspension).

iv) Repulsion between moving magnets with DC excitation and eddy currents induced in nearby conductors by virtue of the relative motion (electrodynamic suspension).

Among these options, the consideration of electromagnetic suspension (attraction force) is common for low speed applications whereas for high speeds applications the electrodynamic system is often a more favourable choice. This technique uses the repulsive force between superconducting magnets, mounted on the underside of the vehicle, and eddy currents induced in aluminium conductors on the guideway surface by the moving magnets. There is no levitation without motion.

The magnetic levitation increases rapidly at low speeds and tends to be reduced while the speed increases. The second force, magnetic drag force also rises rapidly at low speeds to its peak and drops off with increasing speed. The biggest advantage of using this system that it can operate with a large guideway clearance or air-gap and no control system is needed to control this gap. The system is stable, without a control system.

In this work, only a super conducting field coil which is levitated above an aluminium guide way strip is examined. All the technical side of the Maglev system and its design are ignored here. Only the numerical solution methods of the moving conductor problem are concerned.

3.3.1 The Theory

The governing partial differential and its equivalent 3D FE equations for the moving part were derived earlier. The partial differential governing equation in 3D was:

$$curl\,\gamma\, curl\bar{A} = \sigma(\bar{u}\times curl\bar{A} - gradV) \tag{3.15}$$

The terms involving velocity require a special treatment to prevent oscillations occurring in the solution. As in the 2D case, the treatment is upwinding. In the 3D problem, the upwinding procedure can be implemented in a similar manner, to that described for the 2D problem. Different sampling points are used for evaluating the velocity terms only of equation (3.6). For element e:

$$\int_e W_j \, \sigma(\bar{u} \times Curl\bar{A}) \, dv$$

is replaced with

$$\sum W_j(\tau) \left(\sigma \bar{u}(0) \times curl\bar{A}(\tau) \right) J_C \, (0) \, C \qquad (3.16)$$

In this formula, C=8 as the problem is 3D, and the optimum position for τ is also determined by equation (3.9).

3.3.2 Results

A filamentary rectangular coil shown in fig. (3.12) is modelled in 3D. The current in the coil is as high as 10^5 A . Because of symmetry only half of the coil is represented in the model. The coarse mesh and fine mesh are displayed in figs. 3.13 and 3.14. The results, force-speed characteristics in which speed varies from 0 m/s to 100 m/s, are displayed in figs (3.15) and (3.16).

The Fourier transform method developed by Reitz and Davis [3.4] is used to predict the accuracy. In the application of the Fourier transform technique, the conducting plate is assumed to have infinite extent so that the results of the FE model should not correspond exactly as in the 2D linear machine problem. However, the agreement in forces obtained by using the Maxwell stress method (outlined in section 4.3) for FE-upwinding and the transform method is still reasonable, (see fig

3.15 and 3.16). And importantly, FE without upwinding failed to converge at speeds higher than 40 m/s.

The formulations of drag and lift forces by the Fourier transform method are given in appendix 3.1. The integrals of the formulas were determined by using the Nag-library facilities.

3.4 Conclusion

The oscillating effect of the standard Galerkin approach to 2D and 3D moving conductor problems have been demonstrated. This effect causes a large inaccuracy in the solution at high Peclet numbers. However, it has been observed that when upwinding is introduced to the velocity term, the inaccuracy problem caused by the oscillating effect has been resolved. The Hughes scheme has been used for upwinding. The biggest advantage of the scheme is that only the velocity term needs to be upwinded therefore, the computational burden, compared with the other schemes, is minimal. Even when using upwinding, it is possible for the conjugate gradient technique to fail to converge. This has been found for Peclet numbers of about 6000 in 3D problems. At this point, the only remedy is to refine the mesh so that the Peclet number can be reduced.

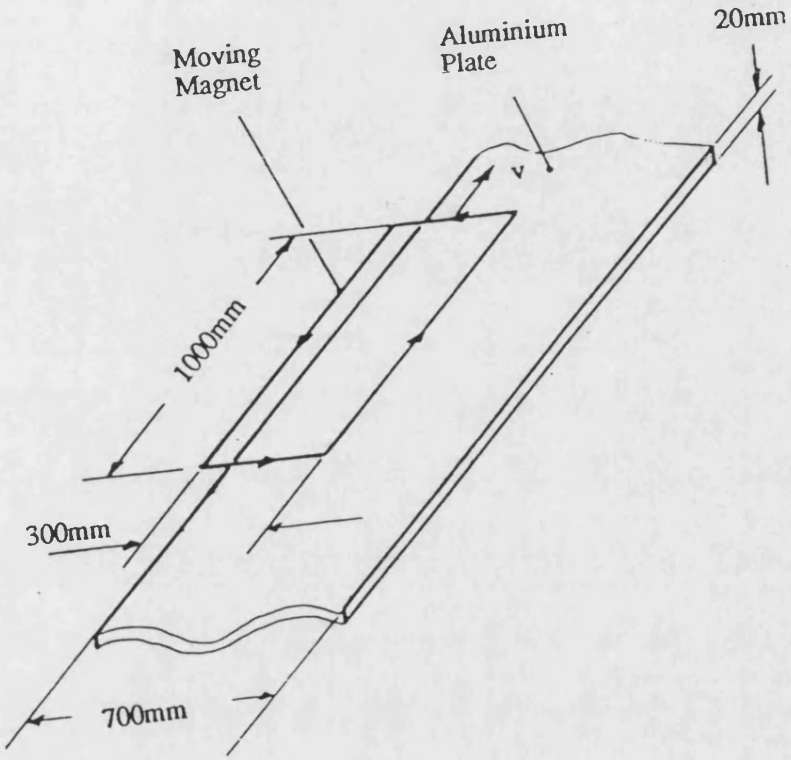

Fig. 3.12 The maglev coil

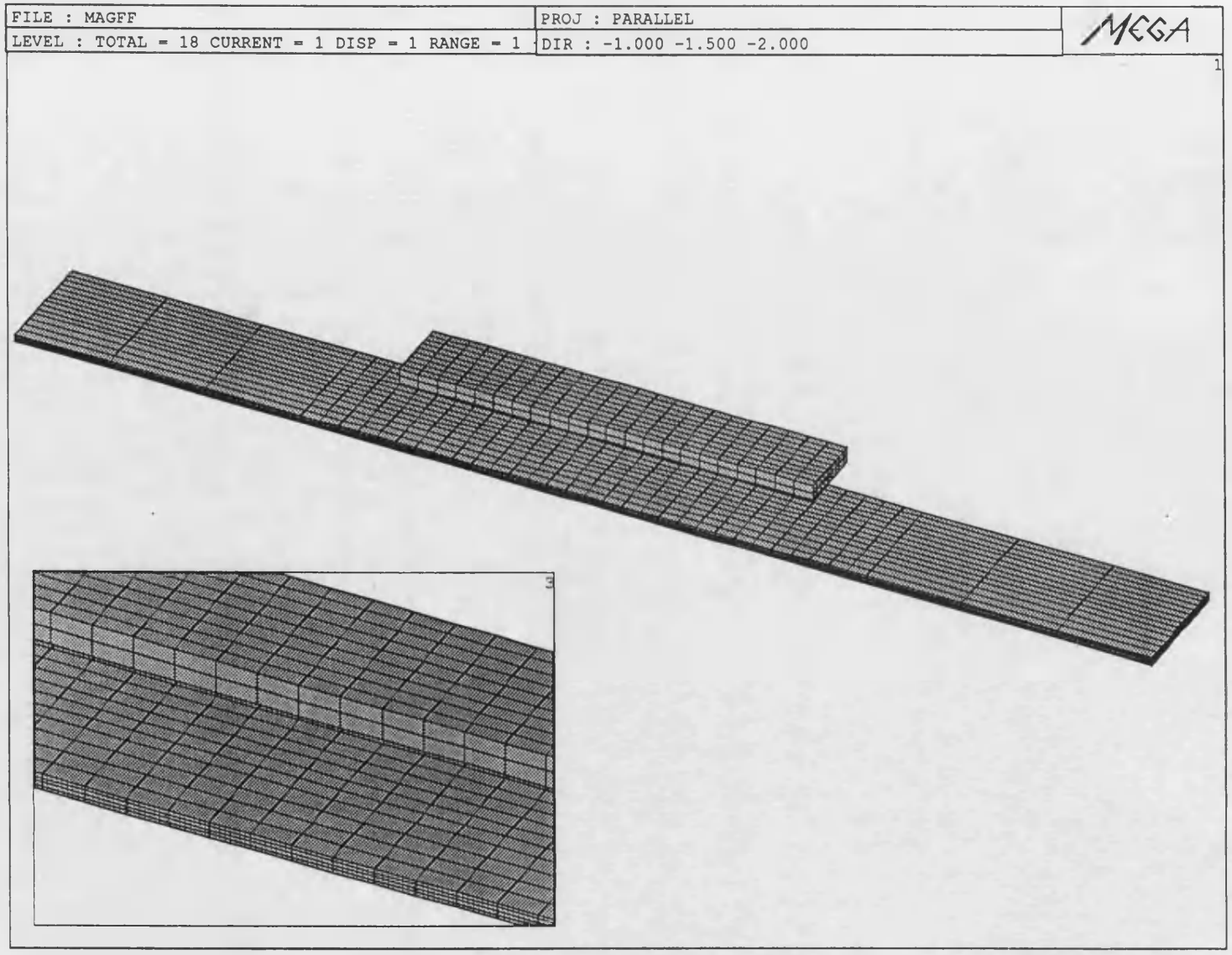

Fig. 3.13 3D Coarse mesh

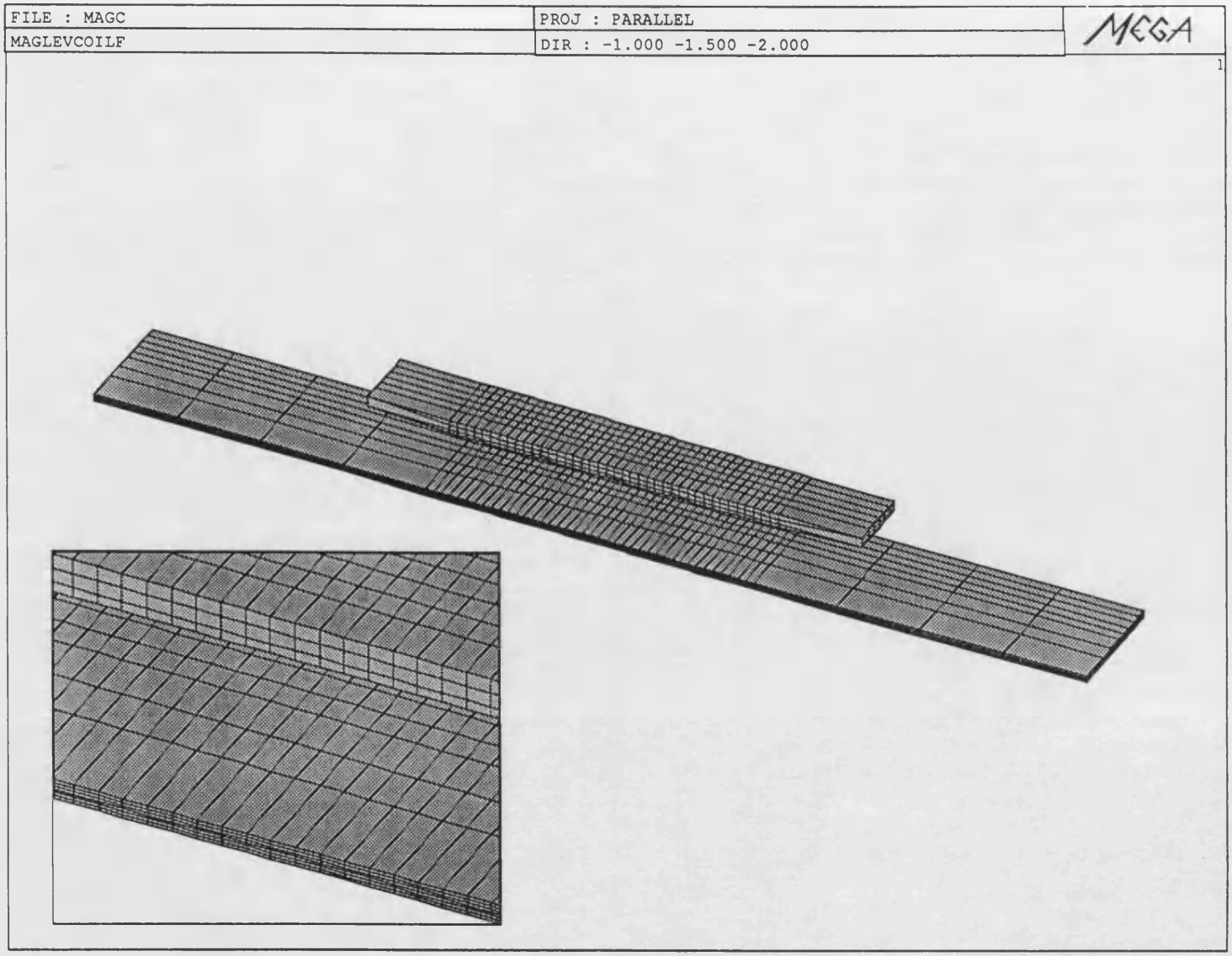

Fig. 3.14 3D Fine mesh

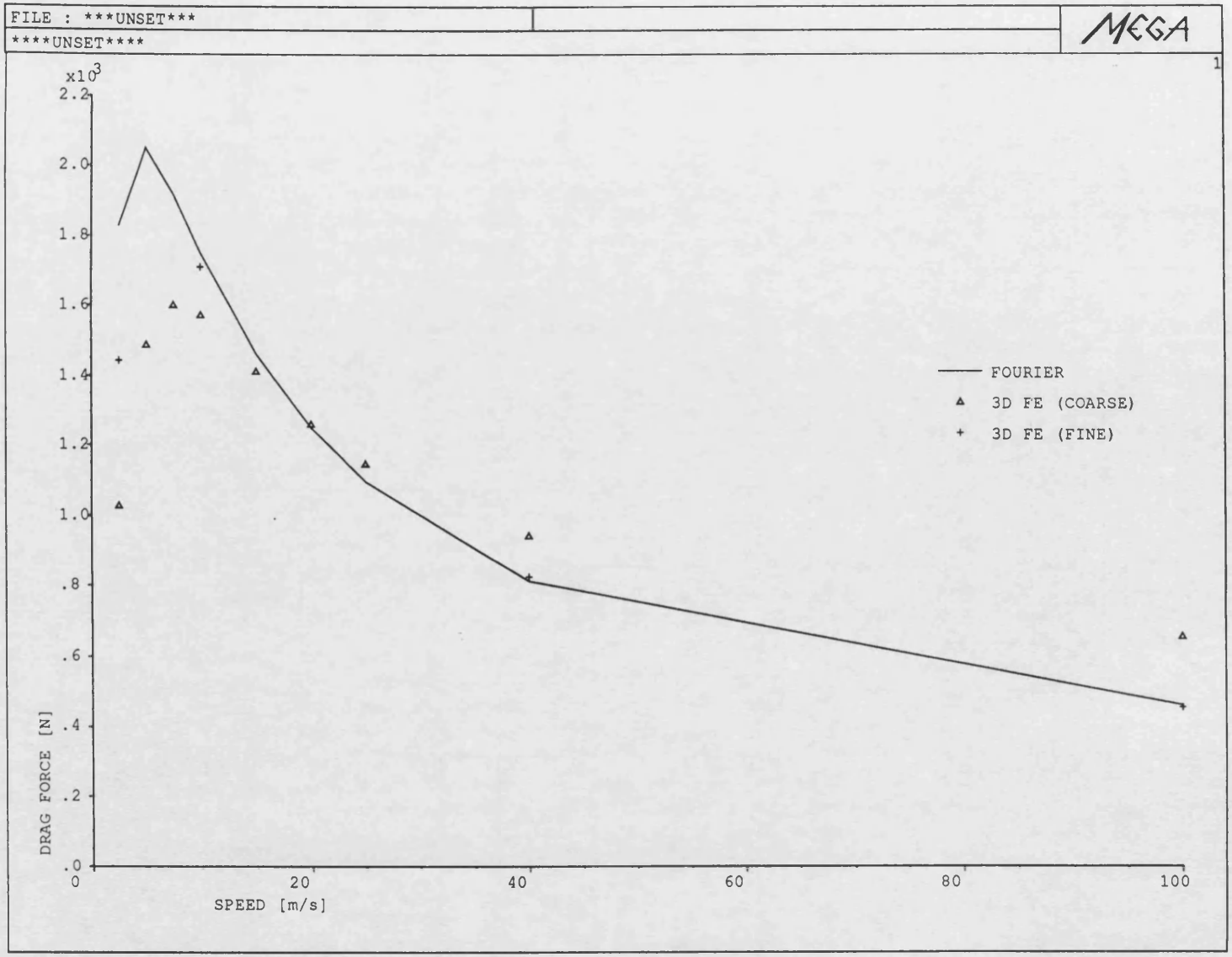

Fig. 3.15 Drag force - speed characteristics for the maglev coil

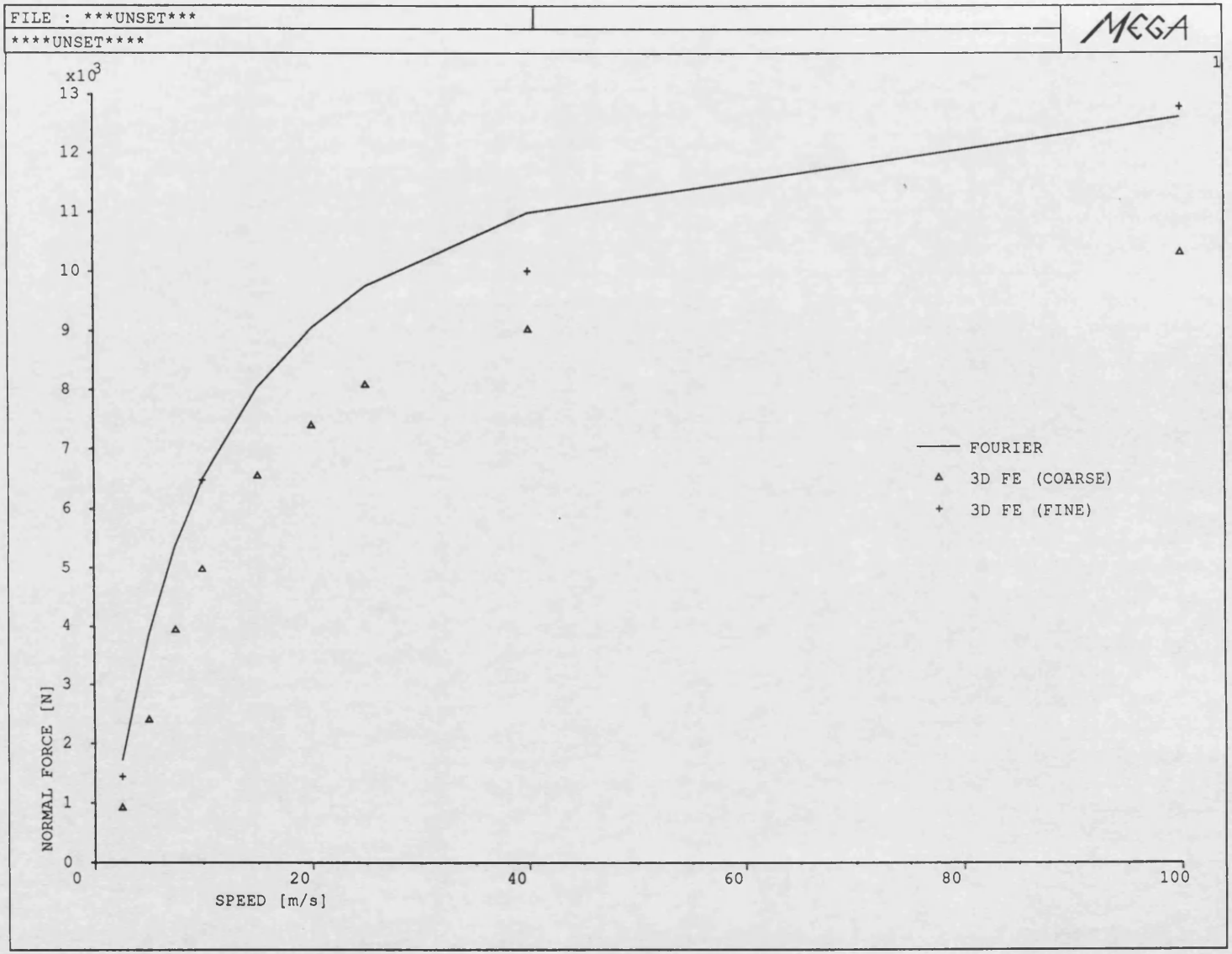

Fig. 3.16 Normal force - speed characteristics for the maglev coil

CHAPTER 4

A NEW OPTIMAL FORMULATION FOR 3D MOVING CONDUCTOR PROBLEMS

4.1 Introduction

A method to solve the 3D moving conductor problem by using the vector and electric scalar potentials in the conducting region, and the magnetic scalar potentials in the rest of the model was described in chapter 2. A new method which does not require the electric scalar potential inside conductors is introduced in this chapter. The new method will have an obvious computational advantage in that only three variables are used for the conducting region rather than four. In addition to this, the final matrix will be better conditioned than before and consequently the solution process will be much faster, when the pre-conditioned bi-conjugate gradient technique is used to solve the final set of equations.

A test rig was set up to verify the substance of the technique experimentally. A DC magnet was designed for the test. The air gap flux density, normal force and drag force measurements are used in the comparison.

4.2 The Formulation

As it was pointed out in chapter 2 that, in general, 3D eddy current formulations, unless the motional effect is negligible, include the **gradV** term. Having considered $\mathbf{div}\bar{\mathbf{J}}=0$ and $\bar{\mathbf{J}}=\sigma\bar{\mathbf{E}}$, the Galerkin procedure, and using the equation

$$\int_v W div\bar{J}\, dv = -\int_v grad W\bar{J}\, dv + \oint_s W\cdot\bar{J}\cdot\bar{n}\, ds = 0$$

the equation below which includes **gradV** was obtained and used in the solution.

$$\oint W\sigma\,(\bar{u}\times curl\bar{A} - gradV)\, n\, ds - \int_v grad W\sigma\,(u\times curl\bar{A} - gradV)\, dv = 0$$

The surface integral term in the formula is important to set $\bar{\mathbf{J}}.\bar{\mathbf{n}}=0$ on the inside surface of conductors. Otherwise, If **gradV** is not contained, the treatment of $\bar{\mathbf{J}}.\bar{\mathbf{n}}=0$ as a natural boundary condition would be incorrect. However, the removal of **gradV** thus the electric scalar potential, would reduce one unknown from the system, and require only one set of equations to be solved. Therefore the formula without **gradV** would be very advantageous. For the removal of the **gradV** from equation (2.15), a study of the $\bar{\mathbf{u}}\times\mathbf{curl}\bar{\mathbf{A}}$ term is useful. Since,

$$\bar{u}\times curl\bar{A} = grad(\bar{A}\cdot\bar{u}) - (\bar{u}\cdot grad)\bar{A} \qquad (4.1)$$

simply defining **V** as below,

$$V = \bar{A}\cdot\bar{u} \qquad (4.2)$$

will achieve the desired removal of **gradV** by obtaining

$$curl\,\gamma\,curl\bar{A} = \sigma\,[(-\bar{u}.grad)\bar{A} + grad(\bar{A}.\bar{u}) - grad(\bar{A}.\bar{u})] \qquad (4.3)$$

And the new formula without **gradV** will be:

$$curl\,\gamma\,curl\bar{A} = \sigma\,(\bar{u}\cdot grad)\bar{A} \qquad (4.4)$$

And Green's theorem yields:

$$\int_v (curl\bar{W}_j\,\gamma\,curl\bar{A} - \sigma\bar{W}_j(u\cdot grad)\bar{A})\,dv - \oint_s \bar{W}_j(\gamma\,curl\bar{A}\times n)\,ds = 0$$

Afterwards, the procedure is the same as described in chapter 2 and chapter 3. The divergence of $\bar{A}$ is enforced by using the penalty technique. And the same upwinding technique as before is used to prevent the possible oscillations occuring in the solution. On the other hand because $\bar{J}$ is defined as, $\sigma(\bar{u}.\mathbf{grad})\bar{A}$, $\bar{J}.\bar{n}=0$ will be obtained when $\bar{A}.\bar{n}=0$ is imposed on the boundary.

4.3 The Maxwell Stress Method and Force Calculations

There are several ways of calculating the forces in electromagnetism [4.1]. The Maxwell stress method is one of the most common ones. In contrast to the virtual work technique which employs a volume integral to determine the stored energy first, the Maxwell stress method finds local stress at all points of boundary surface, then sums the local stresses by means of a surface integral which yields the total net force [4.2]

There are two types of Maxwell stresses, the tensile stress $\mathbf{f}_t$ along the lines of force and the compressive stress $\mathbf{f}_n$, at right angles to the lines of force. These stresses in vacau are expressed in terms of normal and tangential components of **B** as;

$$f_t = \frac{B_n B_t}{\mu_0} \tag{4.6}$$

and

$$f_n = \frac{B_n^2 - B_t^2}{2\mu_0} \tag{4.7}$$

4.4 A DC Magnet and Test Rig

A rig, which is sketched in fig 4.1, and pictured in fig. 4.2 was built to test the validity of both formulations for the moving conductor problem. For this, a 'C' core magnet represents the stator (fig. 4.3). The rotor consists of a steel drum faced by a continuous aluminium plate rotating as the moving conductor. All the eddy currents induced in the plate here are due to the velocity of the moving conductor, as the currents flowing through the coils of the magnet are only DC. The shaft of the aluminum-steel drum is coupled with a DC motor by means of a belt, in order that the speed of the drum can be varied by adjusting the field current of the DC motor.

As it is illustrated in fig 4.4, the magnet involves only one slot in which two coil sides are placed. It is held in a cage, which is free to rotate about the centre of the drum shaft, so that the drag force can be measured. Other load cells holding the

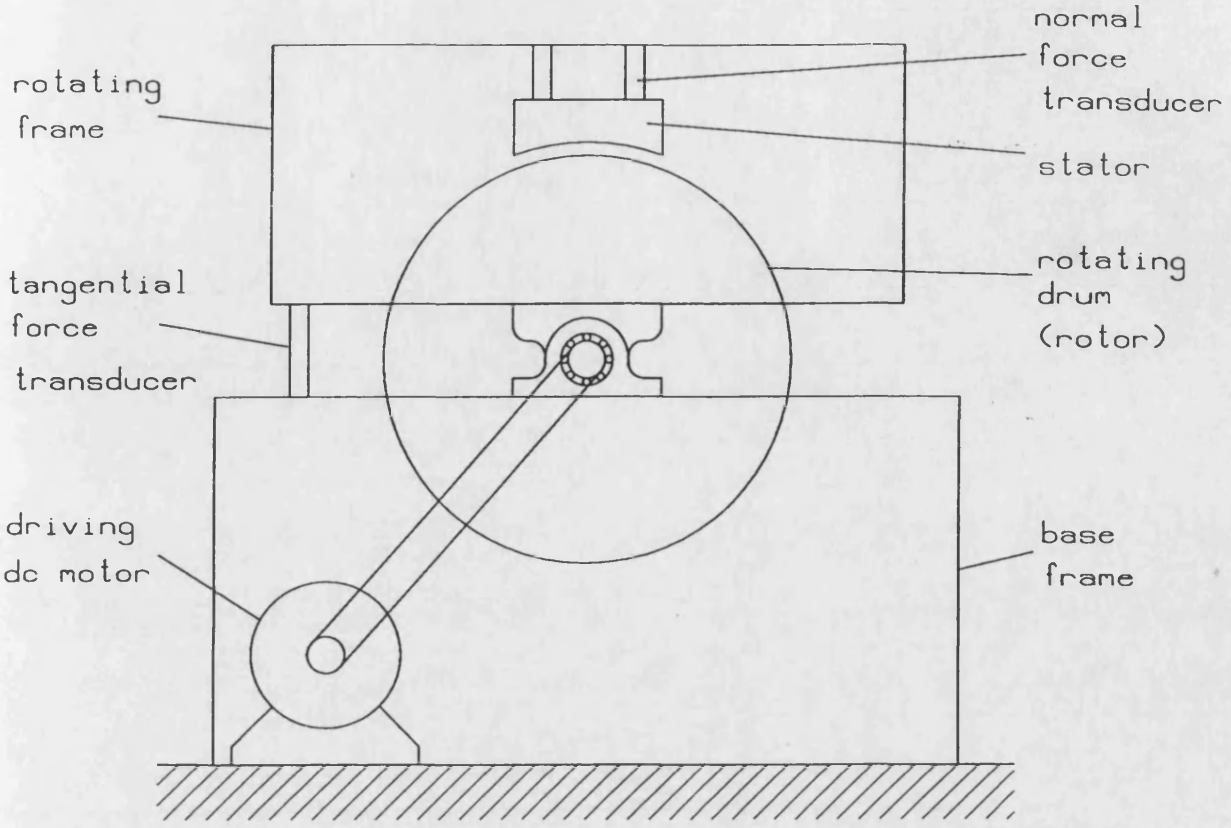

Fig. 4.1 Schematic showing of the test rig

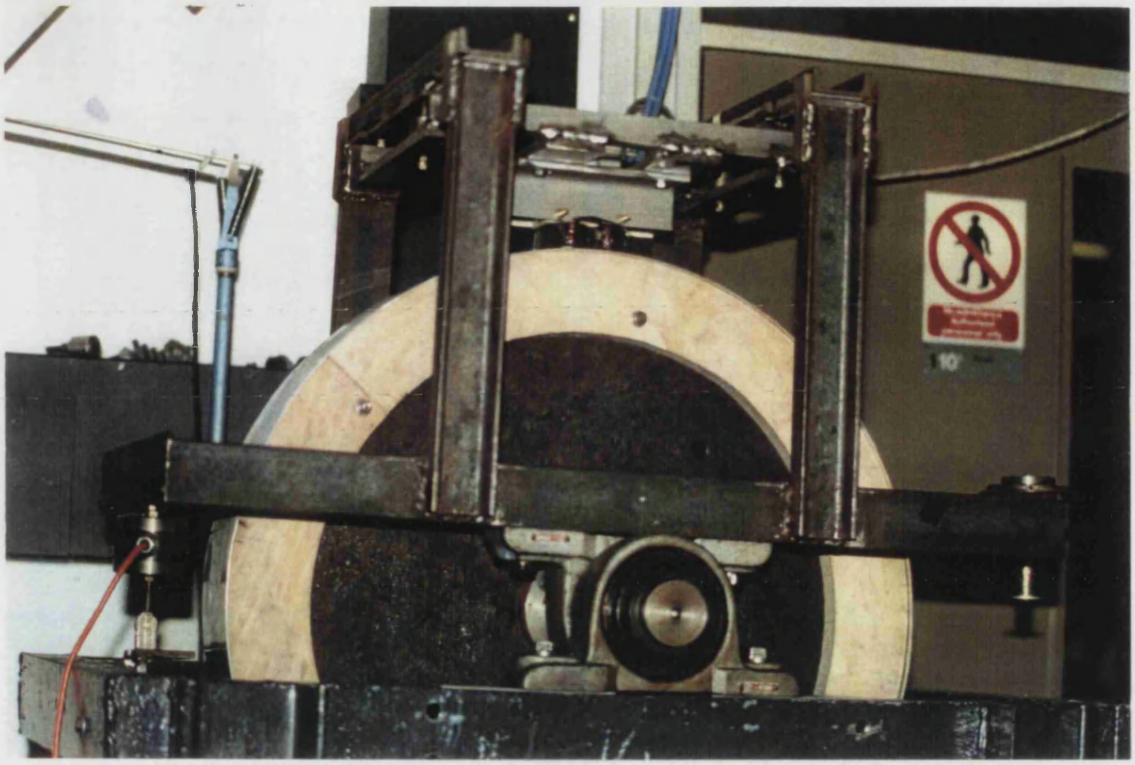

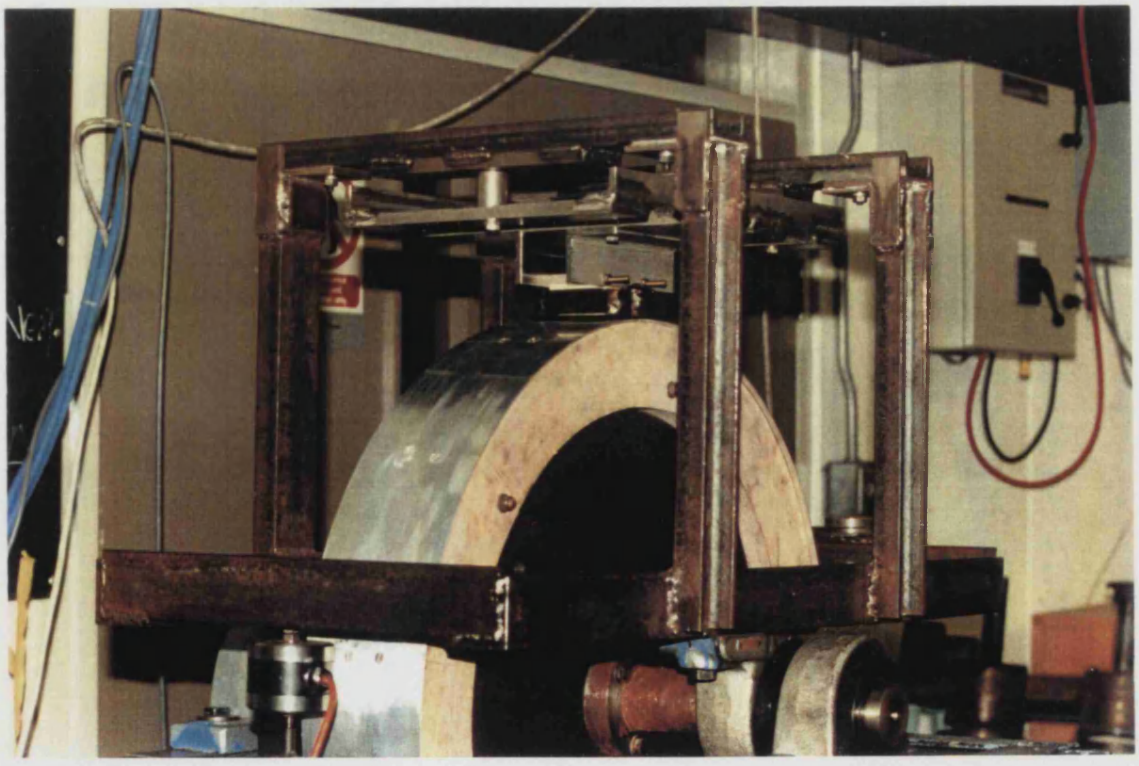

Fig. 4.2 Photographs of the test rig

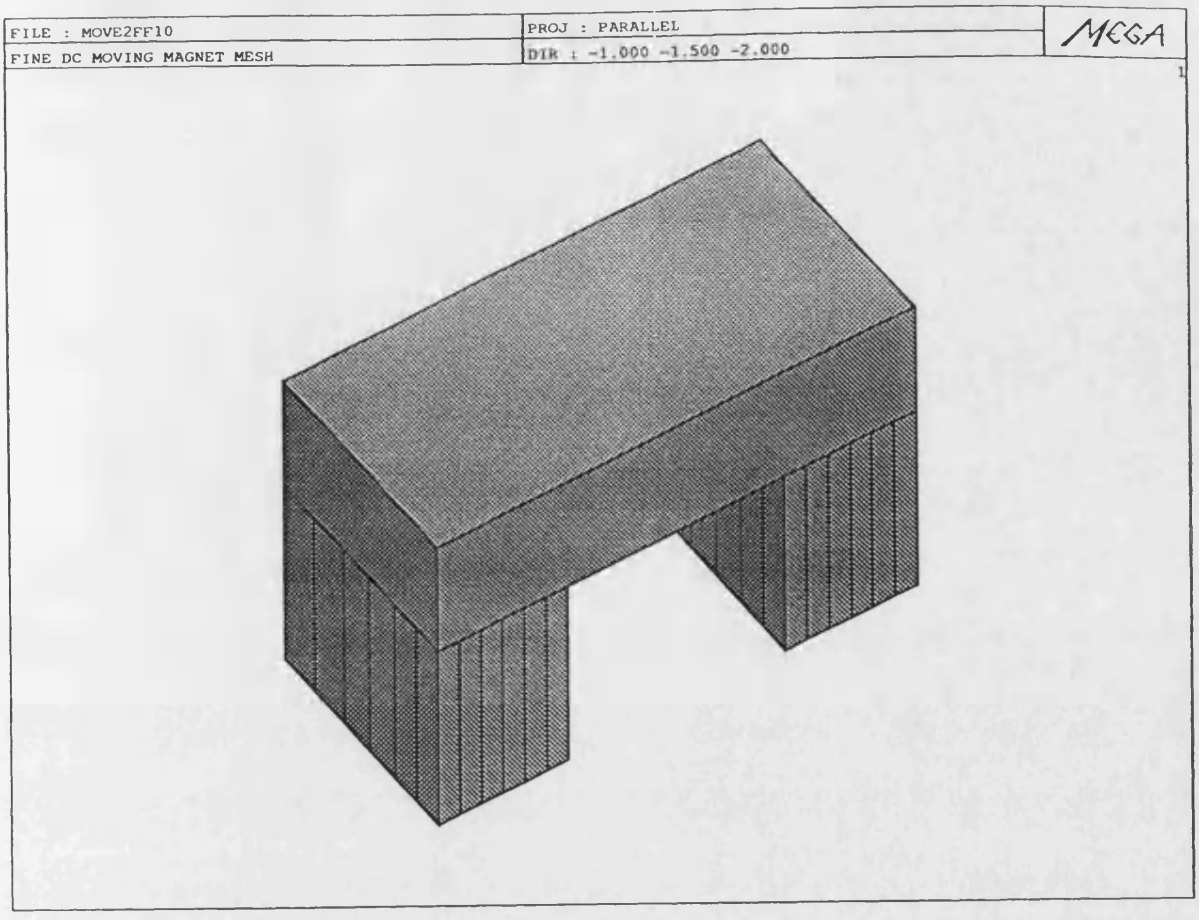

Fig. 4.3 The C core magnet

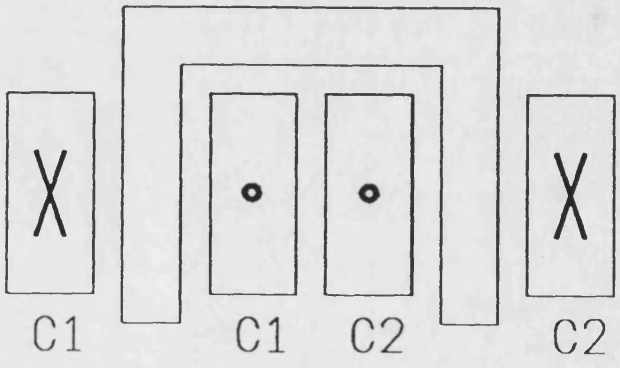

Fig. 4.4 Coils of the magnet and current directions

magnet perpendicularly to the top plane of the cage, are used to measure the normal force. The overall details of the magnet and the drum rotor are exhibited in table 4.1, and fig 4.5 shows a 3D computer view of the magnet with the coils.

4.4.1 Measurements

The normal force, drag force and normal air gap flux density measurements were carried out. A gaussmeter and a hall-effect sensor are arranged for the flux measurements. The sensor is placed in the air gap, and distanced equally from the magnet and the rotor. The results presented in fig 4.8 are obtained at several points along the air gap while the drum rotates at 10 m/s.

Two different types of transducers are employed for the force measurements. The normal force is measured by means of three Kistler type piezo-electric quartz transducers, together with a charge amplifier. The output voltage of the amplifier is read by a digital voltmeter. For the drag force, a strain gauge load cell is used. All the force measurements were carried out at various speeds from standstill to the maximum of 20 m/s. The results taken from force measurements are displayed in table 4.3 and in figs. (4.9) and (4.10).

4.4.2 3D Finite Element Model

A 3D FE representation of the magnet is generated, and modelled with both formulations of which one requires the electric scalar inside the eddy region as in section (2.3.3), and the other does not as in section 4.2.

Due to symmetry, as it is shown in fig 4.6, only half of the magnet is sufficient to be modelled for this particular problem. The boundary conditions resulting from the symmetry must be satisfied. According to the description of symmetry, the currents only exist in the normal direction to the symmetry plane, therefore the magnetic field is tangential to the plane (only x and y components). This will lead to $\mathbf{A_x=A_y=0}$ on the conductor symmetry plane being imposed. If the normal component of the magnetic field is zero on the boundary, in case of **A** modelling the domain, the Dirichlet boundary condition which sets **A=0** is in force, and in case of Φ, the Neumann boundary condition which sets the normal derivative of the field to zero is in force.

The 3D mesh is exhibited in fig. 4.7. Despite the round drum rotor, the model includes only planar elements for simplicity. This can be justified by having a constant air gap between the magnet and the drum. The drum diameter (0.305 m) is quite big compared with the length of the magnet (0.044 m) so errors will be small.

In the model, all the iron parts are assumed to be non-conducting and have a linear permeability. The conductivity of the eddy region is also assumed to be

reduced scalar region where no ferro nor conducting materials exist. Table 4.2 indicates the material property values that are used in the model. Some information about the geometrical mesh such as the number of nodes, elements etc. is included in the same table as well.

4.5 Results and Conclusion

The problem involving 3D eddy currents generated by velocity effects have been investigated. The flux density at u=10 m/s, and the drag and normal forces at various speeds are plotted in figs. 4.8, 4.9, 4.10 respectively. The induced currents in the conducting plate (at u=10 m/s) are also included in figure 4.11. As it can be noted from force and normal flux density results presented in table 4.3, and in figs 4.8-4.10, the new method has produced almost identical results with the old method. However, the removal of the electric scalar, as presented in table 4.4, has led to 2.1 times less consumption of cpu time for the solution. Therefore the use of new method, from the cost point of view, can be extremely significant especially when the number of unknowns involved in the problem is high. The experimental results shown with the computed results verify the point that the removal of $\mathbf{V}$ will not lead to inaccuracy in the solution of moving conductor problems.

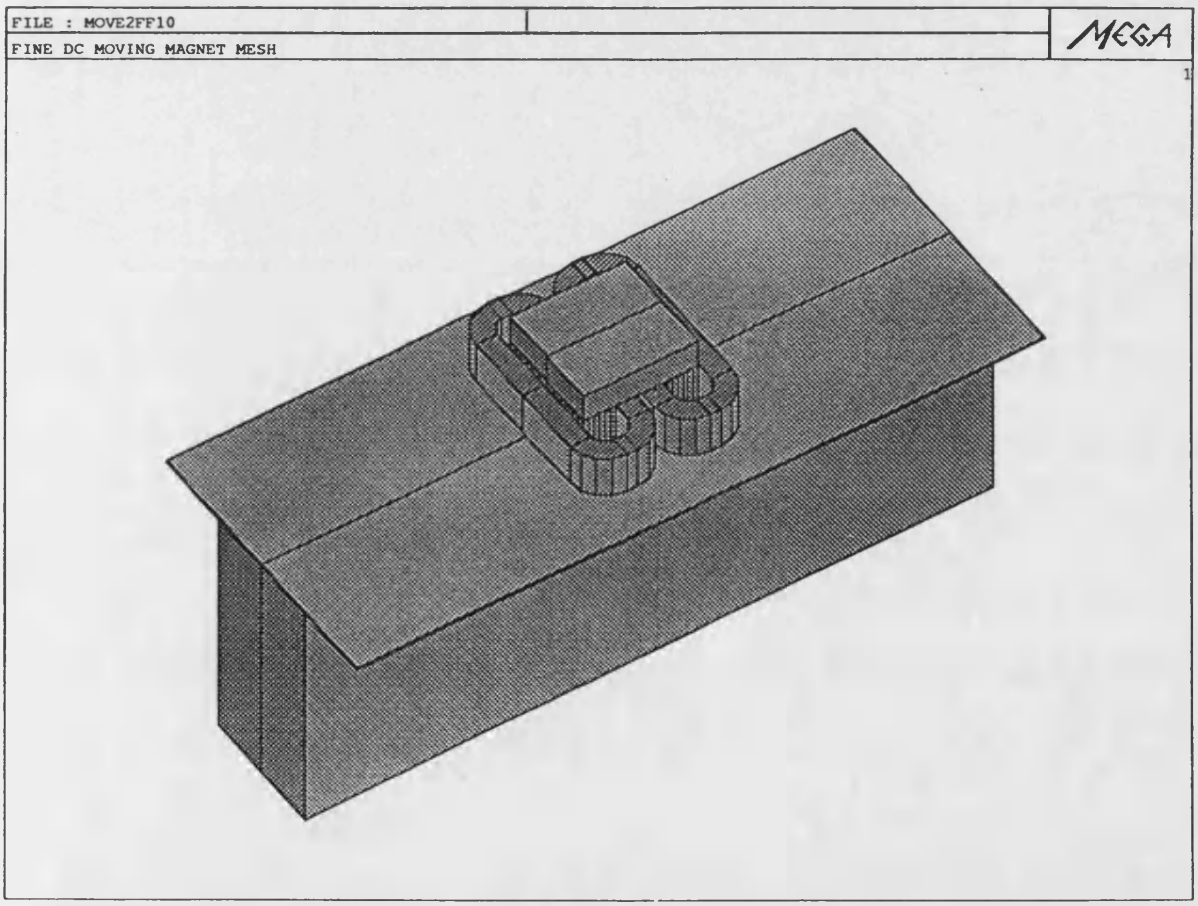

Fig. 4.5 3D view of the magnet

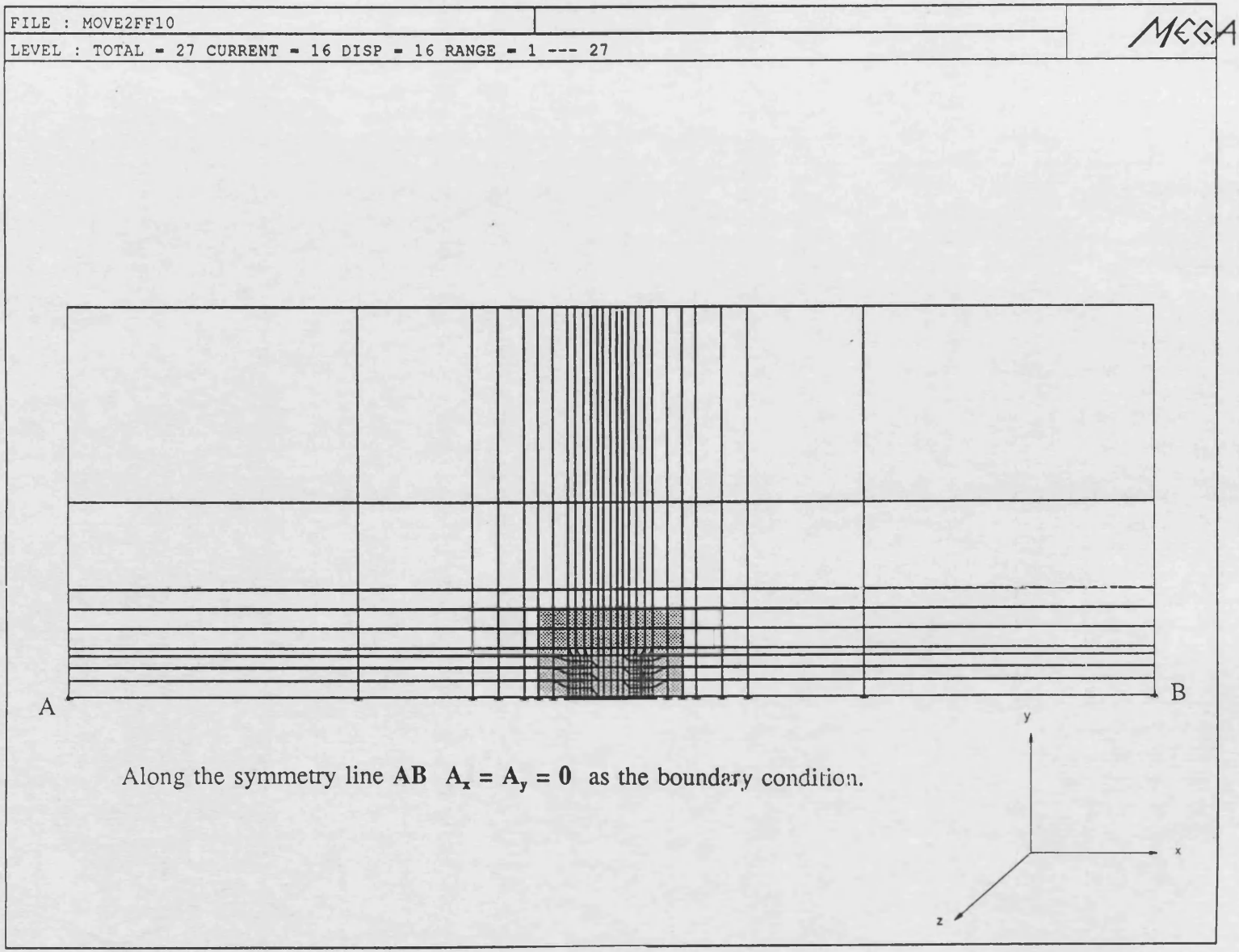

Fig. 4.6 Symmetry line and the boundary conditions

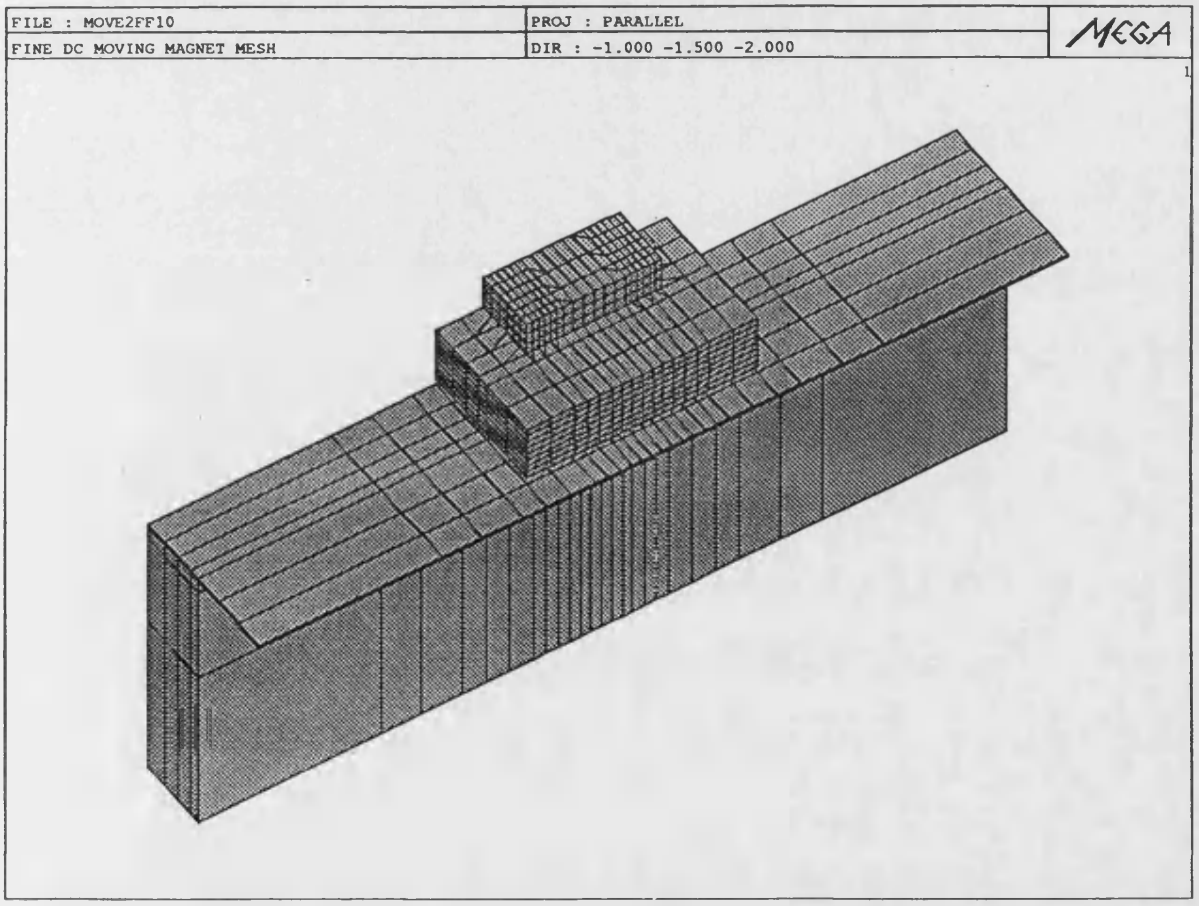

Fig. 4.7 3D mesh

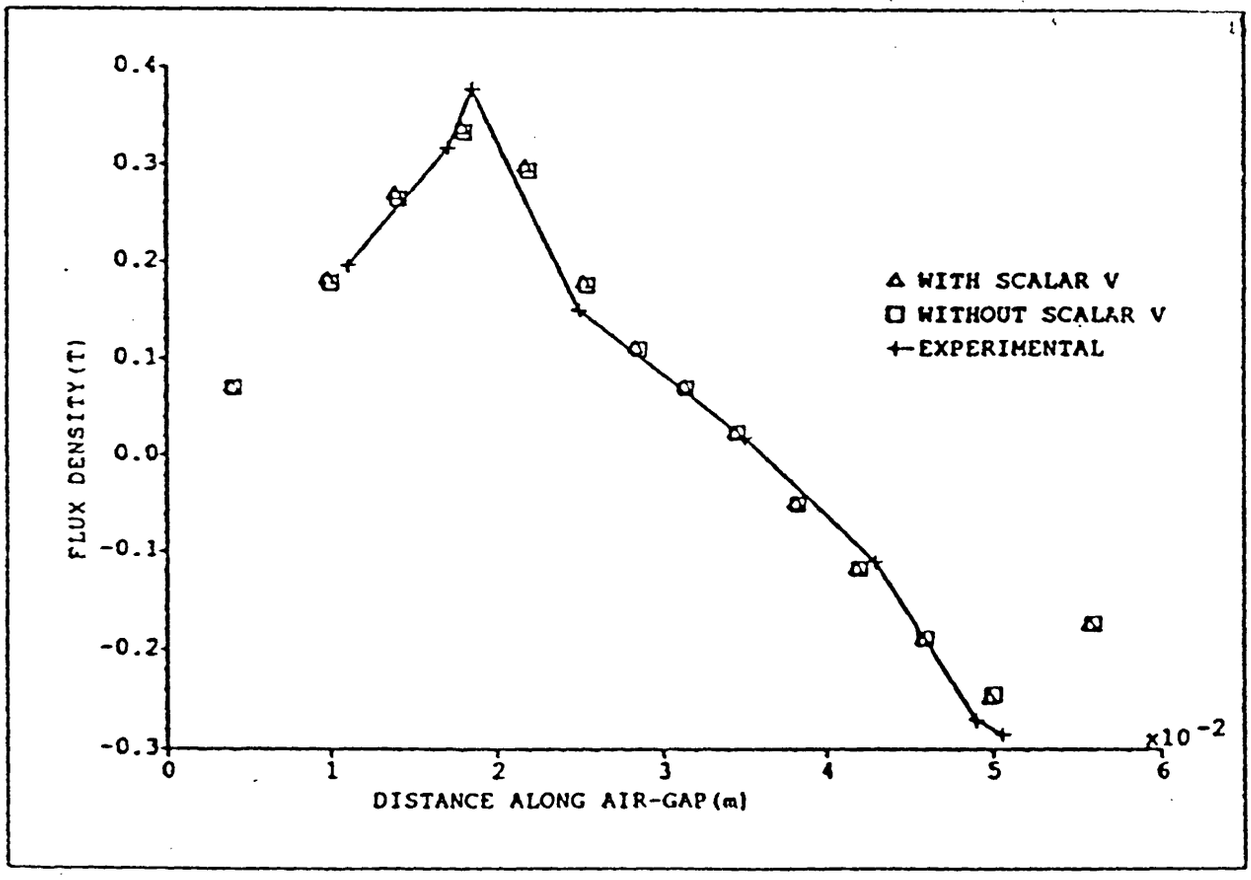

Fig. 4.8 Normal flux density - distance characteristics (in the middle of air-gap)

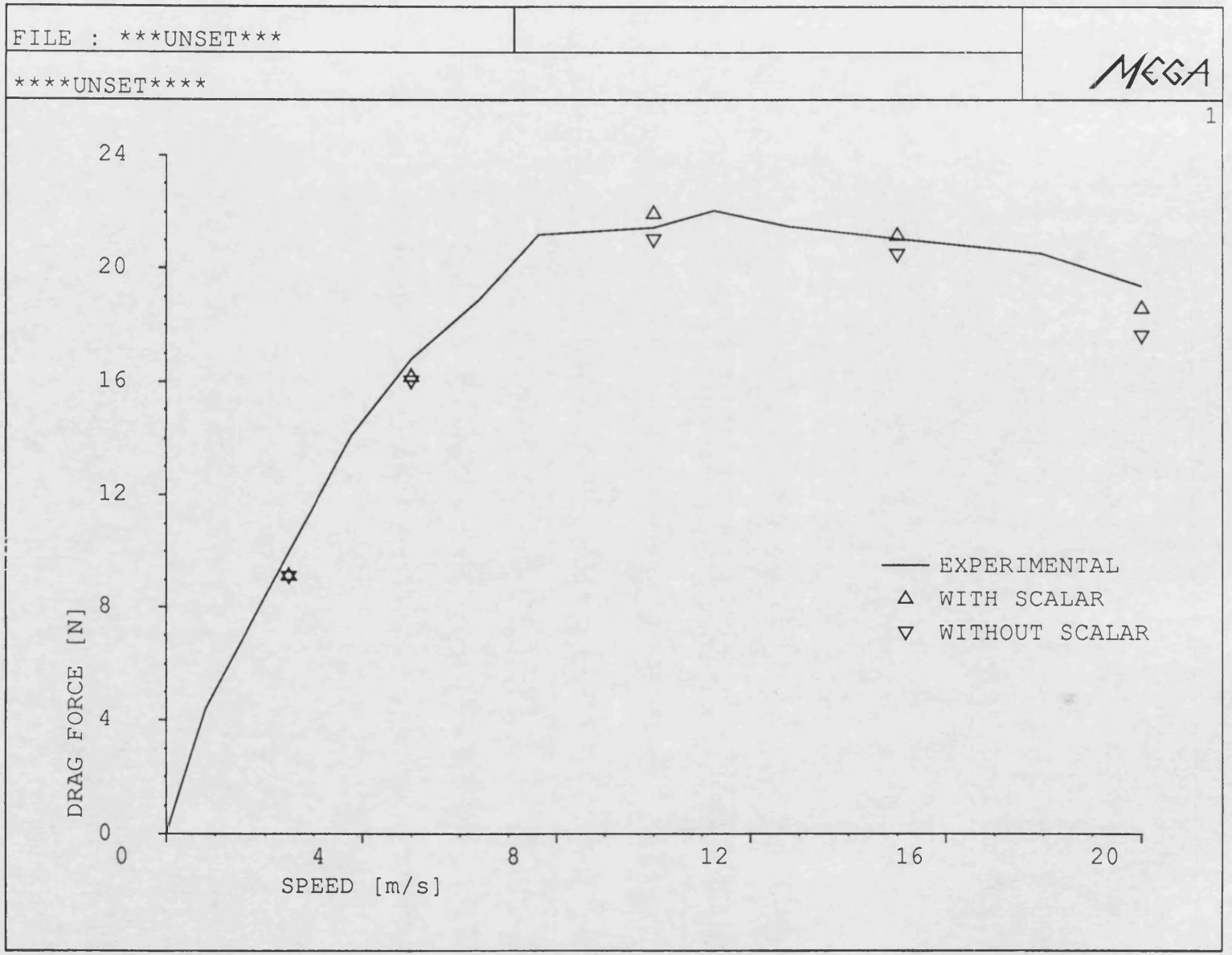

Fig. 4.9 Drag force - speed characteristics with and without V in the formula.

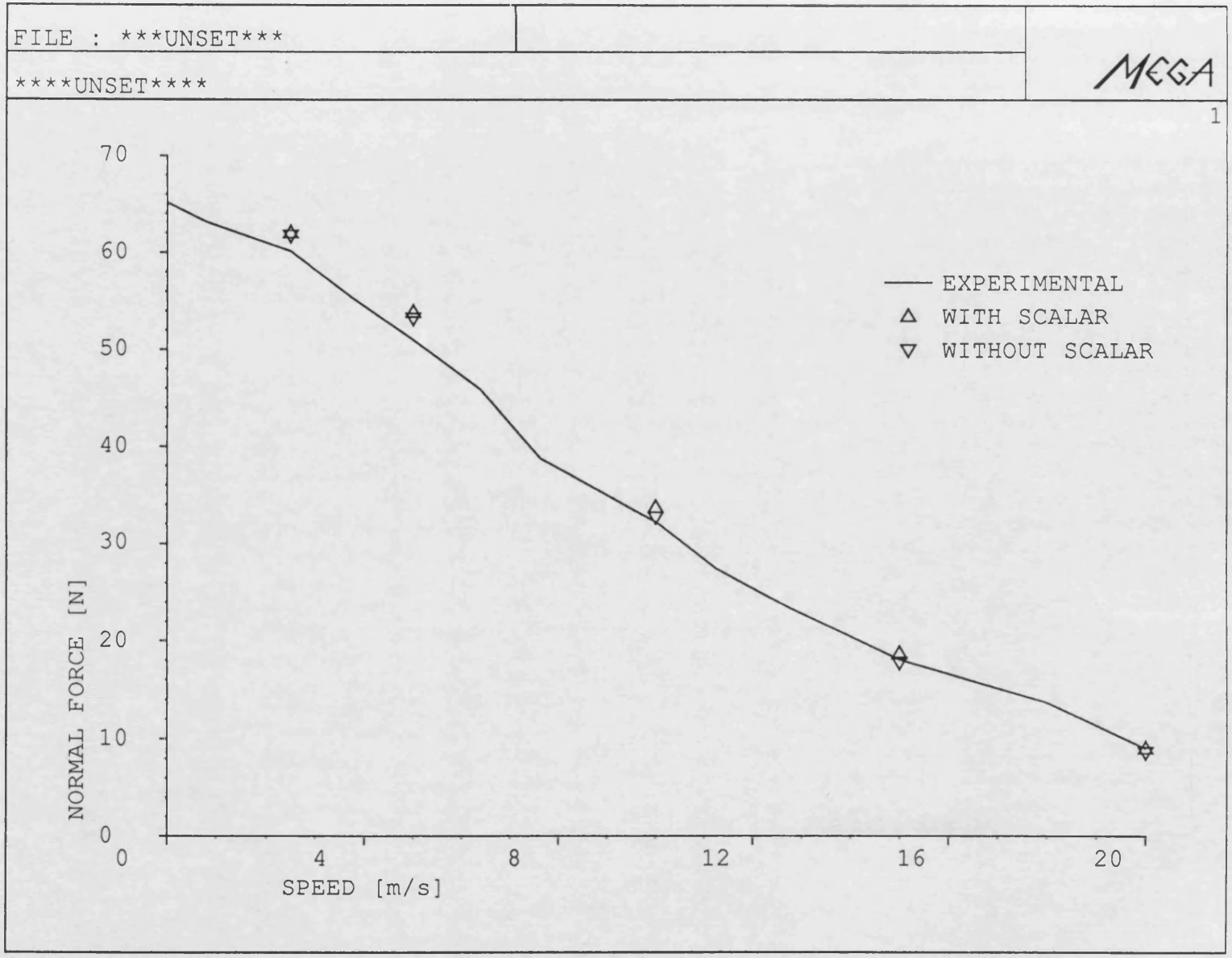

Fig. 4.10 Normal Force - speed characteristics with and without V in the formula

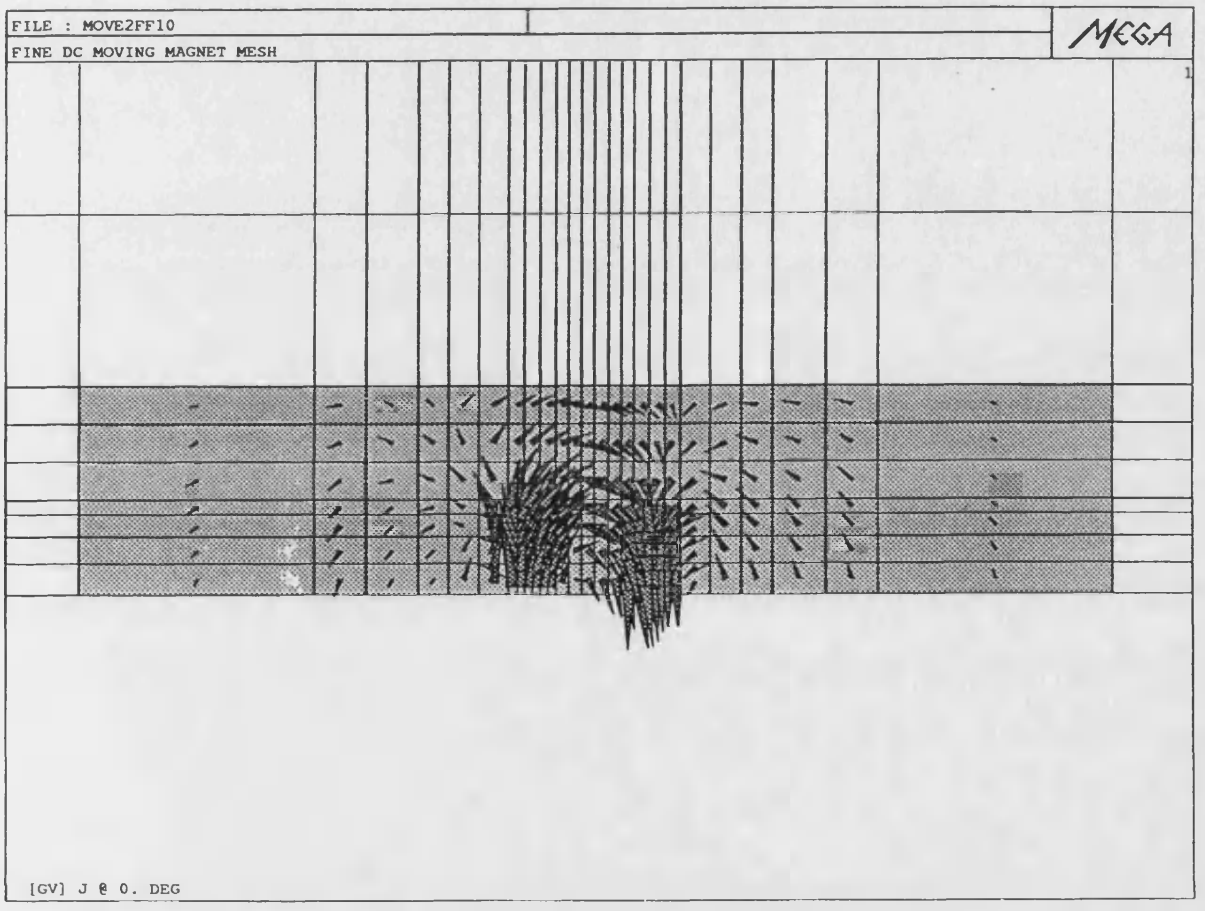

Fig. 4.11 Current vectors on the conducting plate at 10 m/s

Magnet Yoke height	42 mm
Magnet yoke width	12 mm
Magnet slot width	20 mm
Magnet tooth width	12 mm
Magnet air gap	2.5 mm
Drum steel width	50 mm
Drum steel radius	305.88 mm
Drum aluminium	110 mm
Drum aluminium	0.90 mm
Number of turns of coil	189

Table 4.1 Details of the Magnet and drum rotor

Total nodes	5160
Total elements	4256
Nodes per level	258
Elements per level	224
Number of levels	20

Table 4.2.a Details of the 3D geometric mesh of magnet

	Relative permeability (μ_r)	Conductivity (σ) S/m
Magnet iron	500	0
Air	1	0
Aluminium plate	1	$3.2 * 10^7$
Rotor iron	500	0

Table 4.2.b Physical properties used in the model

V Speed [m/s]	F_0 Drag Force [N]	F_N Normal Force [N]
0.00	0.00	65.10
0.80	4.42	63.08
2.50	9.95	60.16
3.80	14.10	55.20
5.00	16.80	51.00
6.40	18.91	45.90
7.65	21.20	38.75
10.00	21.45	32.25
11.25	22.05	27.50
12.80	21.52	23.30
15.00	21.08	18.10
17.95	20.59	13.85
20.00	19.43	9.13

Table 4.3 Force Measurements

	With V	Without V
Number of equations	7351	6763
Number of iterations for the convergence of bi-conjugate gradient method	152	107
Charged CPU time	12:47:30	6:56:23

Table 4.4 The Comparison of the 2 Formulations at 10m/s

CHAPTER 5

TWO PHASE LINEAR INDUCTION SERVOMOTOR

5.1 Introduction

Only DC types of moving conductor problem have been dealt with in the previous chapters. However AC type of moving conductor problems are also common in applications. Therefore the solution of them by means of numerical or analytical methods is significant.

The present chapter comprises the application of the methods that were used in only DC problems earlier, to an AC problem. A two phase linear induction servo motor is selected for the sample problem. Initially a simple procedure is followed for the design. Then the Fourier analysis method is applied for an analytical solution. After solving the problem by means of previously developed FE techniques in 2D and 3D, all these results are compared with the experimentally obtained results.

5.2 The 2-Phase Linear Induction Servomotor and Its Design

2-Phase linear induction machines are simply the linear adaptation of the conventional 2-phase rotary machines. This adaptation from a conventional rotary machine can be easily carried out by a radial plane-cut and, replacement of the rotor by a conducting plate. Servomotors are commonly used in high performance control

systems and most often their power varies from a few watts to 1000 watts so that they are classified as small power machines.

In general use; a servomotor has two windings, called reference and control windings that are electrically 90 degrees displaced from each other. In practice, normally the amplitudes of the currents in the two windings are not the same. The force or torque output is controlled by adjusting the amplitude of the control winding voltage. The schematic of windings of a 2-phase servomotor is shown in fig 5.1.

5.2.1 The Air-gap Equation and Force

For an analytical solution to the performance of the servomotor, it is assumed that the servomotor is connected to a constant current source and the control winding is fed with a current whose phase differs 90 degrees from the reference phase. Due to the very high rotor resistivity that servomotors normally have, the stator impedance can be neglected. This leads to a constant current approach that is more desirable and simple than a constant voltage approach from the analytical solution point of view. The current density of the reference and control phases can be expressed as in ref. [5.1] ;

$$J_R = J_{S1} \cos\frac{\pi x}{s} \sin\omega t \qquad (5.1)$$

and

$$J_C = -J_{S2} \sin\frac{\pi x}{s} \cos\omega t \qquad (5.2)$$

where s is pole pitch. Then the total current density J_s is found as:

$$J_S = \frac{J_{S_1} + J_{S_2}}{2} \sin(\omega t - \frac{\pi x}{s}) + \frac{J_{S_1} - J_{S_2}}{2} \sin(\omega t + \frac{\pi x}{s}) \qquad (5.3)$$

The expression 5.3 includes the forward and backward components of the total current density. If these components are replaced in the air-gap equation which is obtained in appendix 5.1 as

$$\frac{\partial^2 B_y}{\partial x^2} - \frac{\mu_0 \sigma u_x}{g} \frac{\partial B_y}{\partial x} - \frac{\mu_0 \sigma}{g} \frac{\partial B_y}{\partial t} = \frac{\mu_0}{g} \frac{\partial J_S}{\partial x} \qquad (5.4)$$

where g is the air gap length and u_s is the speed of rotor. Then the flux waves can be found for these forward and backward components respectively as

$$B_F = \frac{\frac{1}{2}[J_{S1} + J_{S2}] \left[\left(\frac{\rho_r}{u_s} \right) \left(\sigma + \frac{j}{G} \right) \right]}{\left(\sigma^2 + \frac{1}{G^2} \right)} e^{j(\omega t - \pi x/s)} \qquad (5.5)$$

$$B_B = \frac{-\frac{1}{2}[J_{S1} - J_{S2}] \left[\left(\frac{\rho_r}{u_s} \right) \left((2 - \Omega_s) + \frac{j}{G} \right) \right]}{\left((2 - \Omega_s)^2 + \frac{1}{G^2} \right)} e^{j(\omega t + \pi x/s)} \qquad (5.6)$$

where ρ_r the rotor resistivity and defined as ρ/t_r, (t_r is thickness of the rotor conducting plate), u_s is speed of the stator field, Ω is slip, G is the goodness factor, defined in reference [5.1] as

$$G = \frac{2s^2 \mu_0 f}{\pi g \rho_r} \tag{5.7}$$

Once the flux density and the total surface current density are known at any point along the air-gap of the machine the produced torque or force can be evaluated easily. The torque is decribed as:

$$T = \frac{sp}{2\pi} \int_0^{2sp} Re\{\bar{B} J_s\}\, dx \tag{5.8}$$

By using equations (5.3), (5.5) and (5.6), the torque therefore force can be obtained [5.1]. In general, the force is expressed as:

$$F = T\frac{\omega}{u_s} \tag{5.9}$$

so that, the eqn. above will yield the force at standstill as:

$$F = \frac{\rho_r s p^2}{u_s}\left[\frac{J_{S_1} + J_{S_2}}{1 + G^2}\right] \tag{5.10}$$

5.2.2 Basic Requirements and a Simple Design of the Servomotor

The main function of a servomotor is to provide the position control against the force or torque. This is why one of the factors of the design is that the servomotor should lead to optimum performance of the servo system rather than of the machine itself. The power factor and efficiency of a servomotor are not as significant as they can be for an energy machine. The driving force or torque should be zero at any

speed when there is no signal applied to the control winding. If the motor is current fed, as it is explained in ref [5.1], this condition is automatically satisfied when the goodness factor G is smaller than 1. The rotor resistivity of a 2-phase servomotor is thus made sufficiently high, so that any operation on the reference phase alone is avoided. And also from the solution of the air-gap equation (5.4) maximum torque or force is obtained when the goodness factor is equal one. These points are clearly discussed in reference [5.1]. As the efficiency is insignificant, in this case, the design of a servomotor mainly involves satisfying the condition that $G \leq 1$. From the description of G in equation (5.7), when the pole pitch and air-gap are fixed, the design problem can be reduced to the selection of a suitable thickness of the conduction plate. In this particular design problem, the air-gap is fixed to 3 mm which is as low as manufacturing and operating techniques allow to yield the forces as high as possible.

In a linear machine; due to the slotted structure of the stator and transfer edge effects that ignored in this simple design process, a new air-gap and rotor resistivity values should be considered rather than the actual ones. Since the actual stator is slotted, the air gap reluctance is higher than that of the unslotted model of stator. A new air-gap is found by using the Carter coefficients given in appendix 5.2. The new increased rotor resistivity thereby decreased conductivity is determined by means of Russel and Norsworthy formulas (see appendix 5.2). Furthermore the length and width of the rotor plate should be sufficient to cover the flux which crosses the air-gap from the stator. The frequency of the supply currents can be variable but the most common 50 Hz supplies are preferred so that complex power amplifiers are not needed in the

operation. The size of the motor was kept small so that it would be easy to construct in the workshop.

By taking all these factors into consideration, the dimensions of the motor shown in fig. 5.2 are specified as in table 5.1. The overall 3D view is also included in fig. 5.3. The coils and current directions are illustrated in fig. 5.4.

5.3 The Application of Layer Theory With Fourier Analysis Technique

Before applying powerful but at the same time possibly costly techniques, in some cases of electromagnetic field analysis simple methods could also produce a satisfactory answer to the problem. Therefore the introduction of these rather easy applicable and programmable techniques and their analysis of accuracy and applicability would be very vital. On the other hand these techniques can also be used in comparison and verification of the other specifically developed techniques.

The layer analysis method is one of these useful tools that can be employed. The method uses the theory which is explained in ref [5.6]. Additionally, in this work, the fourier analysis method which considers each harmonic of the excitation, is combined with the layer theory [5.7]. This can be implemented accordingly with the assumption that infinite series of identical machines are spaced in the direction of motion.

5.3.1 The Model and Some Assumptions

The technique is based on the fact that the model has a number of electromagnetically different regions of infinite extent in the x-direction in accordance with fig 5.5 which illustrates the general model and the coordinate system. The travelling field is produced by an applied current sheet at the interface between two layers, distributed sinusoidally and flowing normal to the direction of motion. The slotted primary structure with its windings is not desirable for the technique. Thus, the actual slotted form is replaced with a smooth surface and the current carrying windings are replaced by fictious infinitely thin current elements, called current sheets each having linear current densities (fig 5.6). The actual air-gap of the device is replaced with an effective air-gap, as described previously, the smooth slotless stator leads to more flux crossing the air-gap than the actual case.

Since the excitation is assumed not to vary in the z- direction, the field quantities are also invariant in the same direction. In the technique, the model consists of regions that are assumed to be all planar. Excluding the top and bottom regions which have infinite thickness, all the other regions are represented with having a finite thickness. All end effects of a typical linear machine and saturation effects of high permeable iron regions are neglected. The specified model is given in fig 5.7 and includes the regions of the servomotor and the current sheets on the surface between the stator iron and the air-gap.

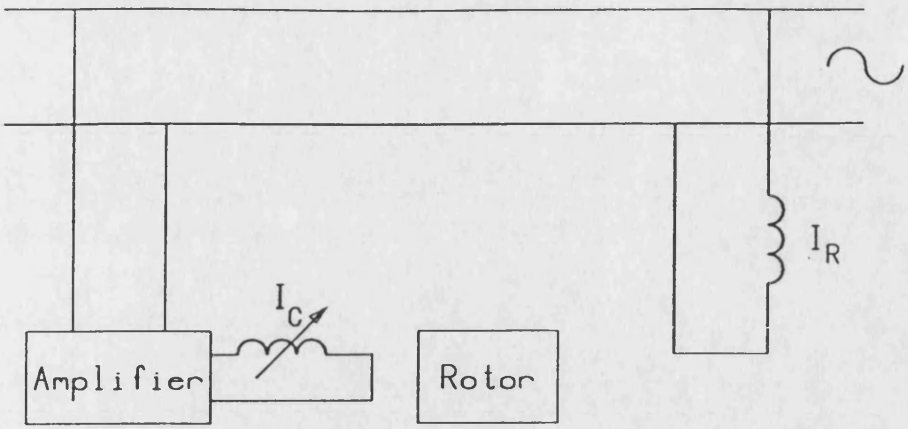

Fig. 5.1 Schematic of windings of a 2-phase servomotor

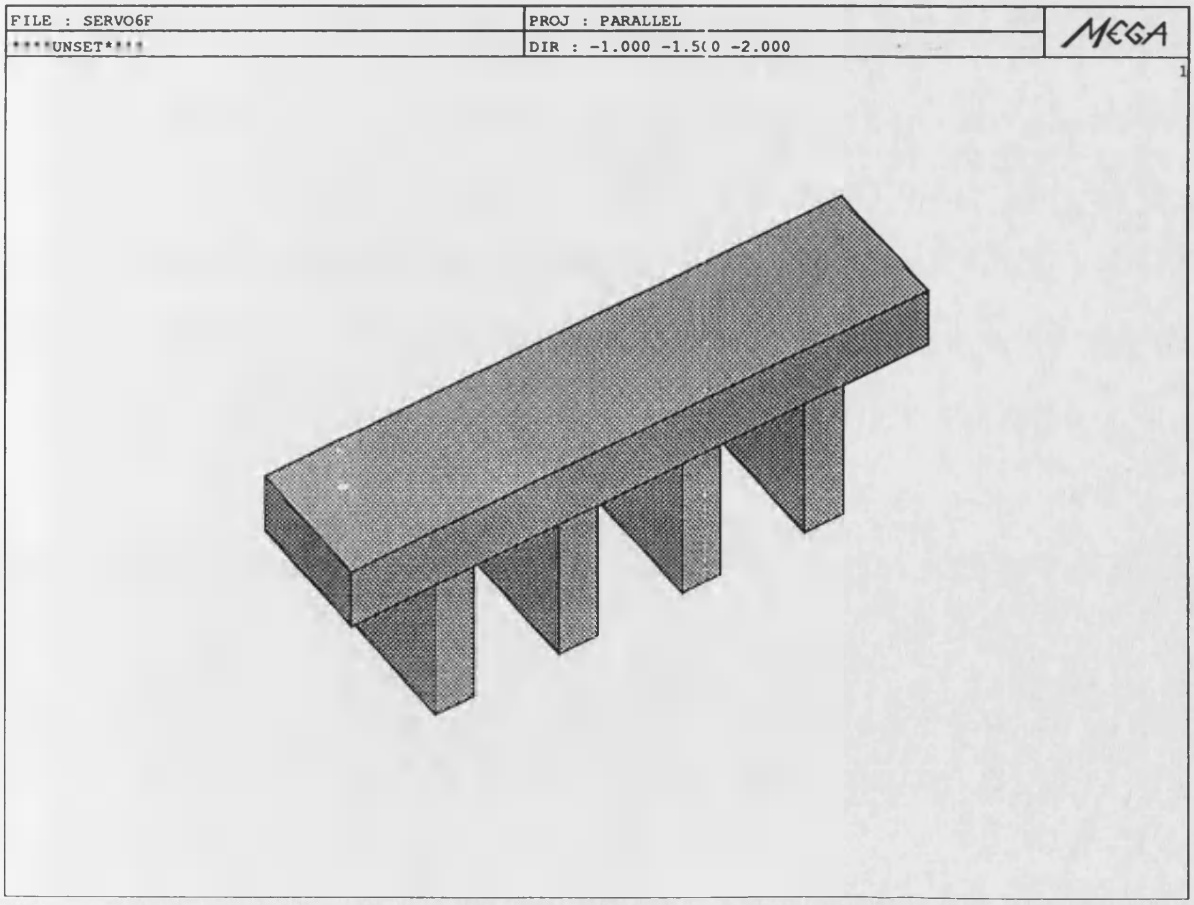

Fig. 5.2 Stator of the servomotor

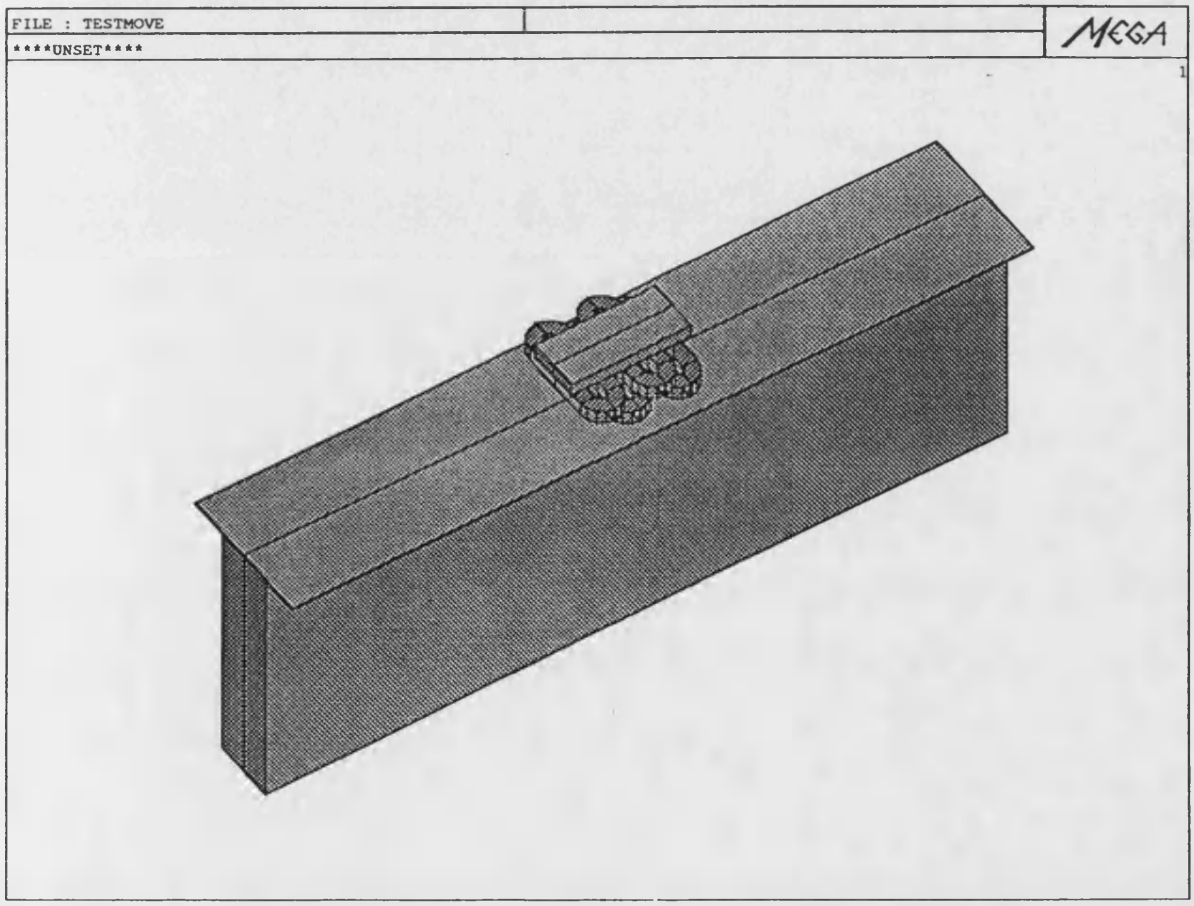

Fig. 5.3 Overall view of the servomotor

Slot width	13 mm
Tooth width	6.5 mm
Air-gap	3 mm
Stator iron width	41 mm
Al-plate width	0.91 mm
Al-plate width	110 mm
Slot depth	25 mm
Back iron stator width	10.5 mm
Diameter of drum	303 mm
Frequency of supply	50 Hz

Table 5.1 Details of the Test Rig and the Servomotor

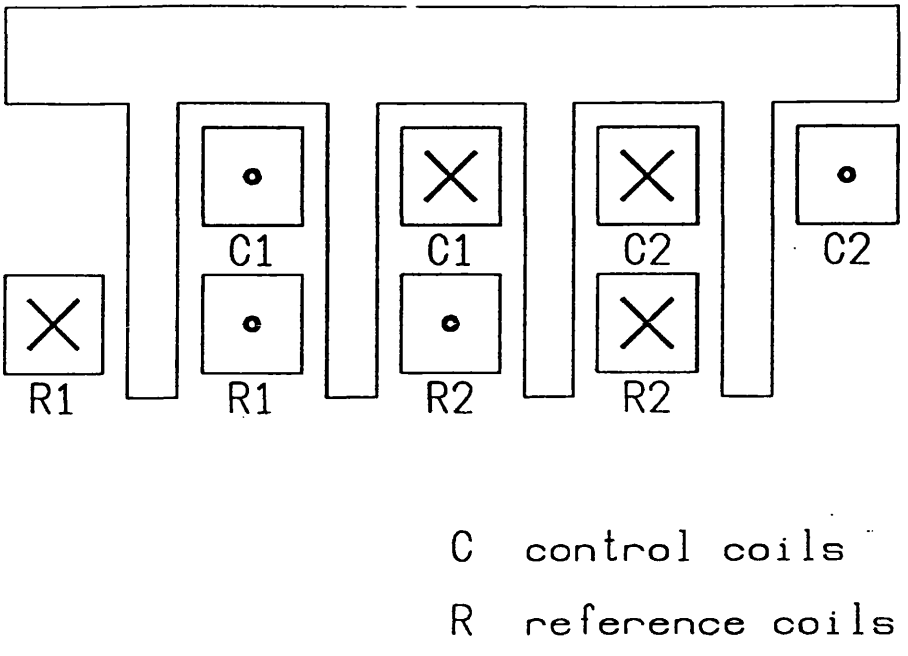

Fig. 5.4 The coils of the servomotor and current directions

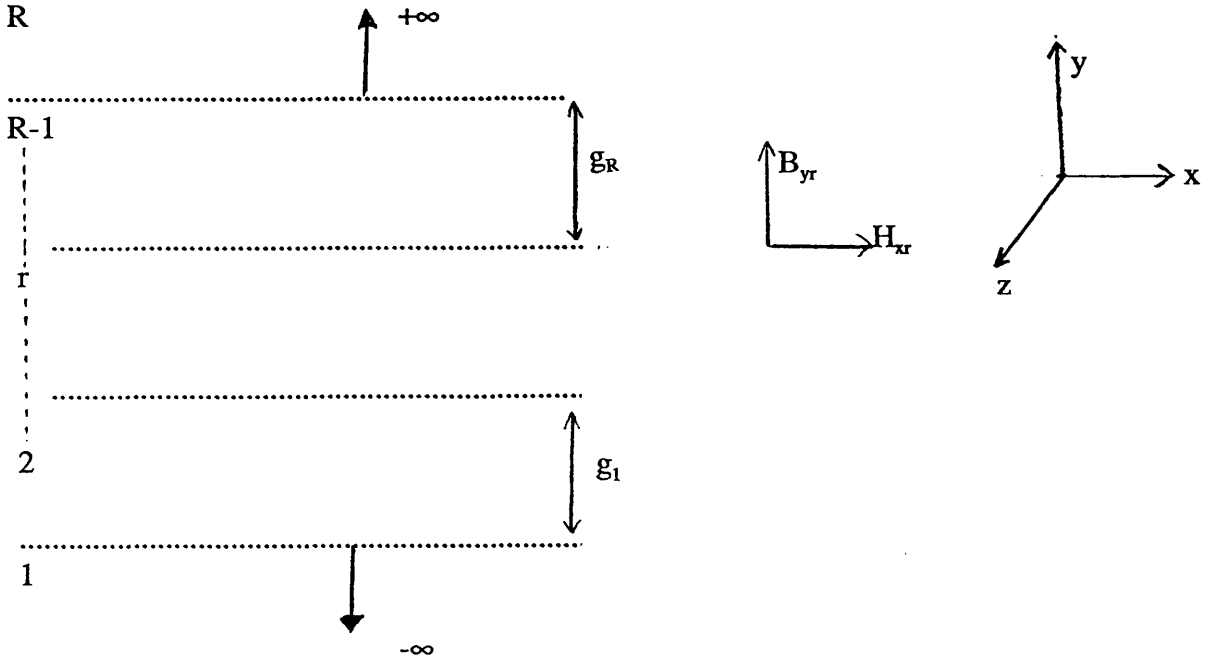

Fig. 5.5 General multi regional layer model

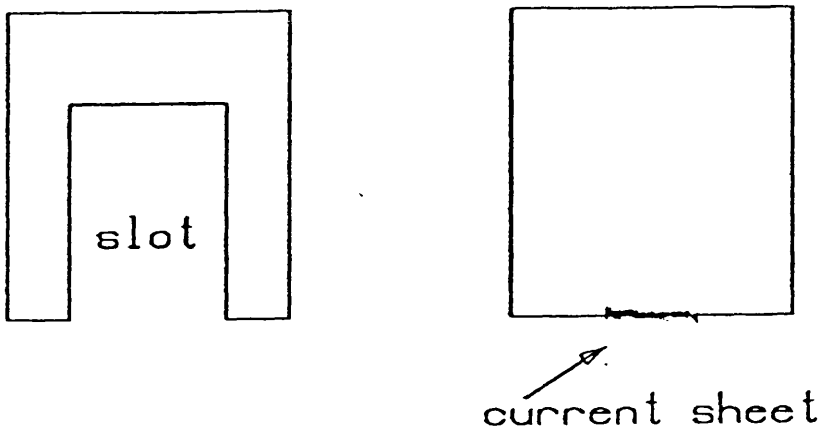

Fig. 5.6 Replacement of a slot with a current sheet

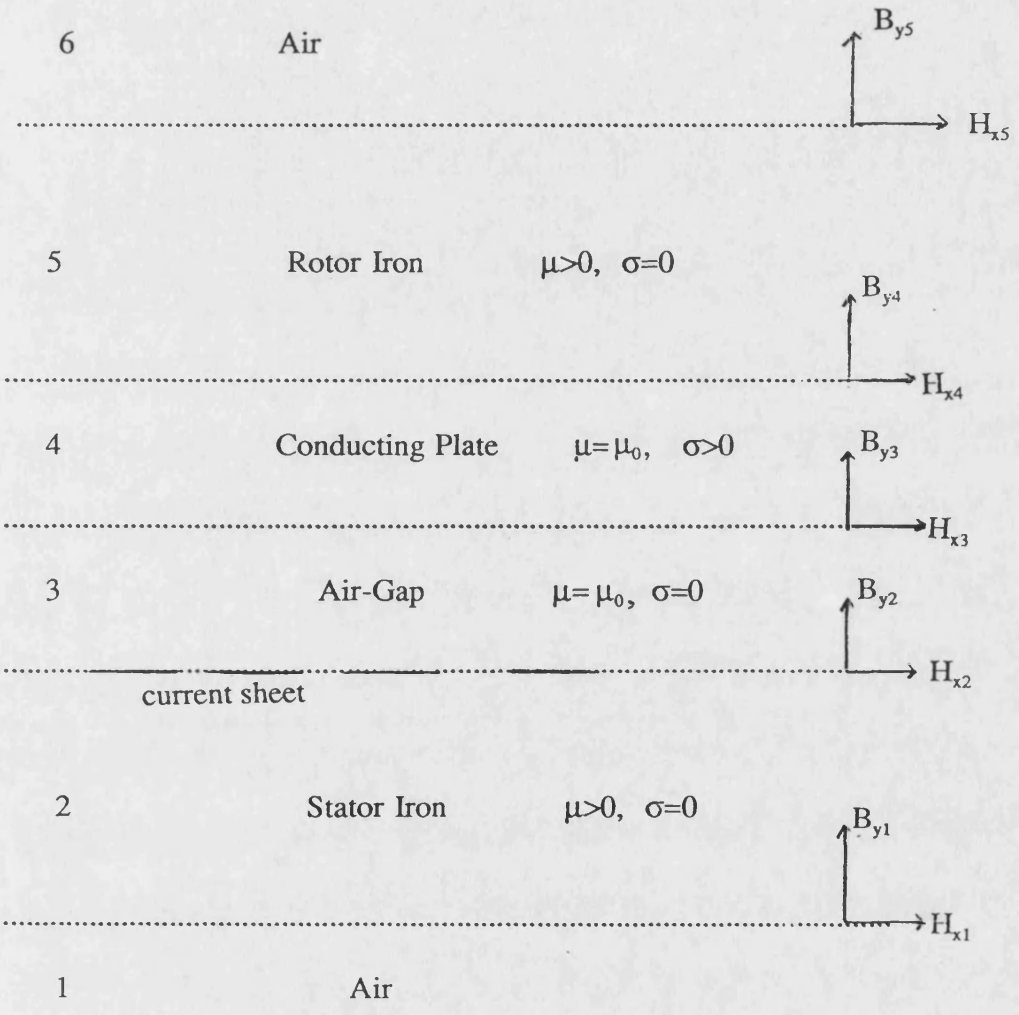

Fig. 5.7 Specified multi layer model for the servomotor

5.3.2 Harmonic Winding Analysis

In general, a slot of machine which is placed on the stator along the air-gap contains a time sinusoidal current represented by I which may be complex. This slot has also N-series conductors of the same phase produces a rectangular pulse of conductor density, fig 5.8. The amplitude of the ***n*.th** harmonic of this pulse can be found by the fourier technique (appendix 5.3). Thus the current density of n.th harmonic for the slot centred at x_m can be determined as described in ref. [5.8]:

$$J_S = \frac{NI}{ML} \sum_{n=-\infty}^{n=+\infty} \frac{\sin(nk\delta)}{nk\delta} \, e^{-jnkx_m} \, e^{j(\omega t + nkx)} \qquad (5.11)$$

In this equation, the forward and backward components of the current density can also be expressed singly when $n<0$ *and* $n>0$ respectively.

If the same procedure is carried out for the other slots and ultimately for the other phases the total current density is obtained by summing up.

5.3.3 The Field Equations

The governing equation to which the layer theory will be applied is also derived from the Maxwell equations. As described in chapter 2; from eqns. (2.2) and (2.7) it can be stated that:

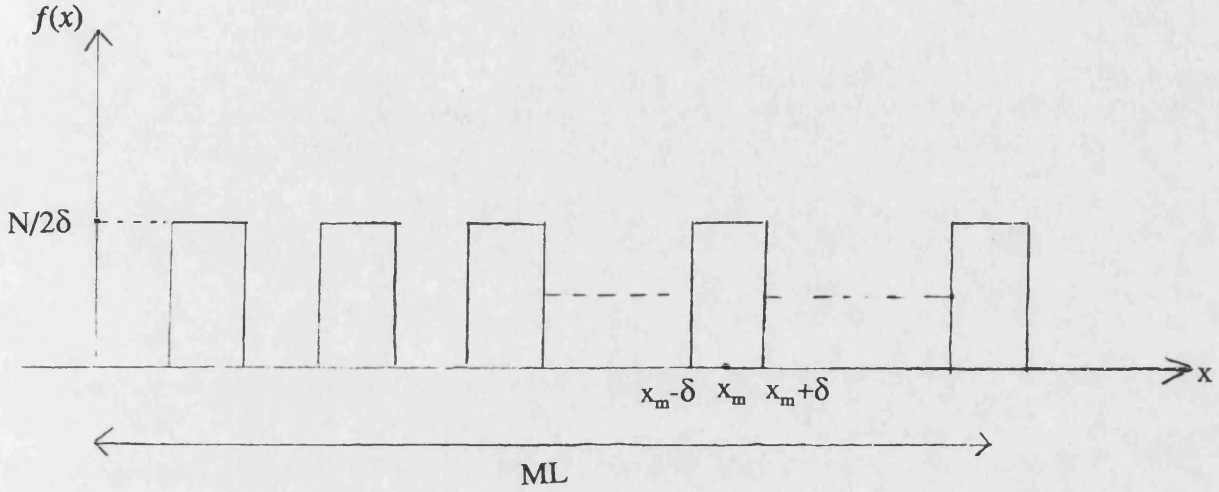

Fig. 5.8 Rectangular pulse of conductor density in slots

$$curl\,\bar{H} = \sigma\,\bar{E} \tag{5.12}$$

If the curl operator is applied to both sides of the equation above, and considering (2.1) and (2.6), while conductivity and permeability are constant then

$$curl\,curl\,\bar{B} = -\sigma\mu\frac{\partial\bar{B}}{\partial t} \tag{5.13}$$

since $curl\,curl\,\bar{B} = -div\,grad\,\bar{B} + grad\,div\,\bar{B}$ and using eqn.(2.3)

$$div\,grad\,\bar{B} = \sigma\mu\frac{\partial\bar{B}}{\partial t} \tag{5.14}$$

is obtained. If the cartesian coordinate system is choosen, and because all the quantities were assumed invarient in the z direction, equation (5.14) can be rewritten as

$$\frac{\partial^2 B}{\partial x^2} + \frac{\partial^2 B}{\partial y^2} = \sigma\mu\frac{\partial B}{\partial t} \tag{5.15}$$

When the normal component of B which is B_y according to the model and the selected coordinate system, are considered together with the form of equation (5.11), then equation (5.15) can be developed further to

$$\frac{\partial^2 B_y^n}{\partial y^2} = (\lambda^2)^n B_y^n \tag{5.16}$$

where $\lambda = (k^2 n^2 + j\mu\omega\sigma)^{1/2}$.

By doing so, the partial differential equation (5.15) has been transformed to an ordinary differential equation (5.16). For the solution of this ordinary diffrential equation, the boundary conditions need to be defined.

5.3.4 The Boundary Equations

Regarding region r in the general model shown in fig. 5.5, the boundary conditions are expressed for 3 different possible cases. The normal component of the flux density By is continuous across a boundary. This is formulated as

$$B_{yr} = B_{yr-1} \tag{5.17}$$

The second condition states that the tangential component of the magnetic field strength H_x is also continuous across a boundary if there is no current sheet, otherwise it is discontinuous.

$$H_{xr} = H_{xr-1} + J_S \tag{5.18}$$

where H_{xr} is just above, and H_{xr-1} is just below the current sheet.
Finally, from the description of the model and the periodic nature of the excitation, all field quantities are specified to vanish at $y = \pm\infty$.

5.3.5 The Solution Method

The general solution of the ordinary differential equation (5.16) is expressed as;

$$B_y = C_1 e^{\lambda y} + C_2 e^{-\lambda y} \tag{5.19}$$

where C_1 and C_2 are the constants to be found.

H_x can also be obtained similarly from eqn. (2.3) which states ***divB=0***, as

$$H_x = -\frac{1}{jkn\mu}\left(C_1 \lambda e^{\lambda y} - C_2 \lambda e^{-\lambda y}\right) \tag{5.20}$$

By obtaining (5.19) and (5.20), the problem is reduced to finding C_1 and C_2 constant values. When using the boundary conditions of (5.17) and (5.18) at a boundary where $y=g_r$, in equations (5.19) and (5.20), C_1 and C_2 can be eliminated. This leads to the solution obtained in transfer matrix form for region r as

$$\begin{bmatrix} B_{yr} \\ H_{xr} \end{bmatrix} = \begin{bmatrix} T_{11}(r) & T_{12}(r) \\ T_{21}(r) & T_{22}(r) \end{bmatrix} \begin{bmatrix} B_{yr-1} \\ H_{xr-1} + J \end{bmatrix} \tag{5.21}$$

where the ***[T]*** matrix is often called the transfer matrix, and the elements of it are given in appendix A5.4

At $y = \pm\infty$, all the field quantities disappear. This requires a different approach for the top and bottom regions. When $y=-\infty$, in equation (5.19) C_2 must be zero, This will yield:

$$B_{y1} = H_{x1} \frac{-jkn\mu_1}{\lambda_1} \tag{5.22}$$

similarly for the top region, the equation below is obtained when $y=\infty$.

$$B_{yR} = H_{xR}\frac{jkn\mu_R}{\lambda_R} \tag{5.23}$$

The value of the field at any point, $y=Y$ which lies between any two layers, for instance $y=g_{r-1}$ and $y=g_r$, may be significant, especially when a precise comparison with the other numerical techniques or experimental results is needed. The values of and B_y at the desired point H_x are obtained as:

$$B_{yY} = \frac{B_{yr-1}}{2}\left[e^{\lambda(Y-g_{r-1})} + e^{-\lambda(Y-g_{r-1})}\right] + \frac{H_{xr-1}(kn\mu)}{2\lambda}\left[e^{\lambda(Y-g_{r-1})} - e^{-\lambda(Y-g_{r-1})}\right]$$

$$H_{xY} = \frac{B_{yr-1}}{2jkn\mu}\left[e^{\lambda(Y-g_{r-1})} - e^{-\lambda(Y-g_{r-1})}\right] + \frac{H_{xr-1}}{2}\left[e^{-\lambda(Y-g_{r-1})} - e^{\lambda(Y-g_{r-1})}\right]$$

The same number of unknowns,(B_y and H_x) and the equations are obtained from (5.21) and the boundary conditions. Thus, the solution of the ***[K] [a] = [b]*** matrix equation (where K is a $m\times m$ dimensional square matrix and mainly consists of the elements of the transfer matrices, b and a are m dimensional column matrixes representing the source excitation term and the unknowns respectively) will be the solution desired.

A simple Fortran 77 programme is used to obtain H_x and B_y values of each region. The region properties such as, frequency, conductivity, thickness etc. are given

as data input. First, the programme calculates the Carter coefficient and the rotor resistivity factor. Then, it determines transfer matrixes of the regions to form the $\boldsymbol{K}$ matrix and the current density to form the $\boldsymbol{b}$ matrix. When these matrixes are obtained, any kind of method which is used to solve a set of simultaneous equations, can be employed. The Gauss elimination method is chosen, as the number of unknowns involved in the problem are relatively small.

By finding all H_x and B_x unknowns all the desirable quantities such as, the flux density distribution in the air-gap, forces, etc can be determined for each harmonic of the excitation. The solution process terminates at the harmonic of n_{max}, further harmonic components of the field are negligible. The total field at any specified point is found by summing all of the harmonics of the field at this point.

5.4 2D Finite Element Modelling of the Servomotor

As already mentioned in the general introduction of the FE method in chapter 2, the 2 dimensional approach can yield much faster and cheaper answers than the 3D one to the problems being tackled here. In the previous section when introducing the layer analysis method to the problem of the servomotor, a considerable number of assumptions were made. Some of these assumptions can be reduced by the 2D FE model. Firstly, the 2D model can model the stator with a finite length so that the end effects which were completely ignored by the Fourier method, can be taken into account. Furthermore the real slotted structure of the stator which was replaced by

fictitious current sheets can also be modelled. Therefore there will be no need in using the Carter coefficients that are introduced for the layer method. However, the general 2D assumption of which the currents are only in the z-direction, and the field does not vary in the same direction, will lead to requiring the Russel and Norsworthy factor to determine the realistic value of the conductivity of the conducting plate.

The methodology for the application of the 2D FE to the servomotor is the same as outlined in chapter 2. But involvement of time variation of the field will renew the description of electric field for the conducting region given in equation (2.8) by adding a new component which represents the new time varying component (transformation effect). Thus, the new formula describing the electric field will be

$$\bar{E} = \bar{u} \times curl\bar{A} - \frac{\partial \bar{A}}{\partial t} - grad V \qquad (5.26)$$

Because the source currents vary sinusoidally, and expressed as in the form of $e^{j\omega t}$ therefore the $\frac{\partial \bar{A}}{\partial t}$ term can be replaced with $j\omega\bar{A}$. If this is considered for a general AC problem, the 2D governing equation for the moving conductor problem can be obtained by simply adding the transformation term into the previous formula used for the DC problems.

$$(div\gamma\, grad)\bar{A} + \sigma(\bar{u} \times curl\bar{A}) - j\omega\sigma\bar{A} = 0 \qquad (5.27)$$

Two meshes were generated to represent the two dimensional geometry of the servomotor. The curvature of the designed stator is taken into account in the mesh shown in fig 5.9. However, by using the mesh which represents the servomotor as

planar, in fig 5.10, very close force results are obtained. Therefore this effect has been ignored for the sake of simplicity in the mesh generation, especially when 3D models are created.

The numerical solution procedure to equation (5.26) follows the same pattern as described in chapter 2 and chapter 3. The upwinding method used for the conducting region when the motion is involved. On the outside boundaries, the homogeneous Neumann condition which sets $\frac{\partial \bar{A}}{\partial n} = 0$ is used. This can only be done if the motor is assumed to be surrounded by infinitely permeable iron box. The magnitude of the current density for each slot is determined by using the ratio of the total current in the slot and the slot area.

5.5 3D Finite Element Modelling of the Servomotor

To obtain the real representation of the motor is impossible unless the third dimension of the motor is modelled. Although the 3D models are more costly than 2D ones, they need to be used when high accuracy is required.

Because of the presence of a time varying field in the servomotor problem, the governing equation of the conducting region will include the additional $j\omega\sigma\bar{A}$ term. And by removing $gradV$ by eqn. (4.2) as explained in chapter 4, the formula is obtained as

$$curl\gamma\ curl\bar{A} + \sigma(\bar{v}\cdot grad)\bar{A} + j\omega\sigma\bar{A} = 0 \qquad (5.28)$$

The solution of field in the non conducting regions is not effected by the presence of the time varying field so that the equations derived for these regions in previous chapters are valid here too.

In the 3D model of the servomotor, similar with the example of the DC magnet, a plane of symmetry exists. Therefore, half of the geometry can be used in modelling, provided with satisfying the necessary conditions arising on the symmetry plane (see section 4.5). On the outside boundaries, the scalar magnetic potentials are set to zero in accordance with the assumption that the motor is surrounded by a highly permeable iron box.

As the number of the unknowns is expected to be very high (up to 30000) initially a coarse mesh was used for modelling shown in fig 5.11. Then the solution is obtained for the finer meshes generated by simply refining the coarse mesh (figs. 5.12 and 5.13). A further refinement is not required as the solution converges when using the finest mesh. This will be discussed in section 5.7.

5.6 Test Rig and Measurements

The prototype servomotor whose dimensions were given in table 5.1 was tested on the test rig which was previously used for testing the DC magnet.

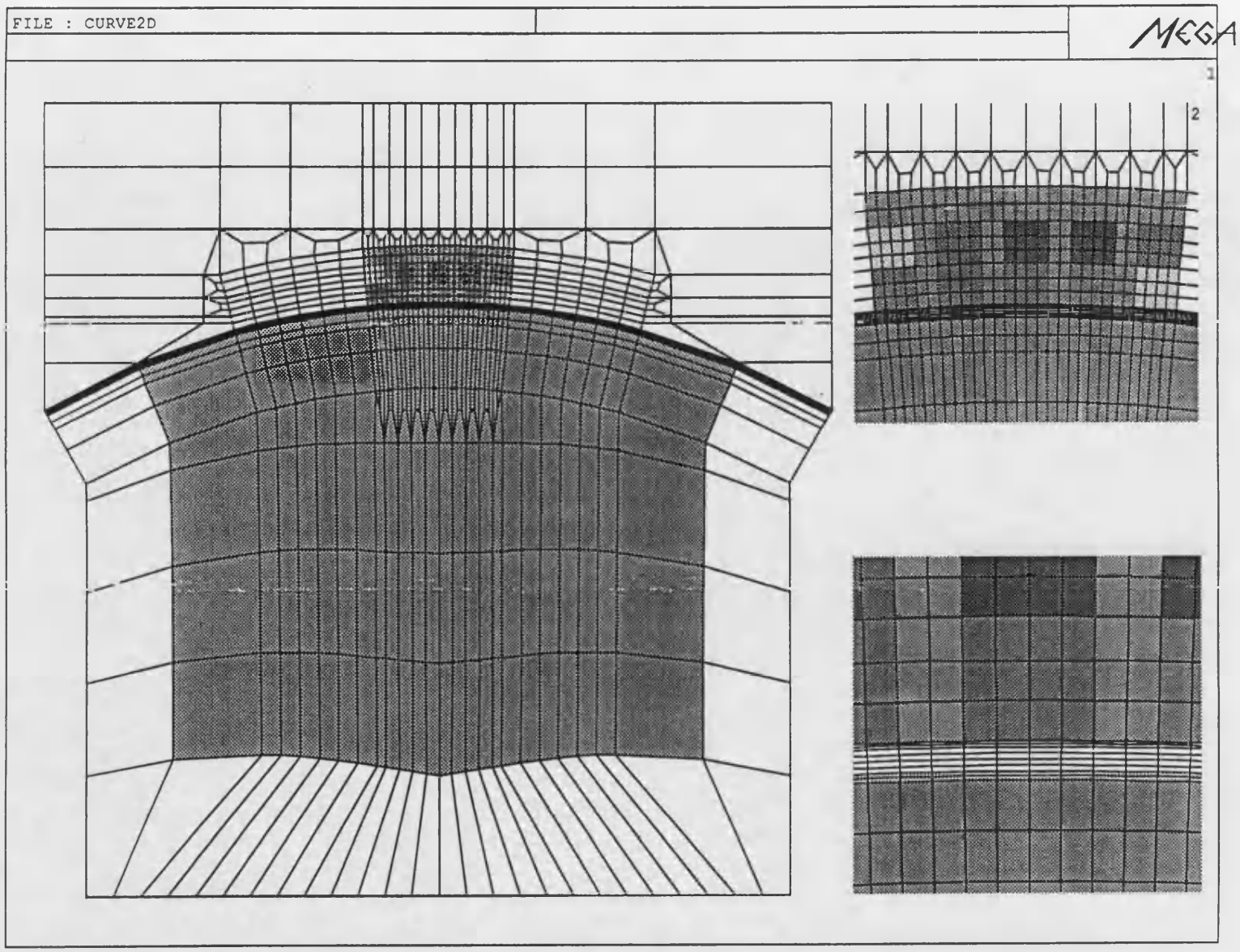

Fig. 5.9 2D FE mesh (curveture)

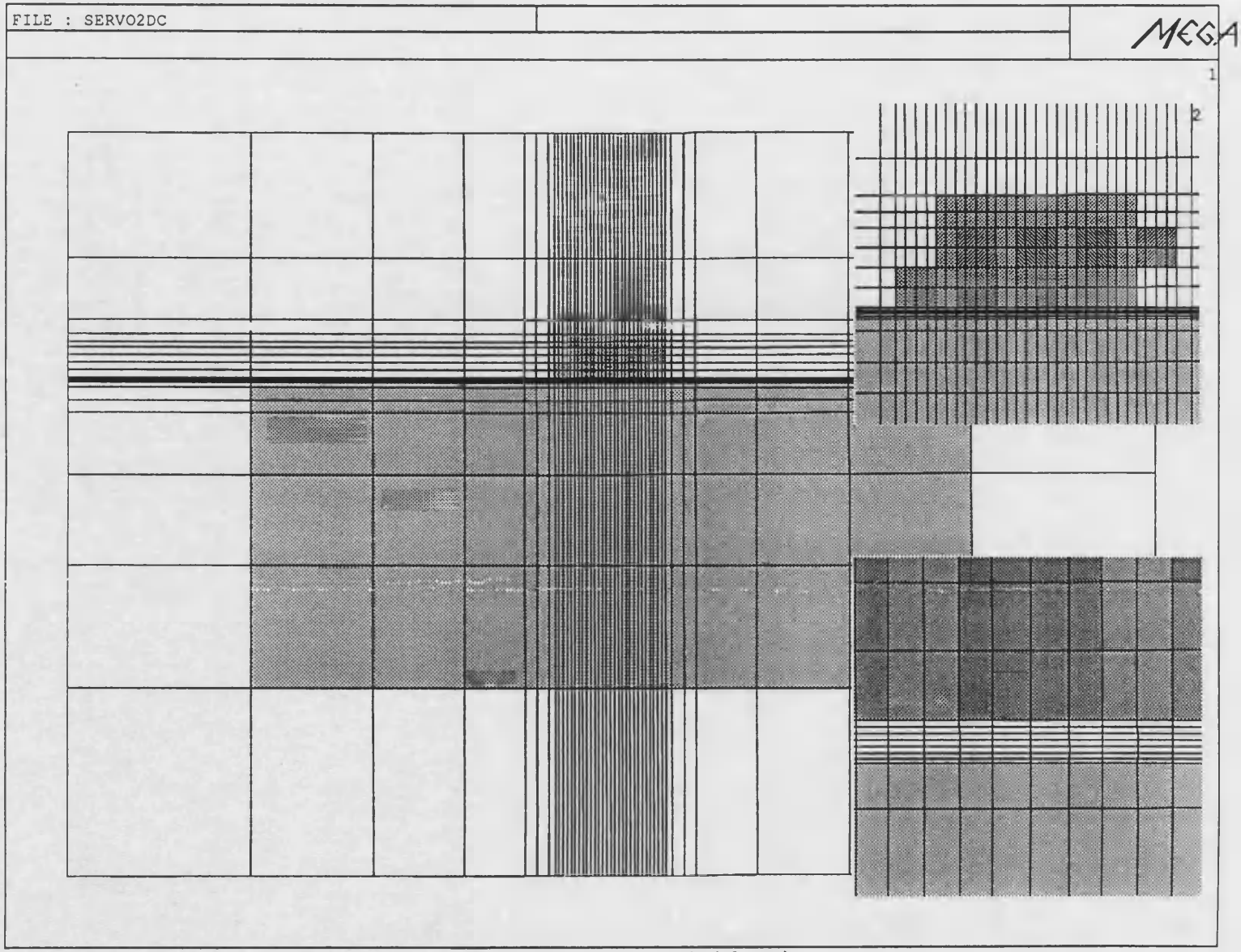

Fig. 5.10 2D FE mesh (planar)

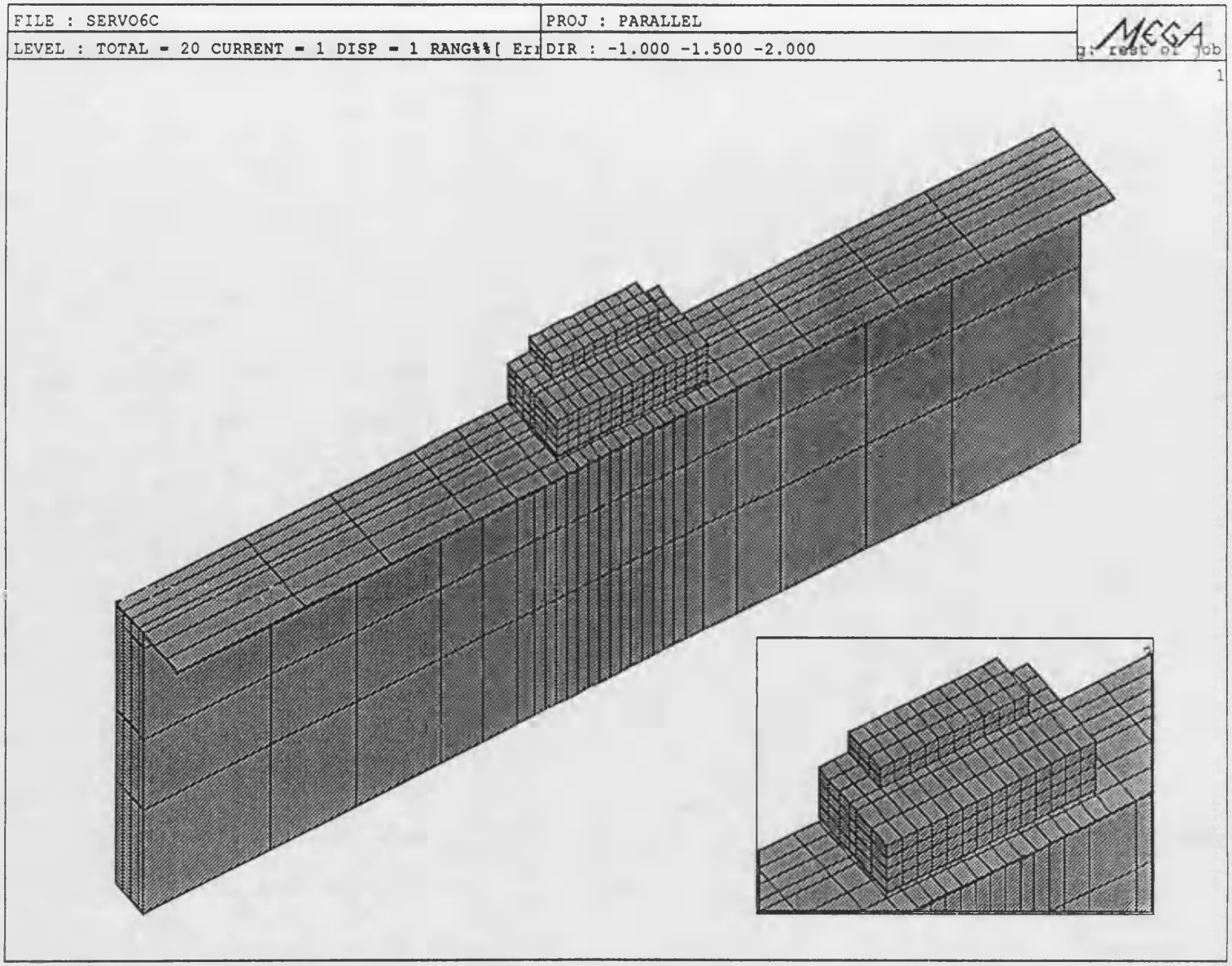

Fig. 5.11 3D FE coarse mesh

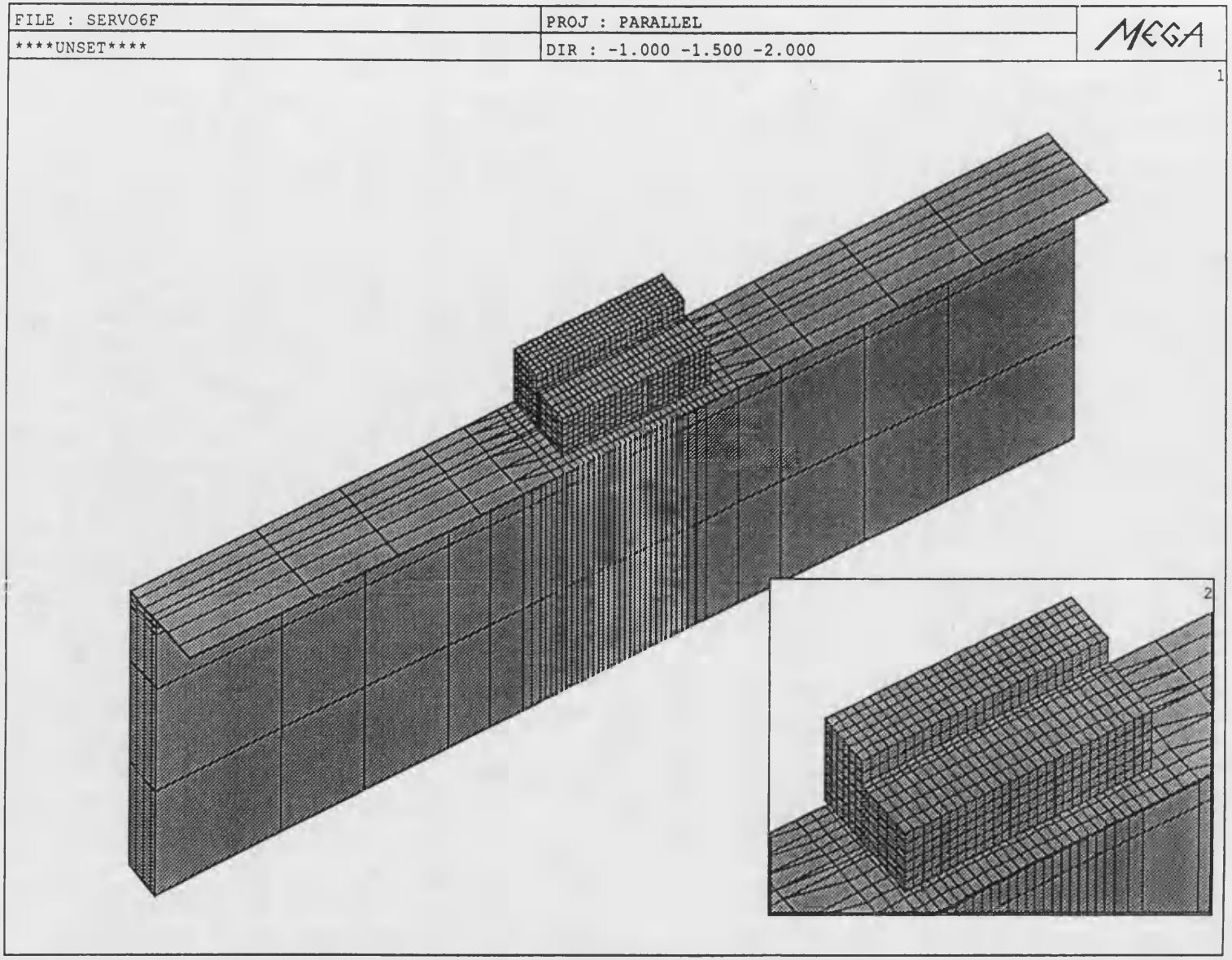

Fig. 5.12 3D FE fine mesh

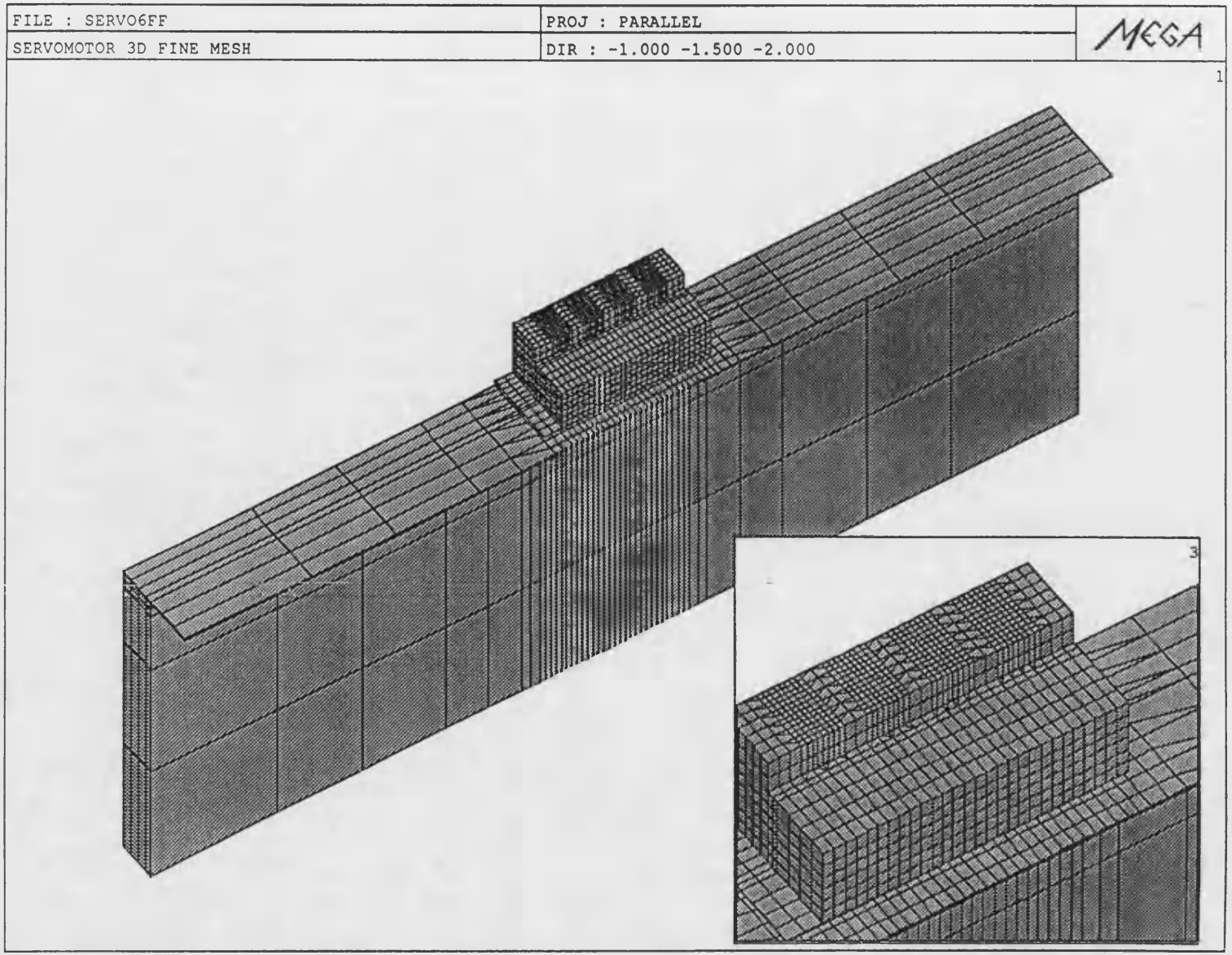

Fig. 5.13 3D FE finer mesh

The windings of the servomotor are fed from an AC source with 50 Hz frequency. The 90 degree phase shift to the phases is obtained by means of the Scott connection, illustrated in fig. 5.14. All the measurements are carried out while both phase currents are fixed at 0.715 A or 500 A-turn. This is considered as an optimum value to be able to avoid the possible nonlinearity effect that ferro materials have, and to obtain measurable drag and normal forces. The BH curve of the laminated iron is included in fig 5.15.

The forces are measured by using the same force transducers used in testing the magnet. However, the flux densities on stator iron were measured by a rather simple method, employing some search coils at certain parts of stator. Actually with this method, initially, the induced voltages between the terminals of the search coils are measured. And, by using the Faraday's law, the time integration of these induced voltages will determine the flux thereby flux densities.

The positions of the search coils are shown in fig 5.16. Two sets of flux density measurements with the drum rotor at standstill, and moving with the speed of 5 m/s, are included in table 5.2. The drag and normal forces measured at different speeds varying from 0 to 10 m/s are also exhibited in table 5.3.

5.7 Results and Conclusion

The results obtained from the layer theory, 2D FE and 3D FE methods are presented in figs.(5.17 - 5.32). The layer theory used in conjunction with the Fourier

analysis method is the simplest and the cheapest one for the solution of the moving conductor problems. The required characteristics for the initial design such as, force-current and force-frequency, etc. can be easily met. Because the layer theory does not consider the end effects, the flux and force are expected higher than the real ones. Even further inaccuracy and poor results are inevitable as the slots are replaced with the current sheets, and the motor is assumed infinitely long in the third direction. This inaccuracy can be easily observed from the force-speed characteristics presented in figs. 5.17 and 5.18. From the same characteristics it can also be observed that if the Carter coefficients and the Russel and Norsworthy factor are determined and used in the solution, considerably high accuracy can still be achieved. And also, as the layer mode involves 6 regions, only 10 unknowns to be found from 10 equations, the time and storage requirement is minimum.

As shown in figs. 5.19 and 5.20, the FE technique can model the end effects. However, it can be concluded from the characteristics depicted in figs. 5.21, 5.22, 5.29 and 5.30 that there is a strong effect of the third dimension in the solution. The error in drag force calculations by the 2D method can be as high as 20%. Therefore, despite being expensive, the 3D models are required for accurate results. The error is reduced to within reasonable 5% band by using 3D meshes. Initially, a coarse mesh involving 7569 unknowns is used. However, the results obtained with a fine mesh with 22093 unknowns differ 9% from the coarse mesh results therefore, a finer mesh is necessary to obtain the convergence. As the mesh involving 33569 unknowns led to only 1% difference with the fine mesh, it is believed that at this point, no further refinement is required. At different speeds and phases, the plots of induced current distribution on the conducting plate, and the flux density vectors, which are obtained

from the fine mesh displayed in figs. 5.23-26. The details of the 2D and 3D models (number of equations, number of iterations, required CPU time, etc) are summarized in table 5.4.

The force results obtained from the numerical methods are all compared with the results obtained from the test rig in fig 5.31 and 5.32. It is obvious that the 3D FE yields the best results. However, the importance of 2D FE and the Layer theory can not be ignored. But without the coefficients it should be accepted that the results look rather poor.

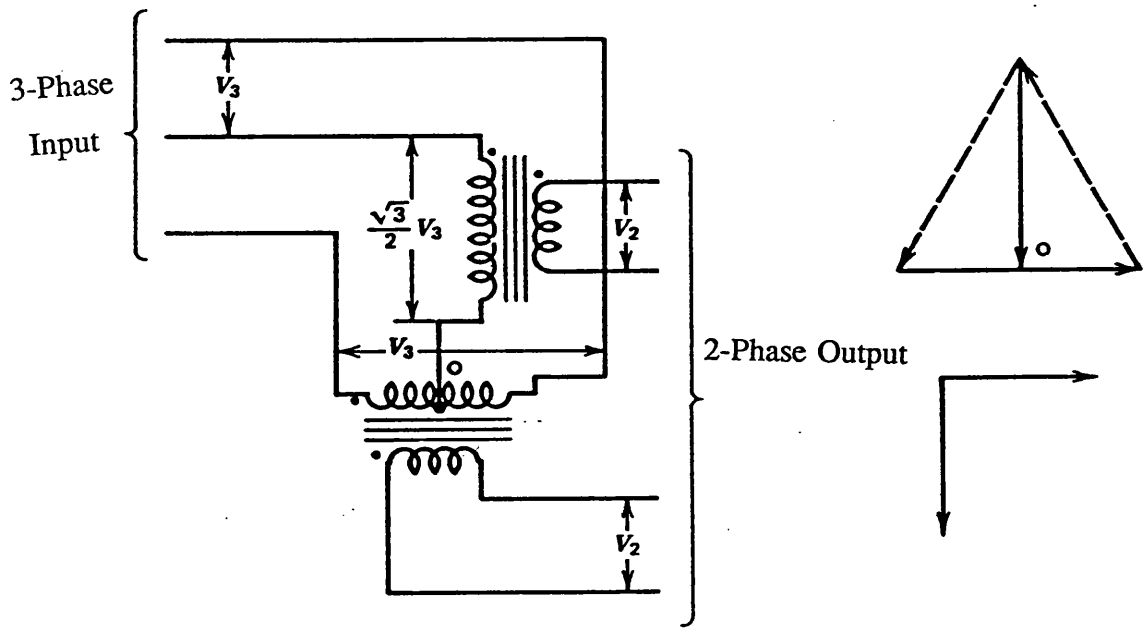

Fig. 5.14 Scott connection

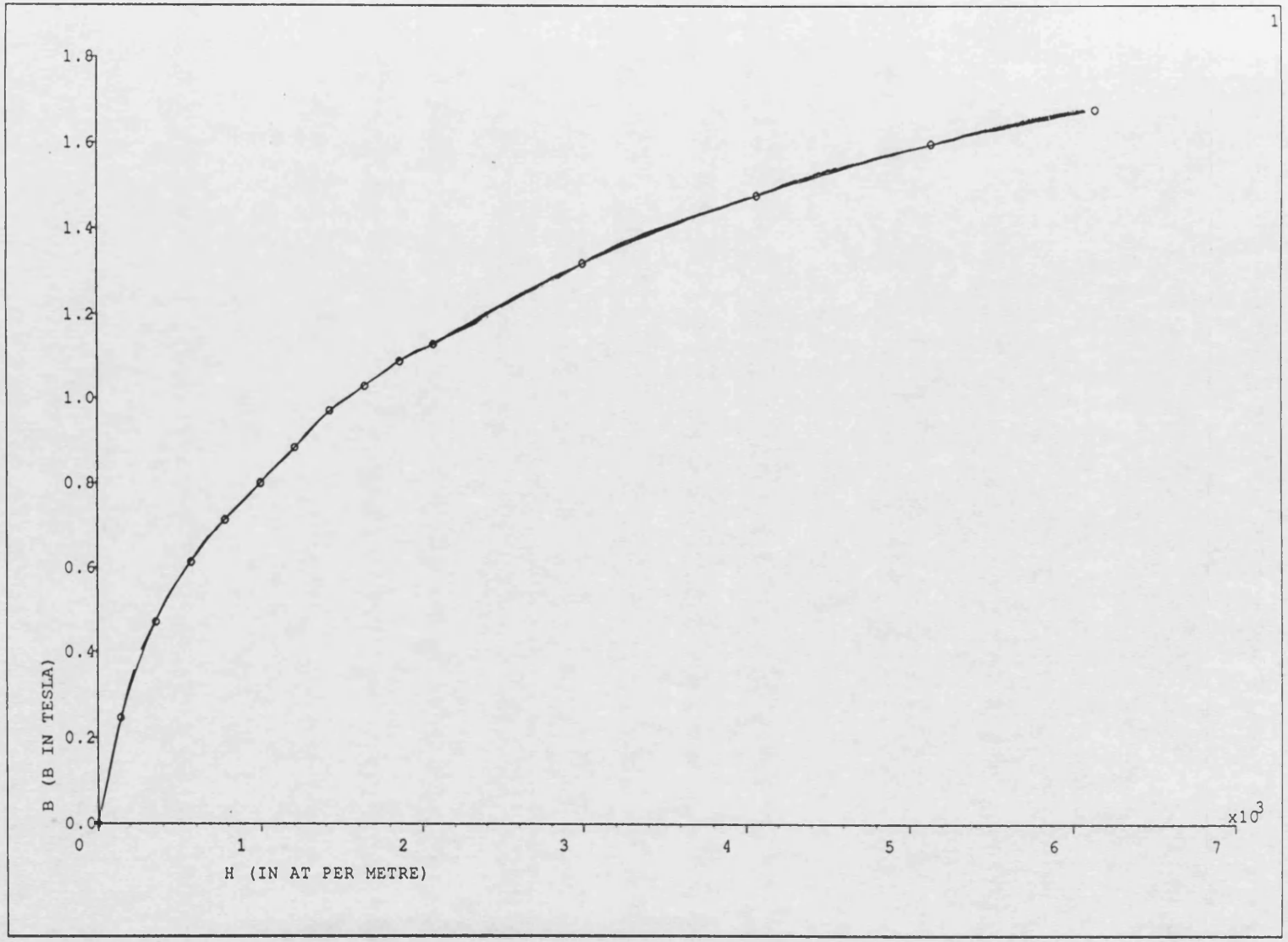

Fig. 5.15 B-H curve of the stator ferro material

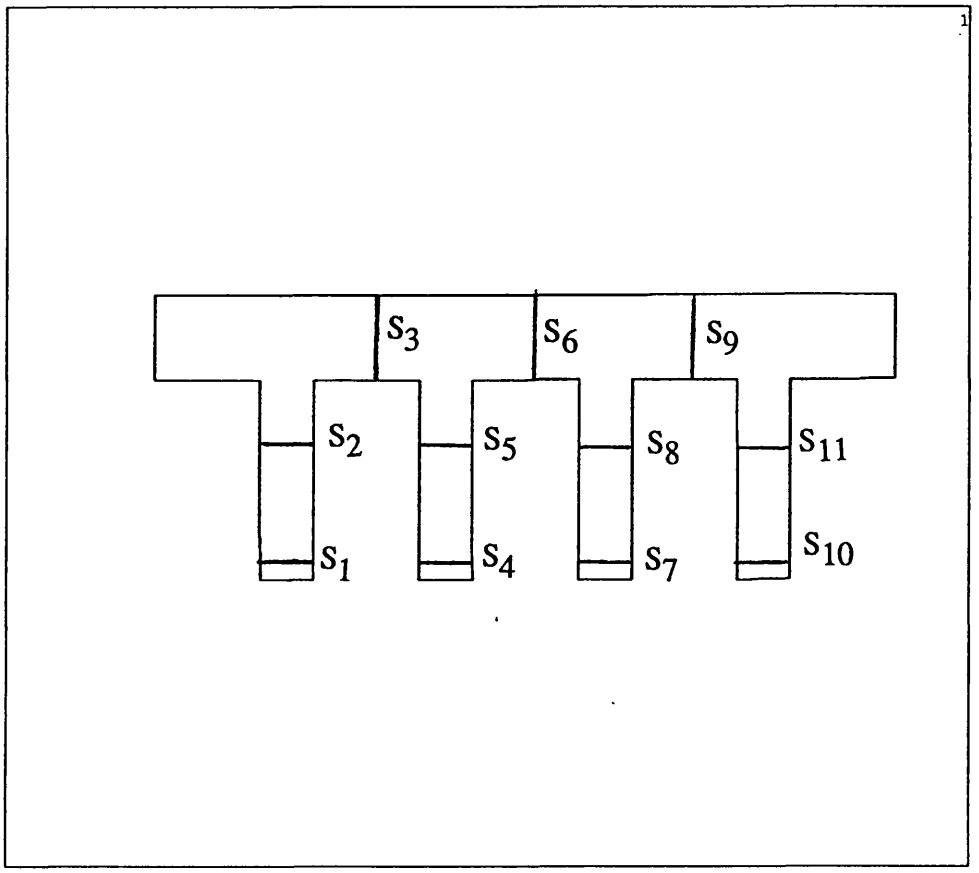

Fig. 5.16 The position of search coils

V Speed [m/s]	F_0 Drag Force [N]	F_N Normal Force [N]
0.00	3.98	23.76
1.28	2.53	26.72
2.24	1.50	27.10
3.84	-0.94	27.55
4.16	-1.52	27.54
5.60	-3.83	27.40
6.73	-5.27	26.63
7.53	-6.29	25.70
8.17	-7.00	24.46
8.97	-8.23	23.80
9.45	-8.79	22.70
10.00	-9.30	22.30

Table 5.2 Measured drag and lift force results at various speeds (IR=IC=0.72 A)

	$V = 0\ m/s$		$V = 5\ m/s$	
Search Coils	$e\,(v)$	$B\,(T)$	$e\,(v)$	$B\,(T)$
S_1	0.264	0.462	0.312	0.545
S_2	0.329	0.575	0.363	0.635
S_3	0.320	0.333	0.358	0.372
S_4	0.336	0.612	0.370	0.674
S_5	0.514	0.936	0.544	0.991
S_6	0.488	0.521	0.510	0.544
S_7	0.326	0.584	0.359	0.643
S_8	0.362	0.650	0.391	0.643
S_9	0.540	0.577	0.592	0.616
S_{10}	0.361	0.664	0.365	0.671
S_{11}	0.534	0.982	0.550	0.988

Table 5.3 Measured induced voltage and flux density results in the search coils

	Coarse Mesh	Fine Mesh	Finer Mesh
Number of Equations	7569	22093	33569
Number of Iterations	75	112	185
CPU Time (on IBM 6091)	13:44	50:21	1:29:53
Drag Force [N] (At u=0 m/s)	4.81	4.32	4.28
Normal Force [N] (At u=0 m/s)	25.25	24.64	24.46

Table 5.4 Comparison of 3D meshes

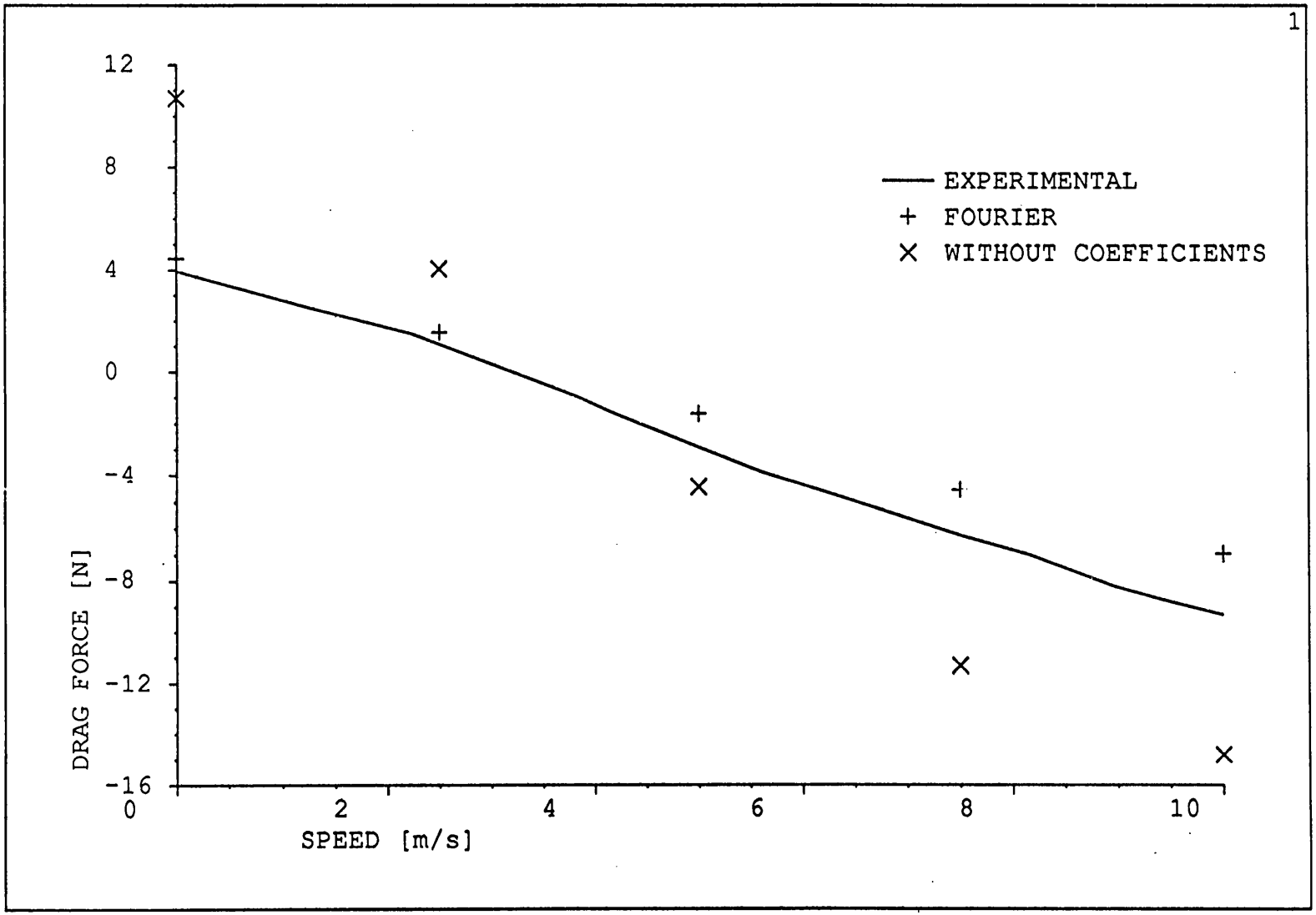

Fig. 5.17 Drag force - speed characteristics (Fourier analysis and exp.)

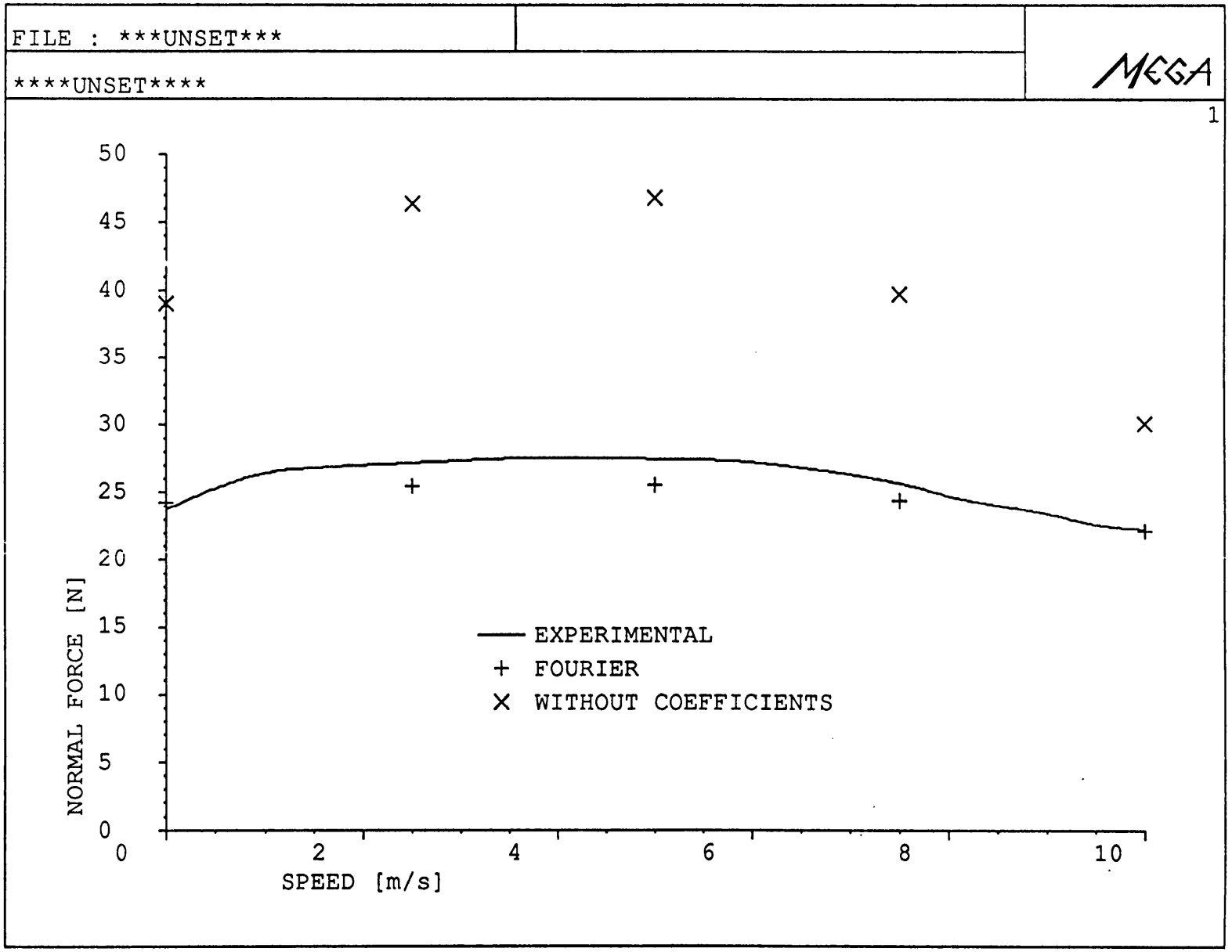

Fig. 5.18 Normal force - speed characteristics (Fourier analysis and exp.)

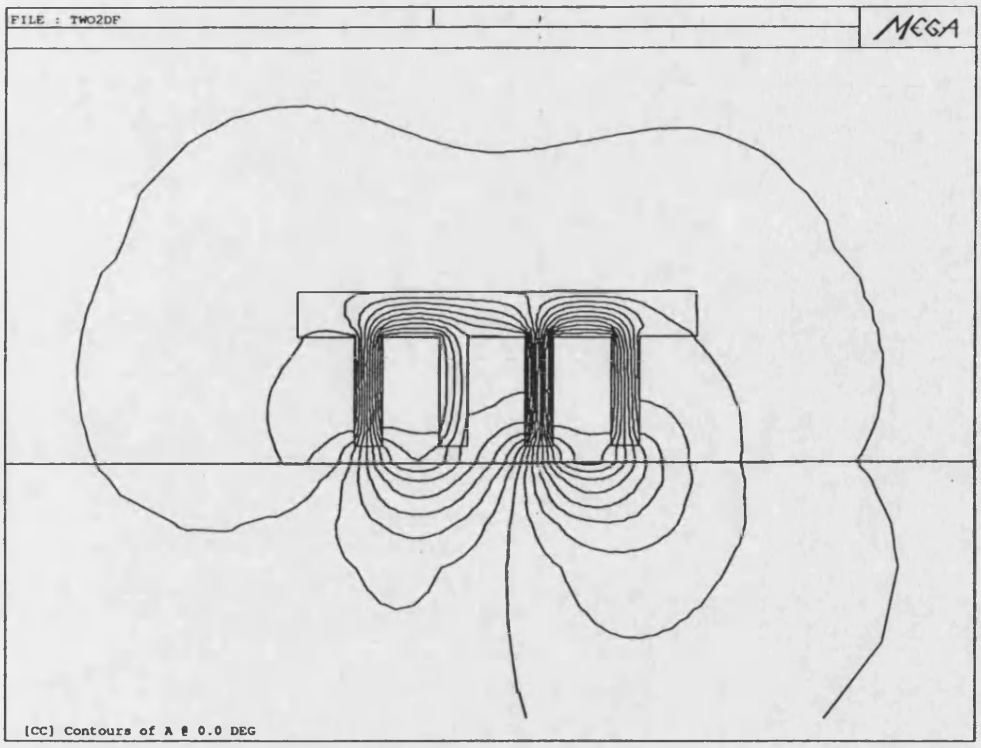

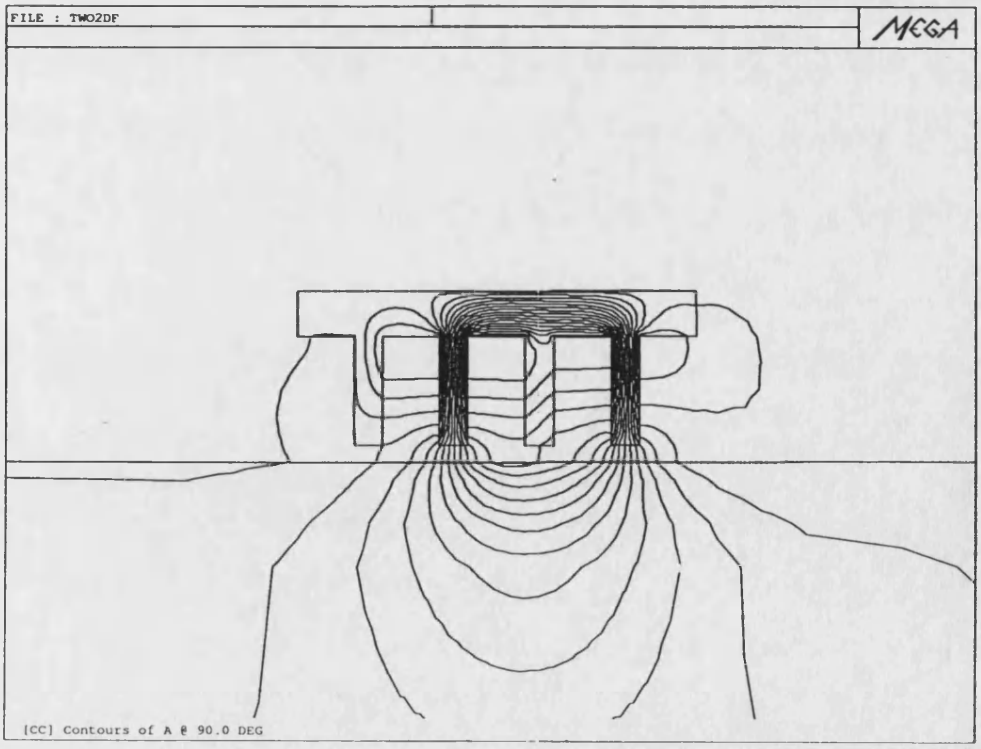

Fig. 5.19 Plots of contours at standstill (2D FE)

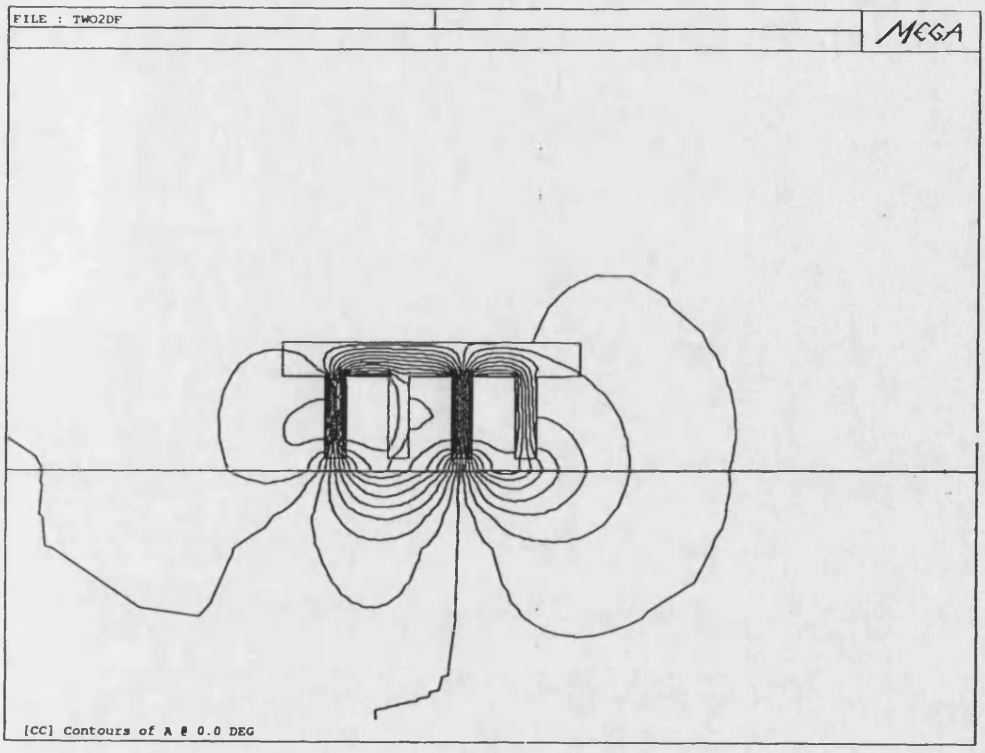

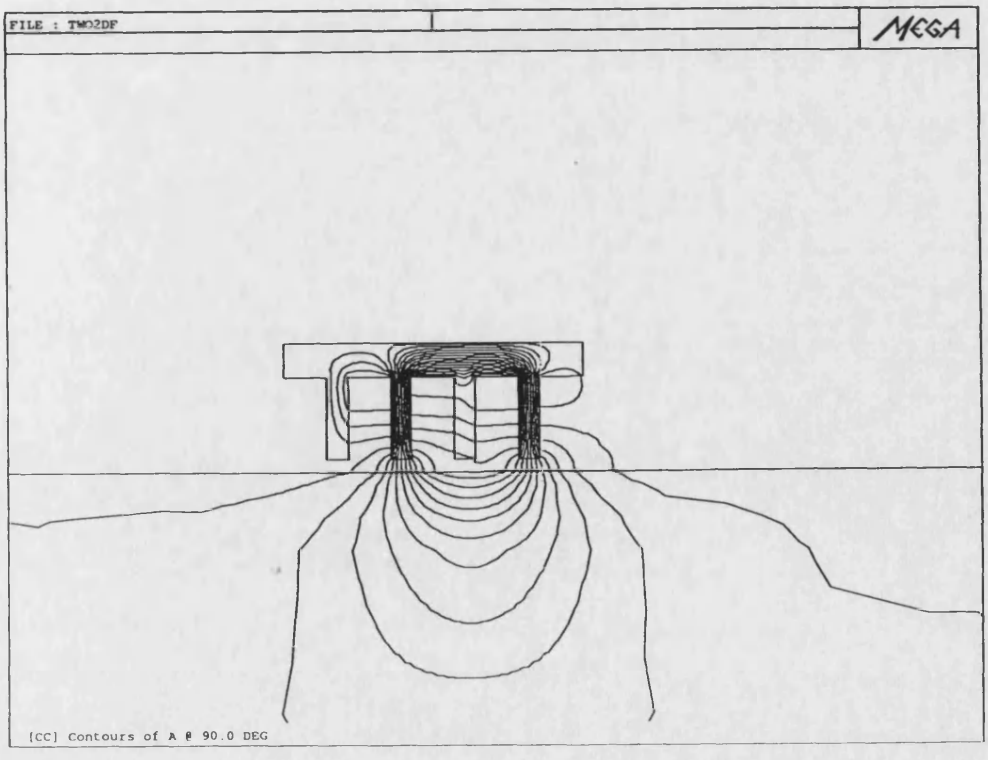

Fig. 5.20 Plots of contours at 5 m/s (2D FE)

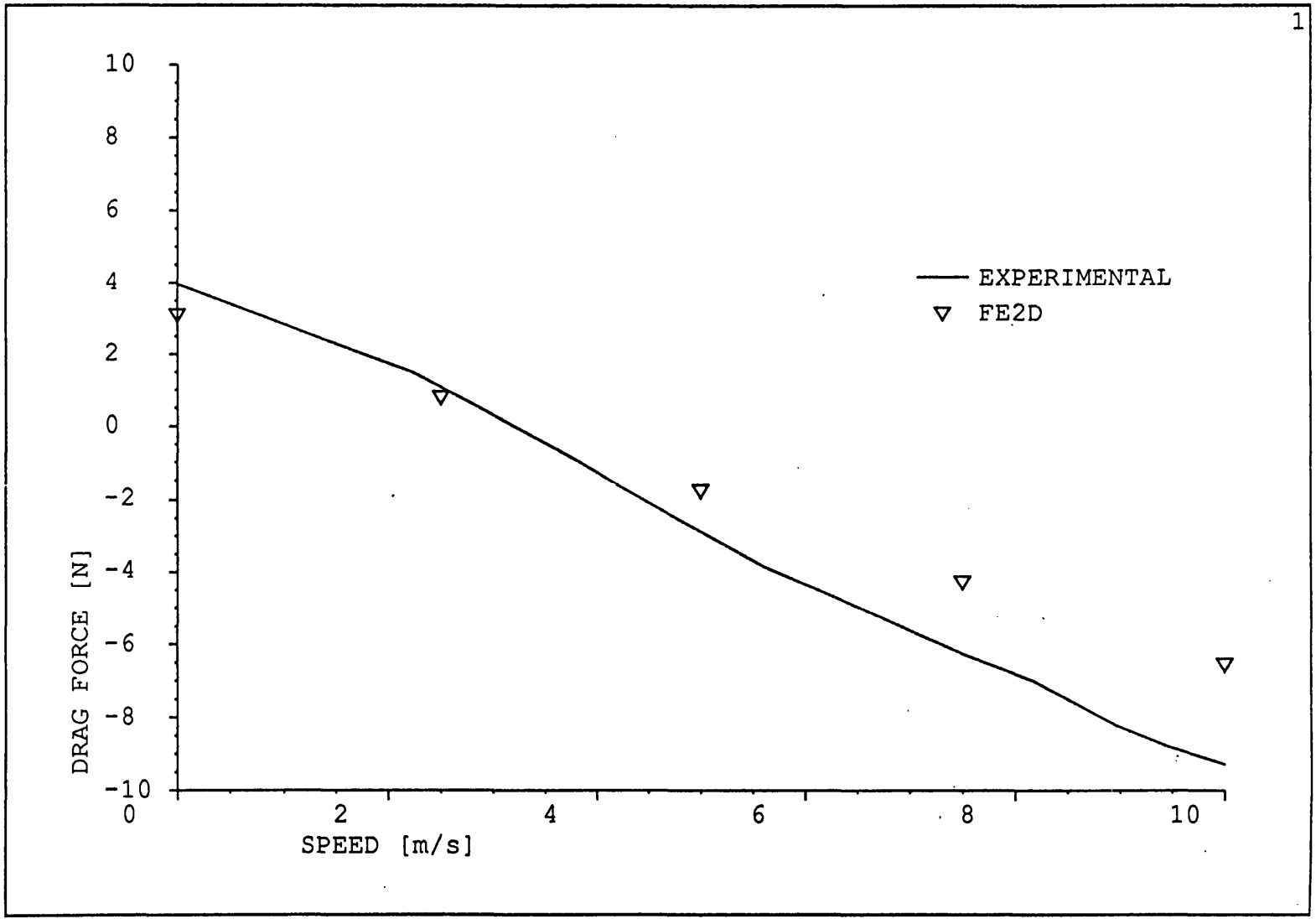

Fig. 5.21 Drag force - speed characteristics (2D FE and exp.)

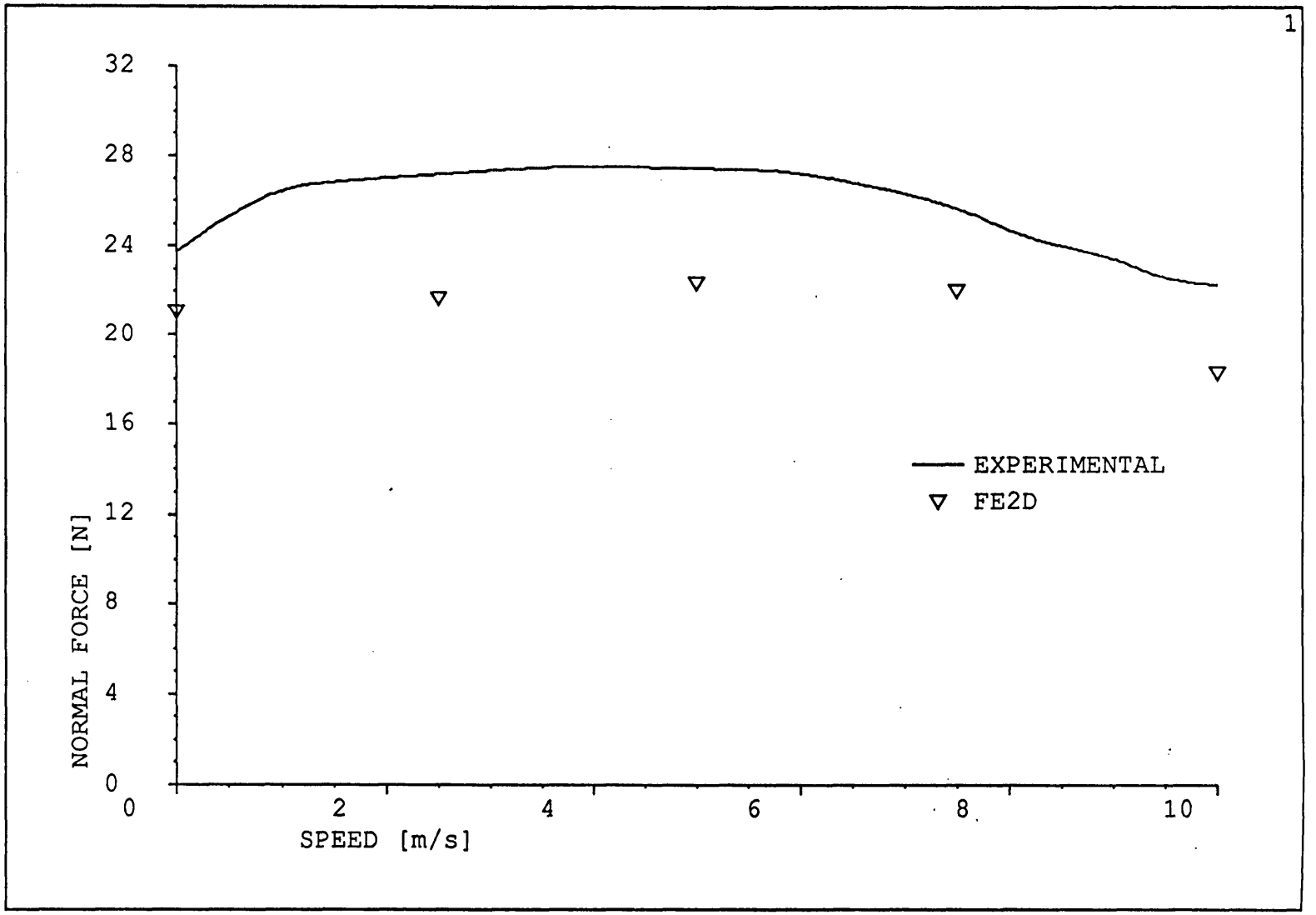

Fig. 5.22 Normal force - speed characteristics (2D FE and exp.)

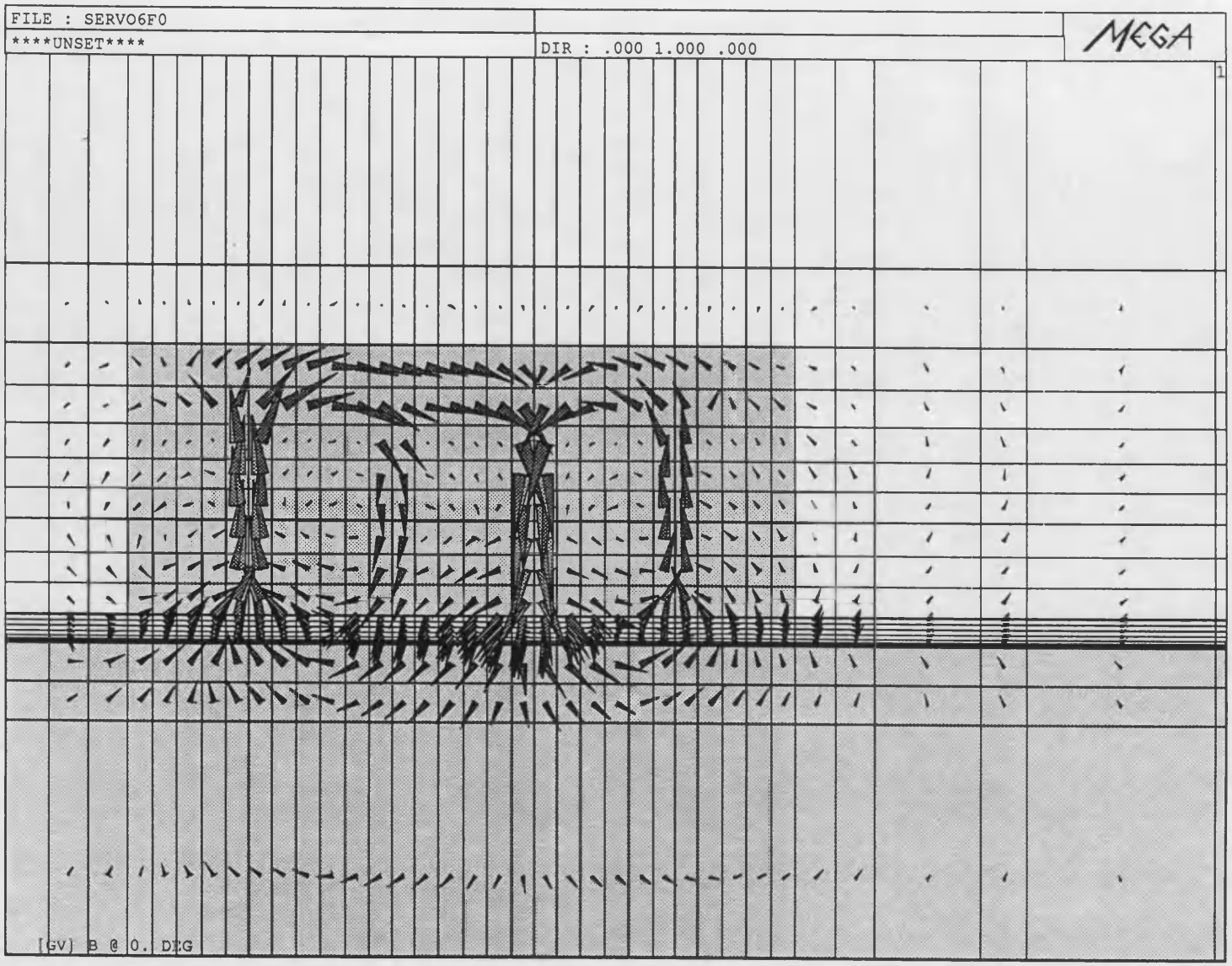

Fig. 5.23 a) Flux density vectors at 0 m/s, 0 phase angle (3D FE)

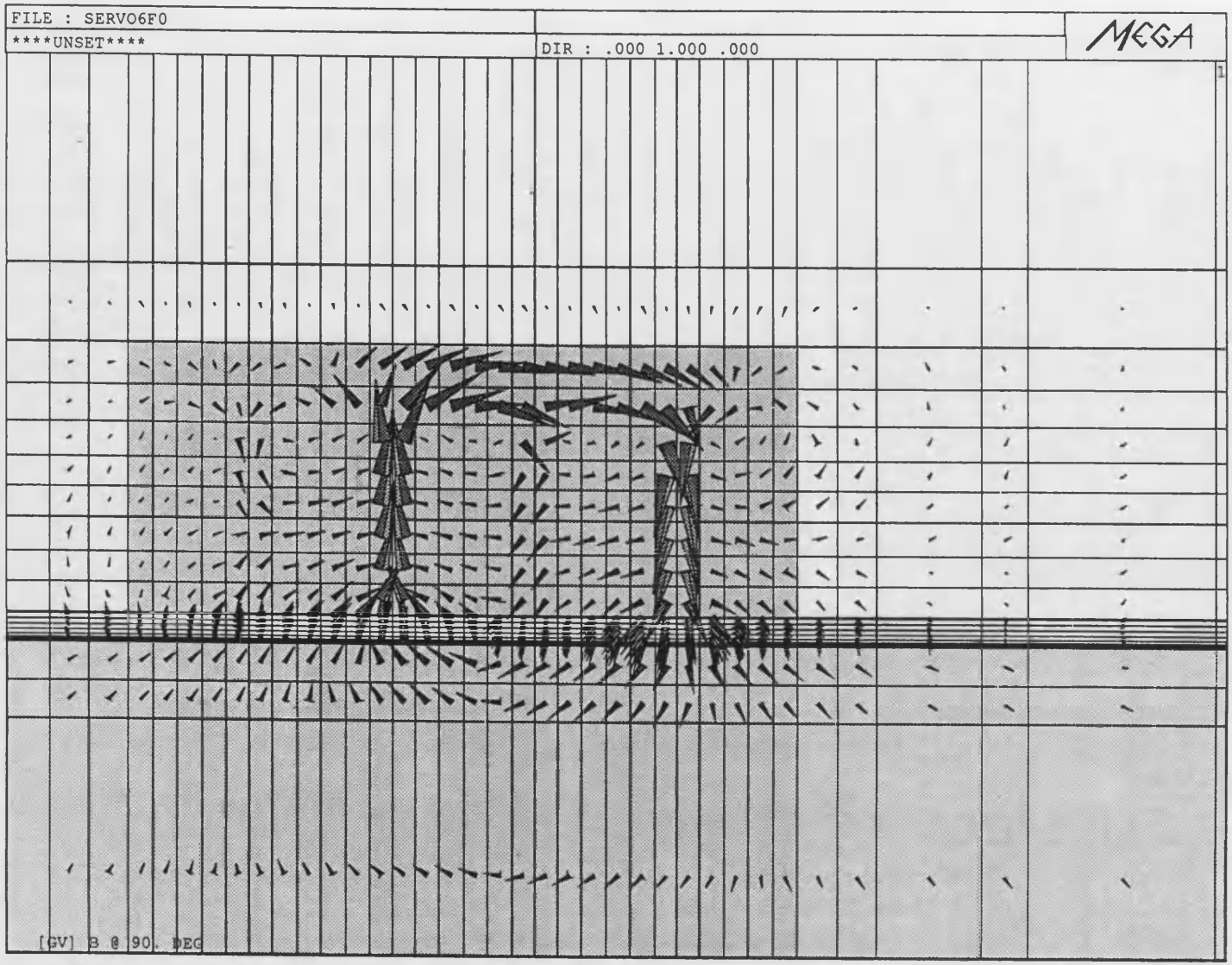

Fig. 5.23 b) Flux density vectors at 0 m/s, 90 phase angle (3D FE)

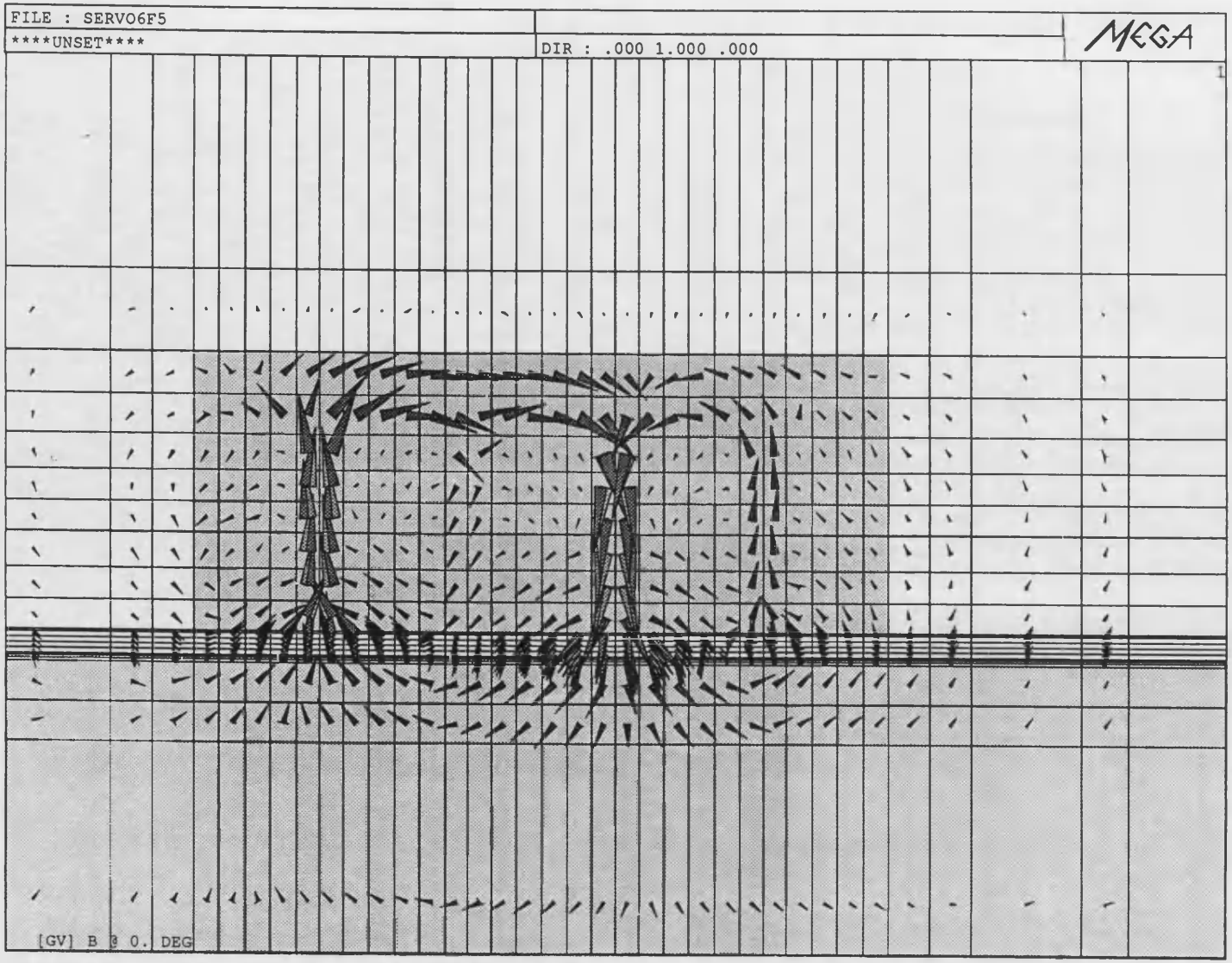

Fig. 5.24 a) Flux density vectors at 5 m/s, 0 phase angle (3D FE)

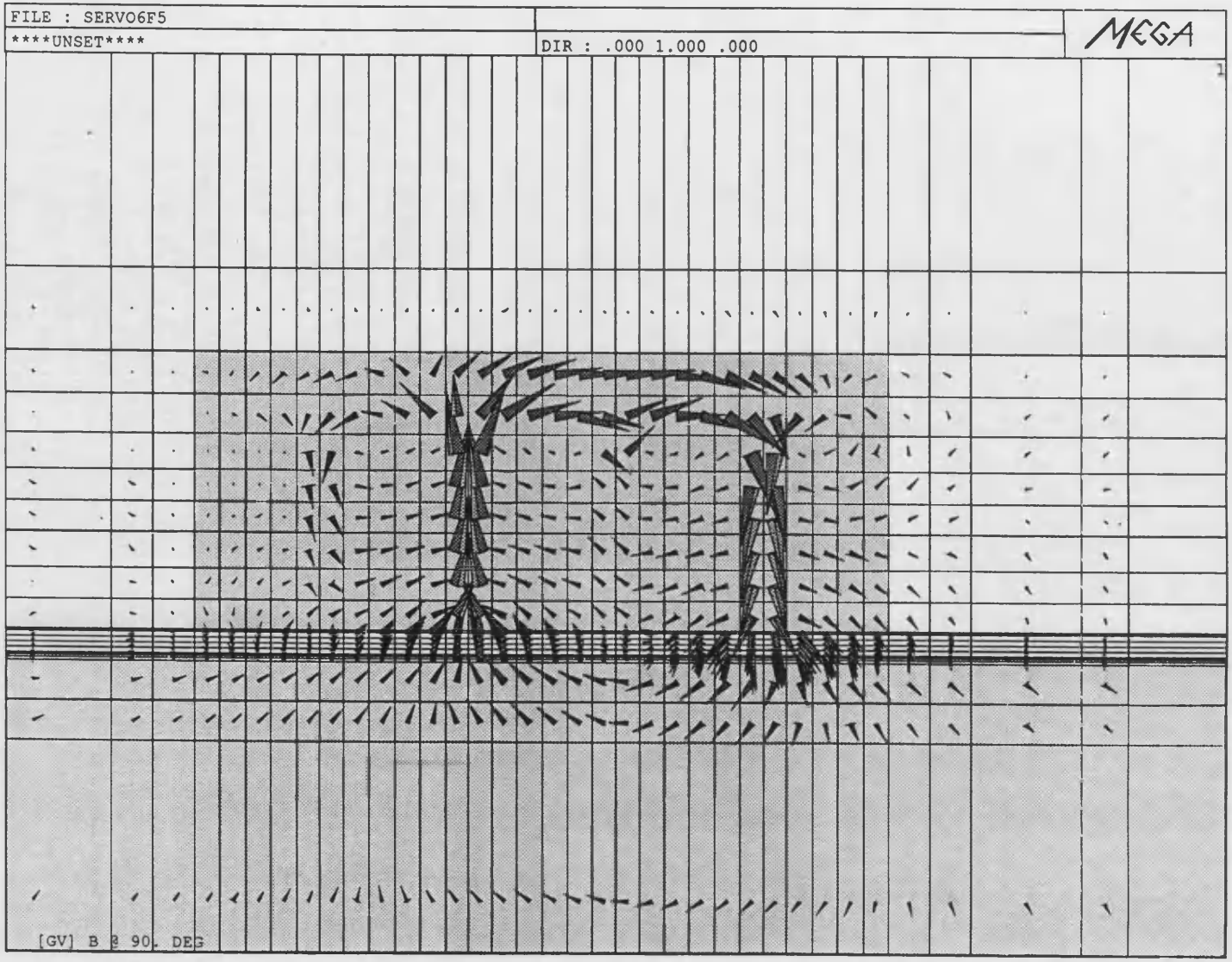

Fig. 5.24 b) Flux density vectors at 5 m/s, 90 phase angle (3D FE)

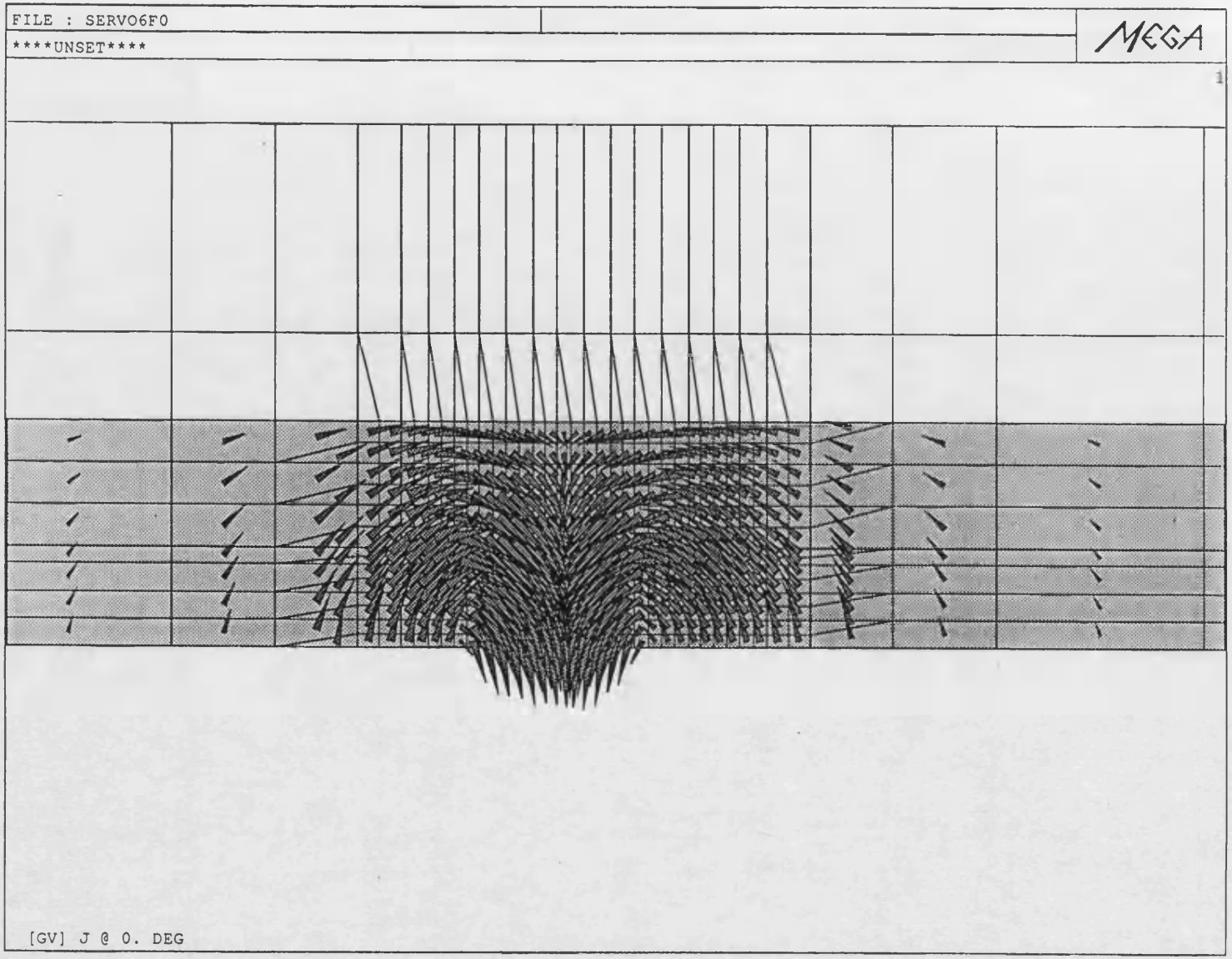

Fig. 5.25 a) Currents in the conducting plate at 0 m/s, 0 phase angle (3D FE)

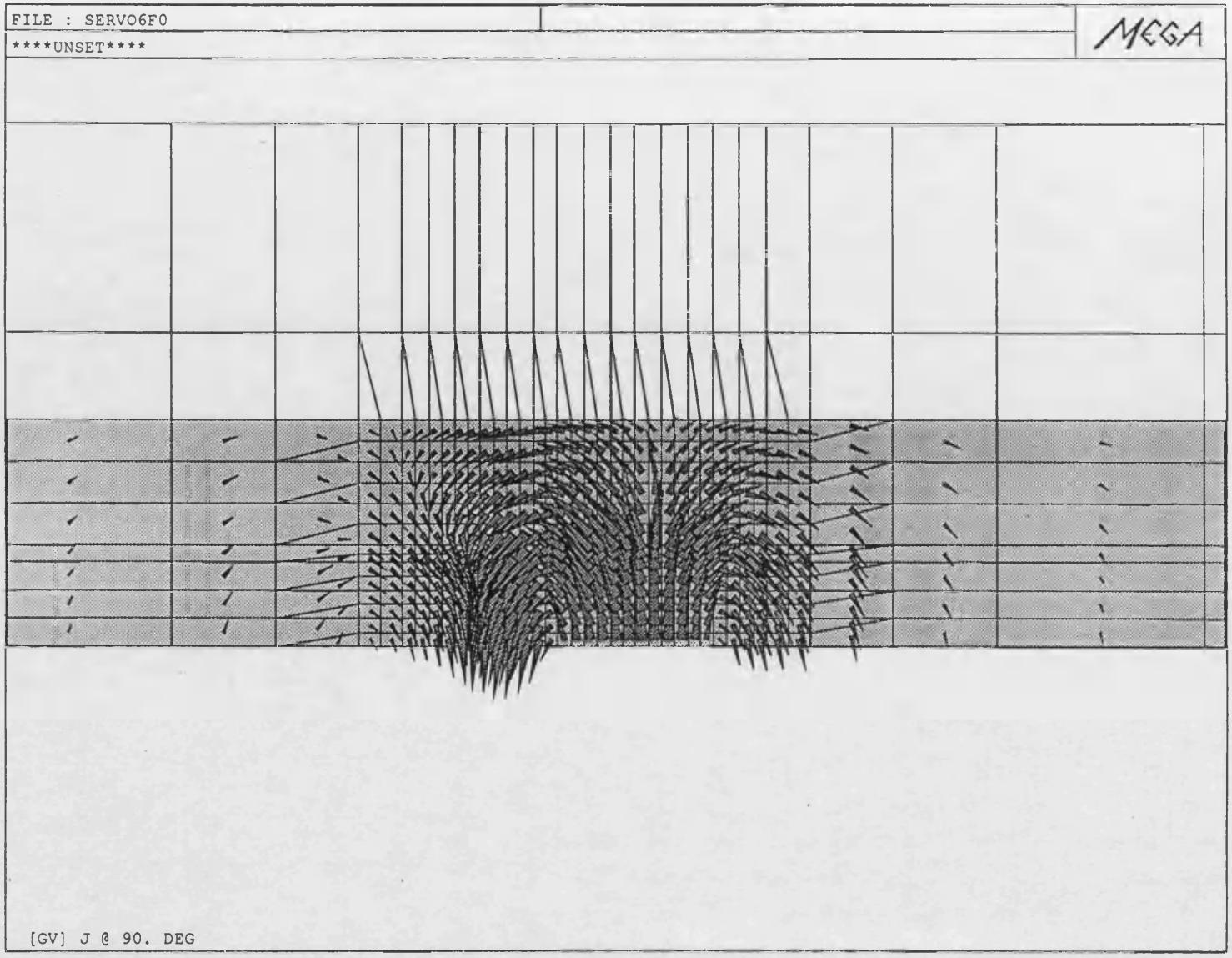

Fig. 5.25 b) Currents in the conducting plate at 0 m/s, 90 phase angle (3D FE)

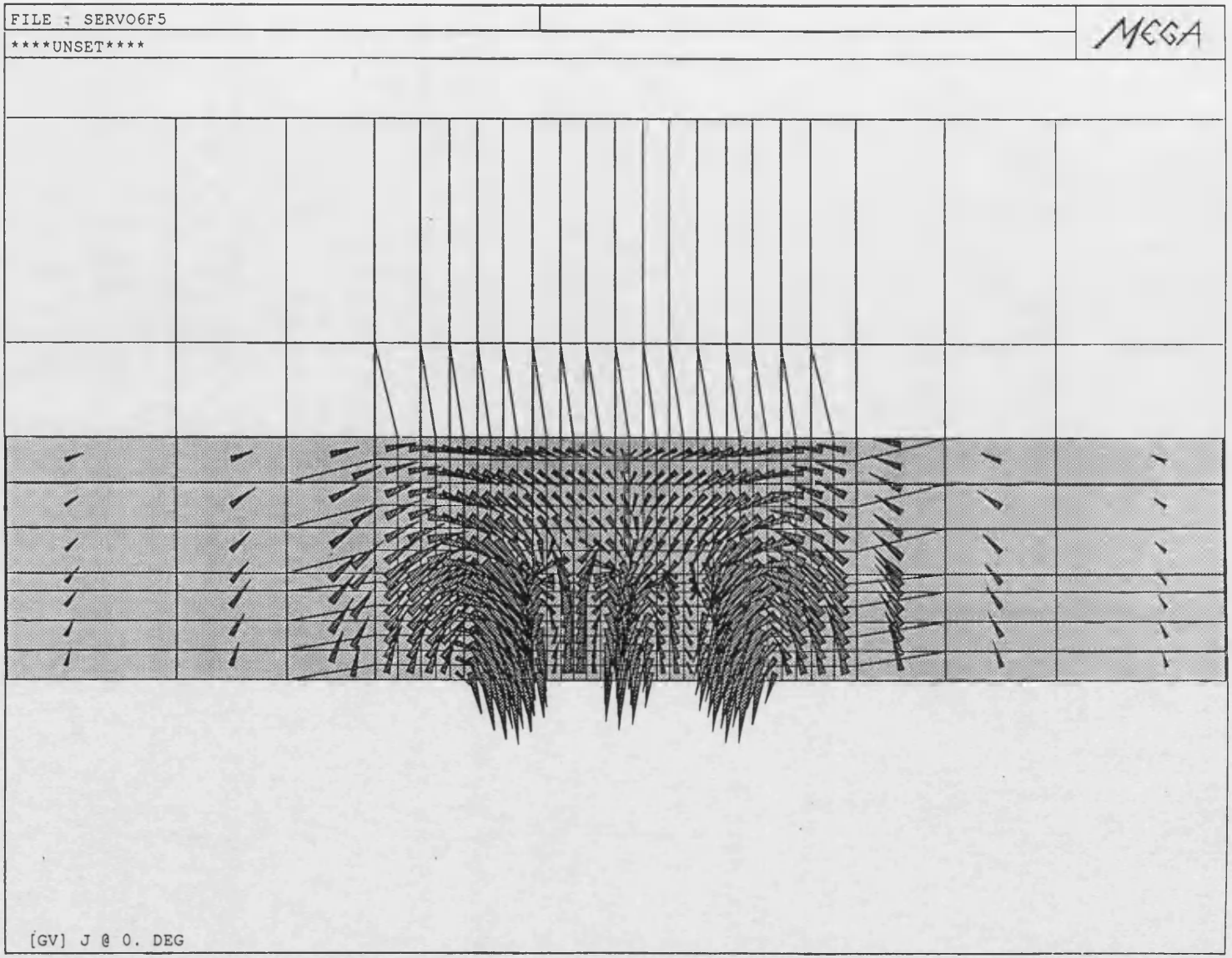

Fig. 5.26 a) Currents in the conducting plate at 5 m/s, 0 phase angle (3D FE)

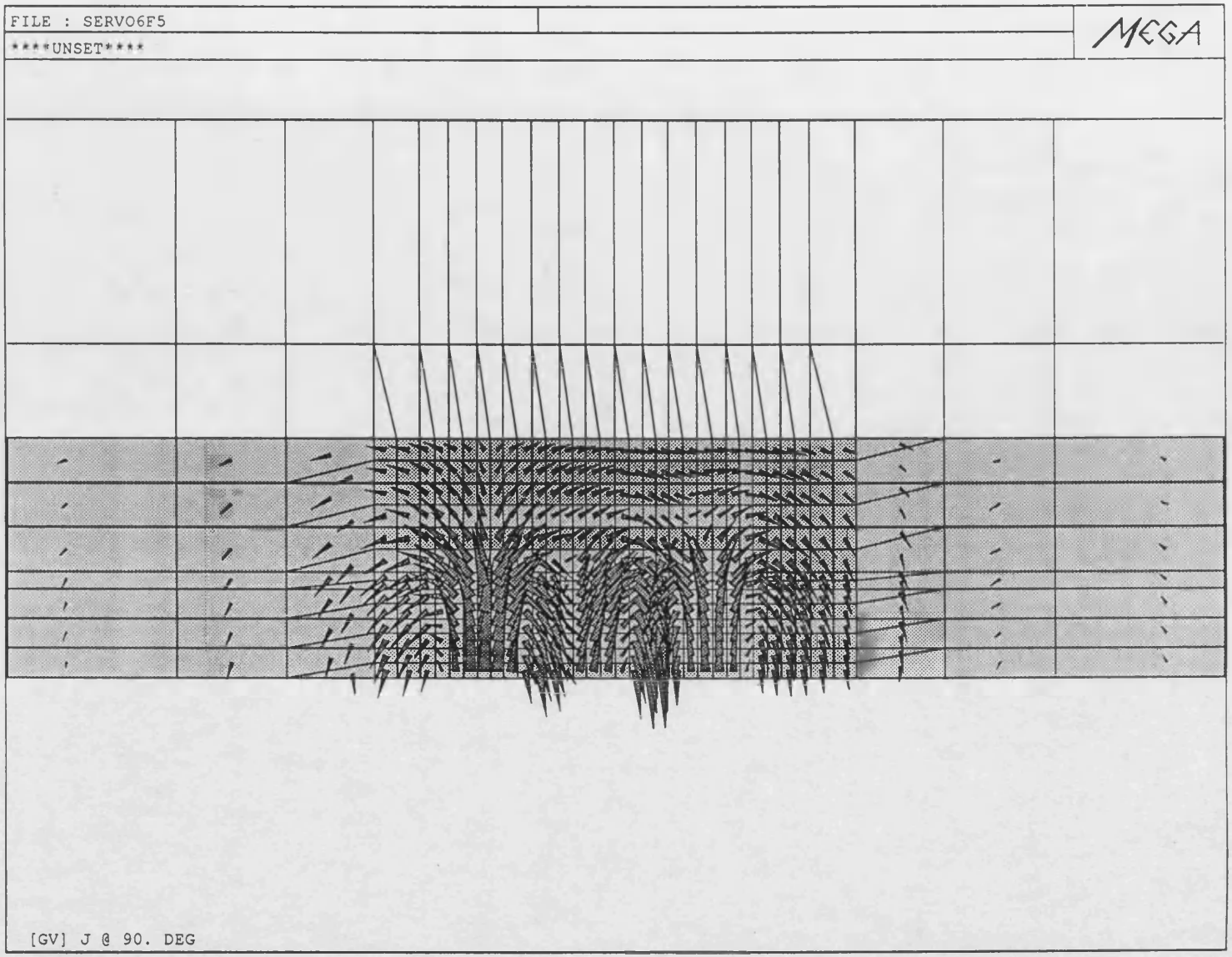

Fig. 5.26 b) Currents in the conducting plate at 5 m/s, 90 phase angle (3D FE)

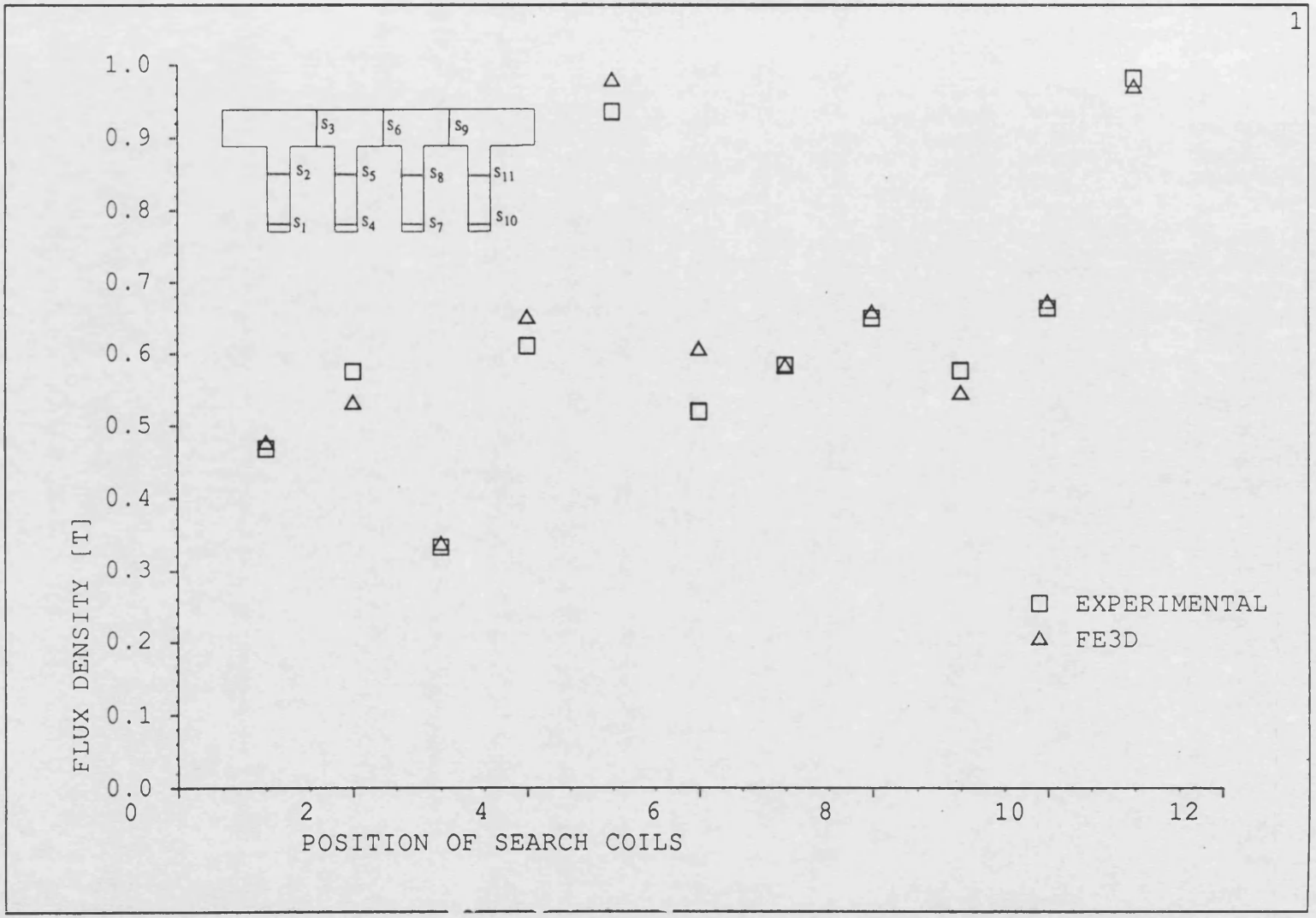

Fig. 5.27 Flux density results at u=0 m/s (3D FE and exp.)

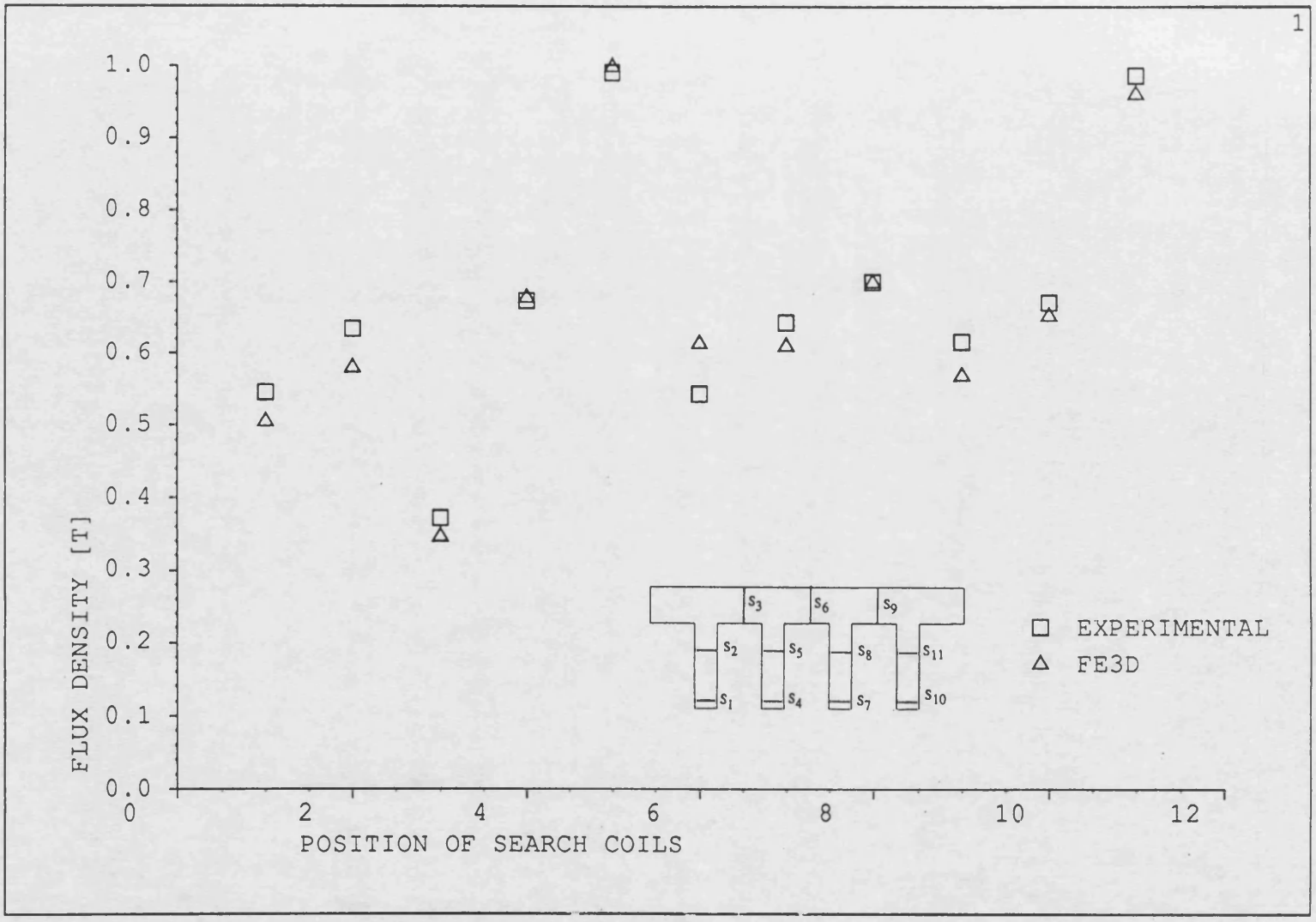

Fig. 5.28 Flux density results at u=5 m/s (3D FE and exp.)

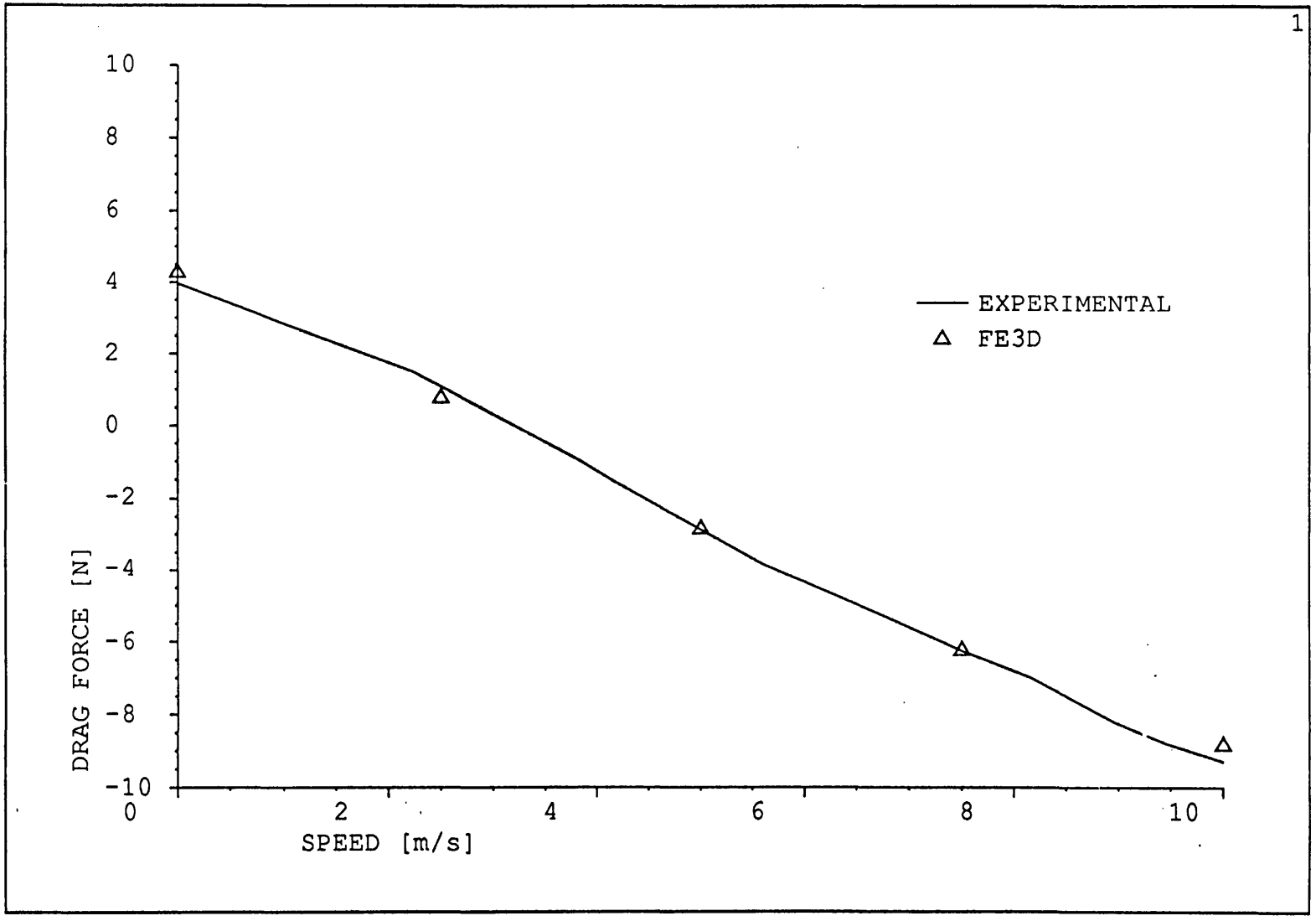

Fig. 5.29 Drag force - speed characteristics (3D FE and exp.)

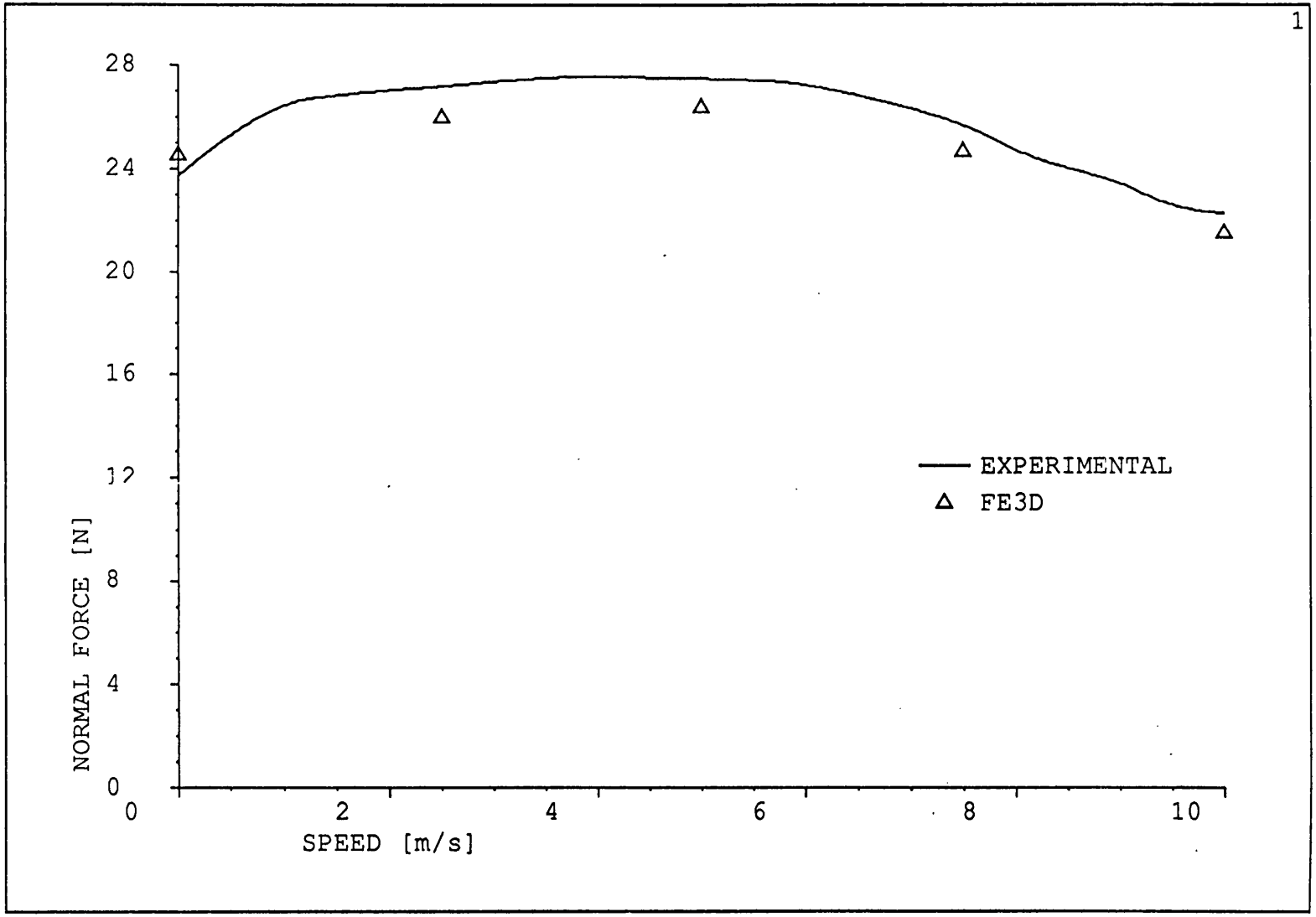

Fig. 5.30 Normal force - speed characteristics (3D FE and exp.)

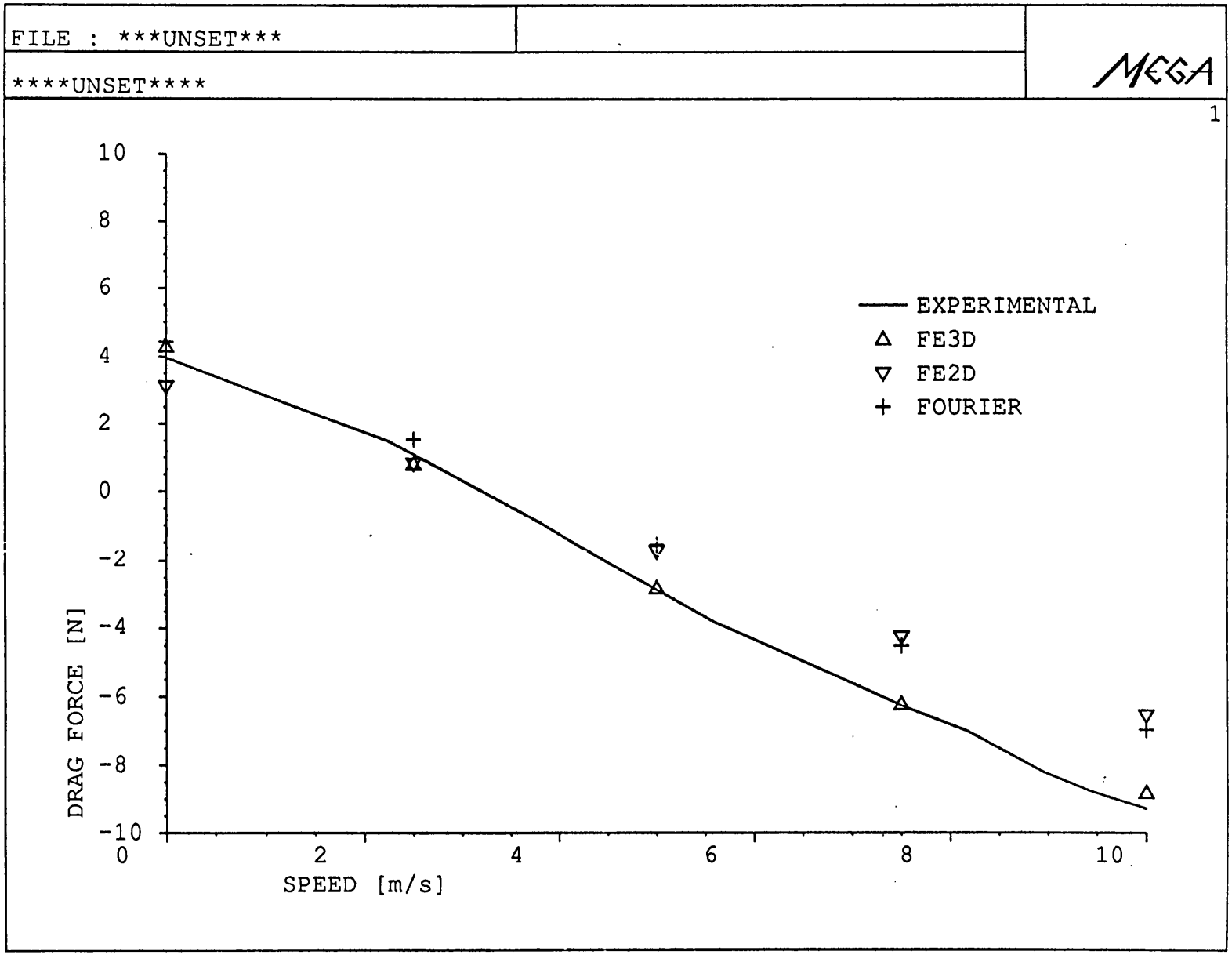

Fig. 5.31 Comparison of drag force results with experimental results

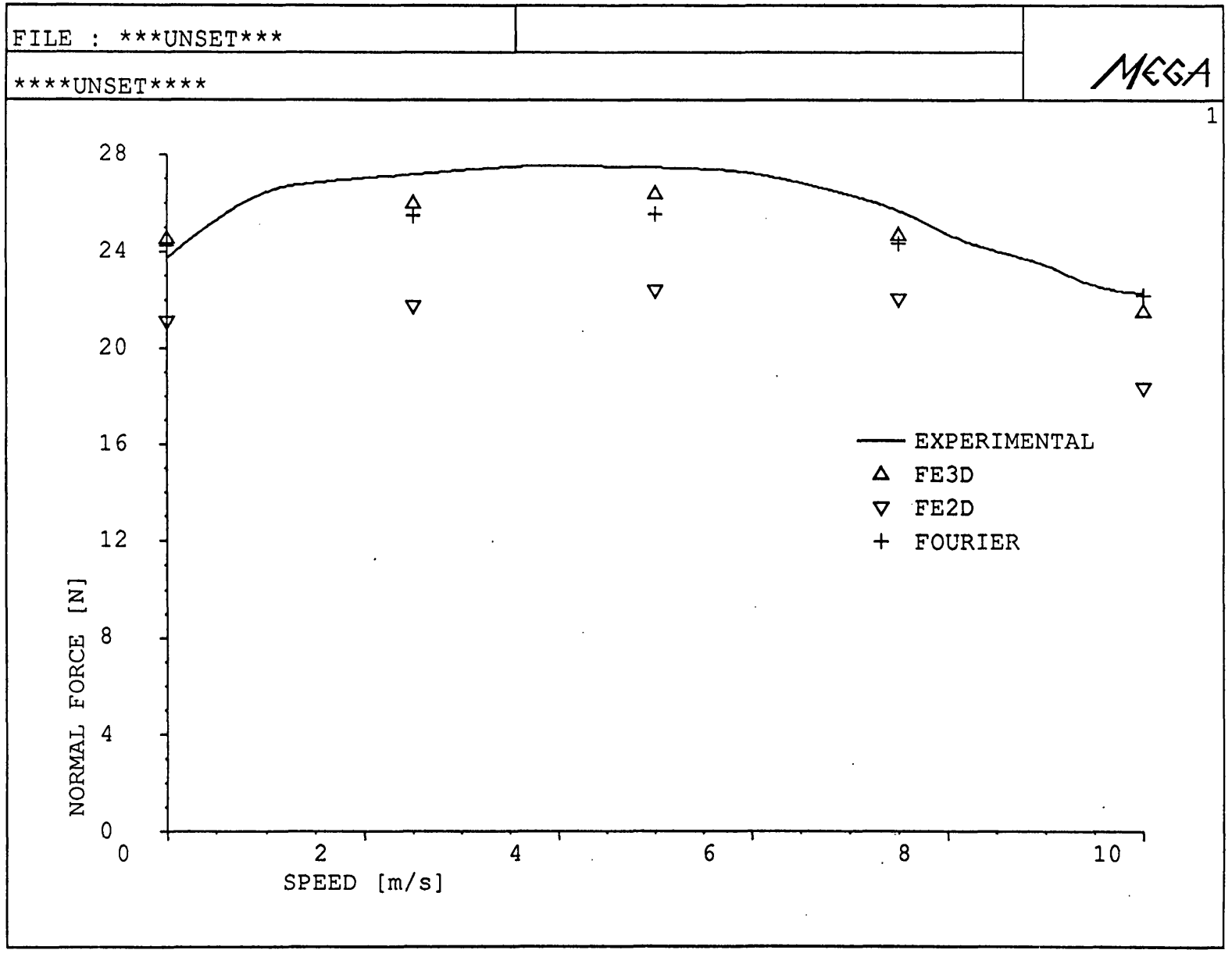

Fig. 5.32 Comparison of normal force results with experimental results

CHAPTER 6

CONCLUSION AND FUTURE WORK

6.1 Conclusion

The main aim of this project was to develop and modify numerical methods for solving the 2D and 3D moving conductor problems. The finite element method from the Galerkin technique point of view is adopted to obtain the solution of the moving conductor problem in both DC and AC (at power frequencies) cases. The difficulties are overcome by using this adaptation.

Despite involvement of some other regions in the models, the difficulties mainly originated from conducting regions which move. The first problem to overcome is that, the possible occurrences of oscillations in the solution when the Peclet number exceeds one. By applying the Hughes's scheme which is upwinding, vast inaccuracy taking place particularly in the drag force calculations was removed. However, at the speed of 100 m/s while the Peclet number is about 6000 in a 3D problem, even upwinding failed to converge. At this point, the only solution is probably to refine the mesh in order to lower the Peclet number.

Secondly, when using the A-Φ formulation in only solving the 3D problems in the conduction region, the use of electric scalar potential along with the magnetic vector potential requires another set of equations which cause an expensive operation

from cost and time point of views. Therefore the removal of the electric scalar potential is desirable. The technique which removed **V** from the formula was introduced. The new technique without **V** has produced an almost identical result with the old technique. The experimental work indicated that these results are valid.

The experimental work on the prototype two-phase linear induction servomotor also verified that the extension of the applications of numerical techniques to an AC problem is successful. Nonlinearity effect of ferro material has not been modelled for simplicity in the calculations. Because of that, in the experimental work, the currents to the stator windings were limited in a way that the maximum value of flux density remained in the relatively linear part of the **B-H** curve. This arrangement is found satisfactory, as the aim of testing of the servomotor is only to verify the validity of the techniques using the optimum formulation, rather than designing the servomotor.

In the beginning of the project, the use of the 3D techniques in the solution of such problems was much more costly than now. The existence of any homogeneity or invariance in the 3D direction of the model would make the 2D techniques more appealing, but rapid developments in hardware technology enables the 3D techniques to be employed more widely. And also powerful software techniques have reduced the amount of effort required in generating 3D meshes. It can be predicted that the use of 3D techniques in the analysis and design of devices will be much widespread. Therefore any contribution to reduce the required computing time and cost in solving problems in 3D is expected to be significant. The results presented in this work show that an important contribution in the field of moving

conductor problems has been made. The new technique without V in the formula yields the solution 2.5 times faster, and involves 1.2 times less unknowns than the previously used method with V in the formula for a typical problem. For problems containing a higher ratio of moving conductor region to non conducting region, these ratios would be even higher. However despite their failure of producing highly accurate results, the importance of the 2D methods as powerful tools to initiate the analysis or design of machines or devices, can still be substantial.

6.2 Future Work and Recommendations

Despite the fact that the moving conductor problem has been widely analyzed, by considering a few more points, even further generalization which would lead to the inclusion of all the possible aspects of the problem, can be made.

One of the shortcomings of the application is that of the neglect of nonlinearity effect of iron parts in the model. In many practical applications, the value of flux density may well fall into the saturation line of the B-H curve of the material. At this point to assume linear permeability can cause some inaccuracy in the solution. Therefore for a general approach to the problem, this effect must be modelled. Furthermore, a discontinuity of conductivity in the conducting plate can be modelled too. This is not a common problem that can be encountered in these particular cases, examined here. However, in some applications, such as the rail gun problem, it may appear due to excessive heat effect on the conductivity of the plate. The solution to

this problem is the use of a thin surface element between the two regions having different conductivities.

The application can be extended to the problem that the motion is not necessarily to be one directional, and the moving member changes in cross section with time. The solution can only be obtained by using a time step algorithm that allows the mesh to move at each step.

APPENDIX 1

AN OPTIMAL FORMULATION FOR 3D MOVING CONDUCTOR EDDY CURRENT PROBLEMS WITH SMOOTH ROTORS

D Rodger, P J Leonard, T Karaguler
University of Bath, Bath, Avon BA2 7AY, UK

Abstract – A new finite element technique for modelling 3D transient eddy currents in 'smooth rotor' conductors moving at a constant velocity is described. This has been implemented in the MEGA software package for modelling 2 and 3D electromagnetic fields. Eddy current regions are modelled using a magnetic vector potential. Non conducting regions require magnetic scalar potentials. Validation by comparison with experiment has been carried out.

INTRODUCTION

Moving conductor eddy current problems are very common. Some of these problems are extremely complex and, although they could probably be modelled in 3D using existing software, the required computer resources would be beyond the means of most organisations. However, many of the 'smooth rotor' type of devices in which the moving member does not change in cross section with time may be conveniently solved using the classical Minkowski transformation. All other types of device require a time stepping solution and a mesh which can move position at each step. This contribution is concerned with the smooth rotor type of device, which includes MAGLEV vehicles, linear induction machines and electromagnetic rail launchers. There are various formulations which can be used to model 3D eddy current problems; we have tended to use magnetic scalar potentials in non conducting regions coupled to magnetic vector potentials $\bar{A}$ in conductors. A method for moving conductors which uses $\bar{A}$ and V, the electric scalar potential, inside conductors coupled to magnetic scalars in non-conductors is described in ref [1]. A new method which does not require V inside conductors is described here. This new method has an obvious computational advantage in that only three variables are used inside conductors rather than four. In addition to this, the final matrix is better conditioned than before and consequently solution is faster using the pre-conditioned bi-conjugate gradient technique. There are some disadvantages associated with the new method. However, it is shown that most of these can usually be overcome. We first describe the previous technique, as the new method is derived from it.

THE A-V-φ FORMULATION FOR MOVING CONDUCTORS

In the laboratory reference frame, the moving region electric field can be written, using the Minkowski transformation, as:

$$\bar{E} = \bar{u} \times \bar{B} - \frac{\partial \bar{A}}{\partial t} - \text{grad } V \qquad (1)$$

$\bar{u}$ is the velocity of the region with respect to the laboratory.

Using curl $\bar{A} = \bar{B}$ and curl $\bar{H} = \bar{J}$, we can obtain:

$$\text{curl} \frac{1}{\mu} \text{curl } \bar{A} - \sigma \left[\bar{u} \times \text{curl } \bar{A} - \frac{\partial \bar{A}}{\partial t} - \text{grad } V \right] \qquad (2)$$

Also from div $\bar{J} = 0$, we have

$$\text{div } \sigma \left[\bar{u} \times \text{curl } \bar{A} - \frac{\partial \bar{A}}{\partial t} - \text{grad } V \right] = 0 \qquad (3)$$

It is well known that eqn (3) is implied by eqn (2), as eqn (3) is obtained by taking the divergence of eqn (2). Eqn (2), however, comprises three equations and four unknowns, so that clearly another equation is necessary for a solution. Eqn (3) does not actually introduce any new information and this is reflected in the fact that eqns (2) and (3) are not unique.

The divergence of $\bar{A}$

The divergence of $\bar{A}$ is not specified by eqns (2) and (3). A number of schemes are possible, however we have chosen to impose the condition div $\bar{A}$ = 0 throughout the volume using a penalty technique. Together with $\bar{A}.n$ = 0 on the inside of conductor surfaces, this ensures a unique $\bar{A}$ [1].

Non conducting regions

The non conducting regions in the same problem may be modelled in terms of the magnetic scalar potential:

$$\text{div } \mu \text{ grad } \varphi = 0 \qquad (4)$$

Eqns 2, 3 and 4 can be solved using the Galerkin weighted residual technique [1].

Upwinding

When the Galerkin technique is applied to the velocity terms of eqn (2), large -ve numbers are generated on the diagonal of the final matrix. This causes oscillations and poor results when the Peclet number, $p = \sigma h \mu u / 2.0$ is greater than 1.0 (h is the length of an element in the direction of velocity). This problem can be cured by using small meshes, effectively using h to keep p down, but this is expensive. It has been more effective to use upwinding, familiar in fluid dynamics [2].

Using the Galerkin scheme leads to the following integral:

$$\int \bar{N}_e \, (\sigma \, (\bar{u} \times \text{curl } \bar{A})) \, d\Omega \qquad (5)$$

$\bar{N}_e$ represents the shape functions of element e.

This is generally evaluated using Gaussian quadrature, sampling at the usual quadrature points. The upwind scheme [2] uses different points, which depend on the value of p.

Eqn (5) becomes:

$$\sum \bar{N}_e(\epsilon) \, . \, (\sigma \, (\bar{u}(o) \times \text{curl } \bar{A} \, (\epsilon))) \, J(o) w \qquad (6)$$

$\bar{u}(o)$ is the velocity evaluated at the origin of the isoparametric co-ordinates of the element, J(o) is the Jacobian of the isoparametric transform, w equals 8 for a 3D element and 4 for a 2D element. $\bar{N}_e(\epsilon)$ represents the shape function evaluated at point ϵ within the element. This is a local co-ordinate, $-1 < \epsilon < 1$ and $\epsilon = \coth p - 1/p$.

THE $\bar{A}$-φ FORMULATION FOR MOVING CONDUCTORS

It is possible to remove the electric scalar V from the above formulation by making the substitution $V = \bar{A}.\bar{u}$ in eqn (2):

$$\text{curl}\ \frac{1}{\mu}\ \text{curl}\ \bar{A} = \sigma\left[\bar{u} \times \text{curl}\ \bar{A} - \frac{\partial \bar{A}}{\partial t} - \text{grad}\ (\bar{A}.\bar{u})\right] \quad (7)$$

Using $\bar{u} \times \text{curl}\ \bar{A} = \text{grad}\ (\bar{A}.\bar{u}) - (\bar{u}.\text{grad})\bar{A}$ we can obtain:

$$\text{curl}\ \frac{1}{\mu}\ \text{curl}\ \bar{A} = \sigma\left[-\frac{\partial \bar{A}}{\partial t} - (\bar{u}.\text{grad})\bar{A}\right] \quad (8)$$

Eqn 8 implies nothing about the divergence of $\bar{A}$. Taking the divergence of eqn (8), the left hand side is of course zero:

$$0 = \text{div}\ \sigma\left[-\frac{\partial \bar{A}}{\partial t} - (\bar{u}.\text{grad})\bar{A}\right]$$

For a constant σ and $\bar{u}$, this simplifies to:

$$0 = -\sigma\ \text{div}\left[\frac{\partial \bar{A}}{\partial t}\right] - \sigma\ (\bar{u}.\text{grad})\ \text{div}\ \bar{A}$$

In the general case, this has many non trivial solutions, so that div $\bar{A}$ is not specified.

The divergence of $\bar{A}$ is enforced in exactly the same way as for the previously described method.

Using the Galerkin scheme, eqn (8) becomes:

$$\int \bar{N}.\left[\text{curl}\ \frac{1}{\mu}\ \text{curl}\ \bar{A} + \sigma\frac{\partial \bar{A}}{\partial t} + \sigma(\bar{u}.\text{grad})\bar{A}\right] d\Omega$$

$$= \int \frac{1}{\mu}\ \text{curl}\ \bar{N}.\text{curl}\ \bar{A} + \sigma\,\bar{N}.\frac{\partial \bar{A}}{\partial t} + \sigma\,\bar{N}.\ (\bar{u}.\text{grad})\bar{A}\, d\Omega$$

$$- \oint \bar{N}.\left[\frac{1}{\mu}\ \text{curl}\ \bar{A} \times \bar{n}\right] d\Gamma = 0 \quad (9)$$

A device with a moving region of constant cross section not in contact with any conductor moving at a different speed may then be modelled in terms of eqns (4) (which could represent the total or reduced magnetic scalar potentials) and eqn (8).

Table 1 – Details of the C core magnet

magnet stack height (A)	42 mm
magnet yoke width (B)	12 mm
magnet slot width	20 mm
magnet tooth width	12 mm
magnet AT (each coil)	189 mm
magnet airgap	2.5 mm
drum steel width	50 mm
drum steel radius	305.8 mm
drum aluminium width	110 mm
drum aluminium thickness	0.9 mm
drum aluminium conductivity	3.2×10^7 s/m

A dc magnet moving past a conducting rail

A rig designed to test moving conductor formulations has been built. A steel drum faced by a continuous aluminium plate rotates under a 'C' core magnet carrying DC current (details, Table 1 and Fig. 1). All of the eddy currents induced in the plate are hence due to velocity and the problem can be modelled with the $\partial/\partial t$ terms in eqns (2, 3) or eqn (8) set to zero since there is no time variation. The magnet is held in a cage which is free to rotate about the centre of the drum shaft so that drag force can be measured. Other load cells also measure the force normal to the drum. Fig. 2 shows a view of the computer model of the magnet. Figs. 3 and 4 show drag and normal force respectively. Measurements are compared with 3D calculations done using the A-V-φ and the A-φ methods. The coil source currents are modelled by the reduced and total scalar potential technique. Fig. 5 shows a set of results for the airgap flux normal to the drum, taken along a line at the centre of the airgap from the 'entry edge' of the magnet to the 'trailing edge'.

Both sets of computed results are acceptable; it is noteworthy that the A-V-φ method used up to almost 2.5 times as much cpu time as the A-φ method.

Moving conductors at different speeds in sliding contact

This type of problem arises when modelling electromagnetic launchers of the 'rail gun' type. The armature slides between the rails and is in electrical contact with them (Fig. 6). In order that the Minkowski transformation remains valid, it is possible to solve the problem with the rails moving and the armature stationary. The interface between the rails and armature requires that $\bar{E} \times \bar{n}$ and $\bar{J}.\bar{n}$ are continuous. At the interface between two regions, moving (1) and stationary (2), this leads to:

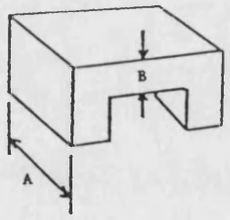

Fig. 1 Showing details of the 'C' core magnet of Table 1

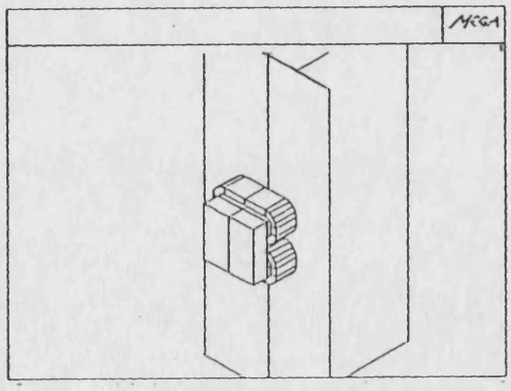

Fig. 2 A view of the computer model of the magnet

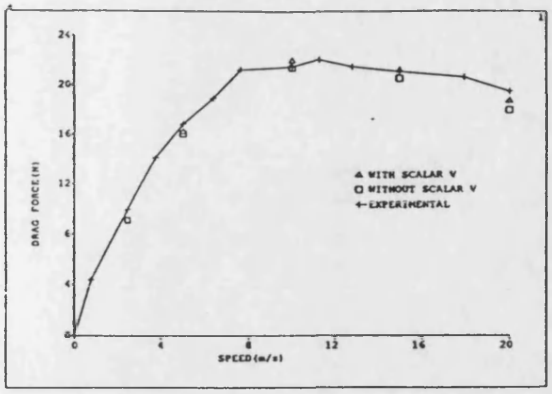

Fig. 3 Drag force versus speed for the 'C' core magnet

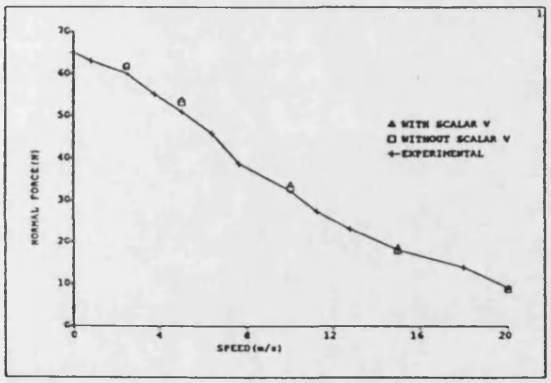

Fig. 4 Normal force versus speed for the 'C' core magnet

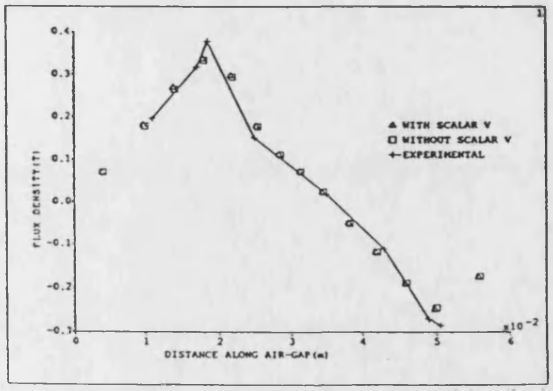

Fig. 5 Airgap flux density for the 'C' core magnet at 10 m/s

$$\left[-\frac{\partial \bar{A}_1}{\partial t} - (\bar{u} \cdot \text{grad})\,\bar{A}_1\right] \times \bar{n} - \left[-\frac{\partial \bar{A}_2}{\partial t}\right] \times \bar{n} \qquad (10)$$

and

$$\sigma_1 \left[-\frac{\partial \bar{A}_1}{\partial t} - (\bar{u} \cdot \text{grad})\,\bar{A}_1\right] \cdot \bar{n} - \sigma_2 \left[-\frac{\partial \bar{A}_2}{\partial t}\right] \cdot \bar{n} \qquad (11)$$

Clearly, the interface conditions cannot be satisfied using a continuous $\bar{A}$ vector, unless the electric scalar V is also present. If V is not used, we must define a discontinuous $\bar{A}$ field and join it using the interface conditions of eqns (10) and (11).

Fig. 7 shows a thin 'surface' element which exists between region 1 and region 2. A local co-ordinate system is shown, n is normal to the interface and r and s are on the interface. In the thin element, from curl $\bar{E} = -\partial\bar{B}/\partial t$ and using the Galerkin scheme, we have:

$$\iint \left[\bar{N}.\text{curl}\,\frac{1}{\sigma}\,\text{curl}\,\bar{H} + \bar{N} \cdot \mu \frac{\partial \bar{H}}{\partial t}\right] d\Omega$$

$$- \iint \left[\frac{1}{\sigma}\,\text{curl}\,\bar{N}.\text{curl}\,\bar{H} + \bar{N}.\mu \frac{\partial \bar{H}}{\partial t}\right] d\Omega$$

$$- \oint \bar{N}.\left[\frac{1}{\sigma}\,\text{curl}\,\bar{H} \times \bar{n}\right] d\Gamma = 0 \qquad (12)$$

If the element is shrunk in the n direction,

$$d\Omega \to d\,ds\,dr \quad \text{and} \quad \frac{\partial}{\partial n} \to 0$$

We then have, from eqn (12)

$$\iint \left[\frac{1}{\sigma}\frac{\partial N_r}{\partial s}\left[\frac{\partial H_r}{\partial s} - \frac{\partial H_s}{\partial r}\right] + \mu N_r \frac{\partial H_r}{\partial t}\right] dr\,ds$$

$$+ \oint N_r E_s\,dr\,ds = 0 \qquad (13)$$

and

$$\iint \left[\frac{1}{\sigma}\frac{\partial N_s}{\partial r}\left[\frac{\partial H_s}{\partial r} - \frac{\partial H_r}{\partial s}\right] + \mu N_s \frac{\partial H_s}{\partial t}\right] dr\,ds$$

$$- \oint N_s E_r\,dr\,ds = 0 \qquad (14)$$

The right hand surface integral terms in eqns (13) and (14) are only non zero on the two sides of the element parallel to the interface. We can substitute for $\bar{E}$ in those integrals from eqn (10). The $\bar{A}$ elements will each give rise to a surface integral involving $\bar{H}$ (from eqn (9)). $\bar{H}$ values from the thin surface element are substituted in these surface terms.

The $\bar{J}.\bar{n}$ terms of eqn (11) are enforced directly using Lagrange mutlipliers. This scheme yields a final set of eqns which is symmetric for the case of $\bar{u} = 0$.

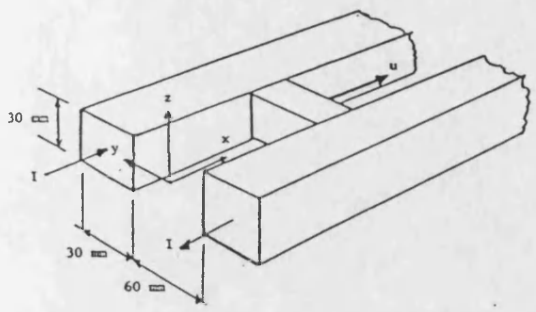

Fig. 6 A sketch of a rail gun

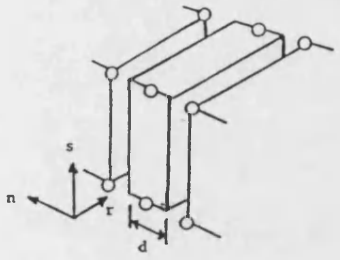

Fig. 7 A thin interface element

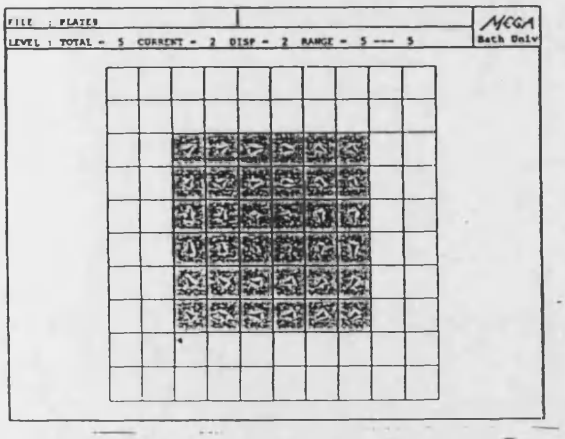

Fig. 8 Currents in a plate solved with discontinuous $\bar{A}$

Eddy currents in a flat plate

The above scheme for joining $\bar{A}$ fields at an interface can easily be tested for the case $u = 0$. This was done for the plate shown in Fig. (8). The plate is modelled with two different $\bar{A}$ fields joined along the line shown using the thin element scheme. The plate is subject to a changing magnetic field from two pole sources above and below the plate. The plate was modelled in 3D.

It may be observed from the symmetry of the current pattern in the plate that the interface does not affect the flow lines. The results are identical to those from the plate modelled using 'conventional' $\bar{A}$-φ, typically to 4 significant figures.

Eddy currents in an electromagnetic launcher

Fig. 6 shows a rail gun launcher. This can be modelled in 2D by assuming that it is invarient in the z direction, and modelling fields in terms of Hz [3,4,5]. This case can also be modelled using $\bar{A}$-φ, using the 'sliding contact' technique at the rail-armature interface. Results for magnitude of current along a line parallel to the x axis and 1.66 mm into the rail are shown on Fig. 9 for a velocity of 20 m/s and 4 msecs after a step switch on transient. It may be observed that the 3D methods show a non physical spike in current around the area shown as x = 0.05 m on the graph. This is where there is a 3:1 jump in mesh size in the x direction. The results are particularly poor for the upwind case. Treating the velocity terms in the usual way, not using upwinding, improves the situation at this low speed, but this is not possible at higher speeds. The spike can be removed by grading the mesh, as shown. This is at present a disadvantage of the upwind scheme and work is in progress to cure this problem. Fig. 10 shows a 3D rail gun at 20 m/s and 2 msec after a step switch on transient. As the mesh used contains few large changes in size, the results are acceptable.

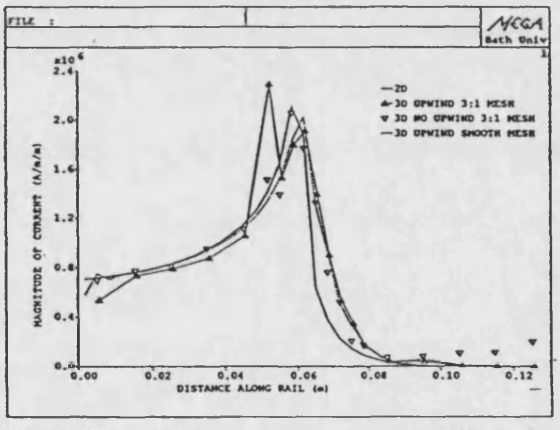

Fig. 9 Magnitude of current along a rail

CONCLUSIONS

A new method which does not require the electric scalar potential inside conducting regions in moving conductor problems has been described. The interface between moving and stationary conductors requires a jump in magnetic vector potential when the electric scalar is not present. This is handled using a 'thin surface' element. The upwind method does not work well when jumps of about 3:1 are encountered in the mesh size in the direction of motion. We have resisted the temptation to call this the velocity modified magnetic vector potential technique.

REFERENCES

[1] D. Rodger, T. Karaguler, P.J. Leonard: 'A formulation for 3D moving conductor eddy current problems', IEEE Trans Mag, Vol. 25, No. 5, Sept 1989, pp. 4147–4149.

[2] T.J.R. Hughes: 'A simple scheme for developing 'upwind' finite elements', IJNME, Vol. 12, pp. 1359–1365.

[3] Long: 'Rail gun current density distributions', IEEE Trans on Mag, Vol. MAG–22, No. 6, Nov 1986.

[4] S.P. Atkinson: 'Electromagnetic modelling of rail guns', 5th Symposium of Electromagnetic Launch Technology, 2 April 1990.

[5] D. Rodger, P.J. Leonard and J.F. Eastham: 'Modelling electromagnetic launchers at speed using 3D finite elements' (ibid).

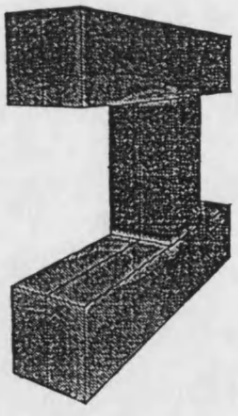

Fig. 10 3D view of a rail gun showing contours of magnitude of current at 20 m/s and 2 msecs after switch on

A FORMULATION FOR 3D MOVING CONDUCTOR EDDY-CURRENT PROBLEMS

D. Rodger, T. Karaguler, P.J. Leonard
University of Bath, Bath, Avon BA2 7AY

A 3D finite element formulation for moving conductor problems is outlined. Upwinding is shown to be important at high values of Peclet number.

Introduction

Many devices, for instance, electromagnetic launchers and linear induction machines, involve conducting parts which move. The geometry of these machines is often such that full 3D computer models are required. In this contribution we describe a new formulation for 3D eddy current moving conductor problems and show how the technique of upwinding, borrowed from the field of fluid flow, is very important in achieving accurate numerical solutions. The technique is implemented using standard 3D finite elements.

We only consider the type of moving conductor problem in which the moving member is invarient in the cross section which is normal to the direction of motion. This allows motion to be taken into account using the usual Minkowski transformation, which leads to a steady state solution for constant speed moving conductor problems. All other geometries would lead to a full time transient analysis. Eddy currents can be generated in the same region by a combination of time varying source fields as well as by motion ('transformer' and 'flux cutting' emfs). In this paper we only deal with the latter.

Theoretical Development

The $\bar{A}-\psi$ method has been used for some time for solving 3D eddy current problems which are either harmonic or transient in time [1-4]. The problem volume is partitioned into conducting and non-conducting regions. Magnetic scalars are used to model fields in non-conducting regions, reduced magnetic scalars [5] in regions containing known source currents and total scalars elsewhere.

Eddy current regions are modelled using the magnetic vector potential $\bar{A}$, with [2,4,6] or without [1,3] an auxiliary electric scalar potential V. The regions are conveniently joined together at the common interface by invoking the continuity of $\bar{H}\times\bar{n}$ and $\bar{B}.\bar{n}$.

Moving conductor formulation

In the laboratory reference frame, the moving region electric field has two components:

$$\bar{E} = -\bar{u} \times \bar{B} - \text{grad } V \qquad (1)$$

In the above, $\bar{u}$ is the velocity of the region with respect to the laboratory and V is the electric scalar potential.

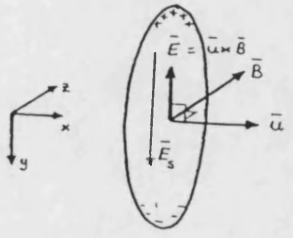

fig. 1 Fields in a moving rod

The two components of $\bar{E}$ can be readily recognised from fig. 1, which shows a conducting bar moving in the x direction through a constant z directed magnetic field. There is a force on each charge of q coulombs given by: $\bar{F} = q\bar{u} \times \bar{B}$. This leads to a displacement of mobile charges as shown. These charges give rise to an electrostatic field shown as $\bar{E}_s$ which is represented in eqn (1) as $-$ grad V.

Using $\bar{B} = \text{curl } \bar{A}$, we can obtain:

$$\text{curl } \frac{1}{\mu} \text{curl } \bar{A} - \sigma\,(\bar{u} \times \text{curl } \bar{A} - \text{grad } V) \qquad (2)$$

From div $\bar{J} = 0$:

$$\text{div } \sigma\,(\bar{u} \times \text{curl } \bar{A} - \text{grad } V) = 0 \qquad (3)$$

Eqns 2 and 3 do not define a unique system. The Helmholtz theorem states that a vector field is unique if its curl and divergence are known throughout a volume, together with the normal component on the boundary. Here we choose div $\bar{A} = 0$ throughout and $\bar{A}.\bar{n} = 0$ on the boundary. The condition div $\bar{A} = 0$ can be imposed on eqn (2) by means of Lagrange multipliers [1] or by a penalty technique $-$ the latter is used here.

Numerical Implementation

As usual, the Galerkin weighted residual technique is used to find an approximate solution to eqns (2) and (3).

Equation 2

This leads to a standard set of equations:

$$\int \frac{1}{\mu} \text{curl } \bar{N}.\text{curl } \bar{A} + \bar{N}.(\sigma(\bar{u} \times \text{curl } \bar{A}) - \text{grad } V)d\Omega - \oint \bar{N}.(\frac{1}{\mu} \text{curl } \bar{A} \times \bar{n})d\Gamma = 0 \qquad (4)$$

$\bar{N}$ are the shape functions.

In order to impose div $\bar{A} = 0$, we add the term

$$\int \alpha \text{ div } \bar{N} \text{ div } \bar{A}\, d\Omega$$

to eqn (4), where α is a large number (usually of the same order as $\frac{1}{\mu}$). Best results are obtained if this set of constraints is singular [7], therefore numerical integration one order less than that which would lead to an exact evaluation of these integrals should be used (order 1 for first order elements).

Incidentally, a different argument can be used [8] to show that the addition of the term

$$\int \bar{N}.\text{grad}(\frac{1}{\mu_0} \text{ div } \bar{A})d\Omega$$

leads to the same results, if $\alpha = \frac{1}{\mu_0}$

The terms involving the velocity $\bar{u}$ require special treatment, upwinding, as outlined below.

0018-9464/89/0900-4147$01.00©1989 IEEE

Equation (3)

Since

$$\int N \operatorname{div} \bar{J} = \oint N \bar{J}.\bar{n}\, d\Gamma - \int \operatorname{grad} N.\bar{J}\, d\Omega,$$

from eqn (3) we have:

$$\oint N\sigma(\bar{u} \times \operatorname{curl} \bar{A} - \operatorname{grad} V).\bar{n}\, d\Gamma$$

$$-\int \operatorname{grad} N.\sigma(\bar{u} \times \operatorname{curl} \bar{A} - \operatorname{grad} V)\, d\Omega - 0$$

The surface integral is important as it yields $\bar{J}.\bar{n} = 0$ as the natural boundary condition on the inside of the conductor.

We need to include V in this formulation as this models the electrostatic field which is the mechanism for controlling the flow of current within the conductor and obtaining $\bar{J}.\bar{n} = 0$ on the conductor-air interface surfaces. Without the electrostatic component of $\bar{E}$ (given by $-$ grad V in eqn (1)), we would have to try and impose $\bar{E}.\bar{n} = 0$ on $\bar{u} \times \bar{B}$ at these surfaces. Obviously this is impossible in the general case without introducing erroneous constraints on $\bar{B}$.

Upwinding

When the Galerkin technique is applied to eqn (4), large -ve terms are generated on the diagonal of the final global matrix. This typically causes oscillations in the solution and very poor results when the Peclet number, $p = \frac{\sigma h u \mu}{2}$, is greater than 1.0 (h is the average element length in the direction of the velocity).

This problem has long been familiar in fluid dynamics. The solution is known as upwinding. A finite element scheme which allows different degrees of upwinding in each moving conductor element has been developed for fluid flow [9].

Usually the integrals of eqn (4) are evaluated using Gaussian quadrature, sampling at the normal quadrature points. Using an upwind scheme, different sampling points are used for evaluating the velocity terms only of eqn (4) as follows, for element e:

$$\int_e \bar{N}.(\sigma(\bar{u} \times \operatorname{curl} \bar{A}))\, d\Omega \triangleq$$

$$\Sigma_e \bar{N}(\epsilon).(\sigma(\bar{u}(o) \times \operatorname{curl} \bar{A}(\epsilon)))J(0)W$$

$\bar{u}(o)$ is the velocity evaluated at the origin of the isoparametric co-ordinates of the element, J(o) is the Jacobian of the isoparametric transform, W equals 8 for a 3D element and 4 for a 2D element. The location of point ϵ (this is a local co-ordinate, $-1 \leq \epsilon \leq 1$) determines the degree of upwinding.

The optimal position for ϵ has been shown to be [9]:
$\epsilon = \coth p - \frac{1}{p}$

This scheme is very easily implemented, some earlier schemes were rather complex.

Results

2D test problem illustrating upwinding

It is interesting to demonstrate the value of upwinding. A very simple test problem which can be solved using a Fourier series analysis is shown in fig. 2. This involves a moving iron rotor, a μ_r of 2000 leads to high values of p. Results for 2D finite elements with and without upwinding are shown on fig. (3). The drag force for the no upwind case is poor, (5 m/s represents a Peclet number of about 125 for the mesh used).

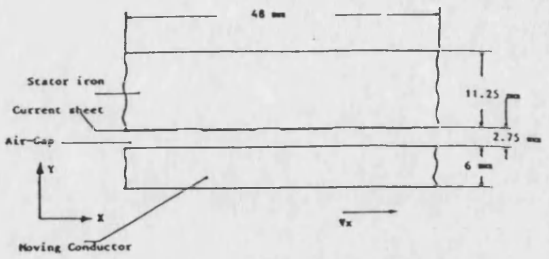

fig. 2 2D test problem with steel rotor

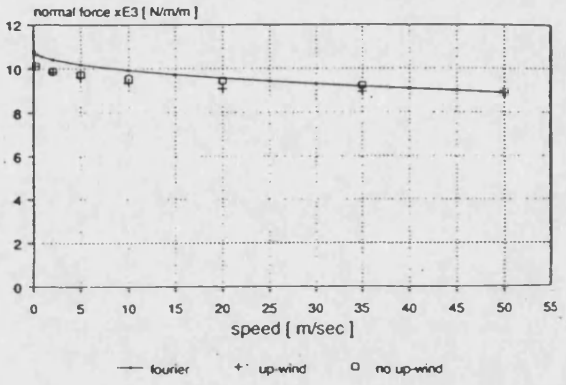

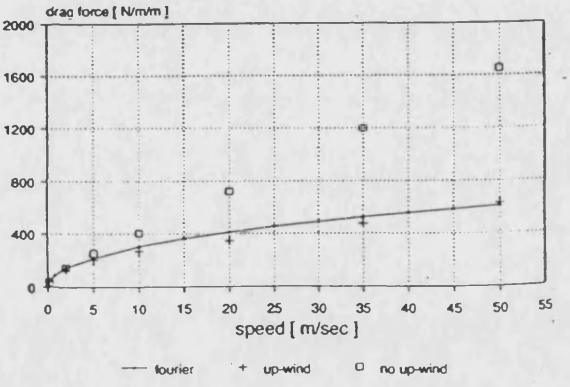

fig. 3 Forces on the 2D rotor

3D problem – filamentary coil moving over an aluminium track

This problem is of interest in MAGLEV advanced transport system design. The coil would normally be superconducting and would, of course, carry DC current. The dimensions are shown on fig. 4. Lift and drag forces are shown on fig. 5. Also shown are forces obtained from a Fourier transform technique applied to a conducting plate of the same thickness and infinite extent. The agreement is probably reasonable.

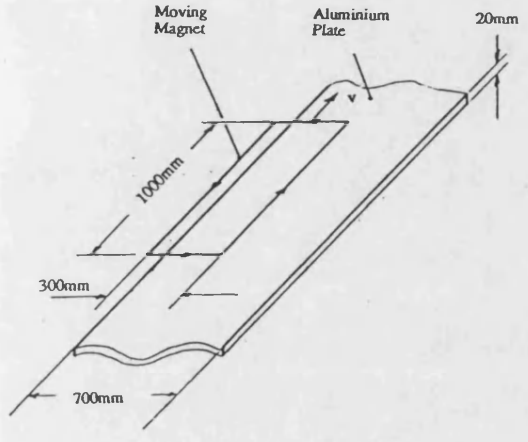

fig. 4 Rectangular coil moving over an aluminium rail

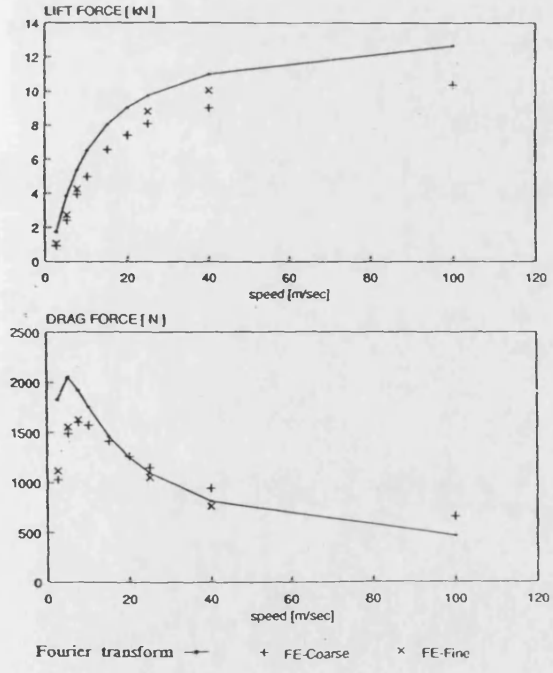

fig. 5 Forces on the rectangular coil

Conclusions

Problems involving 3D eddy currents generated by velocity effects have been investigated. The scalar V is needed inside conductors when using this formulation. It is well known that time varying eddy current problems can be solved using only the vector $\underline{A}$ (without V) inside conducting regions, linked to ψ elsewhere. In this case we rely on the $\underline{J}.\underline{n} = 0$ condition being weakly enforced [3] on the inside surface of conducting regions. This condition will remain approximately true for problems in which the eddy current effect is predominantly due to time variation of fields, with a small component due to velocity. An earlier paper [10] illustrates results for this case. This is valid only where speeds are relatively low, and although more economic than the present implementation, should be used with extreme caution.

Even when using upwinding, it is possible for the conjugate gradient technique to fail to converge. This has been found for Peclet numbers of about 6000 in 3D problems. At this point, the only remedy is to refine the mesh, which is likely to be too coarse from other points of view (accuracy, skin depth).

References

[1] D. Rodger 'A finite element method for calculating power frequency three dimensional electromagnetic field distribution' IEE Proc.A, Vol.130(5), 1983, pp. 233–238.

[2] R.D. Pilsbury 'A three-dimensional eddy-current formulation using two potentials: the magnetic vector potential and total magnetic scalar potential' IEEE Trans 1983 MAG-19(6), pp. 2284–2287.

[3] C.R.I. Emson and J. Simkin 'An optimal method for 3D eddy currents ibid 1983, MAG-19(6), pp. 2450–2452.

[4] A. Kameari 'Three dimensional eddy current calculation using finite element method with A-V in conductor and Ω in vacuum' IEEE Trans Mag, Vol.24, No.1, Jan 1988, pp. 118–121.

[5] J. Simkin and C.W. Trowbridge 'On the use of total scalar potential in the numerical solution of field problems in electromagnetics' Int JNME 1979 14, pp. 423–440.

[6] P.J. Leonard and D. Rodger 'A finite element scheme for transient 3D eddy currents' IEEE Trans Mag, Vol.24, No August 1987, pp. 90–93.

[7] O.C. Zienkiewicz 'The finite element method' (McGraw-Hill 1977, 3rd Ed).

[8] W. Renhart, H. Stogner and K. Preis 'Calculation of 3D eddy current problems by finite element method using either an electric or a magnetic vector potential' IEEE Trans Mag, Vol.24, No.1, Jan 1988, pp. 122–125.

[9] T.J.R. Hughes 'A simple scheme for developing 'upwind' finite elements' IJNME, Vol.12, pp. 1359–1365.

[10] D. Rodger and J.F. Eastham 'Characteristics of a linear induction tachometer – a 3D moving conductor eddy current problem' IEEE Trans Mag, Nov 85, 2412–2415.

APPENDIX 2.1

Integration by Parts and Green's Theorem

The operation of integration by parts is derived from the divergence theorem which states

$$\int_v div(k\bar{F})\, dv = \oint_s k\bar{F}\cdot\bar{n}\, ds \qquad \text{(A2.1)}$$

where k is a scalar, $\bar{F}$ is a vector function, v is the volume and s is a closed surface with outward normal $\bar{n}$. By using the distributive characteristic of divergence over a scalar multipalication of a vector function

$$div(k\bar{F}) = grad\, k.\bar{F} + k\, div\bar{F} \qquad \text{(A2.2)}$$

equation A2.1 can be rewritten as:

$$\int_v div\bar{F}\, dv = \int_v -grad\, k\cdot\bar{F}\, dv + \oint_s k\bar{F}\cdot\bar{n}\, ds \qquad \text{(A2.3)}$$

The expression of Green's theorem can be obtained if $\bar{F}$ is substituted with a gradient of a scalar function, $grad\, l$ in the equation above

$$\int_v k\, div\, grad\, l\, dv = -\int_v grad\, k\cdot grad\, l\, dv + \oint_s k(grad\, l)\cdot\bar{n}\, ds \qquad \text{(A2.4)}$$

APPENDIX 2.2

Pre-conditioned Conjugate Gradient Methods

The gradient methods in general, seek the position of the minimum of an error function derived from the residual vector given as

$$R = B - KX_t \tag{A2.5}$$

where **B** is the right hand side matrix, **A** is the sparse matrix and X_t is the trial solution vector. The positive error function can be obtained from the residues vector as:

$$h^2 = R^T K^{-1} R \tag{A2.6}$$

in fact, X_t can be expressed as a line through the point X_p

$$X_t = X^{(m)} + k d^{(m)} \tag{A2.7}$$

m is the iterative number, **k** is a parameter proportional to the distance of X_t from **X**, **d** is the direction vector. If eqn. (A2.7) is substituted into (A2.6)

$$h^2 = k^2 [d^{(m)}]^T A d^{(m)} - 2k [d^{(m)}]^T R^m + [X^m]^T A X^{(m)} + B^t A^{-1} B \tag{A2.8}$$

And the local minimum which defines the succeeding trial vector is obtained from

$$\frac{\partial h^2}{\partial k} = 0$$

as;

$$x^{(m+1)} = x^{(m)} + k_m d^{(m)}$$

where $\mathbf{k_m}$ is defined as:

$$k_m = \frac{[d^{(m)}]^T R^{(m)}}{[d^{(m)}]^T A\, d^{(m)}}$$

All the gradient methods follow this pattern and only differ from each other in the choice of the direction vectors. For instance in the method of steepest descent, the direction vector $\mathbf{d^{(m)}}$ is chosen to be the direction of maximum gradient of the function at the point $\mathbf{X^{(m)}}$. However the conjugate gradients method chooses the directin vector to be a set of mutually conjugate $\mathbf{P^{(0)}}$,$\mathbf{P^{(1)}}$, ... vectors which are also in the directions of the steepest descent points $\mathbf{X^{(0)}}$,$\mathbf{X^{(1)}}$,..., and orthogonal with respect to **A**. Therefore they satisfy the condition of

$$[P^i]^t A P^j = 0 \qquad for \quad i \neq j \tag{A2.10}$$

The algorithm for the conjugate gradient method for the (m+1).th step can be written as follows;

$$\begin{aligned} U^{(m)} &= A p^{(m)} \\ k_m &= \frac{[R^{(m)}]^T R^{(m)}}{[P^{(m)}]^T U^{(m)}} \\ X^{(m+1)} &= X^{(m)} + \alpha_m P^{(m)} \\ R^{(m+1)} &= R^{(m)} - \alpha_m U^{(m)} \end{aligned} \tag{A2.11}$$

$$l_m = \frac{[R^{(m+1)}]^T R^{(m+1)}}{[R^{(m)}]^T R^{(m)}}$$

$$P^{(m+1)} = R^{(m+1)} + l_m P^m$$

Despite the fact that the conjugate gradient method converges much faster than any other well known numerical method, it possesses the drawback of being heavily dependent on the eigenvalue spectrum of the **K** matrix. If the eigenvalue spectrum is wide, the convergence can be slow. This is why the pre-conditioned conjugate gradient method is developed. The pre-conditioned method uses a pre-conditioning matrix **C** in such a way that the **K** matrix is replaced with $\mathbf{C\,K\,C^T}$ in the process. This modification which leads to a much faster convergence, redefines the conjugate vectors $\mathbf{P^m}$ and conjugate parameters $\mathbf{l_m}$ as

$$P^{m+1} = C R^{(m+1)} + l_m P^m \qquad \text{(A2.12)}$$

and

$$l^m = \frac{[P^{(m)}]^t A C R^{(k+1)}}{[P^{(m)}]^t A P^m} \qquad \text{(A2.13)}$$

APPENDIX 3.1

Forces on a Moving Rectangular Coil

The lift and drag forces results (used in comparesin with the 3D FE method in chapter 3) a rectangular coil moving above a conducting sheet of finite thickness are obtained by using the exact substitutions of the Reitz and Davis formula, which is based on the Fourier transform method [3.5]. With reference to fig 3.7, a coil filament whose dimensions are (2a × 2b), moves in the x-direction with a constant velocity over an infinitely long aluminium track. The coil is placed in a plane parallel to the surface of the plate, at a suspension height of h (in the z-direction). By using Maxwell's equations, (2.1) and (2.2) together with Ohm's law, (2.7), the governing equation for the conducting region is obtained in terms of each component of **B**.

$$\frac{\partial^2 B}{\partial^2 x} + \frac{\partial^2 B}{\partial^2 y} + \frac{\partial^2 B}{\partial^2 z} = -\mu_0 \sigma \frac{\partial B}{\partial t} \tag{A3.1}$$

As the conducting region is assumed infinitely long, the Fourier method can be applied to eqn. (A3.1) for the solution. By doing so (since the calculation of Fourier coefficients and transforms is clearly given in the reference publication, it is omitted here) the drag and lift forces can be obtained as:

$$F_L = \frac{8\mu_0 I^2}{2} \int_0^{\infty}\int_0^{\infty} dxdy \sin^2\left(\frac{a}{h}y\right) \sin^2\left(\frac{b}{h}x\right) e^{-2\sqrt{x^2+y^2}} \left(\frac{1}{x^2}+\frac{1}{y^2}\right) \cdot \frac{R - S - T}{m(1 + c^2(A^2 + D^2) - 2c(A\cos\alpha + D\sin\alpha)}$$

and

$$F_D = \frac{8\mu_0 I^2}{\pi^2} \int_0^{\infty} \int_0^{\infty} dx\,dy \sin^2\left(\frac{a}{h}y\right) \sin^2\left(\frac{b}{h}x\right) e^{-2\sqrt{x^2+y^2}} \left(\frac{\sqrt{x^2+y^2}}{xy^2}\right) \cdot \frac{R - S - T}{m\left(1 + c^2(A^2+D^2) - 2c\left(A\cos\alpha + D\sin\alpha\right)\right)}$$

where

$$R = 2c^2 B_2 D - (1-d)(1+c^2 A)$$

$$S = c\cos\alpha\,[2B_2 D - (1-d)(1+A)]$$

$$T = c\sin\alpha\,[2B_2(1-A) - D(1-d)]$$

$$U = 2B_2(1+c^2 A) + c^2 D(1-d)$$

$$V = c\cos\alpha\,[(1-d)D + 2B_2(1+A)]$$

$$W = c\sin\alpha\,[(1-d) + 2B_2 D$$

$$\lambda_1 = \mu_0 \sigma u$$

$$d = \left[\left(\frac{\lambda_1 h u}{x^2+y^2}\right)^2 + 1\right]^{\frac{1}{2}}$$

$$B_1 = [0.5(d+1)]^{\frac{1}{2}}$$

$$B_2 = [0.5(d-1)]^{\frac{1}{2}}$$

$$C = \exp\left(\frac{-2B_1\sqrt{x^2+y^2}\,t}{h}\right)$$

$$m = 1 + d + 2B_1$$

$$A = \frac{d^2 - 4d + 3}{m^2}$$

$$D = \frac{4(d - 1)B_2}{m^2}$$

$$\alpha = 2B_2\sqrt{x^2 + y^2}\ \frac{t}{h}$$

σ conductivity of the aluminium plate [Ohm m]$^{-1}$

2a width of the coil [m],

2b length of the coil [m]

t thickness of the conducting plate [m]

h suspension height

I current [AT]

u speed [m/s]

APPENDIX 5.1

The Air-Gap Equation

The stator and rotor current sheets are assumed to be only in the z-direction, and the permeability of rotor and stator iron to be infinite. With respect to fig. A5.1, two equations, below, can be derived from Ampere's law.

$$g \frac{\partial H_y}{\partial x} = J_s + J_r \tag{A5.1}$$

$$\frac{\partial E_z}{\partial x} = \mu_0 \frac{\partial H_y}{\partial t} \tag{A5.2}$$

As Ohm's law states that;

$$J_r = \sigma (E_z + u_x B_y) \tag{A5.3}$$

and using $B = \mu_0 H$ for the air-gap from (A5.1), (A5.2) and (A5.3), the air-gap equation is obtained as:

$$\frac{\partial^2 B_y}{\partial x^2} - \frac{\mu_0 \sigma u_x}{g} \frac{\partial B_y}{\partial x} - \frac{\mu_0 \sigma}{g} \frac{\partial B_y}{\partial t} = \frac{\mu_0}{g} \frac{\partial J_s}{\partial x} \tag{A5.4}$$

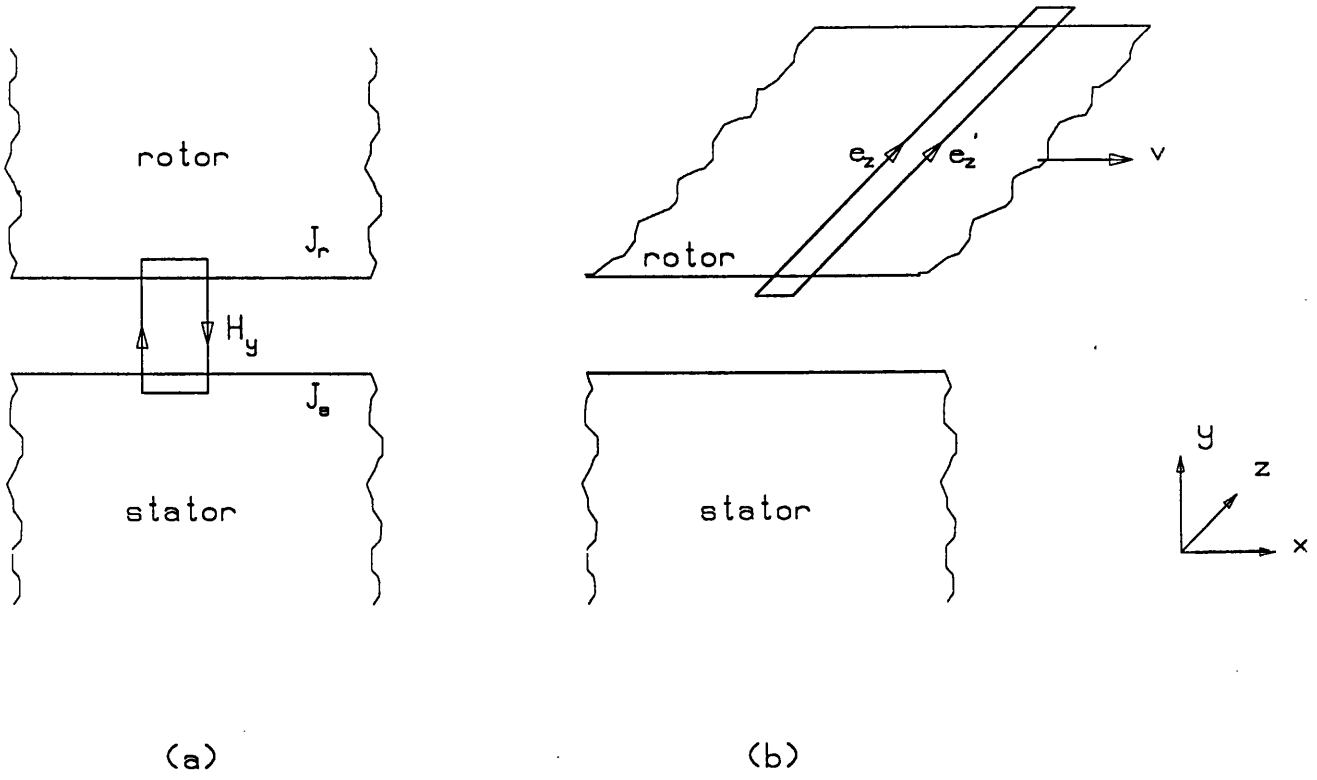

Fig. Ap5.1 Components of fields for the air-gap equation.

APPENDIX 5.2

The Coefficients for the 2D modellings

i) The Carter Coefficient

As mentioned in section 5.2.2, if the stator of an electrical machine is modelled without considering its slotted structure, a coefficient is needed to determine a realistic air-gap for the machine [5.4]. A simple adaptation of Carter's original work [5.5] is used in this work to determine the realistic air-gap of the servomotor.

If the slots are designed as being open the coefficient is determined as:

$$K_{c_1} = \frac{s(5g + s_w)}{s(5g + s_w) - s_w^2} \qquad \text{(A5.5)}$$

and if the slots are partially closed then the coefficient will be

$$k_{c_2} = \frac{s(4.4g + 0.75s_w)}{s(4.4g + 0.75s_w) - s_w^2} \qquad \text{(A5.6)}$$

where s is the pole pitch, g is the air-gap, and s_w is the slot width.

ii) The Rotor Resistivity Coefficient

In the 2D modelling, the returning paths of the currents on the conducting plate are taken into account by using a factor which increases the value of the rotor resistivity. A simple approach [5.7] based on reference work of Russel and Norsworthy [5.6] is used to determine this rotor resistivity factor. If $\mathbf{d_w}$ represents the stator width, and $\mathbf{p_w}$ represents the conducting plate width, the coefficient $\mathbf{k_r}$ is determined as

$$k_r = \frac{1}{1 - \left[\dfrac{\tanh(k_e)}{k_e(1 + \tanh(k_e)\cdot\tanh(k_\phi)}\right]} \qquad \text{(A5.7)}$$

where

$$k_e = 0.5\, d_w \frac{\pi}{5}$$

$$k_\phi = 0.5\,(p_w - d_w)\frac{\pi}{5}$$

APPENDIX 5.3

Harmonic Analysis of Slot Current Density

The m.th slot in fig. A5.2 produces a rectangular pulse of conductor density of magnitude $N / 2\delta$ where 2δ is the slot width. The amplitude of the n.th harmonic of this pulse is the complex Fourier form given as

$$C^n = \frac{1}{ML} \int_{-P}^{+P} f(x)\, e^{-jnkx}\, dx \qquad \text{(A5.8)}$$

If $f(x) = \frac{N}{2\delta}$, $+P = x_m + \delta$, $-P = x_m - \delta$ *and* $k = \frac{2\pi}{ML}$,

C^n becomes:

$$C^n = \frac{N}{ML} \frac{\sin(nk\delta)}{nk\delta}\, e^{-jnkx_m}\, e^{jnkx} \qquad \text{(A5.9)}$$

If C^n is known, the function $F(x)$ can be obtained as

$$F(x) = \sum_{n=-\infty}^{n=+\infty} \frac{N}{ML} \frac{\sin(nk\delta)}{nk\delta}\, e^{-jnkx_m}\, e^{jnkx} \qquad \text{(A5.10)}$$

Since the general sinusoidal form of current is given as $I(\omega t) = I\, e^{j\omega t}$ where I can be complex, the current density is obtained from $J(x, \omega t) = F(x)\, I(\omega t)$ as;

$$J(x,t) = \frac{NI}{ML} \sum_{-\infty}^{+\infty} \frac{\sin(nk\delta)}{nk\delta}\, e^{-jnkx_m}\, e^{j(nkx + \omega t)} \qquad \text{(A5.11)}$$

APPENDIX 5.4

Elements of the Transfer Matrix

When using the layer theory for the solution of magnetic field problems, the regional field quantities are coupled by means of a matrix refered to 'transfer matrix' in the form that is obtained in section 5.3.3

$$\begin{bmatrix} B_{yR} \\ H_{xR} \end{bmatrix} = \begin{bmatrix} T_{11}(r) & T_{12}(r) \\ T_{21}(r) & T_{22}(r) \end{bmatrix} \begin{bmatrix} B_{yR-1} \\ H_{xR-1} + J \end{bmatrix}$$

where the matrix elements are defined as:

$$T_{11}(r) = \frac{1}{2}\left(e^{\lambda_r g_r} + e^{-\lambda_r g_r}\right)$$

$$T_{12}(r) = \frac{1}{2}\frac{jkn\mu_r}{\lambda_r}\left(e^{\lambda_r g_r} - e^{-\lambda_r g_r}\right)$$

$$T_{21}(r) = \frac{1}{2}\frac{\lambda_r}{jkn\mu_r}\left(e^{\lambda_r g_r} + e^{-\lambda_r g_r}\right)$$

$$T_{22}(r) = \frac{1}{2}\left(e^{\lambda_r g_r} + e^{-\lambda_r g_r}\right)$$

REFERENCES

[1.1] **Courant R** 'Variational Methods for the Solution of Problems of Equilibrium and Vibrations,' *Bull Am Math soc, 49: 1-23 (1943)*

[1.2] **Turner M.J, Clough R W, Martin H.C, and Topp L. J.** 'Stiffness and Deflection Analysis of Complex Structures, ' *J Aeron Sci, 23(9), 805-823, 854 (1956).*

[1.3] **Irons B M** 'A Frontal Solution Program for Finite Element Analysis' *International Journal for Numerical Methods in Engineering, Vol.2, No.1, Jan. 1970, pp. 455-472.*

[1.4] **Zienkiewicz O C** 'The Finite Element Method', *McGraw Hill, First Edition, 1967.*

[1.5] **Winslow A A,** 'Numerical Solution of the Quasi-Linear Poisson Equation in a Non-uniform Triangular Mesh.' *J.Comput. Phys.1 p. 149 1971.*

[1.6] **Carpenter C J** 'Finite Element Network Models and Their Applications to Eddy current Problems ' *Proc. IEE. 1975, 122 (4), pp. 455-462.*

[1.7] **Simkin J and Trowbridge C W,**'On the Use of Total Scalor Potential in the Numerical Solution of Field Problems', *Int. Meth. Eng., 1979, 14, pp. 423-440.*

[1.8] **Rodger D** 'A Finite Element Method for Calculating Power Frequency Three Dimensional Electromagnetic Field Distribution', *IEE Proc A, Vol130 (5), 1983, pp 233-238.*

[1.9] **Pillsbury R D** ' A Three Dimensional Eddy Current Formulation Using Two Potentials: The Magnetic Vector Potential and Total Scalar Potential' *IEEE Trans. On Mag. Vol. Mag19. No:6, November 1983 pp. 2284-2287.*

[1.10] **Rodger D and Eastham J** 'A formulation for Low Frequency Eddy Current Solution ' *IEEE Trans. on Mag., Vol. 19, p.2443, November 1983.*

[1.11] **Carpenter C J** ' Comparison of Alternative Formulations of 3D Magnetic field and Eddy current problems at power frequencies ' *Proc. IEEE, 124(11), 1977, pp. 1026-1034*

[1.12] **Simkin J** ' Eddy Current modelling in Three Dimensions ' *IEEE Trans. on Mag., Vol. MAG 22, September 1986.*

[1.13] **Foggia A and Sabonnadiere J C** ' Finite Element Solution of Saturated Travelling Magnetic Field Problems ' *IEEE Trans. on Power Apparatous and Systems, Vol. PAS-94, no: 3, May/June 1975*

[1.14] **Silvester P P and Ferrari R L,** 'Finite Elements for Electrical Engineers' *Cambridge University Press, 1983.*

[1.15] **Rodger D and Eastham J F,** 'Characteristics of a Linear Induction Tachometer - a 3D Moving Conductor Eddy Current Problem', *IEEE, Trans Mag, 1985, 2412-2415.*

[1.16] **Rodger D, Karaguler T and Leonard P J,** 'A Formulation for 3D Moving Conductor Eddy Current Problems, *IEEE Trans, Mag 25, September 1989. pp. 4147-4149.*

[1.17] **Rodger D, Leonard P J and Karaguler T,** 'An Optimal Formulation for 3D Moving Conductor Eddy Current Problems with Smooth Rotors, *IEEE Trans, Vol. Mag-26, p. 2359, September 1990,*

[1.18] **Penman J and Grieve M D,** 'An Approach to Self Adaptive Mesh Generation', *IEEE Tran. on Magn., Vol. Mag-21, No:6, Nov. 1985, p. 2567.*

[2.1] **Hammond P** 'Use of Potentials in Calculation of Electromagnetic Fields' *IEE Proc.,* **Vol. 129,** *No. 2, March 1982 pp. 106-112.*

[2.2] **Renhart W, Stogner H and Preis K** 'Calculation of 3D Eddy Current Problems by Finite Element using either an Electric or an Magnetic Vector Potential' *IEEE Trans Mag, Vol 24, No.1, Jan. 1988 p. 122.*

[2.3] **Hammond P** 'Applied Electromagnetism' *First Edition Pergamon Press, 1971.*

[2.4] **Jennings A,** 'Matrix Computation for Engineers and Scientists' *John Wiley & Sons Press, 1977.*

[3.1] **Hughes T J R** 'A Simple Scheme for Developing 'upwind' Finite Elements'*Int J. Num Meth. Eng.,* **Vol. 12,** *1978, pp. 1359-1365.*

[3.2] **Heinrich J C, Huyorhorn P S, Zienkievicz O C and Mitchell** 'An Upwind Finite Element Scheme for Two-Dimensional Convective Transport Equation' *Int J. Num. Meth. Eng., Vol. 11, p. 131, 1977.*

[3.3] **Odamura M and Ito M** 'Upwind Finite Element Solution of Saturated Travelling Magnetic Field Problems', *4th International Symposium on Finite Element Methods in Flow Problems' pp. 819-826, July 1982.*

[3.4] **Reitz J R and Davis L C** 'Force on a Rectangular Coil Moving above a Conducting Slab' *J Appl. Phys.,Vol 43, No. 4, April 1972 p. 1547.*

[3.5] **Atherton D L and Canadian Maglev Group** 'Magnetic Levitation for High Speed Guided Ground Transportation', *Annual Report for 1973, Queen's University, March 1974.*

[4.1] **Carpenter C J** 'Surface Integral Methods of Calculating Forces on Magnetized Iron Parts', *Proc. Inst. Elect. Eng., 107 C, 1960, pp 19-28.*

[4.2] **Edwards J D** 'Electrical Machines - An Introduction to Principles and Characteristics' *Macmillan, 2nd Ed, 1986, pp 16-19.*

[5.1] **Laithwaite E R** 'Induction Machines for Special Purposes', *George Newnes Limited, 1966, pp 305-306, 23-28, 308-309.*

[5.2] **Carter F W** ' Magnetic Field of the Dynamo-Electric Machine, *JIEE, 64, 1115 (1926)*

[5.3] **Nasar S A and Boldea I** 'Linear Motion Electric Machines'. *John Wiley and sons, 1976, pp 269.*

[5.4] **Bolton H** 'Transverse Edge Effect in Linear Induction Machines' *Proc. IEE, 116, 1969, pp. 725-739.*

[5.5] **Russel R L and Norsworthy K H**'Eddy Currents and Wall Losses in Screened Rotor Induction Motors', *Proc. Inst. Elect. Eng., 105A, 1958, pp 163-175.*

[5.6] **Greig G and Freeman E M** 'Travelling Wave Problem in Electrical Machines' *Proc Inst. El. Eng., Vol 114, no. 11, November 1967, pp 1681-1683.*

[5.7] **Rodger D and Eastham J F** 'Dynamic Behaviour of Linear Induction Machines in the Heave Mode' *IEEE Transactions on Vehicular Techn., Vol VT-3, No. 2, May 1982, pp 100-106.*

[5.8] **Hesmondhalgh D E and Laithwaite E R** 'A Method of Analysing the Properties of two-phase Servomotors and AC Tachometers' *Proc. IEEE 110, 1963, p. 2039.*

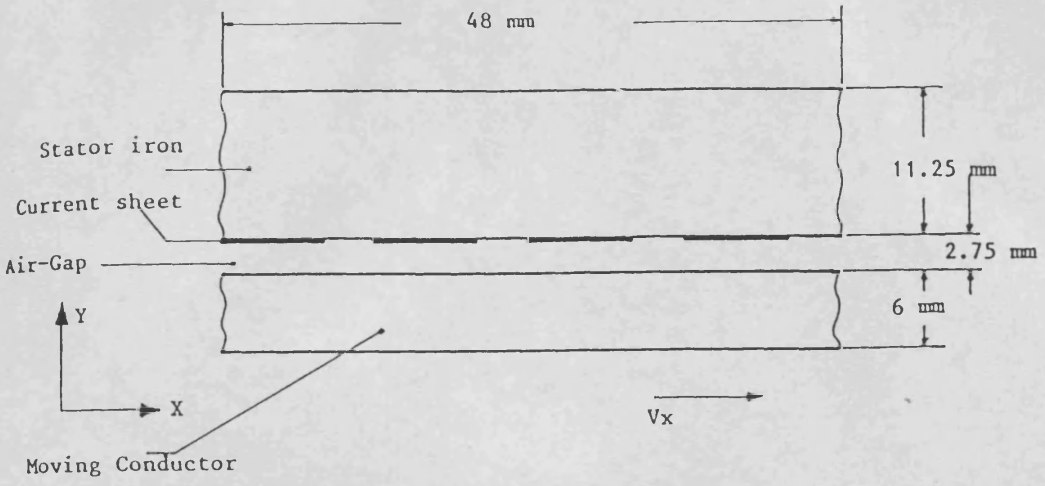

Fig. 3.4 2D test problem with steel rotor

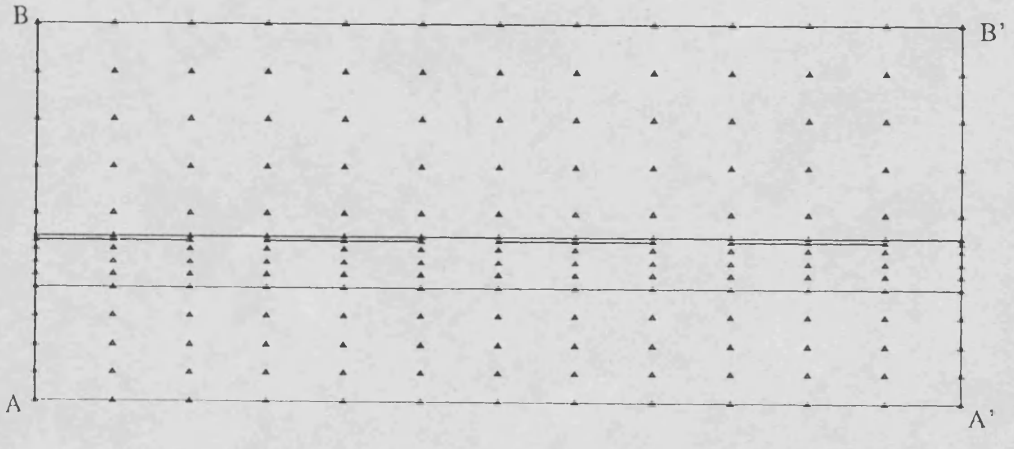

Fig. 3.5 Specification of the periodicity boundaries for the test motor

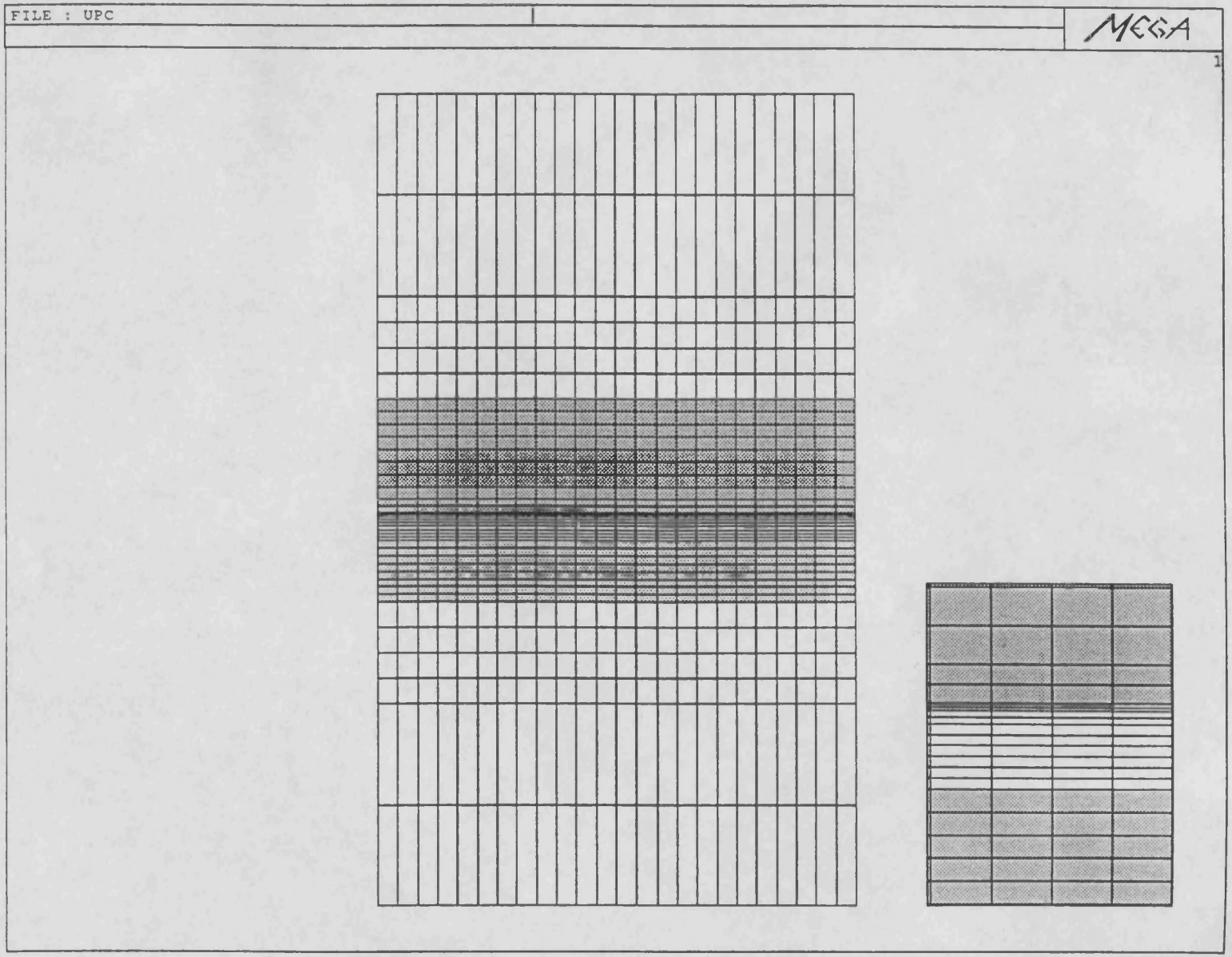

Fig. 3.6 2D Coarse mesh (h=4 mm)

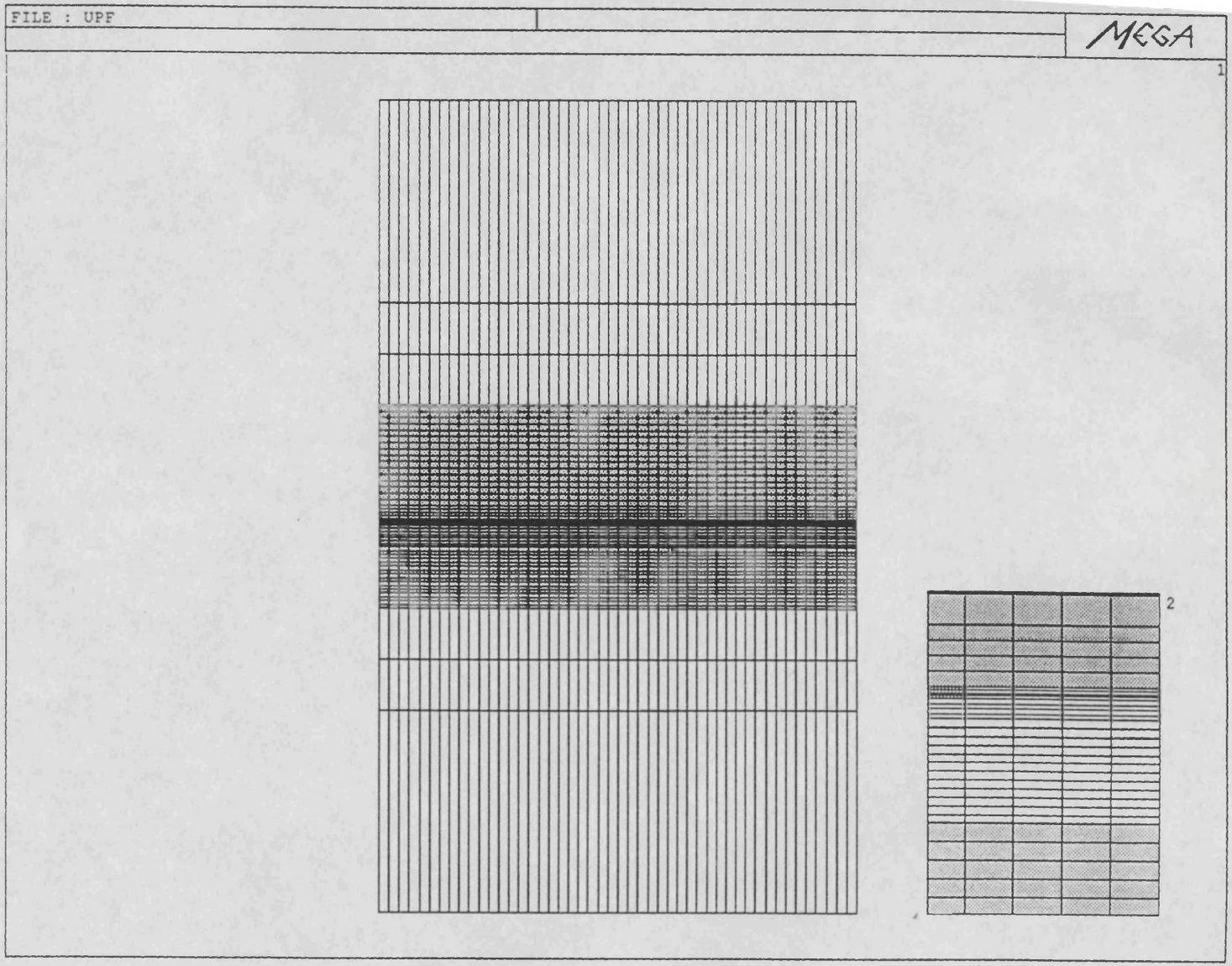

Fig. 3.7 2D Fine mesh (h=1 mm)

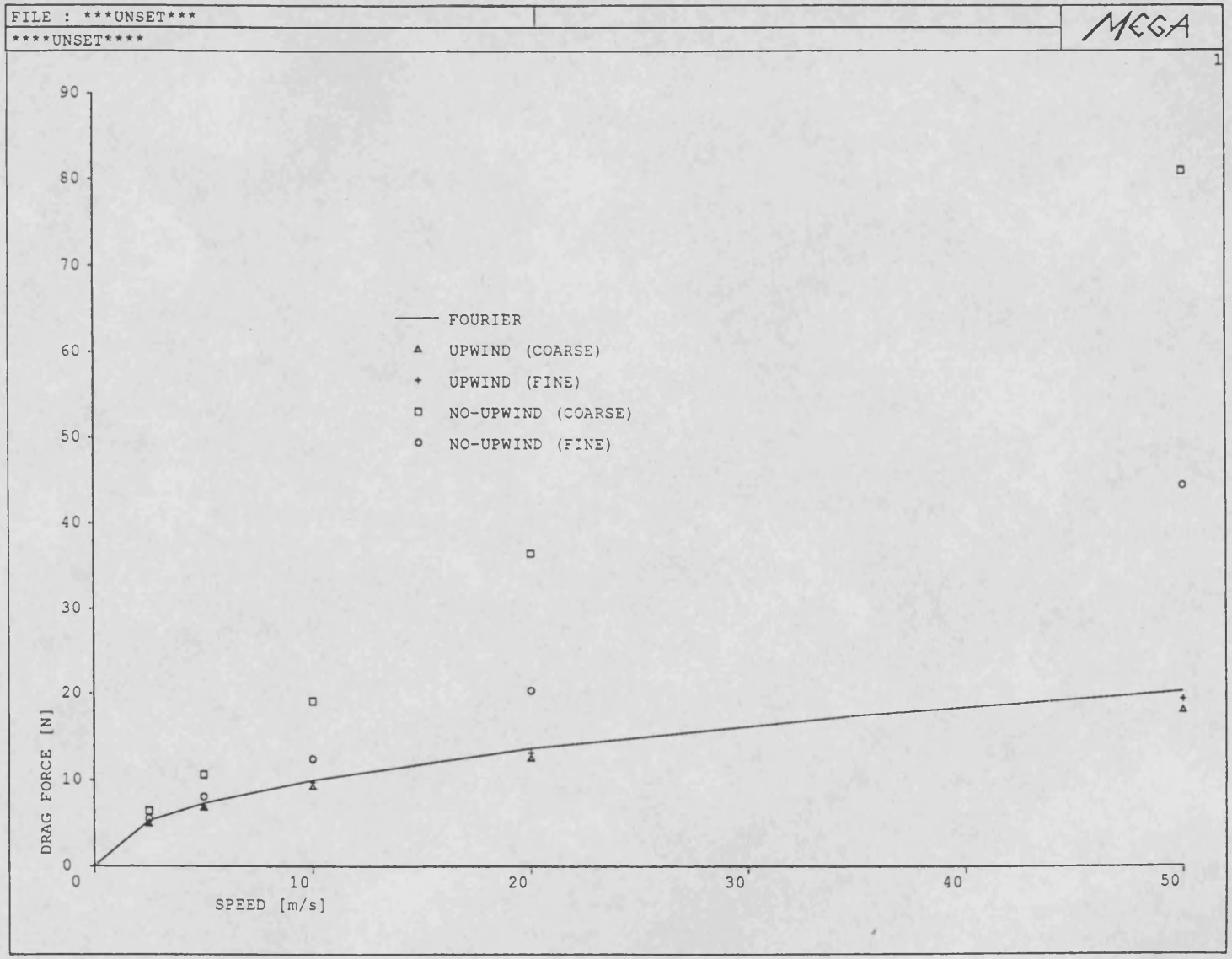

Fig. 3.8 Drag force - speed characteristics with and without upwinding

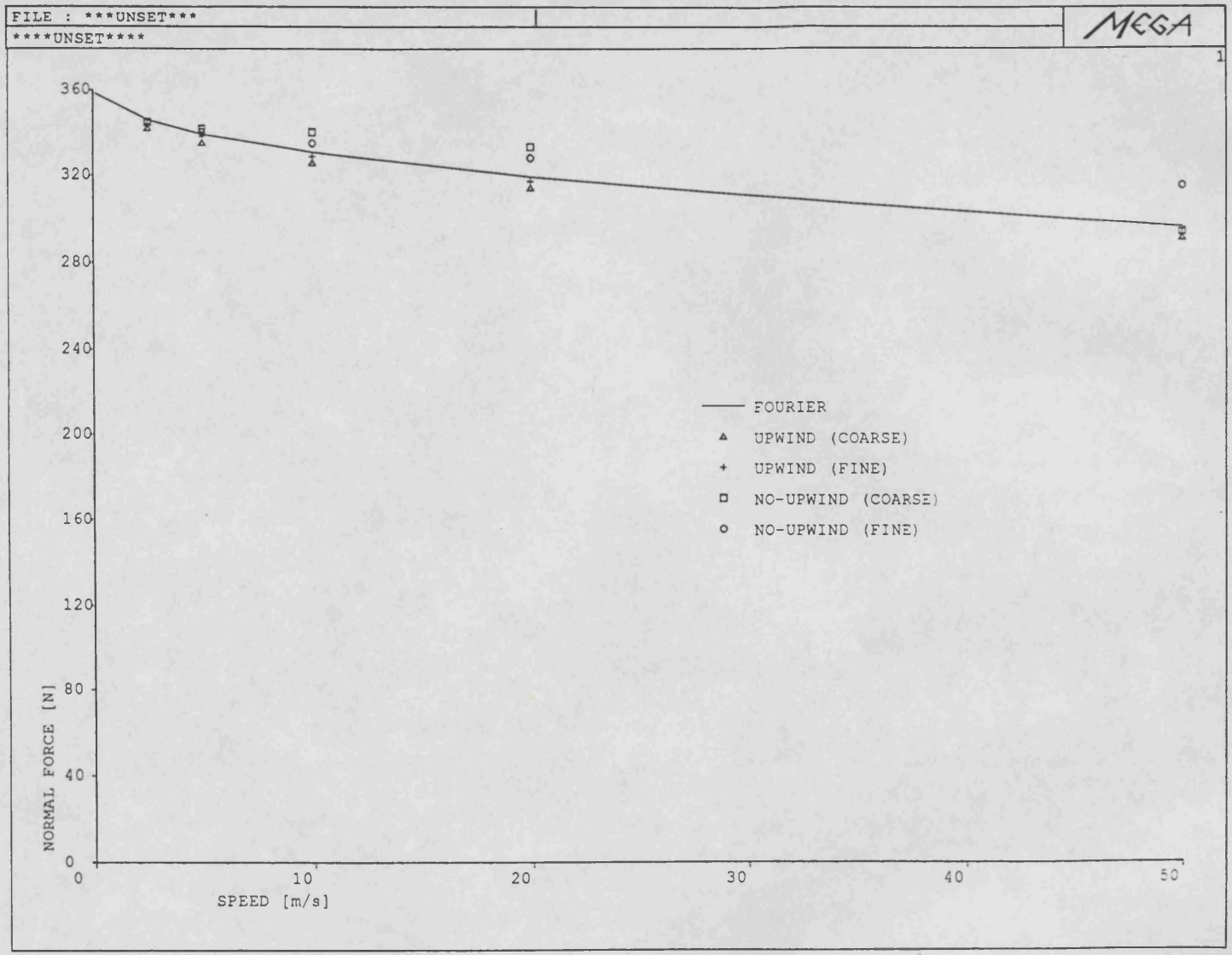

Fig. 3.9 Normal force - speed characteristics with and without upwinding

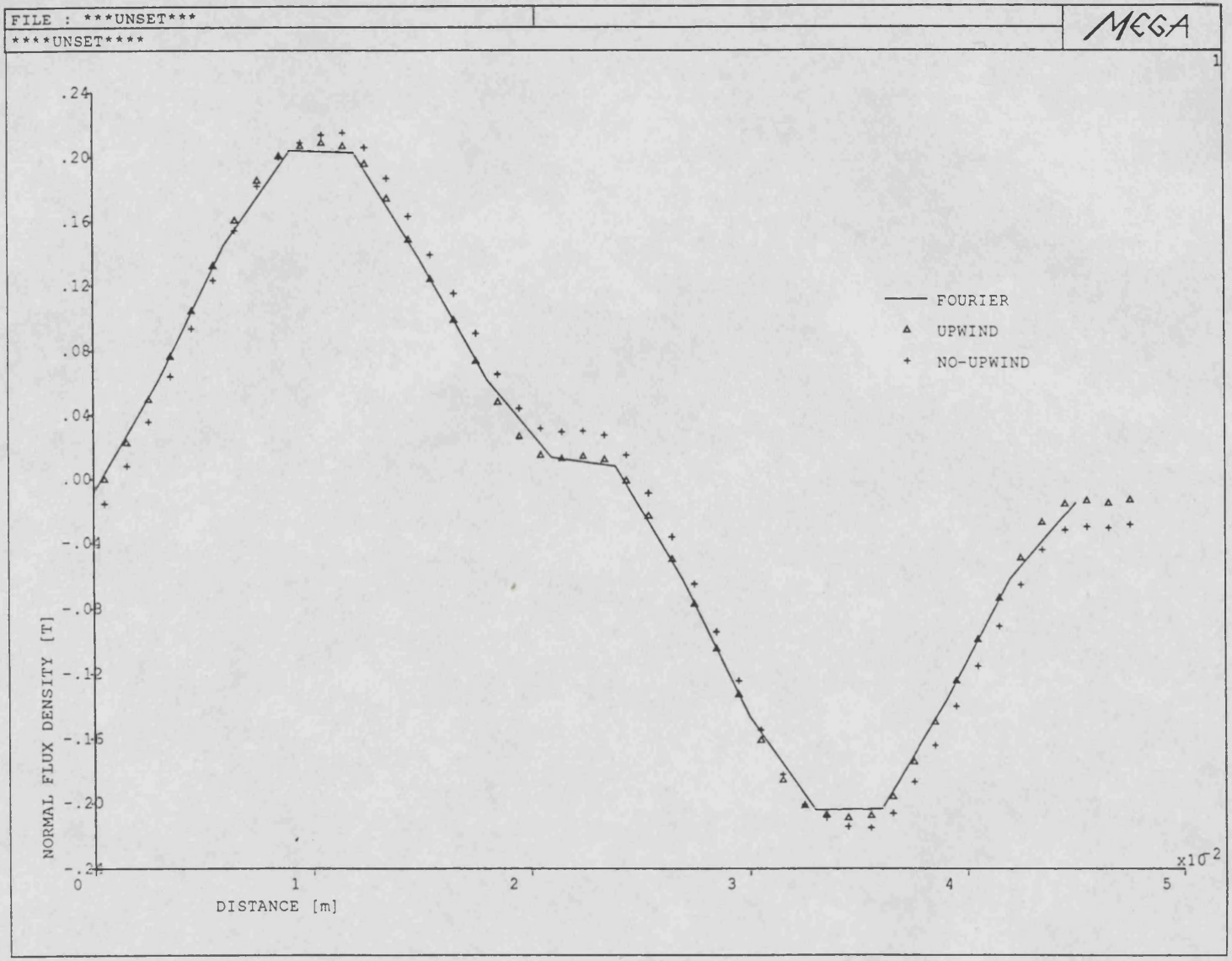

Fig. 3.10 Normal air-gap flux density with and without upwinding at u=50 m/s

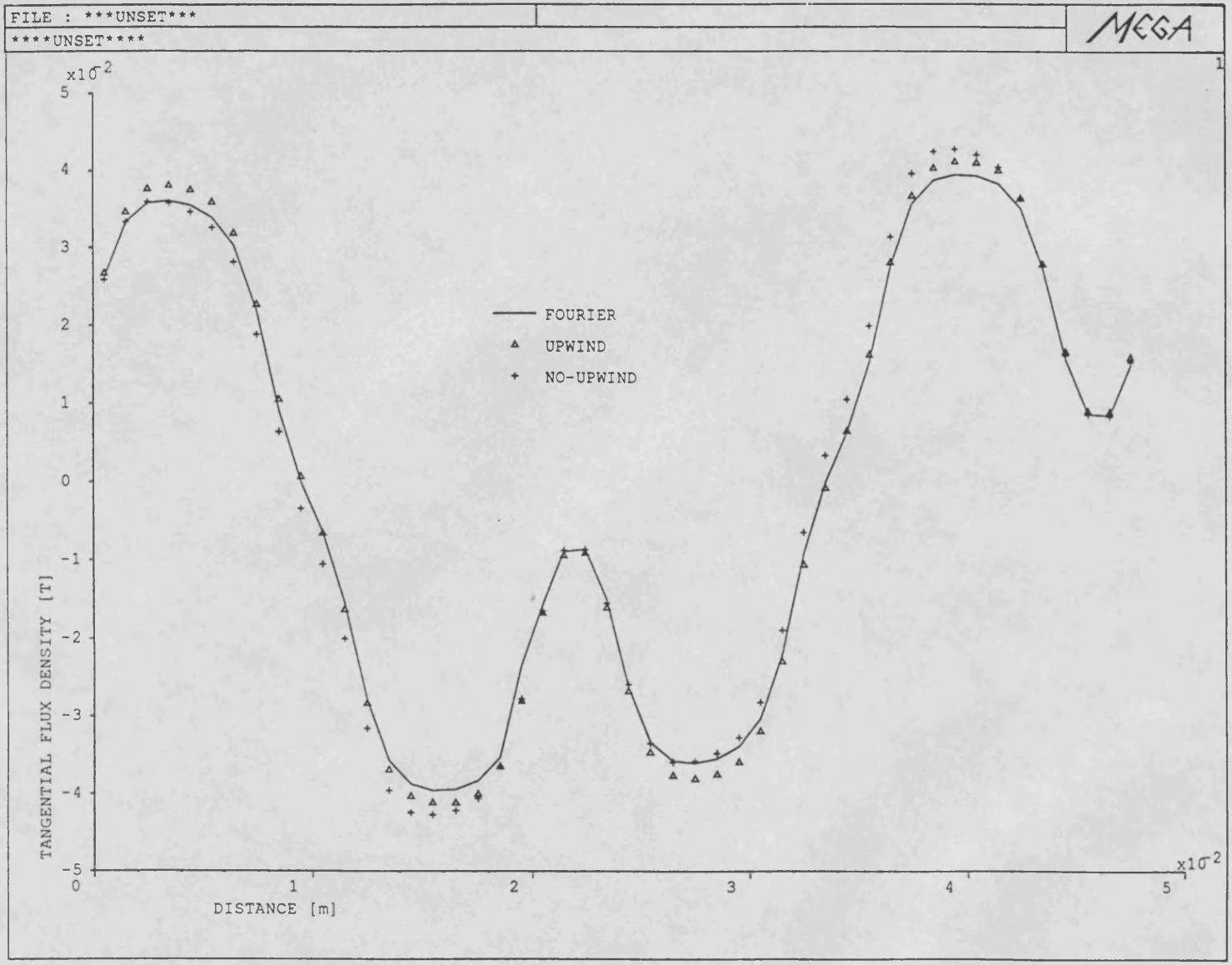

Fig. 3.11 Tangential air-gap flux density with and without upwinding at u=50 m/s

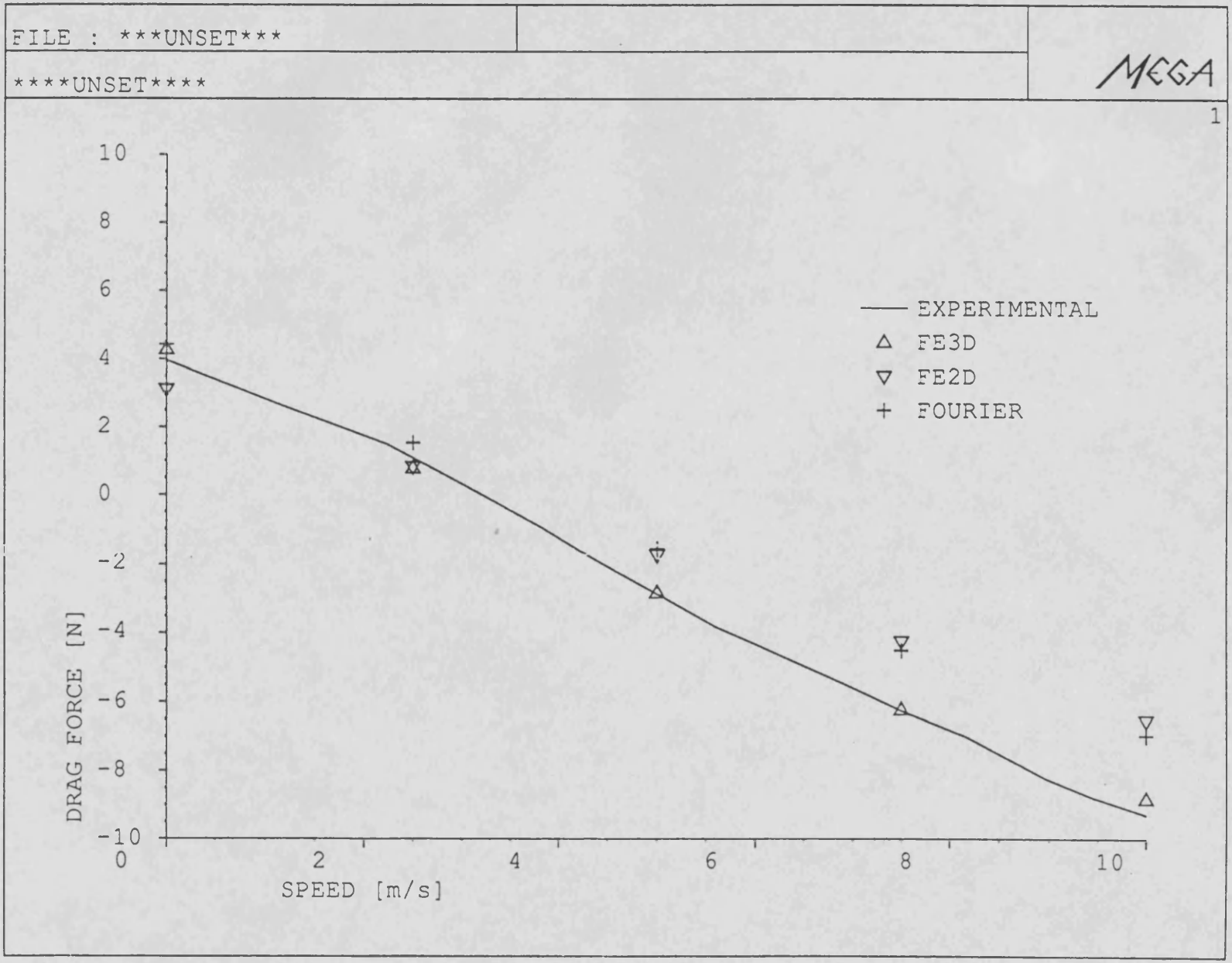

Fig. 5.31 Comparison of drag force results with experimental results

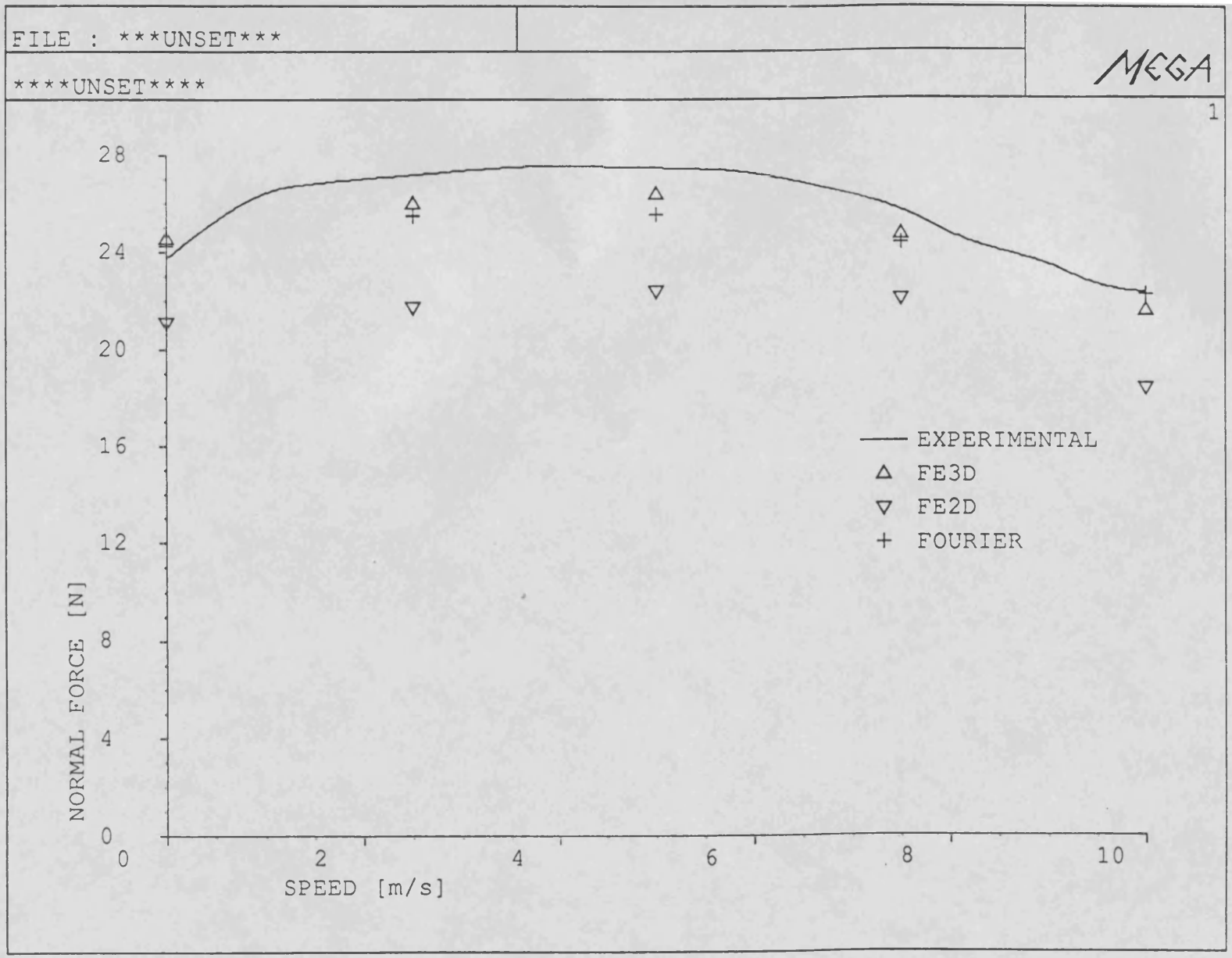

Fig. 5.32 Comparison of normal force results with experimental results